

# SMART FIELD WEIGHING LYSIMETER FOR VALIDATION OF SATELLITE-BASED EVAPOTRANSPIRATION UNDER ARID ENVIRONMENTS

Report to the  
**Water Research Commission**

by

**M.A.M. Abd Elbasit<sup>1</sup> and P.E. Ratshiedana<sup>2,3</sup>**

<sup>1</sup> Department of Physical and Earth Sciences, Faculty of Natural and Applied Sciences,  
Sol Plaatje University, Kimberley

<sup>2</sup> Agricultural Research Council-Natural Resources and Engineering

<sup>3</sup> School of Geography, Archaeology and Environmental Studies,  
University of the Witwatersrand

**WRC Report No. 3163/1/24**

**ISBN 978-0-6392-0648-6**

**August 2024**



**Obtainable from**

Water Research Commission  
Bloukrans Building, Lynnwood Bridge Office Park  
4 Daventry Street  
Lynnwood Manor  
PRETORIA

[hendrickm@wrc.org.za](mailto:hendrickm@wrc.org.za) or download from [www.wrc.org.za](http://www.wrc.org.za)

This is the final report of WRC project no. C2022/2023-00978.

**DISCLAIMER**

This report has been reviewed by the Water Research Commission (WRC) and approved for publication. Approval does not signify that the contents necessarily reflect the views and policies of the WRC, nor does mention of trade names or commercial products constitute endorsement or recommendation for use.

## EXECUTIVE SUMMARY

---

### BACKGROUND

Water scarcity poses a significant and increasing challenge for nations and communities inhabiting arid and semi-arid regions. Research projections suggest that scarcity will reach critical levels by the year 2030, impacting most parts of the South African nation. South Africa is a physically water scarce country where the demand for water far surpasses its available. This challenge is further compounded by the recurrent droughts anticipated in the future of South Africa, as well as the compounding effects of population growth and climate change, which drive the exponential increase in both food demand and water use. Agricultural activities in South Africa use more than 75% of available freshwater resources compared to other water sectors. Addressing this problem requires the implementation of efficient water management practices, focussing on improving water use efficiency and productivity. Optimising agricultural water usage comes with the potential to unlock additional water resources, adding the potential to expand cultivated areas or reallocating water to other sectors that need water. To effectively monitor and evaluate water use efficiency, a robust monitoring system is required. Integrating ground-based and geospatial technologies provides an efficient means of assessing water consumption and utilisation in various landscapes. Although recent advancements in satellite technology have developed products that are capable of monitoring evapotranspiration (ET) and crop water use, their consistency and accuracy remain a subject of concern. The calibration and validation of these remote sensing products are heavily based on ground-based data, which are often lacking or difficult to obtain in arid environments. In response to these challenges, this project was initiated to validate remotely sensed ET, and reference evapotranspiration (ET<sub>o</sub>) models within arid environments.

### AIMS

The main aim of this project was to develop a field-based validation approach using smart lysimeter technique to assess the accuracy and reliability of remotely sensed evapotranspiration (ET) and water-use products within arid environments. Furthermore, four specific objectives were derived to achieve the main aim of this project. The first objective was to determine ET<sub>a</sub> from the water balance components based on the measurements of the smart field weighing lysimeter. The second objective was to find suitable ET<sub>o</sub> models that can be used to determine ET<sub>a</sub> in the absence of smart field weighing lysimeter. The third objective was to evaluate the accuracy and consistency of global ET<sub>a</sub> products using smart field weighing lysimeter data directly and indirectly. The fourth objective was to use the smart field lysimeter data to evaluate remote sensing-based ET<sub>a</sub> calculated from raw Landsat 8 imageries combined with published ET<sub>a</sub> algorithms.

### RESEARCH APPROACH

The study concentrated on both summer and winter crops, specifically barley, maize, and soybean. Evapotranspiration levels were closely monitored within a fully irrigated scheme across various seasons. This scheme, known as the Vaalharts Irrigation Scheme, represents the largest cropping initiative in the arid regions of South Africa. Three distinct methodologies and approaches were used at both the farm and scheme levels, utilizing different sensors and resolutions to assess actual evapotranspiration (ET<sub>a</sub>) and soil moisture balance. These methodologies included the Surface Energy Balance Algorithm for Land (SEBAL) method, vegetation indices such as Crop Water Stress Index (CWSI) and Normalized Difference Vegetation Index (NDVI), and Surface Energy Balance System (SEBS) model. Crop water consumption was analysed based on actual evapotranspiration, crop evapotranspiration, and various water stress indices (WSI). Meteorological data and soil moisture measurements for the calibration and validation of remote sensing-based ET products and water balance calculations were retrieved from the Agricultural Research Council-Natural Resources and Engineering (ARC-NRE) meteorological station network and smart lysimeter measurements conducted at the field level.

## **METHODOLOGY**

The most effective way to increase water use efficiency is to precisely measure plant water consumption by determining all the water balance components and quantifying water losses. Different water balance models can determine irrigation timing/amount and effective rainfall. In this project, two smart field weighing lysimeters were installed to measure  $ET_a$  at field level across four seasons hosting both summer and winter crops. Each lysimeter was equipped with three soil moisture sensors, three temperature sensors, three potential water sensors, and three soil electrical conductivity sensors. The deep drainage component of the water balance from the bottom of the lysimeter was also measured using a drainage container placed on the load cell measuring the amount of water drained out of the lysimeter. The weight of the lysimeter, and drainage container automatically every minute while the sensors measured soil water variables at a 10-minute interval in a field data logger linked to the lysimeters. The daily changes in the lysimeters, weight and soil moisture were used to determine the consumed water after subtracting the total drainage water. From the weight changes  $ET_a$  was determined for all crops. The  $ET_a$  from the lysimeter was compared to the  $ET_o$  calculated from 28 micrometeorological models using data acquired from automated weather stations. The best relationship was selected as the most suitable model for  $ET_o$  in arid environments. Two remotely sensed data processing levels were utilized: 1) evapotranspiration products and 2) raw satellite images. The  $ET_a$  products were directly compared to the lysimeter data at different time scales ranging between daily, monthly, and seasonally. Various methods were applied to determine  $ET_a$  from remotely sensed data, including data at visible (VIS), infrared (IR), and thermal (TIR) spectral ranges. Three methods were examined under different seasons during the period of this project. The NDVI and Land Surface Temperature (LST) were extracted from Landsat 8. The NDVI was used to determine crop coefficients ( $K_c$ ) values which were used to calculate  $ET_a$  as a product of  $ET_o$  multiplied by the  $K_c$  values throughout each cropping season. Using the CWSI,  $ET_a$  was determined as a product of CWSI multiplied by the crop evapotranspiration ( $ET_c$ ). The CWSI used both surface temperature compared to air temperature and vegetation index to estimate the relative water status.

## **RESULTS AND DISCUSSION**

This project focused on the measurement of  $ET_a$  and the evaluation of ET models and satellite ET products using a smart field weighing lysimeter approach.  $ET_a$  was determined for four cropping seasons where barley, maize and soybean crops were used in the lysimeter experiments. Findings demonstrated that  $ET_a$  across all seasons had a similar trend. During the emergence and early development stages of each season,  $ET_a$  was relatively low. This can be attributed to less transpiration processes occurring within the field when crop canopies are at low density stage with few leaves while irrigation water inputs were also low resulting in low evaporation rates. As the crops grew into the season,  $ET_a$  fluxes showed a gradual increase reaching peak at mid-season. The increase in  $ET_a$  at mid-season can be attributed to increased leaf area and increased water inputs where crops were in an active transpiration stage while soil water evaporation was also high.  $ET_a$  gradually declined from peak values as the seasons shifted towards harvest period. The decrease in  $ET_a$  can be attributed to crops reaching senescence while irrigation water inputs are reduced reducing soil water evaporation rates. On assessing the seasonal irrigation inputs versus the total seasonal  $ET_a$ , it was observed that irrigation on the farm did not match the crop water requirements where more water was used than required. This finding makes an emphasis on the significance of  $ET_a$  on irrigation water management.

Upon a successful determination of  $ET_a$  at various time stamps at a farm scale, a total of 28 micrometeorological models for estimating  $ET_o$  were evaluated using a weather station located near the lysimeter installation site. The objective here was to determine the most suitable  $ET_o$  model that can be used to extrapolate  $ET_a$  from point location to the scheme scale using weather stations located within the scheme. Findings demonstrated that the Penman-Monteith model was more suitable for the purpose while other models showed lower agreements. The uncertainties between models and lysimeter  $ET_a$  can be attributed to the fact that some models were developed in areas suiting their climate conditions which may not always yield similar

results in environments where they are transferred to. This finding puts an emphasis on the fact that ET models developed in one area requires local calibrations to fit the local climatic conditions using in situ measurements.

Having determined the Penman-Monteith model as the most suitable,  $ET_a$  was determined at each weather stations in the irrigation scheme using the relationship built between  $ET_a$  and  $ET_o$  at field scale. The values of  $ET_a$  were used to evaluate  $ET_a$  estimated by remote sensing-based ET products which covered the NOAH, MOD16 and WaPOR. The evaluation which was done using the products pixel values on their original spatial resolutions was done using statistical metrics which showed varying accuracies. The disparities between  $ET_a$  from the products and  $ET_a$  on the ground can be attributed to several factors. This includes the coarse resolution of the products which contain multiple land cover types. The parametrization of the algorithms that runs the evaluated products can be attributed to adding more uncertainties of the products. The limitation of lysimeters in the area might have also affected the extrapolation of  $ET_a$  from field to scheme scale due to variability in land cover changes.

With challenges experienced on global ET products, the project further made use of raw Landsat images in generating ET outputs from various algorithms which were evaluated using smart field weighing lysimeter  $ET_a$  data. The SEBS, SEBAL, CWSI-based ET and VI-based ET algorithms were used for this purpose. Varying accuracies were reported for each algorithm. The variabilities can be attributed to the parametrization of the algorithms used while the limitation of Landsat images across some seasons might have played a role in the data points used for the evaluation process.

This study has highlighted the importance of ET in agricultural water management in South Africa with emphasis on the need for development of a network of systems that can be used in the provision of ground-based ET data. The need for ground data is an undisputable gap towards development of models and validation of existing algorithms and products of ET in South Africa. This remains important as more products are developed and validated in countries like Europe and most countries in the United Kingdom which have enough sufficient networks of ground-based ET measurements.

## **KEY MESSAGE**

The project highlights the impending challenges of water scarcity exacerbated by factors such as population growth, climate change, and inefficient water management practices, especially in the agricultural sector. To mitigate these challenges, the project emphasizes the need for efficient water management practices within agriculture, focusing on enhancing water use efficiency and productivity. The project suggests that optimizing agricultural water usage can unlock additional water resources, thereby expanding cultivated areas or reallocating water to other vital sectors. Furthermore, the project discusses the importance of accurate monitoring and evaluation of water use efficiency, advocating for the integration of ground-based and geospatial technologies to assess water consumption and utilization across various land uses. However, the project also acknowledges the challenges associated with the accuracy of remote sensing products and calls for validation efforts as demonstrated. Accurately estimating actual evapotranspiration is essential for water management at different scales. This project has validated actual evapotranspiration and crop water using smart lysimeter measurements. In the agricultural setting,  $ET_a$  data can help farmers to understand the actual water needs of their crops. By matching irrigation schedules to crop water demand based on  $ET_a$ , farmers can ensure efficient water use, avoiding both over- and under-irrigation. This optimization reduces water wastage and promotes sustainable water management practices. South Africa still portrays a huge gap in  $ET_a$  measurements. This study demonstrated the capabilities of determining ET at field scale accurately which highlighted the need for more of these expensive devices. While the devices are cost restricting, having few lysimeters to develop robust models integrating ground data with satellite data will improve agricultural water management through enhanced monitoring and mapping technologies.

## CONCLUSIONS

In this project, the study made use of a smart field weighing lysimeter which is a far much advanced system compared to the systems used in the past decades. Although the lysimeters provided accurate ET outputs, these systems are owned by research institutes and their datasets are not readily available, making ET data a continuous data gap struggle in the South African water management practices. While ET remains a bigger challenge the study made a multi-phased analysis of ET measured from the lysimeter and estimated from various models and satellite products. The study accurately determined ET<sub>a</sub> based on the lysimeter measurement of the water balance components for barley, maize and soybean crops. The study evaluated the relationship between various ET<sub>o</sub> estimation models with the in-situ ET<sub>a</sub> measurements to determine a better model that can be used to extrapolate ET<sub>a</sub> from lysimeter point to other spatial locations using meteorological stations. This action suggests that ET<sub>a</sub> in arid environments can be estimated in the absence of smart field weighing lysimeters or any expensive measuring device if there is a meteorological station on site. The relationship between ET<sub>a</sub> and ET<sub>o</sub> was used to develop new local K<sub>c</sub> values for the Vaalharts irrigation scheme for the three investigated crops which differed from those published by the Food and Agriculture Organization (FAO). This finding made emphasis on the need for local calibrations and development of local K<sub>c</sub> values for each region for accurate water management and irrigation adjustments. With knowledge of ET<sub>a</sub>, farmers can fine-tune irrigation systems to deliver the right amount of water directly to the crop root zone. This precision irrigation reduces losses due to runoff, deep percolation, and evaporation from the soil surface, thereby maximizing water use efficiency. The Vaalharts is well known for its salinity problems. Over-irrigation can lead to waterlogging, soil salinization, and nutrient leaching, causing environmental degradation. By accurately estimating ET<sub>a</sub>, farmers can avoid excessive water application, thereby mitigating these negative impacts on soil and water quality. We acknowledge that, while lysimeters are important devices, they still have their own limitations such as the limitation in spatial extent capturing while they also require knowledge on conversion of weights into water amounts. These devices are expensive, and it might not be possible for farmers to afford for the purpose of irrigation water management and support, but they hold potential in large commercial farms using large volumes of water. These systems also hold promise to be used by the governmental organizations responsible for irrigation water management, distribution, and monitoring purposes.

## RECOMMENDATIONS

- Based on the limitations in ET measuring stations, there is a need to focus on development of ET monitoring network systems across the country with data that is available to the public while the data has potential to help in the validation and calibration of indirect ET models.
- Lysimeters are not cheap, but their accuracy in determining the water balance components make them top priority tools that can be used for crop water use in large commercial farms to aid in irrigation scheduling. As such future research should focus on the development of lysimeters for use at various scales for the purpose of evaluating and calibrating ET models, this can either be from greenhouses or farm scales.
- To our knowledge the smart field weighing lysimeter used in this study is the first in Africa, however the lysimeter of its kind provides more information on the soil-plant-water conditions. More devices of this nature are recommended for future research purposes including those that can be used for horticultural purposes.
- The study was done at a field scale within the Vaalharts irrigation scheme, as such findings obtained here might not actually apply to the entire country, as such evaluation of ET based on the results of this study may not always produce accurate results if used in a different area with different climatic, topographic and soil conditions. We recommend that future research should focus on implementing projects of this nature to solve the issue of environmental variabilities for accurate outputs.
- The current study focused on three crops which were barley, maize, and soybean, we recommend the determination of ET<sub>a</sub> for many other crops which can help in the development of local crop coefficients that can be used for irrigation scheduling.

- During the project, we observed the limitations in the use of SFL-600 lysimeter for maize ET<sub>a</sub> determination where we could only determine ET<sub>a</sub> for early to development stages of the crop with errors being observed on the weighing balance measurement due to long maize roots reaching the lysimeter bottom. We recommend that, future research should focus on the use of larger lysimeters when dealing with crops that have long roots.
- The study made use of micrometeorological models to aid in extrapolating ET<sub>a</sub> from a point level into the larger extent of the irrigation scheme using four weather stations. We recommend the continuous installation of meteorological stations in the study area to capture more variabilities in ET which can be used to develop more robust ET models that could aid in improving the water management practices in the scheme.
- The study made use of ET products at varying scales, the coarse resolutions such as NOAH and MODIS products demonstrated poor results when compared with ET<sub>a</sub> from ground measurements. While on the other side, WaPOR product showed some promising results at 250 m<sup>2</sup> resolution. The WaPOR product in some countries contains a 100 m<sup>2</sup> and 30 m<sup>2</sup> resolution ET products. We recommend the FAO to improve the resolution of WaPOR also covering South Africa and more African countries.
- The project made use of Landsat 8 data for estimation of ET using SEBAL, SEBS, CWSI and vegetation index-based algorithms obtaining varying observations when compared to ground measurements. We recommend the integration of better resolution images such as sentinel datasets and the use of Unmanned aerial vehicles (UAV) for ET estimation. The use of UAV will add more value to solve the issues of spatial and temporal resolutions and weather challenges such as clouds which are common when using satellite images.

## ACKNOWLEDGEMENTS

The research team would like to thank the Water Research Commission for the financial support of this project on the smart weighing lysimeter for calibration and ground validation of satellite-based evapotranspiration and water use products in South African arid region (Project No. C2022/2023-00978). We thank Mr Wandile Nomqophu and Ms Penny Jaca from the Water Research Commission for their help and support, in providing the necessary guidelines for managing the project. We also thank Dr Simba Jombo, Mr Amanda Masana, Mr Eric Benjamin Economon and Mr Phumlani Magnificent Zwane for their assistance during fieldwork and lysimeter installation. We also acknowledge the South African Barley Breeding institute (SABBI) for granting us permission to use their experimental field to set up our field experimental designs which goes to Mr Fagan Scheepers, Mr Willem Vermeulen. Our gratitude to Mr Nkosinathi Nxumalo from AB-INBEV who also assisted during this project.

The project team wishes to thank the following people for their contributions to the project.

### Reference Group

Mr Wandile Nomqophu (Chair)

Ms Penny Jaca (Coordinator)

Dr Thomas Abraham

Dr Khaled Abutaleb

Dr Iqra Atif

Prof John Odindi

Prof Tesfay Araya

Prof Ahmed Mukalazi Kalumba

Prof Elhadi Adam

Mr Terry Newby

### Affiliation

Water Research Commission

Water Research Commission

WILSON GEOSERVICES

Agricultural Research Council

University of the Witwatersrand

University of KwaZulu-Natal

University of the Free State

University of Fort Hare

University of the Witwatersrand

GeoTerra Image

### Others

Dr Tabaro Kabanda

University of Dodoma (Tanzania)

### Project Team

Prof. Mohamed Abd Elbasit

Mr Phathutshedzo Eugene Ratshiedana

### Role

Principal investigator

PhD Researcher

### Capacity Building

Mr Amanda Masana

Ms Katelyn Tamia Cole

Ms Owami Mashaba

M.Sc. Researcher

Hons. Researcher

Hons. Researcher

## LINKED OUTPUTS

---

1. Ratshiedana, P.E., Abd Elbasit, M.A., Adam, E., Chirima, J.G., Liu, G. and Economon, E.B., 2023. Determination of Soil Electrical Conductivity and Moisture on Different Soil Layers Using Electromagnetic Techniques in Irrigated Arid Environments in South Africa. *Water*, 15(10), p.1911. <https://doi.org/10.3390/w15101911>.
2. Ratshiedana, P.E., Abd Elbasit et al. Smart field based lysimeter for the determination of crop water use under arid environments-Technical note. (In preparation).
3. Ratshiedana, P.E., Abd Elbasit et al. Evaluation of reference evapotranspiration in arid environments using smart field lysimeter. (In preparation).
4. Ratshiedana, P.E., Abd Elbasit et al. Field-based evaluation of actual evapotranspiration algorithms using satellite imageries under arid environments. (In preparation).

This page was intentionally left blank

# CONTENTS

<b>EXECUTIVE SUMMARY</b> .....	<b>iii</b>
<b>ACKNOWLEDGEMENTS</b> .....	<b>viii</b>
<b>CHAPTER 1: BACKGROUND</b> .....	<b>1</b>
1.1 INTRODUCTION .....	1
1.2 EVAPOTRANSPIRATION ESTIMATION USING REMOTE SENSING .....	3
1.2.1 Background .....	3
1.3 MOTIVATION.....	4
1.4 RESEARCH APPROACH.....	5
1.5 REMOTE SENSING APPLICATION .....	5
1.6 APPLIED ESTIMATION METHODOLOGY .....	7
1.7 STUDY AREA DESCRIPTION .....	7
<b>CHAPTER 2: SMART FIELD LYSIMETER FOR ACTUAL EVAPOTRANSPIRATION MEASUREMENT</b>	<b>10</b>
2.1 INTRODUCTION .....	10
2.1.1 Lysimeter installation area .....	12
2.1.2 Lysimeter components and installation.....	13
2.2 LYSIMETER DATA MEASUREMENT AND ET DETERMINATION .....	17
<b>CHAPTER 3: LYSIMETER DATA PROCESSING (MULTI-TEMPORAL ANALYSIS)</b> .....	<b>19</b>
3.1 INTRODUCTION .....	19
3.1.1 Lysimeter data selection and processing.....	19
3.1.2 Lysimeter mass balance .....	20
3.2 DETERMINATION OF ACTUAL ET AT DIFFERENT TIME SCALES USING SMART FIELD WEIGHING LYSIMETERS .....	20
3.3 EVALUATION OF LYSIMETRIC MEASUREMENTS .....	22
3.4 RESULTS .....	22
3.4.1 Actual evapotranspiration from smart lysimeters.....	22
3.4.2 Irrigation and ETa assessment .....	25
3.4.3 Lysimeter temperature variability .....	27
3.4.4 Lysimeter soil moisture dynamics .....	31
3.4.5 Relationship between soil moisture and evapotranspiration .....	32
3.4.6 Validation results based on the 2019 season.....	33
3.5 DISCUSSIONS .....	34
3.6 CONCLUSIONS.....	36
<b>CHAPTER 4: EVALUATION OF REFERENCE EVAPOTRANSPIRATION METEOROLOGICAL MODELS</b> .....	<b>38</b>
4.1 INTRODUCTION .....	38
4.2 METHODS AND MATERIALS .....	40
4.2.1 Study area description. ....	40
4.2.2 Ground-based data collection. ....	42
4.2.3 Actual Evapotranspiration Measurement.....	42
4.3 METHODOLOGIES .....	43
4.3.1 Radiation-Based Models.....	47
4.3.2 Temperature-Based Models .....	47
4.3.3 Aerodynamic-Based Models.....	47
4.3.4 Combination Models .....	48
4.3.5 Calculation of the Actual Evapotranspiration .....	48
4.3.6 Development of a relationship between ETa and ETo .....	48

4.3.7	Statistical Analysis .....	49
4.4	RESULTS .....	50
4.4.1	Calculated metrics at the field level during various seasons .....	50
4.4.2	Overall model rankings based on compromise programming ranking. ....	54
4.5	COMBINATION MODEL SELECTION ACROSS SEASONS .....	55
4.5.1	Final ranking and selection of radiation-based models across seasons.....	55
4.5.2	Final selection of the best models for estimating ET <sub>o</sub> in the arid environment. ....	56
4.6	DISCUSSIONS .....	57
<b>CHAPTER 5: ASSESSMENT OF REMOTE SENSED EVAPOTRANSPIRATION PRODUCTS UNDER ARID ENVIRONMENT .....</b>		<b>58</b>
5.1	INTRODUCTION .....	58
5.2	METHODOLOGY.....	59
5.2.1	Lysimeter Installation and Data Collection.....	59
5.2.2	Lysimeters field data measurement operation.....	60
5.2.3	Lysimeter data selection and processing.....	60
5.2.4	Calculation of actual ET at different time scales using smart field weighing lysimeters.....	61
5.2.5	Calculation of reference evapotranspiration at different weather stations.....	61
5.2.6	Relationship between ET <sub>a</sub> and ET <sub>o</sub> .....	61
5.3	RESULTS .....	63
5.3.1	Evaluation of NOAH ET product against in situ ET data across various stations .....	69
5.3.2	WaPOR evaluation across different stations and seasons.....	71
5.3.3	Evaluation of MOD16 across various stations and seasons .....	73
5.4	DISCUSSIONS .....	75
<b>CHAPTER 6: ASSESSMENT OF SATELLITE-BASED EVAPOTRANSPIRATION ALGORITHMS UNDER AGRICULTURAL ARID ENVIRONMENT.....</b>		<b>77</b>
6.1	INTRODUCTION .....	77
6.2	METHODOLOGY.....	80
6.2.1	Study area.....	80
6.2.2	Data Acquisition .....	81
6.2.3	Data Pre-processing .....	82
6.2.4	Actual Evapotranspiration Based on Reference Evapotranspiration and vegetation index. ..	82
6.3	RESULTS .....	88
6.3.1	Statistical analysis between ET <sub>a</sub> from lysimeter and the estimated ET <sub>a</sub> from four models ..	88
6.4	DISCUSSIONS .....	91
<b>CHAPTER 7: CONCLUSIONS &amp; RECOMMENDATIONS.....</b>		<b>93</b>
7.1	CONCLUSIONS.....	93
7.2	RECOMMENDATIONS.....	94
<b>REFERENCES.....</b>		<b>96</b>

## LIST OF FIGURES

Figure 1: South African arid region map.....	3
Figure 2: Conceptual framework for the research approach of ET-Sensing.....	5
Figure 3: Installation area of the smart lysimeter system.....	8
Figure 4: Climate characteristics of the study site; (a) annual rainfall, (b)potential evapotranspiration, (c) mean temperature, (d) aridity conditions.....	9
Figure 5: A view of a Smart lysimeter system, a) Schematic view of weighing lysimeter, b) internal view and display of the lysimeter components.....	12
Figure 6: Locality map of the study area, where (a) is the experimental farm, (b) is the Vaalharts irrigation scheme, (c) is the lysimeter area and (d) shows the location of the study area within South Africa and its provinces.....	13
Figure 7: Depicts different components of the lysimeter. The lysimeter core cylinder and housing barrel (a), lysimeter bottoms with gypsum (b), lysimeter and drainage balances (c), tensiometers (d), drainage bottle and pump (e), lysimeter cylinder with weighing balance (f), lysimeter cylinder with sensors installed, lysimeter battery recharging solar panel and data logger (h) while (i) shows inside the logger box.....	15
Figure 8: Provides an overview of the lysimeter installation during different cropping seasons. The soil monolith extraction using the lysimeter cylinder, straps, and a jack (a-d), lysimeter cylinder bottom closure (e), final lysimeter field setting (f), barely in lysimeter during 2019 (g), maize in 2020 (h), barley in 2020 (i) and soybean in 2021 (j).....	16
Figure 9: Smart field weighing lysimeter setting.....	17
Figure 10: Lysimeter setting during winter barley season 2020 and Soybean in 2021.....	18
Figure 11: Noise associated with various lysimetric distortion vs noise-filtered data.....	19
Figure 12: Lysimeter weight fluxes throughout the 2019 barley cropping season.....	20
Figure 13: Quantified hourly ET <sub>a</sub> during zero-irrigation days and irrigation amounts during the 2019 barley season.....	23
Figure 14: Actual evapotranspiration fluxes throughout the 2019-2020 maize season.....	24
Figure 15: Quantified hourly ET <sub>a</sub> during zero-irrigation days and irrigation amounts during the 2020 barley season.....	24
Figure 16: Quantified hourly ET <sub>a</sub> during zero-irrigation days and irrigation amounts during the 2021 Soybean season.....	25
Figure 17: The relationship between irrigation events and ET <sub>a</sub> .....	26
Figure 18: The ET <sub>a</sub> vs irrigation during winter barley season of 2020.....	26
Figure 19: The ET <sub>a</sub> vs irrigation during the soybean season in 2021.....	27
Figure 20: Temperature fluxes within the lysimeter.....	28
Figure 21: Water potential fluxes within the lysimeter.....	29
Figure 22: Soil electrical conductivity fluxes within the lysimeter.....	30
Figure 23: The influence of soil moisture (SWC) (b) in the variability of lysimetric mass changes (a).....	31
Figure 24: Cumulative soil moisture variability within the lysimeter at three different sensors and depths....	32
Figure 25: Cumulative soil moisture variability within the lysimeter at three different sensors and depths....	33

Figure 26: Relationship between measured irrigation depth from the ONSET rain gauge and depth measured by the smart weighing lysimeter in 2019; 2020 and 2021. ....	34
Figure 27: Locality map of the study area. ....	41
Figure 28: The visual setting of an automatic weather station in relation to the weather station within the field. ....	42
Figure 29: Model rankings throughout the seasons. ....	56
Figure 30: Selected models (Blue is the Penman-Monteith model, black is the Hargreaves and Allen model while orange is the Makkink model). ....	56
Figure 31: Satellite-based evapotranspiration coverage using MODIS data. ....	63
Figure 32: 10-Days WaPOR-FAO evapotranspiration products extracted at the lysimeter site in the period between September 2019 and August 2022. ....	63
Figure 33: Relationship between ETo and ETa using WaPOR products. ....	64
Figure 34: Extraction of MODIS ETa products using Google Earth Engine. ....	64
Figure 35: Annual evapotranspiration data for Vaalharts irrigation scheme using MODIS ETa product. ....	65
Figure 36: Different evapotranspiration products used in this study. ....	65
Figure 37: Relationship between ETo and ETa using meteorological functions and lysimeter data logger ...	66
Figure 38: NOAH ET evaluation at Tadcaster station for all seasons. ....	69
Figure 39: NOAH ET evaluation at SABBI station. ....	70
Figure 40: NOAH evaluation at Ganspan station. ....	70
Figure 41: WaPOR evaluation at Ganspan station. ....	71
Figure 42: WaPOR evaluation at Jan Kempdorp station. ....	71
Figure 43: WaPOR evaluation at SABBI station. ....	72
Figure 44: WaPOR evaluation at Tadcaster station. ....	72
Figure 45: Evaluation of MOD16 at Ganspan station. ....	73
Figure 46: Scatter plot of MOD16 vs in situ data at Jan Kempdorp. ....	73
Figure 47: Scatter plot of MOD16 vs measured ETa at SABBI. ....	74
Figure 48: Scatter plot of MOD16 vs measured ETa data at Tadcaster station. ....	74
Figure 49: The map depicting the study area distinct regions, (a) delineates the Vaalharts Irrigation Scheme, (b) identifies the experimental farm, and (c) indicates the study area's position in relation to various South African provinces. ....	81
Figure 50: Conceptual framework for the determination of crop evapotranspiration based on vegetation index. ....	83
Figure 51: Conceptual framework for the determination of crop evapotranspiration based on CWSI. ....	87
Figure 52: Shows the spatial distribution of ETa values estimated by SEBAL algorithm compared to the lysimeter method. ....	90
Figure 53: Shows the spatial distribution of ETa values estimated by SEBAL algorithm compared to the lysimeter method. ....	91

## LIST OF TABLES

Table 1: Cropping seasons and their associated crops during the experimental period. ....	21
Table 2: Radiation based models for reference evapotranspiration estimated estimation. ....	44
Table 3: Aerodynamic based models for reference evapotranspiration estimated estimation.....	45
Table 4: Combination models for reference evapotranspiration estimated estimation. ....	45
Table 5: Temperature based models for reference evapotranspiration estimated estimation. ....	46
Table 6: Statistical performance indicators used for validation of different ETo models.....	49
Table 7: Radiation-based models ranked according to metrics in the 2019 Barley Season.....	50
Table 8: Aerodynamic-based models ranked according to metrics in 2019 Barley Season.....	50
Table 9: Temperature based models ranked according to metrics in 2019 Barley Season.....	50
Table 10: Combination model metrics in 2019 Barley Season.....	51
Table 11: Radiation based ranked according to metrics in 2020 Maize Season. ....	51
Table 12: Aerodynamic based models ranked according to metrics in 2020 Maize Season.....	51
Table 13: Temperature based models ranked according to metrics in 2020 Maize Season. ....	51
Table 14: Combination model metrics in 2020 Maize Season. ....	52
Table 15: Radiation based ranked according to metrics in 2020 Barley Season.....	52
Table 16: Aerodynamic based models ranked according to metrics in 2020 Barley Season. ....	52
Table 17: Temperature based models ranked according to metrics in 2020 Barley Season.....	52
Table 18: Combination model metrics in 2020 Barley Season.....	53
Table 19: Radiation based models ranked according to metrics in 2021 Soybean Season. ....	53
Table 20: Aerodynamic-based models ranked according to metrics in 2021 Soybean Season. ....	53
Table 21: Temperature-based models ranked according to metrics in 2021 Soybean Season. ....	54
Table 22: Combination model metrics in 2021 Soybean Season.....	54
Table 23: Radiation based models ranking based on CP. ....	54
Table 24: Aerodynamic-based models ranking based on CP. ....	55
Table 25: Temperature based models ranking based on CP. ....	55
Table 26: Global ET products data acquisition.....	62
Table 27: Validation of NOAH pixels with ground data across four seasons .....	67
Table 28: Validation of WaPOR pixels with ground data across four seasons .....	67
Table 29: Validation of MOD16 pixels with ground data across four seasons .....	68
Table 30: Landsat 8 Satellite Data from Operational Land Imager (OLI) and Thermal Infrared Sensor (TIRS) .....	82
Table 31: Details on satellite images used in this study.....	88
Table 32: Showing the daily ETa (mm) from the lysimeter and estimated from four remote sensing models.	88

Table 33: Comparison of estimated and lysimeter ET values using statistical indicators..... 89

---

## ACRONYMS & ABBREVIATIONS

---

ADE	Alpha-derived emissivity
ARC-NRE	Agricultural Research Council-Natural Resources and Engineering
ASCE	American Society of Civil Engineers
ASTER	Advanced Spaceborne Thermal Emission and Reflection Radiometer
ATSR	Along Track Scanning Radiometer
AVHRR	Advanced Very-High-Resolution Radiometer
CWSI	Crop water stress index
DI	Deficit irrigation
ET <sub>a</sub>	Actual evapotranspiration
ET <sub>c</sub>	Crop evapotranspiration
ET <sub>o</sub>	Reference evapotranspiration
FAO	Food and Agriculture Organization
GDVI	Green Difference Vegetation Index
GEE	Google earth engine
GEO	Global Earth Observation
K <sub>c</sub>	Crop Coefficient
kg	Kilogram
km	Kilometres
LST	Land Surface Temperature
METRIC	Mapping evapotranspiration at high resolution with internalized calibration
mm	Millimetres
MODIS	Moderate Resolution Imaging Spectroradiometer
MOD16	MODIS Global Evapotranspiration Product
NDVI	Normalised Difference Vegetation Index
NDWI	Normalised Difference Water Index
NGA	National Groundwater Archive
NIR	Near Infrared
NOAA	National Oceanic and Atmospheric Administration
NOAH	Navigation with optical assistance for humanity
NWDACE	Northwest Department of Agriculture, Conservation and Environment
RS	Remote sensing
SABBI	South African Barley Breeding Institute
SAVI	Soil Adjusted Vegetation Index
SEBAL	Surface Energy Balance Algorithm for Land
SEBS	Surface Energy Balance System
SFL	Smart Field Lysimeter
SM	Soil moisture
SWC	Soil water content
SWIR	Short Wave Infrared
TIR	Thermal Infrared
TISIs	Temperature-Independent Spectral Indices
TOA	Top-of-atmosphere (Radiance or Reflectance)

TVDI	Temperature Vegetation Dryness Index
TVTA	Temperature-Vegetation Triangle Algorithm
UAV	Unmanned Aerial Vehicle
VI	Vegetation index
WaPOR	Water Productivity through Open access of Remotely sensed derived data
WP	Water potential

## GLOSSARY OF TERMS

---

**Actual evapotranspiration (ET<sub>a</sub>)** is the combined process by which water is transferred from the Earth's surface to the atmosphere through evaporation from soil and plant surfaces, as well as transpiration from plants. It represents the total amount of water vapour that is physically removed from a specific area over a given time, typically expressed in units of depth (e.g. millimetres or inches).

**Aridity** is defined as any physical limitation of water in an area usually emphasized as situations where ET exceeds the total amounts of precipitation.

**Crop Water Requirements** is the understanding of water needs for different crops at various growth stages. This involves considering factors such as evapotranspiration rates, soil characteristics, crop type, and local climate conditions.

**Crop water stress index** is an indicator used in agriculture to assess the water stress levels experienced by crops which is calculated based on the temperature differential between the crop canopy and the surrounding air, considering factors such as relative humidity, wind speed, and solar radiation.

**Evapotranspiration (ET)** is defined as a combination term that defines the loss of water from vegetation leaves as transpiration and from soil medium as soil water evaporation.

**Heat (thermal) capacity** is the amount of heat to be supplied to a given mass of a material to produce a unit change in its temperature.

**Irrigation Scheduling** is the timing and determination of the amount of water application to match crop water demand.

**Irrigation water management** defines the efficient and effective use of water for agricultural purposes through planning, implementation, and optimization of irrigation systems. It encompasses various practices aimed at ensuring that water resources are used sustainably to meet crop water requirements while minimizing waste and environmental impacts.

**MOD16** is a global evapotranspiration product that provides ET on an 8-day period at a resolution of 500 m.

**Reference evapotranspiration (ET<sub>o</sub>)** is the rate at which water would evaporate from a hypothetical reference surface under standardized conditions. It represents the evaporative demand of the atmosphere when there are no limitations on water availability, such as soil moisture or vegetation cover. ET<sub>o</sub> is typically calculated based on meteorological parameters such as temperature, humidity, wind speed, and solar radiation.

**Remote sensing** is the process of collecting and interpreting data about the Earth's surface or atmosphere from a distance using sensors mounted on aircraft or satellite platforms.

**Smart field weighing lysimeter** is a ground-based instrument that directly measures the water balance components necessary to determine the actual evapotranspiration.

**Thermal conductivity** is the ability of material to transfer (conduct) heat.

**Thermal diffusivity** is the rate of heat transfer of a material from the hot spot to the cold spot.

**Thermal resistivity** is a heat property and a measurement of a temperature difference by which an object or material resists a heat flow.

**WaPOR** is a global evapotranspiration product that provides ET estimates on a decadal period at varying resolutions (250; 100 and 30 m). South Africa is covered by the 250 m resolution.

**Water balance (WB)** refers to the quantitative analysis of the distribution and movement of water within a defined system, such as a watershed, basin, or hydrological cycle. It involves accounting for the inputs, outputs, and storage of water within the system over a specific period, typically daily or seasonally.

**Water scarcity** is defined as a natural condition where the demand for water in a rea surpasses the actual availability of water to meet the demands.

# CHAPTER 1: BACKGROUND

## 1.1 INTRODUCTION

Water scarcity continues to be a continuous global challenge threatening the livelihoods of humans and the sustainability of the natural environment as a system. Over the past decades, more efforts have been channelled towards the objective of ensuring sustainable and efficient access to clean and adequate water to support the steadily increasing global population (Roundy, 1985; Van Vliet et al., 2021). Arid areas which are dominated by extremely high temperatures in summer and low temperatures during winter seasons, are the most threatened environments with very limited precipitation rates and high ET fluxes (Raziei et al., 2011). Consequently, agricultural activities in such areas are highly affected, resulting in low crop yields, low grazing and browsing productivity due to reduced biomass and plant density (Costa and Gianquinto, 2002; Lohman et al., 2020). In trying to achieve efficient water use, knowledge in the water-energy balance is critical in accounting for the water budget. With that being of interest ET has gained much attention in accounting for water losses from various environments ( Yang et al., 2000; Van Halsema and Vincent, 2012; Cheng et al., 2022; Groh et al., 2019). ET quantifications are crucial in understanding the role played by temperature and sunlight hours in water loss from soil through evaporation and from vegetation through transpiration post known precipitation or irrigation amount (Thomas, 2000; Wang et al., 2012). Understanding these roles aid in water management and efficient resource management and productivity. The measurement and quantification of ET is not an easy process due to the different parameters required to estimate ET components on the hydrological cycle (Rodell et al., 2004; Zhao et al., 2013). Various researchers have measured and estimated ET using different possible direct and indirect ways to quantify water losses, such as the water balance, energy balance, Bowen ratio, Lysimeters, Eddy covariance stations, weather stations; satellite-based remote sensing products and recent satellite products at different scales ( Yang et al., 2000; Buttar et al., 2018; Denager et al., 2020; Jiang et al., 2020; Niu et al., 2020). The eddy covariance and the lysimeters are the most common direct measurement methods and the lysimeters are known to have the highest accuracies in estimating the actual ET fluxes (Sobrino et al., 2021). Using direct ground-based methods such as meteorological data, lysimeters and eddy covariance can provide highly reliable estimations for evapotranspiration. However, they cannot be used to represent regional or global scales because they provide point information rather than spatially distributed information ( Kumar et al., 2021). Due to landscape diversity, hydrological and soil heterogeneity, these methods are unsuitable for representing larger areas away from their location ( Walker et al., 2019; Cuxart and Boone, 2020). The fact that they produce estimates with high precision and accuracy, they are crucial to calibrate and validate other indirect methods (Bardsley and Campbell, 2000; Jarchowet al., 2022). Remotely sensed satellite data of different resolutions have been applied to solve the issue of spatial evapotranspiration extent at no cost than it would cost to spatially distributed ground-based devices and stations (Elnmer et al., 2019; Chen and Liu, 2020; Ghaderi et al., 2020; Chen et al., 2021). Although remotely sensed ET data exists, there is a need to have an improved model that integrates ground-based ET and satellite derived ET products at small time intervals because satellites sometimes have saturation problems when retrieving land surface energy components (Corbari et al., 2020). As the water scarcity issue becomes a daily concern, there is a need to establish baseline data and models to quantify ET, especially for arid regions more affected by water shortages (Anapalli et al., 2019). Various studies have addressed the quantification of ET using coarse resolution products to have a global coverage (Ma et al., 2005; Zhao et al., 2015; Sun et al., 2020). However, improved products over certain regions with better resolutions are required for local or regional water use planning and management due to data requirements. This includes the integration of satellite coarse and high-resolution data with

ground-based ET products. Developing better resolution ET products for arid regions, which are potential food production zones, will aid in water management strategies and policy developments. According to the study undertaken by various scientists under the auspices of the committee on irrigation requirements of the American Society of Civil Engineers (ASCE), focusing on 20 Methods which were validated using lysimeters, the standard panman monteith method was found to overestimate the ETo (Doorenbos and Pruitt, 1981). They suggested that local calibrations are required to yield sound results. They further pointed out that the use of the method has problems in arid areas where the aerodynamic term is low. They also pointed out that ET estimations using the Pan method have problems for open water bodies.

The use of weighing lysimeters in South Africa was conducted by Hutson (1980) in Roodeplaat to investigate crop evapotranspiration. They used three lysimeters which had a square design to fit in row cropping. Their daily evapotranspiration ranged between 0 and 120 mm with high evapotranspiration being observed during rain and irrigation days. Their continuous investigation for two years led them to conclude that lysimeters are accurate and reliable devices for evapotranspiration estimation. They further suggested improvements in the lysimeter systems to increase understanding of the interaction between water, soil, crops and the atmosphere.

Berliner and Oosterhuis (1987) used two field plots set under different conditions to install lysimeters to test the lysimeter's representativeness in crop water stress determination; one lysimeter was well irrigated while the other was left in dry condition. They planted winter wheat in each lysimeter and monitored ET, soil water content and canopy temperature to determine water stress conditions. They monitored crop water stress by assessing the leaf water potential in each lysimeter. Changes in evapotranspiration were observed with changes in soil water content with higher evapotranspiration being observed in dryer conditions. They concluded that crop water stress could be determined well by using lysimeters in plots representing the field conditions. They mentioned that conclusions on the relationship between canopy conditions and soil conditions influence water stress could not be made. Gebler et al. (2015) investigated the use of lysimeters in actual evapotranspiration (ETa) and precipitation which they compared with Eddy Covariance and tipping bucket in Germany Rollesbroich. Six weighing lysimeters were used to estimate evapotranspiration. The Eddy Covariance and Penman-Monteith methods were used to estimate the actual and the reference evapotranspiration. They reported that comparisons between eddy covariance and lysimeters are limited in the literature. They obtained their hourly evapotranspiration ranging between 0 and 0.5 mm for the lysimeters, eddy covariance and the Penman-Monteith method. They concluded that the evaluation of the two methods showed good agreement with a small difference.

Ratshiedana (2022) investigated the utility of unmanned aerial vehicles and smart field weighing lysimeters in estimating the barley crop water use using surface energy balance algorithms for irrigation scheduling. His studies found that lysimeters offer more accurate crop water use and irrigation scheduling because of their temporal resolution, which is every minute, including at night. When the lysimeter weights dropped, the soil moisture content within the lysimeters and the entire field were also dropping. He also noticed that ETa increases from sunrise and reaches peak at mid-day and becomes very small after sunset.



**Figure 1: South African arid region map.**

## **1.2 EVAPOTRANSPIRATION ESTIMATION USING REMOTE SENSING**

### **1.2.1 Background**

#### *1.2.1.1 Surface Energy Balance Algorithm for Land (SEBAL)*

The Surface Energy Balance Algorithm for Land (SEBAL) predicts hydrological features such as ET and water deficit using energy balance principles; Professor Bastiaanssen developed the model in the late 1990s (Bastiaanssen et al., 1999). The model has been validated under a variety of conditions for various locations ( Bastiaanssen, 2000; Allen et al., 2003; Santos et al., 2010; Ruhoff et al., 2012; Singh et al., 2013; Sun et al., 2020). To estimate ET per pixel in each area, the SEBAL model employs a set of mathematical equations and meteorological data, including atmospheric corrections, surface albedo, net radiation, surface temperature, vegetation index, and heat flux.

#### *1.2.1.2 Atmosphere Land Exchange Inverse (ALEXI)*

The Atmosphere-Land Exchange Inverse (ALEXI) model links geostationary satellite time-differential LST observations to the time-integrated energy balance within the surface-atmospheric boundary layer system (Anderson et al., 2018). ALEXI relies on instantaneous air or surface temperature input data as little as possible, resulting in a relatively robust flux determination at the coarse geostationary pixel scale (Anderson et al., 2018). ALEXI flux fields can be spatially disaggregated for finer scale ET applications using higher resolution LST data from polar orbiting systems.

### 1.2.1.3 Mapping Evapotranspiration at high Resolution with Internalized Calibration (METRIC)

The University of Idaho created the METRIC model, a well-known energy balance model used to calculate ET (Morse et al., 2004). The model uses an hourly ground reference evapotranspiration procedure for self-calibration (Gowda et al., 2008). The near-surface temperature gradient is used by the SEBAL model, on which the METRIC model is based. At the same time, it does not consider sensible heat flux to be zero, does not calculate aerodynamic surface temperature, and chooses the cold pixel in the agricultural setting rather than employing biophysical considerations. Evapotranspiration is calculated using a typical Penman-Monteith equation.

### 1.2.1.4 Temperature-Vegetation Triangle Algorithm (TVTA)

The triangular model is built around two components: the Normalized Vegetation Index (NDVI) and the radiant surface temperature ( $T_{ir}$ ), from which other parameters for calculating evapotranspiration fractions are derived (Carlson, 2007). The NDVI is divided into two parts: NDVI<sub>v</sub>, which represents the portion of an image covered by dense vegetation, and NDVI<sub>o</sub>, which represents bare soil surfaces. Surface radiant temperature is scaled from 0 to 1, with temperatures close to zero representing wet areas or densely vegetated areas and temperatures close to one representing dry surfaces covered only with bare soil ( Yang et al., 2008; Minacapilli et al., 2016; Fuzzo and Rocha, 2018).

## 1.3 MOTIVATION

The South African food production system has rapidly grown throughout the country to meet governmental food security goals and market demands. Farmers are often bound to supply more than the crop evapotranspiration (ET<sub>c</sub>) empirically under irrigated systems; these amounts are sometimes inappropriate. The sustained deficit irrigation (DI) methods can be proposed as a helpful practice to apply Irrigation amount at the cumulative-daily crop water needs. However, a rational way to keep the crop performance as close as possible to its maximum potential ensure the highest potential yield. The estimation of the ET<sub>c</sub> is usually either calculated from the reference evapotranspiration (ET<sub>o</sub>) retrieved from the climatic data and then multiplied by the crop coefficients (K<sub>c</sub>) to get the ET<sub>c</sub>. Another method is a reduced percentage of ET<sub>c</sub> is applied throughout the irrigation season (Fernández et al., 2010). Irrigation scheduling is often based on soil water balance, in which ET is estimated using ET<sub>o</sub> and K<sub>c</sub> values, according to the procedure proposed by FAO (Allen et al., 1998). There are some techniques to determine water consumption at the plant level, such as weighing lysimeter; the method is very accurate but high-cost, and a limited number of lysimeters can be installed. The new development in remote sensing data acquisition and analysis provides advanced techniques for monitoring ET<sub>a</sub> from the single plant level to the basins and national scales. Using these advanced technologies in determining ET<sub>a</sub> is of great importance for producers and decision-makers. The crop growth has been monitored effectively using optical sensors working at red and infrared spectral range from various sensing platforms ranging from satellite-based sensors to ground. On the other hand, the spectral range at the long-wave infrared, and thermal infrared avail new dimension in monitoring the water balance in agricultural and non-agricultural fields using the energy partitioning approaches. The basic concept of energy partitioning is to quantify the latent heat flux necessary for water evaporation from the soil surface and plant leaves, ET distribution. The ET is a significant component of the field water budget. It can calculate the crop water requirements, irrigation water depth/frequency, evaluate water stress level, and stem and quantify the total field water consumption. The distributed water consumption can be extrapolated to the field level using the crop type maps to quantify the water consumption of each crop type at a particular basin. The water consumption maps can be used effectively to evaluate the water allocation at the basin level per crop type and field.

Recently, various remotely sensed ETa products have been developed using satellite data with various resolutions. The development of these products can range from the simplified method used on the thermal infrared data to the much more complex model that integrates the vegetation indices and ground data with the remote sensing thermal images. In general, four major development schemes were adopted: 1) direct empirical method, 2) residual method of the energy balance, 3) deterministic method, and 4) vegetation indices method. These methods can use TIR data from satellites such as Landsat 8 (30 m), MODIS (1 km), and Visible Infrared Imaging Radiometer Suite (VIIRS). The critical question is to what extent we can trust these products? Previous research works have compared the remote sensing estimation of the ETa with relatively low-quality ground data or estimated ET using climatic data. In this project, different ET products such as MODIS, NOAA, FAO-WaPOR and calculated products using Landsat 8 imageries will be calibrated and validated using smart lysimeter ETa measurements installed under an arid environment.

### 1.4 RESEARCH APPROACH

The research approach can be summarised in the following conceptual diagram (Figure 2).

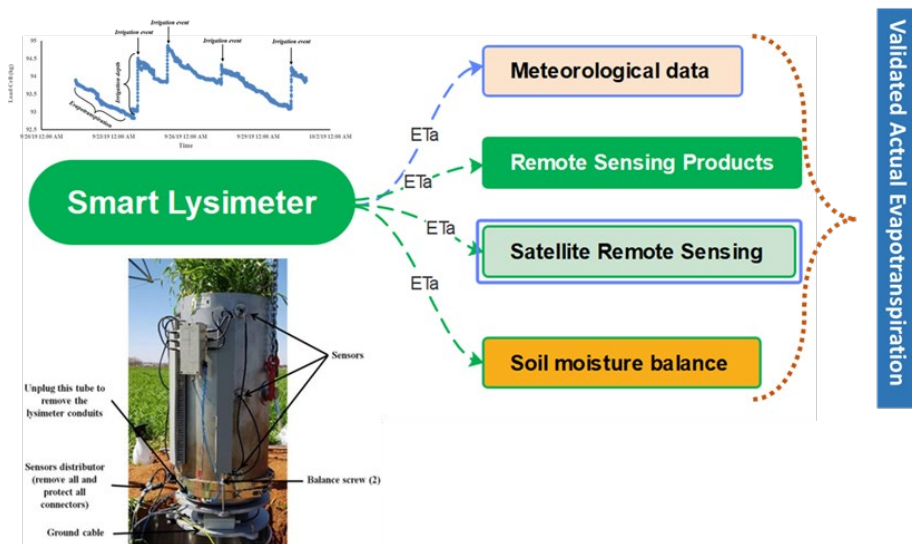


**Figure 2: Conceptual framework for the research approach of ET-Sensing.**

The ground monitoring techniques can be used as a validation source of information while satellite-based monitoring can be utilised as a continuous and low-cost source of information. The smart lysimeter can measure ET accurately at the local scale. These measurements can be used to develop a large-scale validation proxy using meteorological information. The combination of the lysimeter measurements and soil moisture dynamic at the local scale will be used to develop relationships that consider the scarcity of the data in the arid land environment.

### 1.5 REMOTE SENSING APPLICATION

Every object emits energy proportionally to the fourth power of its surface temperature (Stefan-Boltzmann law). The amount of energy emitted depends on the wavelength, the wavelength where the emission is maximum is greater as the temperature decreases. For most of the land surface vegetation

(between -20 and 50°C), this maximum corresponds to a wavelength near 10  $\mu\text{m}$ . Thermal infrared remote sensing has been proven of great potential in many environmental studies. Thermal infrared has been utilised in urban microclimate (Santamouris et al., 2001; Ngie et al., 2014; Abutaleb et al., 2015), water quality monitoring, vegetation stress (Stoll et al., 2008; Labbé et al., 2012; Sobrino et al., 2021) fire detections and sea surface temperature (Franc and Cracknell, 1994).

Attempts to extract the land surface temperature (LST) from remote sensing data have been undertaken for several decades (Zhang et al., 2006). Remote sensing data supply a practicable approach for the investigation of LST on wide spatial and temporal scales. Satellite thermal infrared (TIR) sensors measure top of the atmosphere (TOA) radiances, from which brightness temperatures can be derived based on Planck's law (Dash et al., 2002). The TOA radiance is the mixing result of three fractions of energy, earth's surface emitted radiance, atmosphere upwelling radiance, and sky down welling radiance. Top of atmosphere and land surface brightness temperature differences generally range from 1 Kelvin to 5 Kelvin in the 10-12  $\mu\text{m}$  spectral regions, and such differences depend on the atmospheric conditions (Prata et al., 1995). Therefore, atmospheric effects, including absorption, upward emission, and downward irradiance reflected from the surface, must be corrected before land surface brightness temperature is obtained (Franc and Cracknell, 1994). These brightness temperature should be further corrected with ground emissivity values prior to the computation of LST to account for the roughness properties of the land surface, the amount and nature of vegetation cover, and the thermal properties and moisture content of the soil (Friedl, 2002).

Methods to retrieve LST are depending on how the sensor's thermal bands were designed. one can classify satellites according to the number of thermal bands to a) single thermal band such as Landsat satellites, b) two thermal bands such as NOAA, AVHRR, ASTR (Along-track scanning radiometer) and GOES (Geostationary operational environmental satellite) satellites, c) multiple thermal channels such as ASTER and MODIS satellites. The split-window algorithms have been widely used for estimating LST from two thermal bands in the 10.5-12.5  $\mu\text{m}$  region with given surface emissivity. Many split-window formulas are published in the literature such as those implemented by (Price, 1984; Sobrino et al., 1994; Francois and Ottlé, 1996).

For multiple thermal band satellites, other formulas were developed to retrieve more accurate LST and emissivity from the satellite image. Among these formulas are: the day/night algorithm which is used for MODIS (Wan et al., 2002), the reference channel method (Lyon *et al.*, 1965; Kahle *et al.*, 1980) Alpha-derived emissivity (ADE) method (Kealy, 1990; Hook et al., 1992; Kealy and Hook, 1993) which is known as alpha-residual technique, Temperature-Independent Spectral Indices (TISIs) (Becker and Li, 1990; Watson, 1992) Optimisation Algorithm and the ASTER Algorithm (Realmuto, 1990; Gillespie et al., 1998; Li et al., 1999; Liang et al., 2002).

There are three basic modules in the ASTER algorithm 1) normalised emissivity method, 2) ratio module and 3) maximum-minimum difference module. The main difference between the three modules is the way to estimate the ground emissivity from the ASTER image. Numerical simulations show that ASTER algorithm can estimate LST to within error of 1.5 K and emissivity to within 0.015 (Gillespie et al., 1998). However, Dash et al. (2002) reported that algorithm requires an accurate atmospheric correction. Running ASTER algorithm on airborne multispectral thermal data applied this algorithm to TMS (Thermal Infrared Multispectral Scanner) resulted in LST with typical errors of 3 K (Schmugge et al., 1998). However, for satellites with a single thermal band, such as Landsat TM and ETM+, obtaining LST is more difficult. In addition to an accurate radiative transfer model and some knowledge of the atmospheric profile, emissivity information is also required (Qin et al., 2001).

The most common methods adapted for retrieving LST from the Landsat TM and ETM+ thermal data are: 1) the radiative transfer equation, 2) mono-window algorithm, and 3) Jiménez-Muñoz and Soprano's algorithm (Sobrino et al., 2004). The first method requires in situ measurements of atmospheric data simultaneously with the satellite pass which in turn may be constrain for using that method. Meanwhile, the second and the third one could be used in the absence of these data. The second and the third methods use NDVI for calculating ground emissivity.

## 1.6 APPLIED ESTIMATION METHODOLOGY

Remotely sensed data was used to calculated  $ET_a$  under different seasons and crop types. The satellite data will be used to classify crop plant cover. Normalised Difference Vegetation Index (NDVI) and Land Surface Temperature (LST) will be extracted from Sentinel-2, Landsat, NOAA/AVHRR and MODIS satellite data. Crop Water Stress Index (CWSI) uses both surface temperature compared to air temperature and vegetation index to estimate the relative water status. According to the Penman-Montieth method,  $ET_o$  will be estimated from meteorological data. The CWSI and  $ET_c$  will be used to estimate  $ET_a$ . Details of the methodology will be shown in the next steps. Jackson et al. (1981) showed that there is a unique mathematical relationship between CWSI and evapotranspiration from the vegetation surface as follows:

$$ET_a = (1-CWSI) * ET_c$$

Where  $ET_a$  is actual evapotranspiration,  $ET_c$  is potential crop evapotranspiration and CWSI is Crop Water Stress Index. CWSI approach was preceded and developed by Jackson et al. (1981). They proposed the empirical and theoretical methods to estimate CWSI as follows:

$$CWSI = (dT - dT_m)/(dT_x - dT_m)$$

Where:  $dT$  is the difference between measured surface and air temperature,  $dT_m$  is the difference between minimum surface and air temperature and  $dT_x$  is the difference between maximum surface and air temperature. Since all variables have the same units, CWSI is a dimensionless ratio. The lower limit of  $dT$  occurs under non-water-stressed conditions when ET is only limited by atmospheric demand. On the other hand, the upper limit of  $dT$  is reached under non-transpiring conditions when ET is stopped due to the lack of water. The values of CWSI are ranged between zero and one, where zero indicates no stress and the value of one indicates maximum stress.

## 1.7 STUDY AREA DESCRIPTION

The study area was the Vaalharts irrigation scheme which is located on the confluence of the Northern cape and Northwest provinces of South Africa. Within the Vaalharts scheme a selected experimental farm was located around the coordinates: 24.739827° East and -27.720237° South. The Vaalharts irrigation is the biggest irrigation scheme in South Africa receiving water from the Bloemhof dam which is supplemented by the Vaal and the Harts rivers reaching the scheme through gravity canals (Figure 3). The scheme was developed to alleviate hunger and starvation in the area as well as for job creation for the surrounding communities back in 1938. The area is the biggest producer of pecans while a variety of crops are also grown. Water transfers remains the key source of irrigation water while challenges with salinity problems prevents the use of groundwater for irrigation purposes. The scheme is dominated by pivot irrigation systems while other forms of irrigation which includes drip irrigation, flood irrigation and sprinklers amongst others. The climate in Hartswater is characterised by long hot

summer days and freezing winter days, with most of the rain occurring during the summer seasons between 1 November and 28 February (Seshoka *et al.*, 2004). Recordings of the average annual rainfall in the study area from 1975 to date have been 35 mm, while the minimum and maximum rainfall have been 13.5 mm and 77 mm, respectively. The mean maximum temperatures have been recorded at 31.8°C and mean minimum temperatures at 7°C during the 1975 to 2019 period (Ratshiedana, 2022). Since 1975, there has been an increase in gradient for the mean annual maximum temperatures in summer and a decline in mean yearly minimum temperatures (Ratshiedana, 2022). The decrease in trends explains the shift in climate variability, which has a greater influence on water resources when temperatures become extremely high or too low with less precipitation. The study area is in an arid environment (Figure 4).

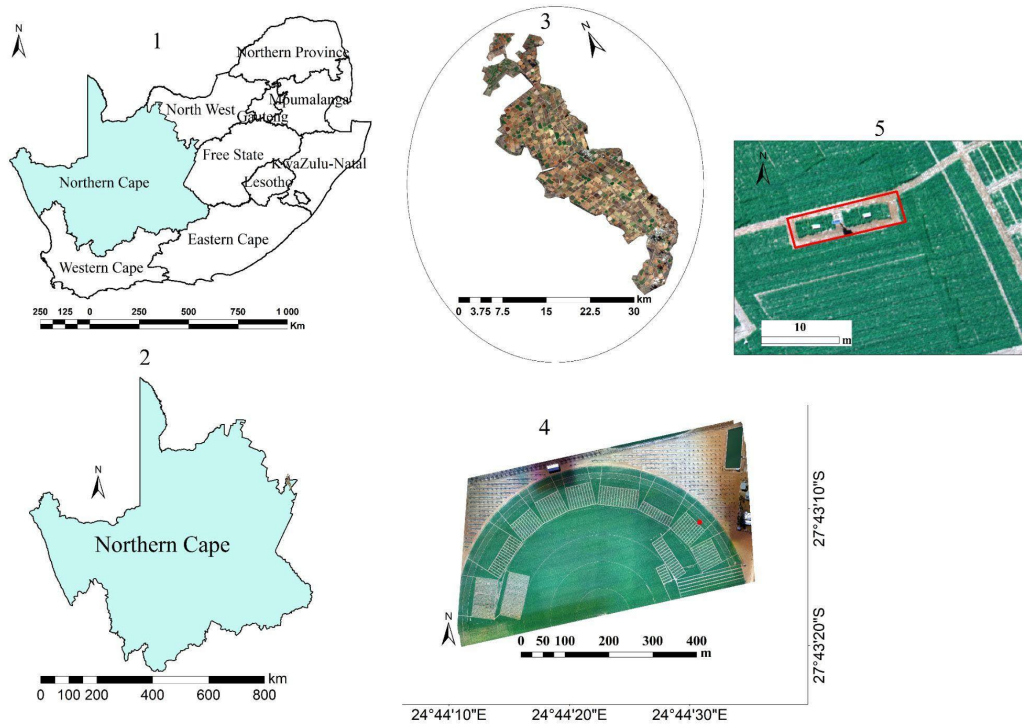


**Figure 3: Installation area of the smart lysimeter system.**

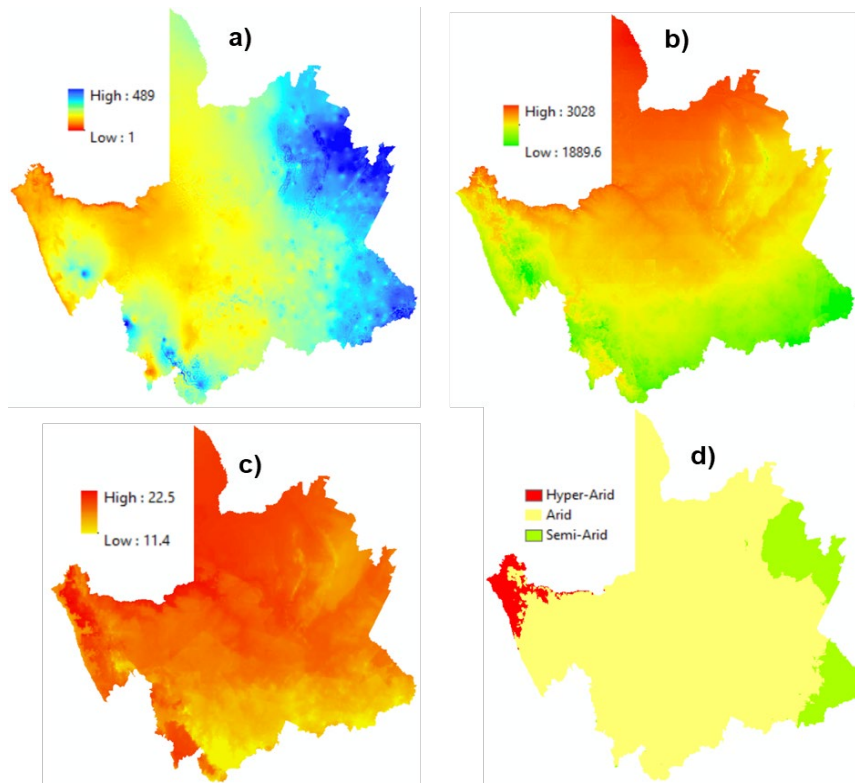


**Figure 4: Climate characteristics of the study site; (a) annual rainfall, (b) potential evapotranspiration, (c) mean temperature, (d) aridity conditions.**

## CHAPTER 2: SMART FIELD LYSIMETER FOR ACTUAL EVAPOTRANSPIRATION MEASUREMENT

### 2.1 INTRODUCTION

Water use monitoring is one of the major challenges faced globally affecting the availability, control, and distribution of natural water resources amongst various water reliant users. The lack of monitoring techniques hinders the determination of acceptable ways to reduce the overuse and misuse of the available limited water resources. Agriculture in most countries uses more water than other industries through irrigation practices which are not guided by the actual crop water demands. The combination of soil water evaporation and transpiration termed evapotranspiration (ET) which is the principal component of the water cycle plays a crucial role in scheduling and designing irrigation approaches (Van Vliet et al., 2021). Several researchers have made efforts to quantify ET in irrigated agricultural environments with the aim of reducing water use in the agricultural environments to improve water scarcity problems (Tanner, 1967; Hargreaves and Samani, 1982; Pereira et al., 2020). The water scarcity challenges are exacerbated by the rapid increase of populations which puts more pressure on water resources through increased water demand and food demands triggering the agricultural sector to use more water in the context of changing climate. In agricultural practices, the most important component of the water budget is crop evapotranspiration (ETc) or the actual crop evapotranspiration (ETa) which define the actual amount of water lost after precipitation or irrigation events (Allen, 1998). Crop evapotranspiration plays a crucial role in determining crop water requirements, crop coefficients and scheduling of irrigation events. After every irrigation or precipitation event in arid environments more water is lost due to evapotranspiration while a little amount goes for deep percolation (Wang et al., 2012).

Lysimeters are mainly classified in two class types being: weighing lysimeters and non-weighing lysimeters (Shahrajabian and Soleymani, 2017). Weighing lysimeters are built with several sensors and weight load cells providing weight changes data records continuously (Sagar et al., 2022) on the other hand; non-weighing lysimeters do not contain any load cells or sensors but the water balance components are measuring using volumetrically approaches which can only be done on non-continuous intervals. Weighing lysimeters due to their capabilities of offering continuous weight changes depending on soil moisture changes can provide information on crop water use from an interval of minutes, hours, and daily recordings (Hoffman, 2014). Weighing lysimeters have record of use over many years to quantify crop water use or evapotranspiration fluxes and for computations of crop coefficients for different crops (Tolk and Evett, 2009; Ávila-Dávila et al., 2021). As a function of changes in weight, weighing lysimeters provide measurements which are direct and accurate for the water amount lost as evaporation and transpired by vegetated surfaces (Johnson et al., 2005).

Smart Field Weighing Lysimeters (SFL-600, developed by METER Group) which are the focus devices in this study are point based measurement devices which provided advanced crop water use or evapotranspiration in a real-time and actionable time frame for human interference in water use applications which have high temporal measurement resolution of one minute significant for monitoring crop water use post each irrigation event (Doležal et al., 2018). Figure 5 depicts a general view of the field weighing lysimeter. The benefit of using these real-time water use monitoring and informing devices is that they reduce the likelihood of crop loss and poor yields. The availability of real-time lysimetric crop water use measurement at the field level enables prompt mediation throughout the growing season, resulting in better crop and water productivity output (Kim et al., 2011; Pereira et al., 2015). Smart Field Weighing Lysimeters are more intelligent lysimeters compared to others (Figure 5).

These systems are the only systems which consist of a bi-directional pump that maintains the true field conditions automatically representing the surrounding field environment within the lysimeter. Changes in storage or lysimeter weight were recorded every minute. For every 10 minutes soil moisture content in the lysimeters was measured and sent to the central lysimetric logger control system, at any case when the soil contained within the lysimeter was becoming more drier as compared to the surrounding field conditions, the water in the drainage container was automatically pumped back into the lysimeter system to maintain homogeneity between the field conditions and the lysimeter system. Contrary, when the soil contained within the lysimeter systems becomes very wet compared to the surrounding field conditions, the system pump drains the water out of the lysimeter until there was a balance in moisture between the field conditions and the lysimeter system, always maintaining the actual true field conditions. Compared to other methods which have known inaccuracies, the Smart Field Weighing Lysimeters are the only devices that can measure with high accuracy the field-level actual evapotranspiration fluxes (Allen et al., 1998). The Smart Field Weighing Lysimeter makes use of very sensitive load cells when weighing the amount of water that comes into the system as precipitation or irrigation as well as the amount of water that leaves the lysimetric system as soil water evaporation or plant transpiration.

Weighing lysimeters have a long history of use in accurately quantifying and validating ET fluxes, as well as computing crop coefficients for different crops (Green, 1974; Ávila-Dávila et al., 2021; Sagar et al., 2022). These lysimeters offer direct and accurate measurements of water loss through evaporation and transpiration from vegetated surfaces (Wang et al., 2021). Over the years, lysimeters of various designs, sizes, shapes, and measurement systems have been constructed (Mukammal *et al.*, 1971; Payero and Irmak, 2008). However, older non-weighing lysimeters suffered from issues such as manual sampling of drainage components, which introduced human errors in sampling, measurement, and data recording (Shahrajabian and Soleymani, 2017).

While lysimeters have been used extensively for hydrological research and crop water use investigations in the past (Kovacs, 1976; Hutson, 1980), recent advancements in lysimeter technology have brought renewed attention to their utility worldwide. Studies in the United States (Hashem et al., 2020), China (Liu et al., 2020), Iran (Valipour et al., 2020), Japan (Takahashi et al., 2022), Nigeria (Chiwetalu et al., 2022), and elsewhere have demonstrated their effectiveness. However, the use of lysimeters in South Africa remains relatively limited, making direct ET measurements one of the scarcest data gaps in hydrological research (Green, 1974; Ratshiedana, 2022). Despite this scarcity, such data is crucial for understanding water dynamics, irrigation scheduling, water allocation, and the development of water management monitoring algorithms applied to various ET-related platforms, ranging from meteorological stations to satellite geospatial approaches.

Considering the critical importance of water management in agriculture, this study aimed at exploring the potential of accurate  $ET_a$  measurement and monitoring by using the latest generation smart field weighing lysimeters (Fig. 5) for directly measuring the rate of barley, maize, and soybean crop water consumption in between irrigation events. Furthermore, the study targeted to showcase the principle of operation behind the smart field weighing lysimeter, detailing how its precision weighing system accurately quantifies crop water use and water loss from the crop-soil system. Additionally, the study will demonstrate the integration of cutting-edge sensors and data acquisition systems, which enable real-time measurements of the water balance components, further enhancing the device's utility in understanding crop response to fluctuating water inputs and climate conditions. The findings of this study aim at facilitating accurate irrigation scheduling and improving water-use efficiency in agricultural practices, particularly in the Vaalharts irrigation scheme located in arid regions facing water scarcity and drastic climatic challenges.

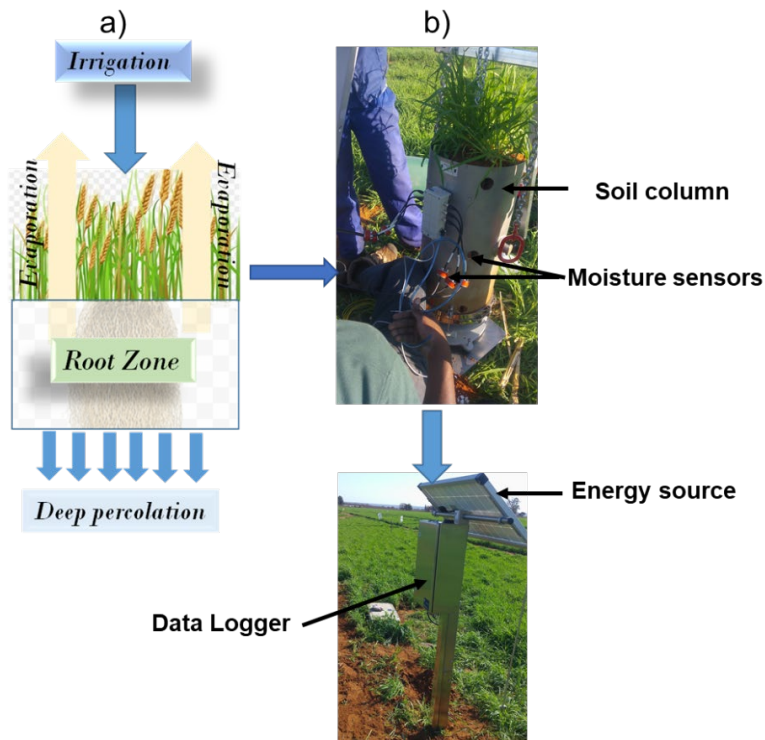


**Figure 5: A view of a Smart lysimeter system, a) Schematic view of weighing lysimeter, b) internal view and display of the lysimeter components.**

### 2.1.1 Lysimeter installation area

The study area for this experimental research is the South African Barley Breeding Institute (SABBI) experimental farm number 5JII, situated in the Northern Cape province of South Africa, approximately around 24°44,21.47"E and 27°43,16.02"S (Figure 6). The farm covers a total area of 18 hectares and is located at an elevation of 1081 metres above sea level. The farm featured a uniformly even and level surface, exhibiting a remarkable absence of any variations in terrain. This consistent topography provided an ideal setting for modern farming machinery and lysimeter setting to be representative of the field. The experimental farm is part of the Vaalharts Irrigation Scheme, which is the largest irrigation scheme in South Africa. The climate in the study area is characterized by long hot summer days and freezing winter days, with the majority of rainfall occurring between 1<sup>st</sup> November and 28<sup>th</sup> February during the summer season (Seshoka et al., 2004). The average annual rainfall in the area from 1975 to the present has been recorded as 35 mm, with minimum and maximum rainfall of 13.5 mm and 77 mm, respectively (ARC, 2023). The mean maximum temperatures have been recorded at 31.8°C and mean minimum temperatures at 7°C during the 1975 to 2019 period (ARC, 2023). Sandy soils dominate the study area with high silica content. Hough and Rudolph (2003) described the soil as the Kalahari sands, the sandy soil in Hartswater is susceptible to salinization and waterlogging conditions, due to a poor drainage system (Maisela, 2007). As a result, a drainage network has been constructed in open canals, and subsurface drainage pipes have been installed to control water-logging conditions (Verwey and Vermeulen, 2011). According to Streutker (1977), the study area consists of two soils: Sunbury and Hutton. Irrigation on sandy soil replenishes soil water content to sustain the healthy growth of plants and crops. Consequently, the rate at which water infiltrates this type of soil determines the frequency of irrigation which can be high; clay soil is only found at one-meter depth to two metres, which is far

below the root zones of many crops (Verwey and Vermeulen, 2011). Various forms of irrigation exist within the Vaalharts irrigation scheme, including surface flow irrigation using water from the canals, primarily used for plant irrigation, pivot irrigation systems, drip irrigation, bubblers, and sprinklers. Pivot irrigation systems are dominant in the area (Annandale et al., 2011).

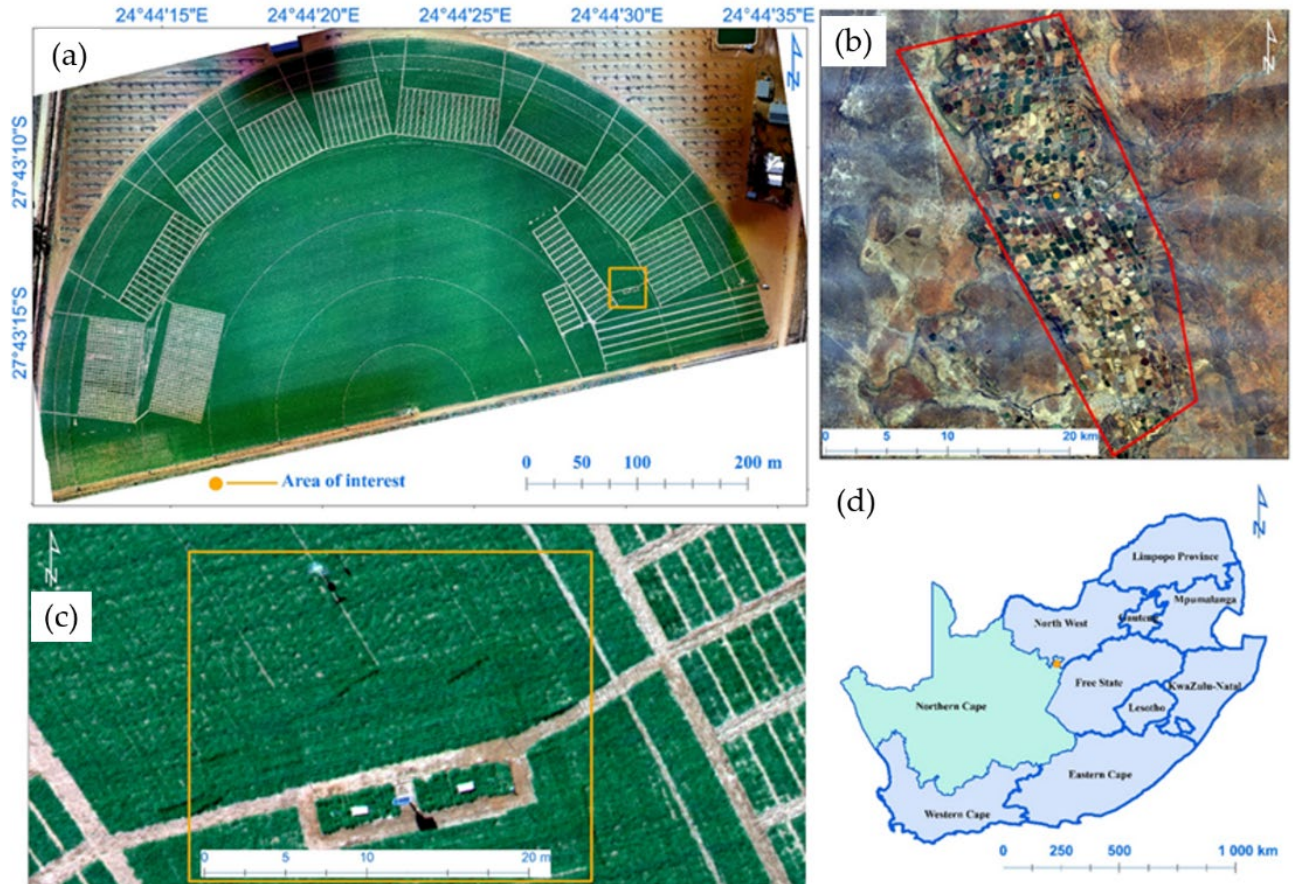


**Figure 6: Locality map of the study area, where (a) is the experimental farm, (b) is the Vaalharts irrigation scheme, (c) is the lysimeter area and (d) shows the location of the study area within South Africa and its provinces.**

### 2.1.2 Lysimeter components and installation

The smart lysimeter is a system that directly measures the water balance components through a set of components that are interconnected to measure various components and store the measured data. This section provides an overview of the lysimeter components and the lysimeter installation process.

Two smart-field weighing lysimeters (SFL-600) were installed within an 18-hectare experimental field, as illustrated in Figure 6. Each lysimeter featured a stainless-steel core cylinder with dimensions of 60 cm in height and 30 cm in width. Within these lysimeters cylinders, a soil monolith was present hosting cultivated crops that replicated the environmental conditions of the surrounding field with the crop matching the one planted in the entire farm. Retrieving the soil monolith core from each lysimeter involved the utilization of three rope straps which were fixed to steel hook anchors embedded in the ground. These straps were used to secure a jack positioned on top of the cylinder which effectively drove the cylinder into the soil (Figure 7). The process continued until a sufficient volume of soil was

filled reaching the bottom level of the cylinders. At the base of the lysimeters cylinder the closing process was done using gypsum-filled ceramic caps, which contributed to effective sealing. These caps played a significant role in establishing a suitable boundary between the external field environment and the controlled internal environment within the lysimeters. Within the gypsum filled caps, two pumps were secured to maintain the balance in conditions of wetness between the lysimeter and the field condition. Preventive measures against potential leakage included the incorporation of a rubber seal between the cylinder walls and the contact point of the ceramic cap which were further reinforced by a metallic strap to ensure a secure connection. A weighing balance platform was positioned below these caps, secured using metal fasteners and tensioned nut and bolts (Figure 7).

Each individual lysimeter was outfitted with a set of twelve sensors. These sensors were designed to monitor important parameters in soil which included temperature ( $^{\circ}\text{C}$ ), electrical conductivity ( $\text{mS}/\text{cm}$ ), soil moisture (%) and water potential ( $\text{kPa}$ ). Three sensors measuring the same parameter were installed at three different depths 5, 30 and 55 cm depth. To ensure stable and accurate measurements, the lysimeter system was housed within a protective barrel which was carefully levelled using a spirit level prior to its surrounding being filled with soil to create a level ground surface for the weighing balance. The installation process also incorporated a tripod which facilitated the lifting of the sensor-equipped lysimeter. A controlled descent into the protective barrel was accomplished using a chain block. Prior to the descent of the lysimeter, wires were connected linking each lysimeter to drainage control pipes, tensiometric cables and other necessary components.

To sustain uniform conditions both within and outside the lysimeters, a special tensiometer was installed alongside each lysimeter. Additionally, a drainage bottle equipped with a weighing platform was positioned within the field box located at one metre from each lysimeter. This arrangement enabled the monitoring of water drainage from the lysimeters (Figure 8). To centralize data collection and management the lysimeters were interconnected through power cables to a central data logger system. This included important components such as solar panels, batteries, and a SIM card for facilitating remote storage connection (Figure 8). The interconnected network of components ensured the efficient and accurate gathering of data for further analysis and interpretation.

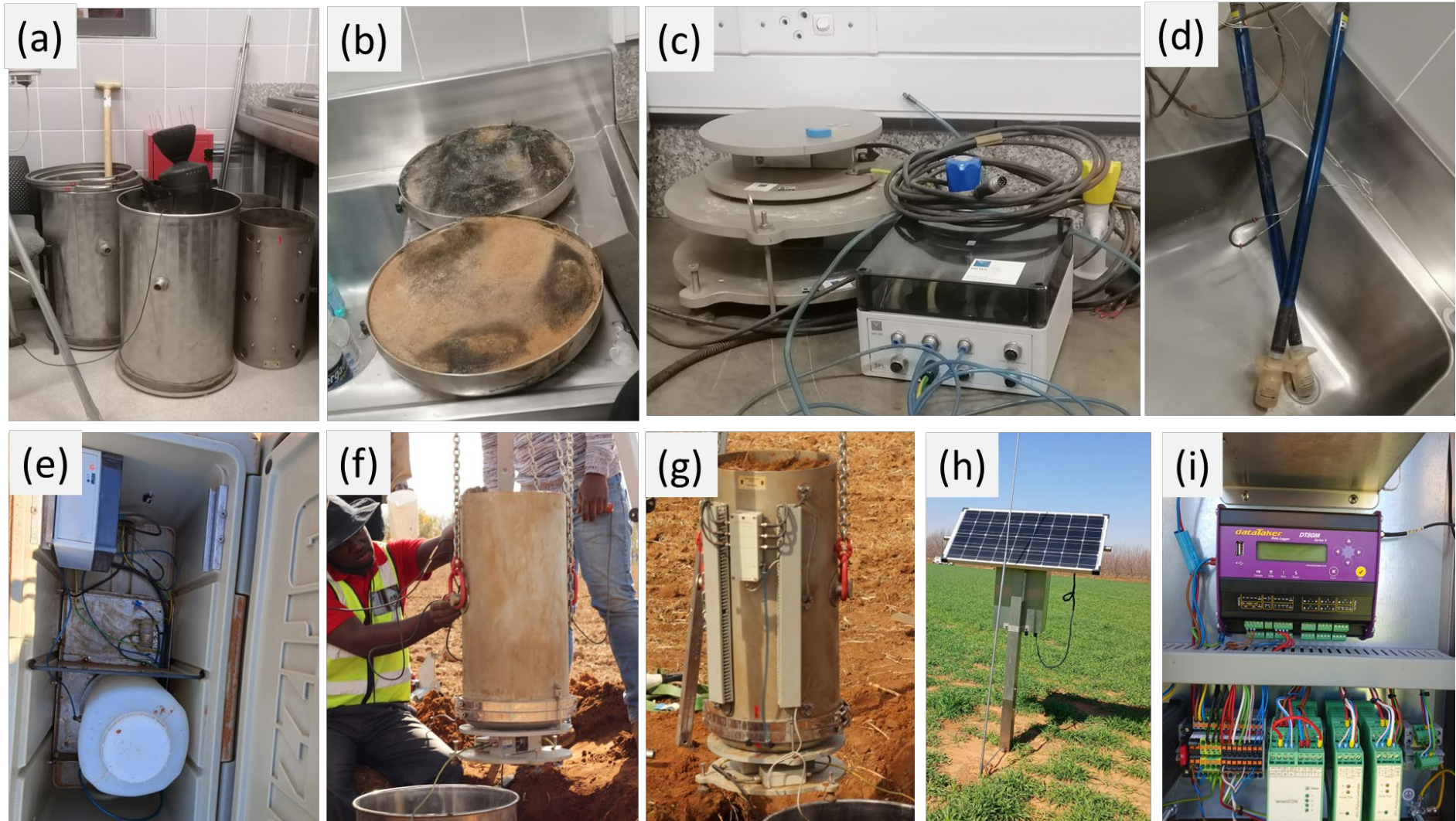


**Figure 7: Depicts different components of the lysimeter. The lysimeter core cylinder and housing barrel (a), lysimeter bottoms with gypsum (b), lysimeter and drainage balances (c), tensiometers (d), drainage bottle and pump (e), lysimeter cylinder with weighing balance (f), lysimeter cylinder with sensors installed, lysimeter battery recharging solar panel and data logger (h) while (i) shows inside the logger box.**

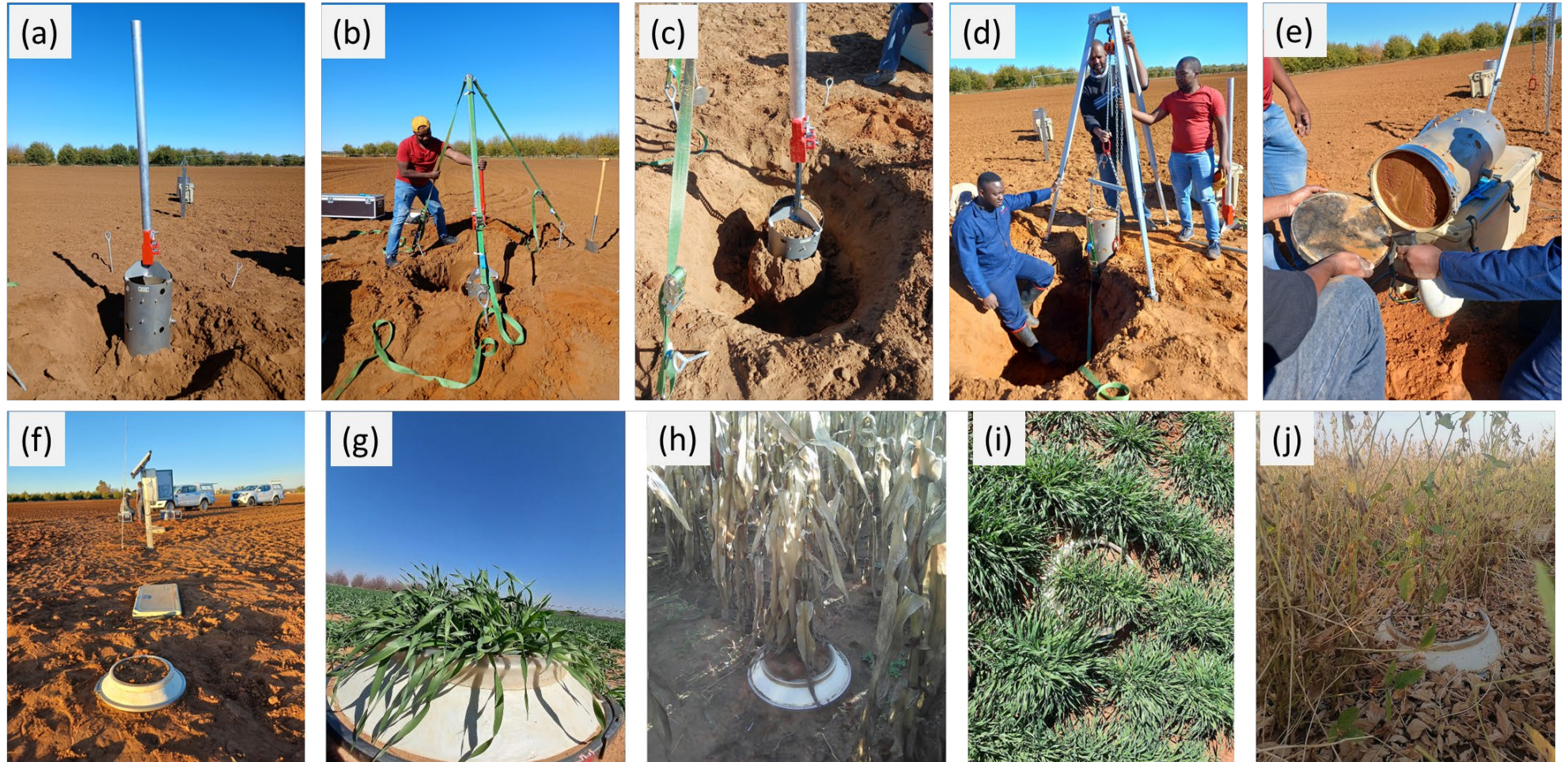


Figure 8: Provides an overview of the lysimeter installation during different cropping seasons. The soil monolith extraction using the lysimeter cylinder, straps, and a jack (a-d), lysimeter cylinder bottom closure (e), final lysimeter field setting (f), bare in lysimeter during 2019 (g), maize in 2020 (h), barley in 2020 (i) and soybean in 2021 (j).

## 2.2 LYSIMETER DATA MEASUREMENT AND ET DETERMINATION

To measure  $ET_a$  for different crops, two smart field lysimeters (SFL-600, METER Group®) were installed during the 2019, 2019-2020; 2020 and 2021 cropping seasons. The pictures depicting the barley 2020 and soybean 2021 seasons are shown on figure 10. Each lysimeter consisted of a stainless-steel cylinder, 60 cm in height and 30 cm in diameter, which was specifically designed to replicate the field conditions of the soil and barley crop. The lysimeters were equipped with weighing balances to continuously measure changes in mass (Kg) throughout the cropping period. The primary component measured by the lysimeters was the change in storage ( $\Delta S$ ), representing the variation in soil moisture levels. The weight of the lysimeters was recorded at one-minute intervals throughout the season, providing high temporal resolution data for immediate decision making in real-time. In addition to mass measurements, each lysimeter was equipped with sensors to measure various soil parameters at different depth intervals (5, 30, and 55 cm). These parameters included volumetric soil water content (%), temperature ( $^{\circ}C$ ), electrical conductivity (mS/m), and water potential (Kpa). The sensors provided real-time data, collected at 10-minute intervals, ensuring that the information retrieved from the lysimeters could be used promptly for decision-making purposes. The measurement data collected by the lysimeters were transferred to a digital data logger (DT80M dataTraker®), which stored the data internally and transmitted it to a cloud-based storage system via a built-in modem equipped with a local network connection Sim card. The cloud storage capability allowed remote data acquisition, reducing the need for frequent field visits to access the data. To measure the drainage component of the water balance, a drainage vessel with a weighing balance was placed below the lysimeters to quantify the excess water from the lysimeter bottom. An intelligent automatic pump was incorporated within the drainage vessel to maintain consistent boundary conditions between the soil within the lysimeter and the field. This innovative feature ensured that the lysimeter accurately represented the field soil water conditions. When the lysimeters soil became drier than the field conditions, the pump automatically returned drainage water from the vessel back into the lysimeter, ensuring equilibrium. Similarly, when the lysimeters soil became too wet, the pump automatically pumped water out of the lysimeter cylinder and into the drainage vessel. The Smart Weighing Field Lysimeter functioned by measuring both the mass of the crop-planted lysimeter cylinder and the quantity of drainage water from the lysimeter.

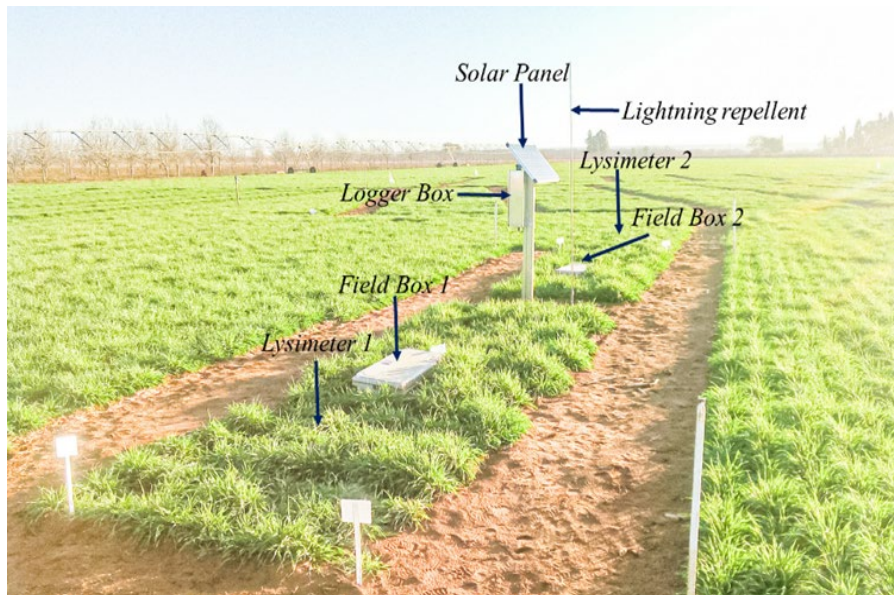


Figure 9: Smart field weighing lysimeter setting.



**Figure 10: Lysimeter setting during winter barley season 2020 and Soybean in 2021.**

The lysimeter evapotranspiration was estimated using the formula:

$$ET_a = \frac{(LYW_n + SWW_n) - (LYW_{n+b} + SWW_{n+b})}{\left(\frac{\pi}{4}\right) 0.3^2}$$

$ET_a$  represents  $ET_a$  on the  $n^{\text{th}}$  day,  $LYW_n$  represents the weight of the lysimeter in kg on the midnight of the  $n^{\text{th}}$  day,  $SWW_n$  represents the weight of the percolate water vessel storage also in kg on the midnight of the  $n^{\text{th}}$  day.  $LYW_{n+b}$  and  $SWW_{n+b}$  represents the lysimeter weight and storage vessel weight on the  $n^{\text{th}}$  day of the next day. The water density was assumed to be  $1000 \text{ kg m}^{-3}$ , while 0.3 is the diameter of the inner core barrel of the lysimeter (Ratshiedana, 2022). To convert the mass of the lysimeter from kilograms to millimetres, the water density assumed to be  $1000 \text{ kg m}^{-3}$  which was converted to  $0.001 \text{ m}^{-3}$ . The water density of  $0.001 \text{ m}^{-3}$  was divided by the surface area of the lysimeter being  $0.0707 \text{ m}^2$ , equal to 0.014 m equivalent to 14 mm.

## CHAPTER 3: LYSIMETER DATA PROCESSING (MULTI-TEMPORAL ANALYSIS)

### 3.1 INTRODUCTION

This section provides a detailed description of the lysimeter data analysis post field measurements. Measured raw data on lysimetric and drainage masses as well as measurements made from the lysimeter sensors are explained and portrayed through graphs throughout the section. A more detailed description of how mass measurements are converted into the actual amount of water lost in between irrigation and subsequent events is provided. The processes involved in the removal of noise between measurements is also narrated while the outputs from various sensors located within the lysimeter are presented.

#### 3.1.1 Lysimeter data selection and processing

Data cleaning and removal of noise that occurs from external activities such as mechanical vibrations, farm attacking animals and strong winds amongst many other factors is crucial before using data for quantification of crop evapotranspiration, data cleaning reduces false quantifications which can lead to wrongful decision making. Data recorded by both lysimeters for different seasons were inspected for anomalous values such as negative values, error readings on the weighing balance and abnormal readings causing spikes which cannot be explained. ET data focus was on rainless days with zero irrigation, zero-dew or and frost days. The purpose of removing water input days was to allow monitoring water use after a known irrigation amount event, nevertheless; irrigation days yield negative ET due to weight differences between the less wet and irrigated soils. Following data cleaning, the data was imported into the origin lab software and plotted against time to enable smoothing of the data for ease interpretation using the Savitzky-Golay filter at 20 minutes window to remove anomalies (Figure 11), manual filtering was also done for the values which could not be smoothed by the automatic filter. The Savitzky-Golay filter was used because it has the capability to enhance the precision of the measured data without removing the important information from the measured weights.

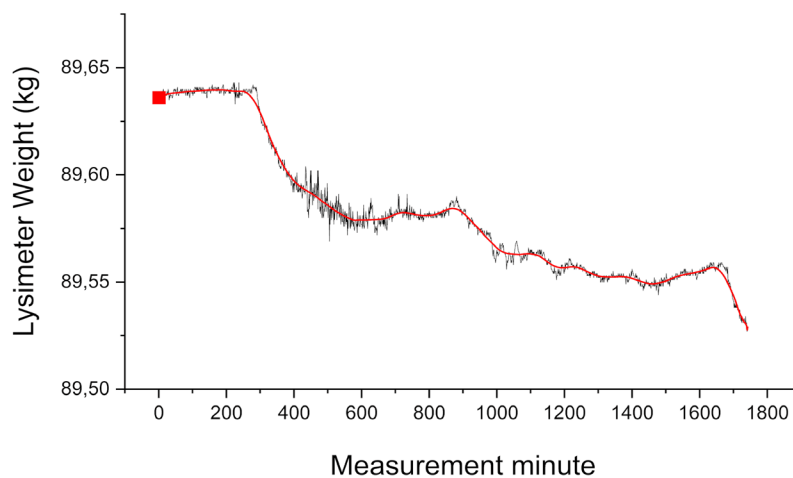


**Figure 11: Noise associated with various lysimetric distortion vs noise-filtered data.**

### 3.1.2 Lysimeter mass balance

Figure 12 illustrates the fluctuations in lysimeter mass (kg) recorded on the weighing balance from September to October 2019. The gradual decline in lysimeter weight corresponds to crop water usage, indicating water consumption by the crops. On the other hand, the sudden vertical increases in weight represent irrigation events and the associated water depth applied to the crops. Such weight increments indicate the addition of water content due to irrigation and not precipitation bearing in mind the experiment was based on irrigated winter barley when there is no precipitation in the area. Conversely, a decrease in lysimeter weight indicates water loss through evaporation and transpiration processes. This decrease signifies the reduction in water content within the lysimeter, caused by the natural water loss from the crops to the atmosphere during their growth and development.

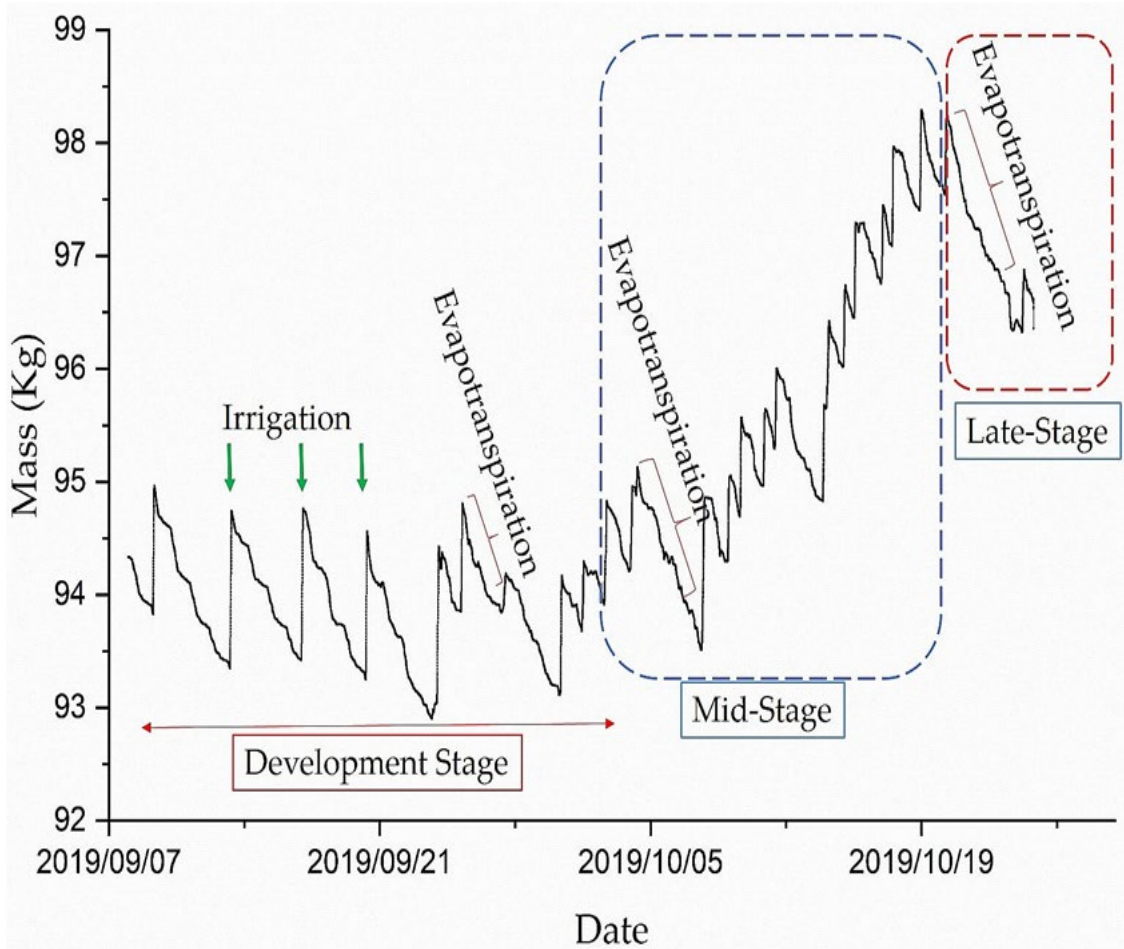


Figure 12: Lysimeter weight fluxes throughout the 2019 barley cropping season.

## 3.2 DETERMINATION OF ACTUAL ET AT DIFFERENT TIME SCALES USING SMART FIELD WEIGHING LYSIMETERS

To calculate the actual evapotranspiration fluxes, lysimetric data from smart field weighing lysimeters recorded from 2019 to the end of 2021 cropping seasons for different crops within the experimental farm were used.

**Table 1: Cropping seasons and their associated crops during the experimental period.**

Season	Year	Crop
Season 1 winter	2019	Barley
season 2 summer	2019-2020	Maize
season 3 winter	2020	Barley
Season 4 summer	2020-2021	Soybean

Pre-processing of the lysimeter data was done to fit the hourly, daily, and monthly ETa requirements. Evapotranspiration was determined using two smart field weighing lysimeters (SFL-600) based on the weight variations of the lysimeter weighing balance when irrigation was discontinued. Evapotranspiration was computed using the lysimeters, in-situ weight readings, indicated as (LYW), and the weight of the storage vessel, designated as (SWW). The two lysimeters were connected to a data logger which was programmed to record, store and transfer measurement data from the load cells every 10 seconds. The data was downloaded from the cloud storage and saved as .csv files for analysis. For quality and maintenance purposes, monthly visits to the location where the lysimeters were installed were undertaken to assess the field conditions, vegetation planted and the drainage containers for flood checks. The decrease in the lysimeter cylinder weight was caused by the evaporation of water from the crop and soil surfaces as well as transpiration of water through the tissues of the crop, the increase in weight was associated with irrigation, precipitation, and dew effects. The lysimeter weight changes measured in kilograms, were converted to the equivalent depth of water in millimetres, by dividing the changes in weight of the lysimeter between periods by the density of water in grams as well as the surface area of the lysimeters in square metres. The hourly ETa was calculated based on the weight changes between two consecutive hours, while daily ETa values were calculated by summing up all the daily ETa values obtained from 08:00 am and 17:00 pm on a 24-hour period in winter for barley crop and 5 am to 18:00 pm for summer crops (maize and soya beans), the purpose of selecting data between the hours was to eliminate the diurnal effects caused by dew or frost which possibly add weight on the lysimeter balance. The choice was influenced by the fact that evapotranspiration occurs between sunrise and sun set when there is sufficient energy to evaporate water from surfaces, transpiration also ceases when the sunlight is reduced stopping the processes, the diurnal variations in this study were taken as dew or frost influenced. The smart field weighing lysimeters directly measure the water balance components being the amount of irrigation or incoming precipitation, frost and dew events as incoming water which causes changes in the lysimeter storage. Irrigation and precipitation were also measured directly using a Hobo-link weather station rain gauge situated 10 metres north of the two lysimeters. At every 10 minutes interval drainage was measured by the lysimeters. Adding all the measured components, the only component not measured remains the actual crop evapotranspiration. The water balance equation is used to calculate evapotranspiration:

$$ET = P - R - \Delta S$$

ET is the water lost through evaporation (E) and plant transpiration (T) while P represents Precipitation and R denotes Rainfall while  $\Delta S$  denotes change in storage. Precipitation in this situation was taken as irrigation input, another input was water pumped back into the systems by tensiometers when the conditions were to overlap. Change in storage was measured by the water accumulation in the drainage system changes. The actual evapotranspiration from lysimeters is calculated as Doležal *et al.* (2018).

$$ETa, i = LYWn + SWWn - LYWn + 1 + SWWn + 1$$

Where  $ET_a$  (mm)  $ET_{a,i}$  is the actual crop evapotranspiration,  $LYW_n$ =Lysimeter Weight at  $n$ th time,  $SWW_n$ =Drainage Weight at  $n$ th time,  $LYW_{n+b}$ =Lysimeter Weight at  $n+b$  time,  $SWW_{n+b}$ =Drainage Weight at  $n+b$  time.

$$LysimeterArea = \pi r^2 = \pi \times 0.152 = 0.0707m^2$$

When the drainage is zero, evapotranspiration can be obtained directly by multiplying the change in storage with the density of water which can be calculated as:

$$1 \text{ kg of seepage water} = 0.001m^3 = 0.001m^3 / 0.0707m^2 = 0.014m = 14mm$$

$$1 \text{ kg of seepage water} = 0.001m^3 = 0.001m^3 / 0.0707m^2 = 0.014m = 14mm$$

### 3.3 EVALUATION OF LYSIMETRIC MEASUREMENTS

To evaluate the effectiveness of the lysimeters in determining  $ET_a$ , irrigation days excluded in the quantification of  $ET_a$  as one of the water balance components was computed as measured by the lysimeters and compared to irrigation measurements measured directly by an automatic weather station (AWS) rain-gauge. Statistical analyses were done to assess the relationship between the two measured observations.

### 3.4 RESULTS

#### 3.4.1 Actual evapotranspiration from smart lysimeters

Figure 14 depicts the daily  $ET_a$  measured by the smart field weighing lysimeters during the 2020 winter barley crop season.  $ET_a$  is low at the beginning of the season when the crop is germinating and increases gradually in different phenological stages. Figure 13 presents a detailed representation of  $ET_a$  fluxes quantified throughout the barley cropping season, starting from approximately the 7<sup>th</sup> of September, and extending towards the end of October 2019. The graph portrays the fluctuations in  $ET_a$  fluxes over time, offering valuable insights about the dynamic nature of water consumption by the barley crop during this period. During the initial days of September, the hourly ET values were relatively lower around 0.55 mm/hour, indicating moderate water consumption by the crop. As the cropping season progressed towards late October, there was a noticeable upward trend in  $ET_a$  fluxes with the average of 1 mm/hour. This observed increase in ET can be attributed to several factors that influenced the barley crop's water demand and transpiration rates in two ways. Firstly, the growth of the barley crop had advanced during this period, leading to an increase in crop biomass. As the crop biomass increases, so does the overall water requirements of the barley plants as well as the weight of the lysimeters. The higher demand for water by the growing crop resulting in an increase on  $ET_a$  fluxes. Secondly, irrigation practices during the cropping season contributed significantly towards the availability of water for the barley plants. As the season advanced, the frequency and volume of irrigation water provided to the crop increased as reflected on Figure 13 around 03/10/2019 and 15/10/2019. This additional water supply was to ensure sustainable crop water needs, supporting robust growth and transpiration rates, thereby reflecting in the rising ET values around the same period of intensive irrigation with  $ET_a$  reaching around 1.2 mm/hour. Furthermore, the influence of temperature on  $ET_a$  cannot be overlooked, as September approaches the end, the temperatures appeared to rise within the lysimeter as depicted in Figure 13, creating a warmer and more favourable environment for plant transpiration. The increased temperature stimulated the barley crops to transpire more actively,

leading to higher ETa fluxes. The dynamic nature of the ETa fluxes depicted in Figure 13 demonstrates the importance of closely monitoring and understanding crop water requirements throughout the cropping season. Accurate estimation of ET fluxes enables farmers to optimize their irrigation schedules, ensuring that the crop's water needs are met efficiently and without unnecessary water wastage. During the initial stages of growth, in the preliminary phase, rate exhibited relatively low rates as the barley crop developed. Throughout this stage, the barley plants laid the foundation for their growth, resulting in a measured ETa that aligned with their growth status. As the barley plants transitioned into the vegetative stage, a notable shift in ETa dynamics became apparent. The ETa values showed an increase, mirroring the increase in growth of the barley plants and the concurrent expansion of their leaf surface area. This growth-driven increase in ETa was closely linked to the transpiration rates as the plants capitalised on their enlarged leaf coverage for water exchange with the atmosphere. Upon entering the reproductive stage, characterized by heading and flowering, a transformation in ETa composition was evident. During this phase, transpiration emerged as a prevailing force in driving ETa, assuming a more pronounced role compared to the prior dominance of evaporation. Continuing along the seasonal timeline into the grain filling and maturation phase, ETa's behaviour changed. The recorded ETa values exhibited a marginal decline, this reduction in ETa demonstrates the crop response as they prioritized grain development. Figure 13 shows ETa fluxes during the maize growing season, while figure 14 shows the 2020 barley cropping season. Figure 15 portrays the hourly ETa fluxes extracted during the 2021 summer soyabean crop season, ETa varies in different days with ETa being more pronounced in hottest days. ETa variability at night-time appears to be low increasing slowly from sunrise and reaching maximum limit around mid-day time gradually decreasing until sunset. This is influenced by the solar radiation pushing more water from the soil medium and out of the crop leaves.

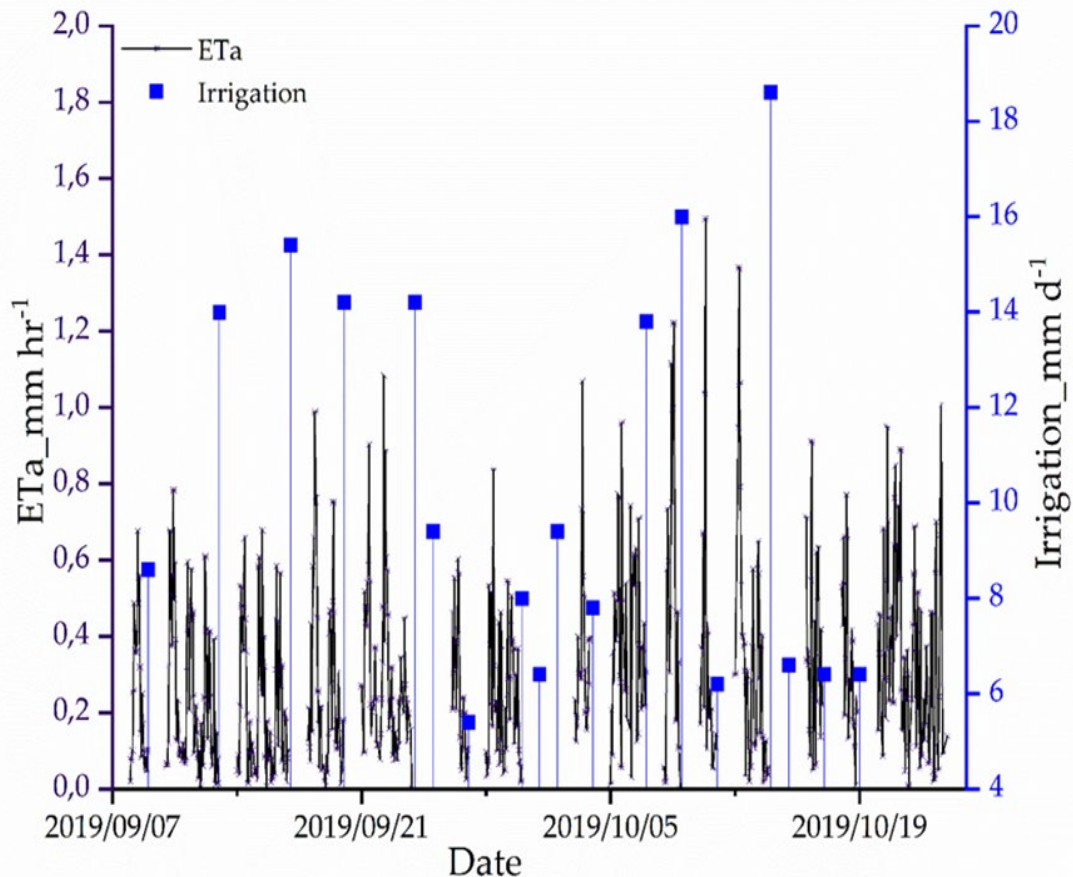


**Figure 13: Quantified hourly ETa during zero-irrigation days and irrigation amounts during the 2019 barley season.**

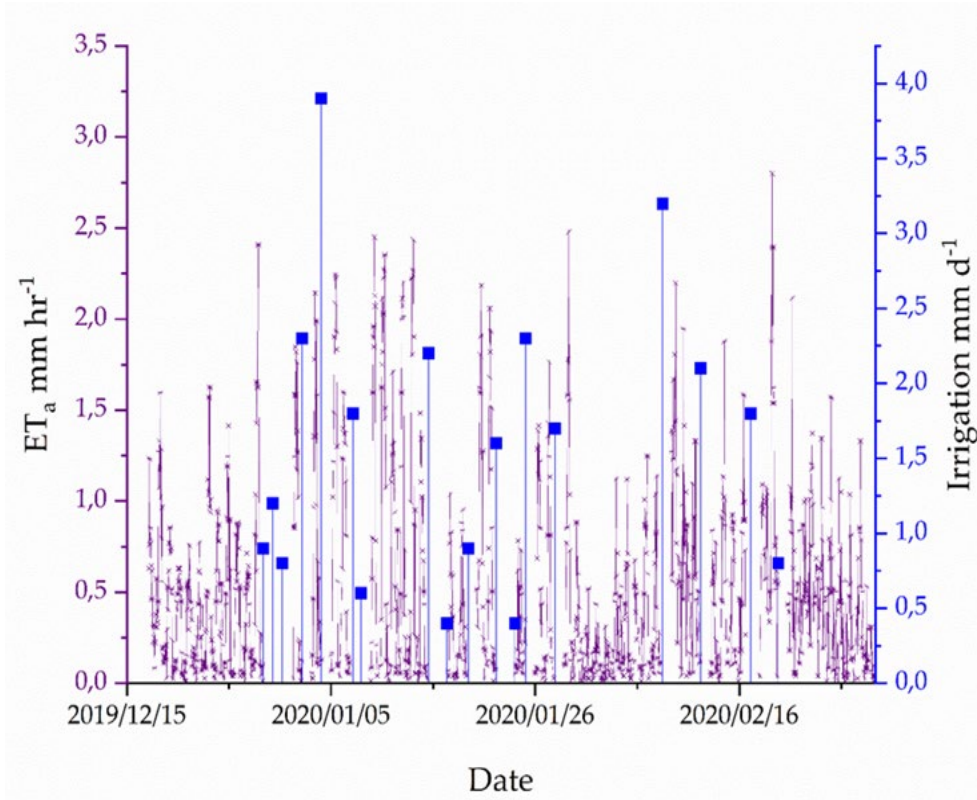


Figure 14: Actual evapotranspiration fluxes throughout the 2019-2020 maize season.

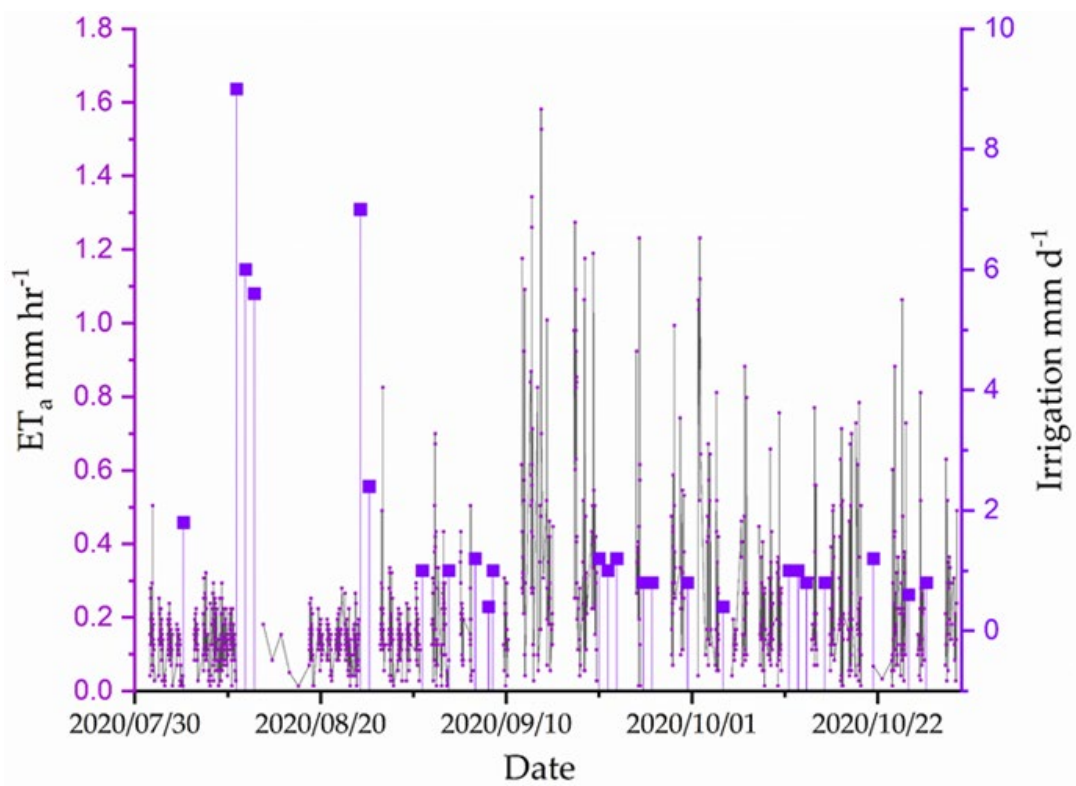
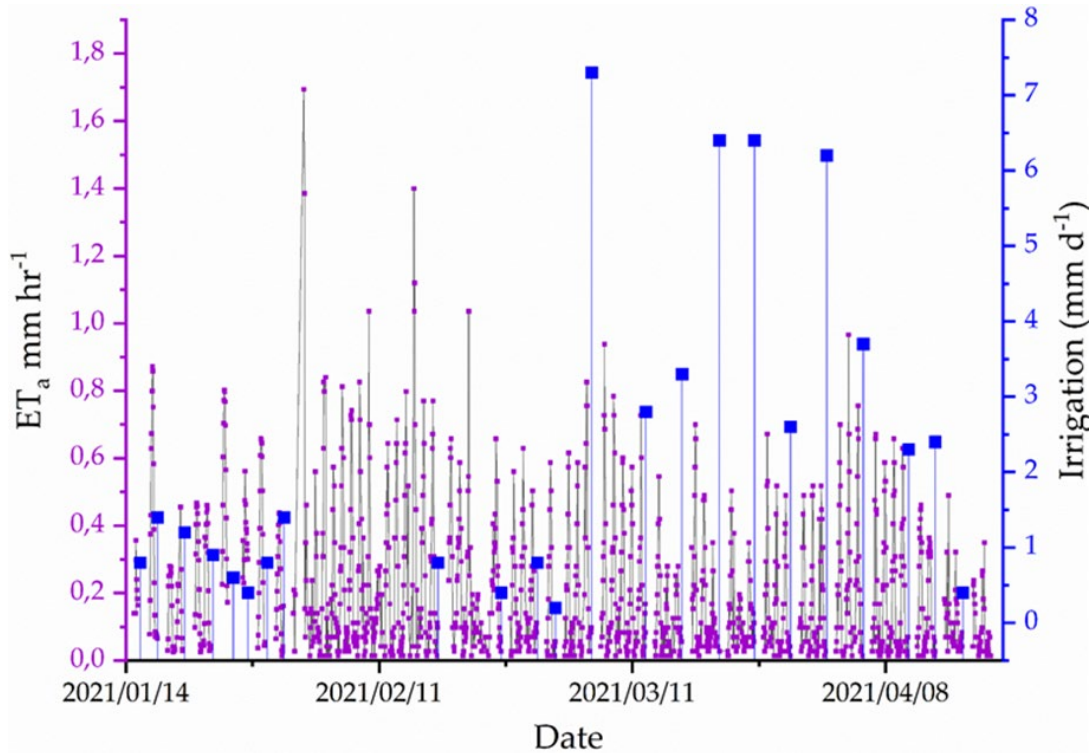


Figure 15: Quantified hourly  $ET_a$  during zero-irrigation days and irrigation amounts during the 2020 barley season.



**Figure 16: Quantified hourly  $ET_a$  during zero-irrigation days and irrigation amounts during the 2021 Soybean season.**

### 3.4.2 Irrigation and $ET_a$ assessment

The illustration provided by Figure 17 depicts the relationship between irrigation events and  $ET_a$ , which represents the crop's water demands. The findings reveal that throughout the duration of the experiment, irrigation did not consistently meet the full water requirements of the crops. However, around the dates of September 27<sup>th</sup> and 28<sup>th</sup>, 2019, irrigation approached the  $ET_a$  values, although it did not precisely match the required water amounts. This alignment is evident in the graph along the zero-line, where the disparity between irrigation and  $ET_a$  is minimized. It is evident that approximately 57% of the time, irrigation exceeded the crop's water demands. Conversely, during 43% of the days, irrigation fell short of providing the necessary water to meet the actual water lost by the crops. When irrigation surpassed the crop water demand, the irrigation- $ET_a$  graph exhibited a positive shift above the zero-line. On the contrary, instances where  $ET_a$  exceeded irrigation resulted in a negative shift, moving further away from the zero-line on the graph.

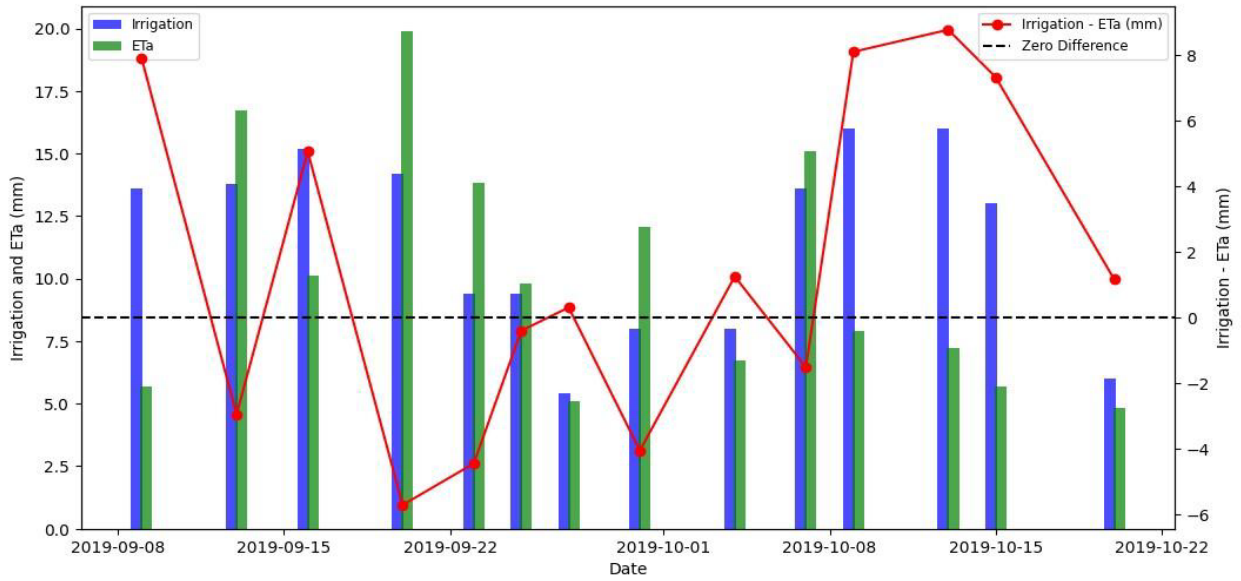


Figure 17: The relationship between irrigation events and ETa.

Throughout the winter barley season of 2020, the variation between irrigation and ETa is visually depicted in Figure 18. It is evident from the data that the quantity of irrigation administered to the crops did not align closely with the genuine water demand of the crops. On certain days, the amount of irrigation exceeded the actual demands, while on other days, it fell short of meeting the required water loss. However, on the 14<sup>th</sup> of August 2020 and the 18<sup>th</sup> of October 2020, instances occurred where the irrigation closely matched the ETa values. This alignment is clearly demonstrated in both the irrigation-ETa difference graph and the zero-line graph. Specifically, the graphs illustrate that during these dates, the disparity between irrigation and ETa was minimal, indicating a close match between the actual irrigation and the crop's water requirements.

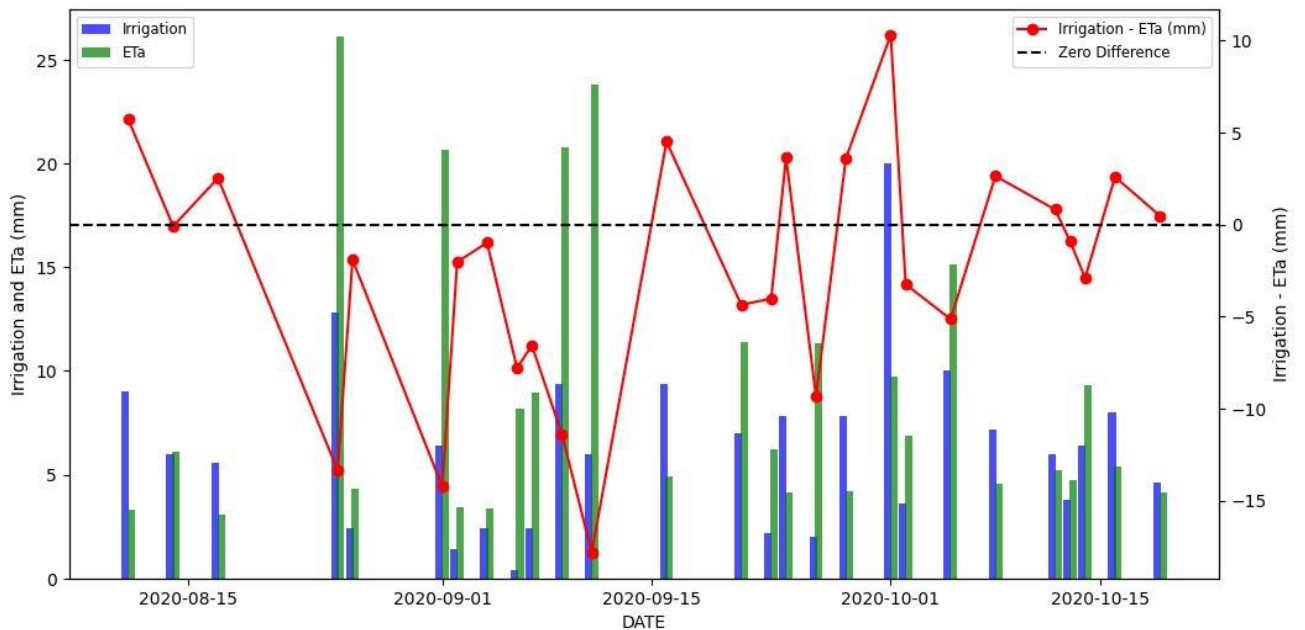
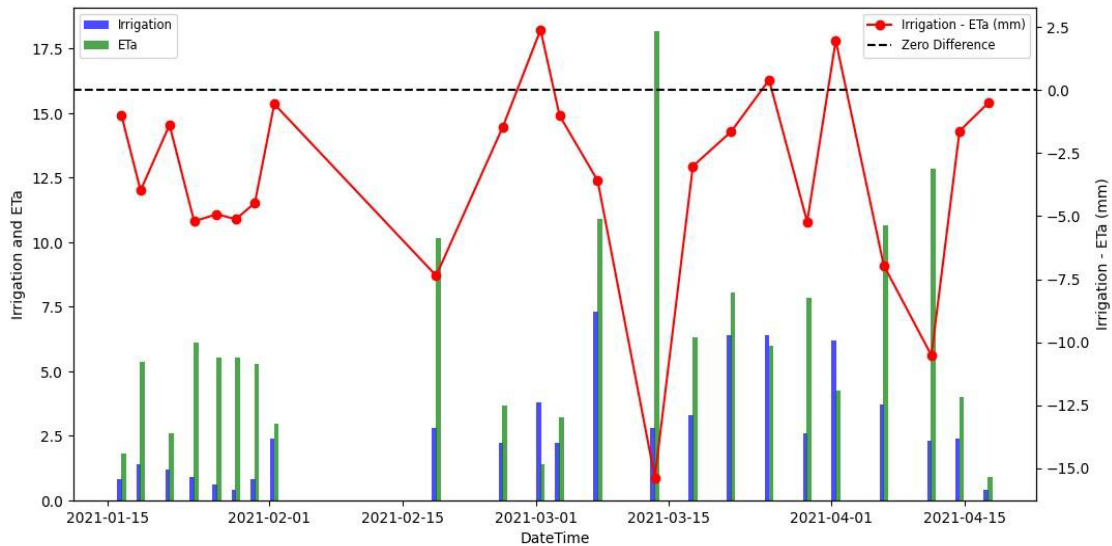


Figure 18: The ETa vs irrigation during winter barley season of 2020.

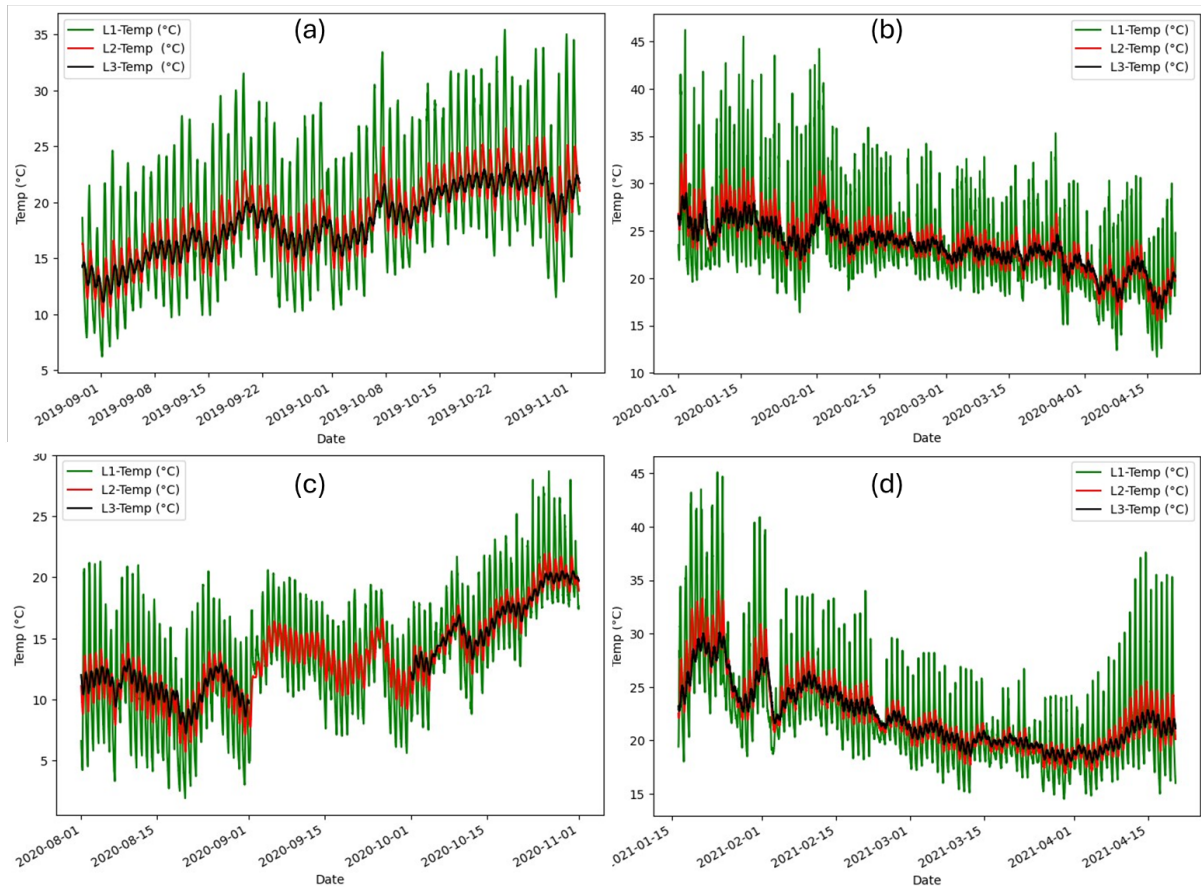
During the soybean season in 2021, the contrast between irrigation and ETa is represented in Figure 19. The findings reveal that on most days during the season, the irrigation levels were insufficient in meeting the actual water requirements of the soybean crops. Throughout most days, the rate of ETa consistently surpassed the levels of irrigation, providing a recurring pattern where the crop's water needs were not adequately addressed through irrigation. However, there were three specific days within the season where the scenario deviated. On these days, the rate of irrigation managed to match the corresponding ETa values.



**Figure 19: The ETa vs irrigation during the soybean season in 2021.**

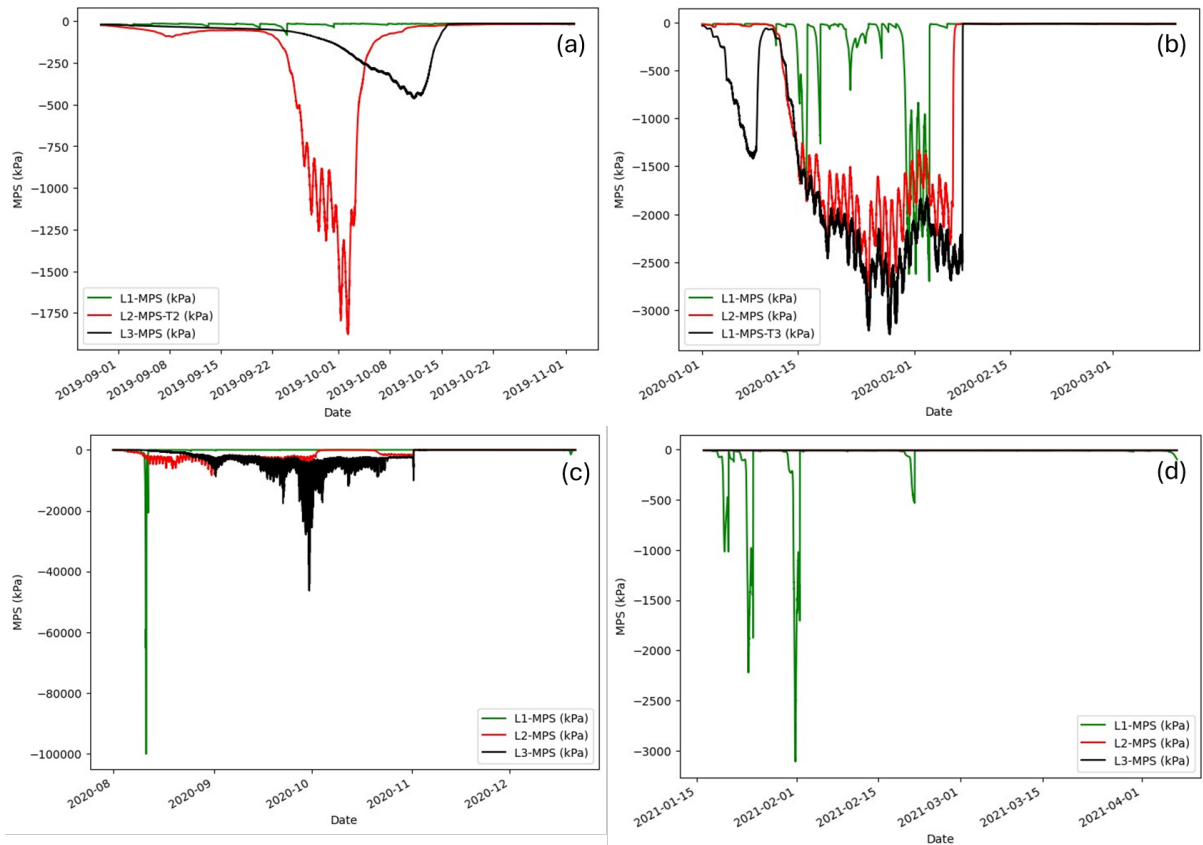
### 3.4.3 Lysimeter temperature variability

Figure 20 presents the response of temperature sensors at various depths within the lysimeter cylinder, offering insights into the soil's thermal dynamics. The temperature sensor, L1, situated close to the surface of the lysimeter column, displays higher temperature fluctuations compared to sensors located at deeper soil depths. The L1 sensor exhibits more sensitivity to diurnal and seasonal temperature changes, as well as variations in air temperature, radiation, and surface cooling and heating effects. Being near the surface, this sensor is directly influenced by these surface-related factors, resulting in more pronounced temperature fluxes. On the other hand, the middle (L2) and bottom (L3) temperature sensors respond at a slower rate to temperature fluctuations. These sensors experience reduced exposure to direct influences from surface temperature variations. Consequently, the lower temperature sensors reflect slower and smaller temperature fluctuations due to the less immediate impact of surface-related factors. The same trend is observed throughout all the seasons as displayed on the figure 20.



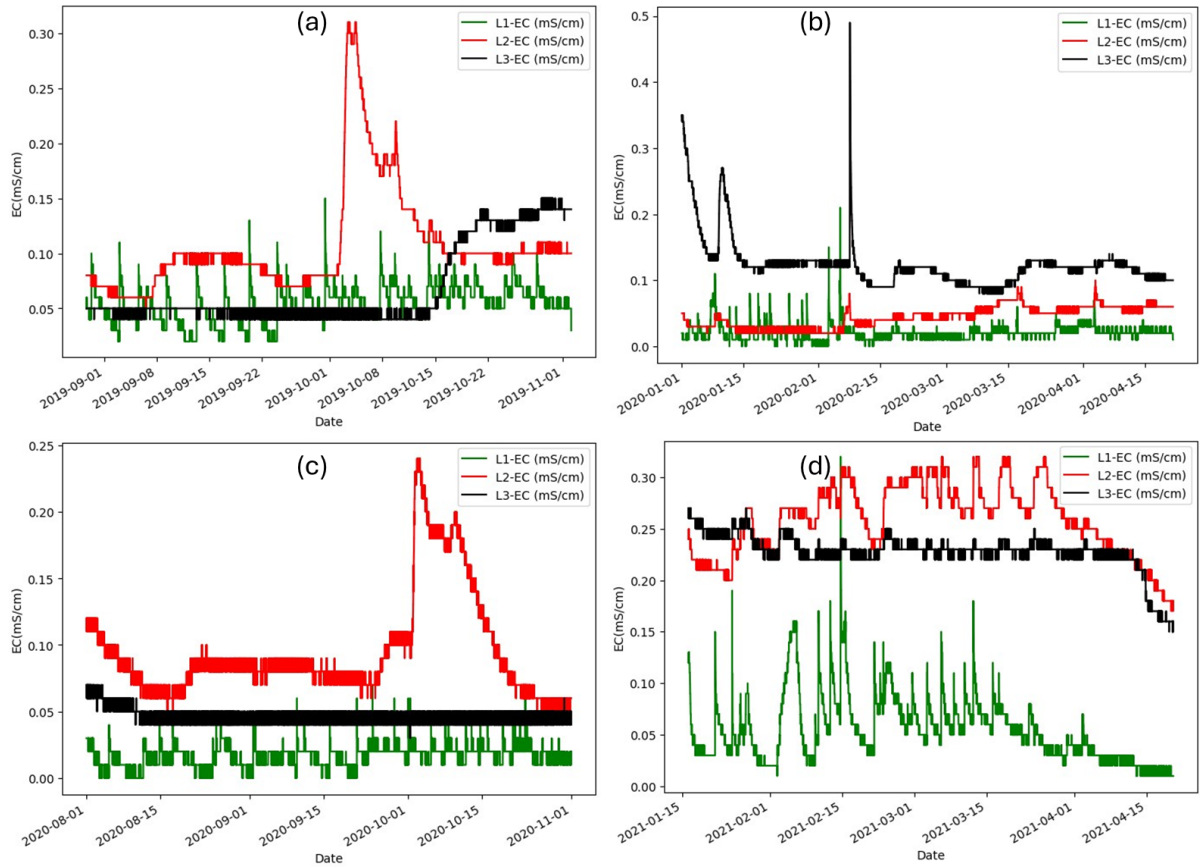
**Figure 20: Temperature fluxes within the lysimeter.**

Figure 21 illustrates the response of three water potential sensors located at different depths: L1, L2, and L3. The upper sensor, L1, situated closer to the soil surface, exhibits more frequent fluctuations in water potential, which can be attributed to variations in the moisture content status. This is because the L1 sensor is directly influenced by irrigation, evaporation, and transpiration processes. When irrigation water is applied to the lysimeter, the water potential near the soil surface changes rapidly, leading to more frequent fluctuations in this sensor's readings. The middle sensor, L2, responds with a slight delay compared to L1. This delayed response is due to the slower movement of water from the upper layer (L1) to the middle layer (L2). The rate of water transfer through the lysimeter column is influenced by hydraulic conductivity fluctuations and the soil's water holding capacity, resulting in a slightly delayed response in L2 compared to L1. The lower sensor, L3, depends on the movement of water from the upper two layers. The rate of water transfer to the lower layer is further slowed down due to hydraulic conductivity fluctuations and the soil's water holding capacity. As a result, the response of the L3 sensor is significantly delayed compared to L1 and L2, reflecting the slower water movement to the deepest layer of the lysimeter.



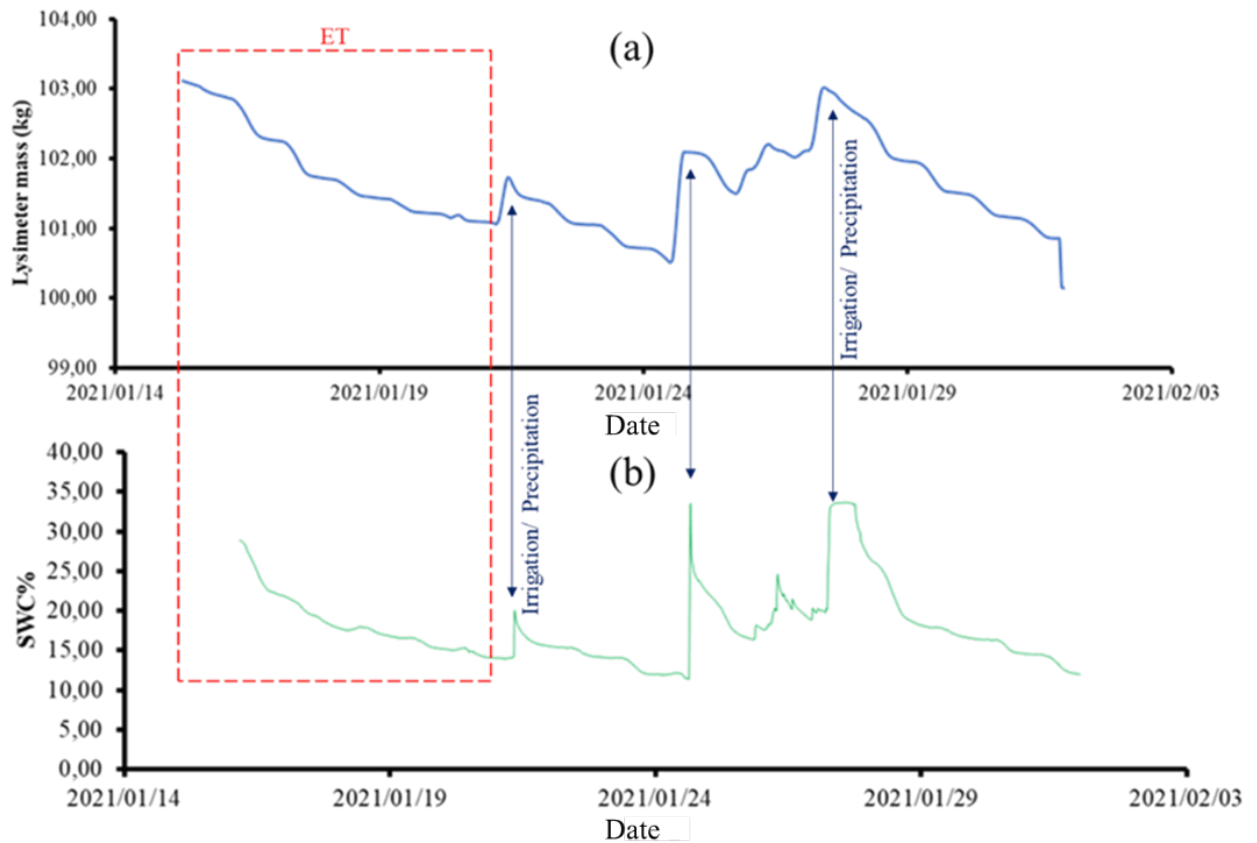
**Figure 21: Water potential fluxes within the lysimeter.**

Figure 22 depicts the variation in electrical conductivity (EC) as measured by three sensors located at different depths within the lysimeters. The response of the EC sensors, similar to the moisture sensors, varies depending on their depth within the lysimeter cylinder. The upper EC sensor, L1, situated near the lysimeter and land surface, exhibits a rapid response to changes in electrical conductivity. This is because when irrigation water is applied, there is an immediate increase in EC near the soil surface due to the dissolution of salts in the more saturated soil. The middle EC sensor, L2, shows a delayed response compared to L1. As irrigation water percolates down through the soil layers, it carries some of the dissolved salts with it. Therefore, the middle EC sensor also records an increase in EC but with a slower response time compared to L1. The bottom EC sensor, L3, located at the deeper soil layer, responds extremely slowly to variations in EC. This is because irrigation water reaching L3 has undergone soil filtering from the upper and middle soil layers, which could have diluted some of the dissolved salts. As a result, variations in EC at the lower depth are less pronounced. Similar observations on the sensors, responses around the 5<sup>th</sup> of September 2019 show that the bottom EC sensor displays an increase in EC, while the middle EC sensor also shows an increase above the near-surface sensor.



**Figure 22: Soil electrical conductivity fluxes within the lysimeter.**

Figure 23 shows the relationship between lysimeter weight changes and soil moisture content (SWC). Post precipitation or any irrigation event, soil moisture content is higher as it is with the lysimetric mass. With time SWC declines as we move away from the irrigation or precipitation event, the lysimeter mass also behaves in a similar pattern as portrayed by (a) and (b).



**Figure 23: The influence of soil moisture (SWC) (b) in the variability of lysimetric mass changes (a).**

### 3.4.4 Lysimeter soil moisture dynamics

Figure 24 presents the variability in soil moisture over time and at different depths, specifically at three sensor locations: L1, L2, and L3. L1 is the sensor closest to the surface, while L3 is positioned at the bottom of the lysimeter cylinder. The response of the sensors to irrigation is influenced by their depth. L1, being near the surface, shows a rapid increase in moisture content upon irrigation since it is the first to receive the irrigation water. The L2 sensor responds to irrigation at a slower rate because it takes considerable time for the irrigation water to infiltrate from L1 to L2. Consequently, the middle L2 sensor demonstrates a delayed response to irrigation. The L3 sensor, situated at the lower end of the lysimeter cylinder, exhibits the slowest response to irrigation events. The water applied as irrigation passes through L1 and L2 layers gradually percolating down to the lower L3 layer, causing a further delay in the response rate of the L3 sensor compared to L1 and L2. Figure 24 (a) also indicates an increase in soil moisture content response on the bottom sensor, L3, around the 5<sup>th</sup> of September 2019. Interestingly, the middle soil moisture sensor, L2, shows an increase above the near-surface sensor, L1. This observation can be attributed to the fact that the near-surface soil is more exposed to atmospheric conditions, including evaporation and transpiration by the cropped barley in the lysimeter. These processes lead to water being drawn out of the soil, resulting in lower moisture levels near the surface (Soulsby et al., 2021). In contrast, the deeper soil layers, such as the location of L3, experience less influence from these atmospheric conditions and may retain moisture for longer periods. Plant roots play a significant role in extracting water from the soil to support their growth and metabolic processes. Near-surface roots are more likely to consume moisture, contributing to lower moisture levels in the

topsoil. However, at deeper soil layers, the presence of roots might be less significant, allowing more moisture to accumulate.

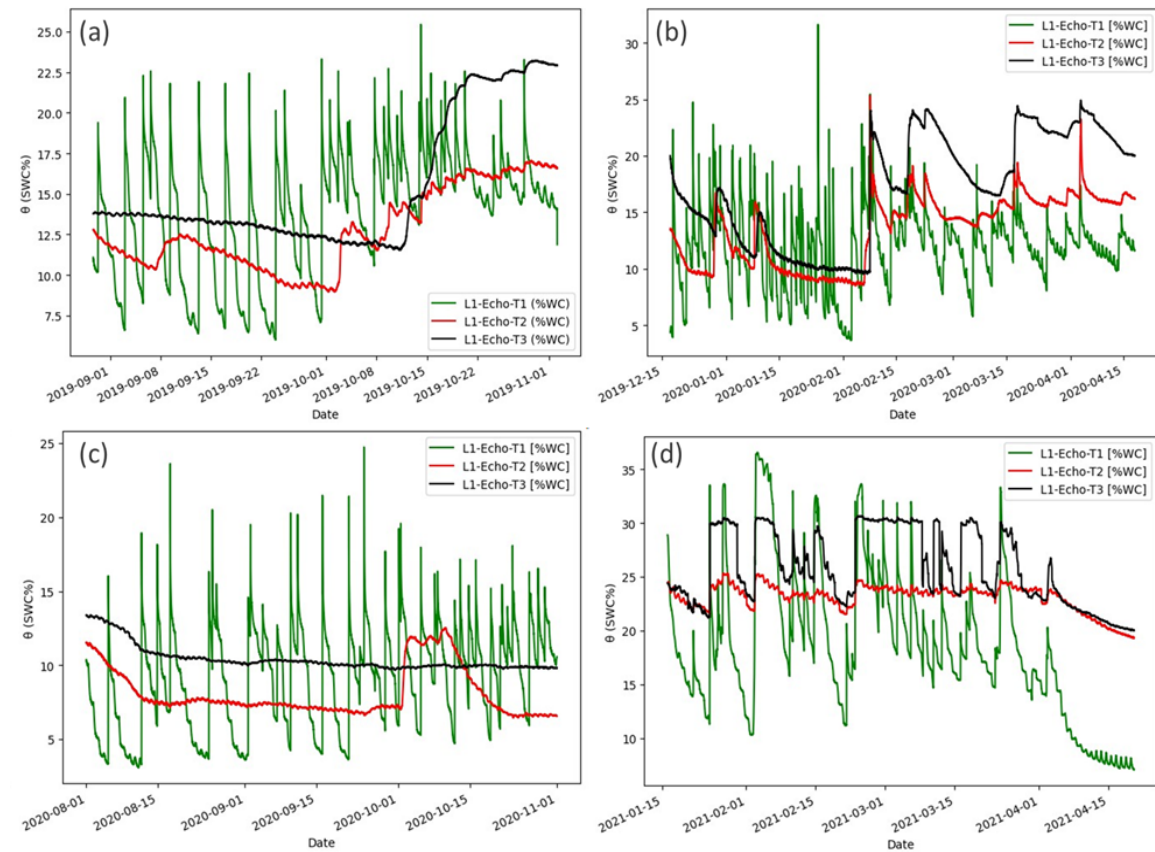


**Figure 24: Cumulative soil moisture variability within the lysimeter at three different sensors and depths.**

### 3.4.5 Relationship between soil moisture and evapotranspiration

Figure 25 shows a comparison of  $ET_a$  with SWC% on selected days with no irrigation or rainfall. The figure shows the relationship in terms of  $ET_a$  pattern against the L1, L2, and L3 moisture sensors. The L1 sensor displays a more pronounced reaction that closely matches the patterns seen in  $ET_a$ . The figure indicates that the uppermost layer, as indicated by L1, plays a significant role in capturing immediate moisture changes that are relevant to  $ET_a$  processes. The strong correlation between the readings of L1 and  $ET_a$  indicates that the near-surface layer has a direct influence on factors that drive  $ET_a$ . While L2 and L3 also offer insights into soil moisture dynamics, their responses might be influenced by deeper soil processes, such as water movement due to gravity or root activity. However, the behaviour of the L1 sensor, which closely reflects  $ET_a$  pattern highlights its importance as a key indicator of immediate soil moisture changes relevant to  $ET_a$ . During season 4 indicated by figure 25 (d), the L3 sensor also demonstrates a similar trend and response as  $ET_a$  pattern.

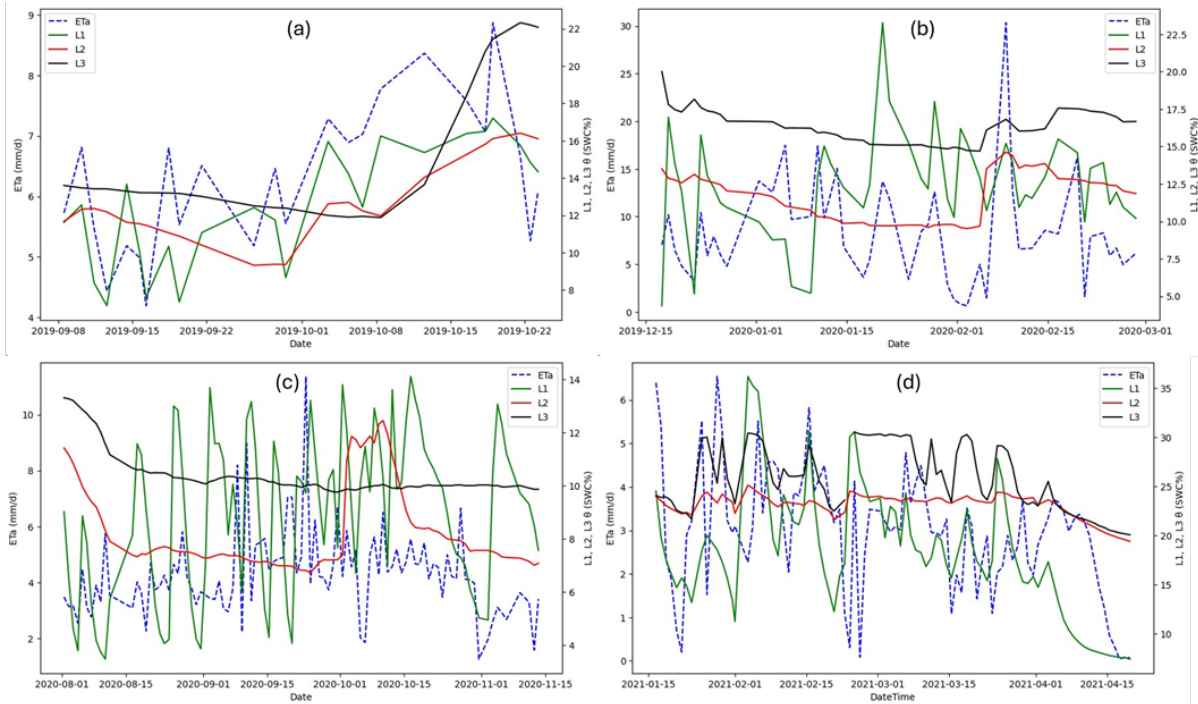


**Figure 25: Cumulative soil moisture variability within the lysimeter at three different sensors and depths.**

### 3.4.6 Validation results based on the 2019 season.

Based on the 2019 data, the statistical analysis revealed a strong positive correlation between the two datasets, with a correlation coefficient calculated to  $r=0.84$ . The  $R^2$  value was calculated to 0.7, indicating a considerable amount of variance in the irrigation depths can be explained by the rain gauge measurements (Figure 26). The significance of the relationship was confirmed by a highly significant p-value, which was found to be less than 0.005. This implies that the likelihood of obtaining such a strong correlation by chance alone is extremely low, thus lending more weight to the validity of the findings. In terms of the actual irrigation amounts, the cumulative total measured by the rain gauge amounted to 188.4 mm, while the smart field weighing lysimeter recorded a slightly lower total of 184.2 mm. The difference between the two measurements was merely 4 mm over the entire evaluation period, indicating a high level of agreement between the two methods. Looking at individual measurements, the rain gauge recorded a minimum irrigation depth of 5.4 mm, whereas the lysimeter registered a slightly higher minimum value of 5.8 mm. Similarly, the maximum irrigation depth recorded by the rain gauge was 16 mm, while the lysimeter recorded a slightly higher value of 16.7 mm. Analysing the mean irrigation amounts, the rain gauge data showed an average of 11.08 mm, while the lysimeter data showed a slightly lower mean of 10.84 mm. These minor differences in minimum, maximum, and mean values suggest that the two methods of measuring irrigation depths yield similar results overall.

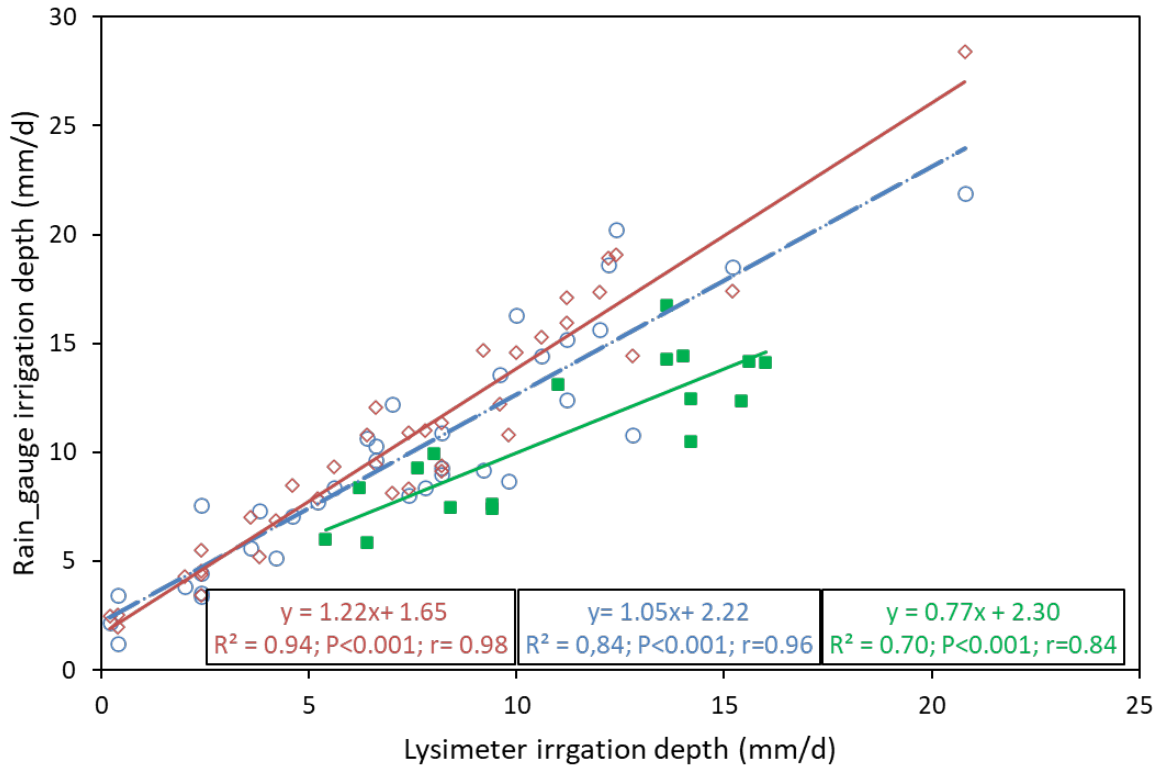


**Figure 26: Relationship between measured irrigation depth from the ONSET rain gauge and depth measured by the smart weighing lysimeter in 2019; 2020 and 2021.**

### 3.5 DISCUSSIONS

The behaviour of the lysimeters during the entire measuring and monitoring period on quantifying the soil water balance components was as expected. The nature and pattern at which the lysimeters weight changed was that, during irrigation events a sharp contact gain indicating a sudden change in weight became prominent, similar observations have been found in several study efforts (Mpelasoka et al., 2001; Shekharet al., 2022). At the beginning of each day, the lysimeters had an initial weight record which represented the total mass of the lysimeter cylinder as a function of the soil monolith, cropped vegetation and soil water content available in the entire system. As the daytime progresses and temperatures increase, soil water evaporation and crop water transpiration rates also increased, these processes led to water vapor escaping directly into the atmosphere and resulted in a decrease in the lysimeters mass. Similar findings have also been reported on efforts made by Salman et al. (2023) in their study using four mini-lysimeters. The net lysimeters weight changes at the end of the day reflects the overall water gain or loss in the lysimeter systems, our results reflect the net water lost between irrigation events, this information is key because it monitors the crop water use post irrigation which then assist in determining the amount required in the next irrigation event. Generally, it is important to note that the weight of a lysimeter can fluctuate throughout the day due to various environmental conditions, Zsembeli et al. (2019) narrated the factors that influence the lysimeter weight. Findings on this study also confirmed the introduction of noise between measurements, to compensate for these effects on ET computations, the raw data was passed through a Savitzky-Golay filter process to smooth the data for accurate estimations, such processes have been undertaken in the studies of (Peters et al., 2014; Moorhead et al., 2019; Gebler et al., 2015). Generally, at sunset when solar radiation

decreases, evapotranspiration also decrease, with lower solar energy input, the rate at which water evaporates from the soil and transpires from plants decreases (Bakhshoodeh et al., 2022). As consequence, the weight of the lysimeter systems changed slowly during the evening and overnight hours where it becomes stable at times. Changes in the lysimeters weight were also observed at night-time, however; these slight variations observed at night within the lysimeters system may not be directly related to the time of day but other effects such as dew or frost as narrated by Groh et al. (2019). Such scenarios have also been reported in various studies where small amounts of weight increases occur at night (Ding et al., 2010; Groh et al., 2019; Ratshiedana, 2022; Tolk and Evett, 2009).

The inclusion of various sensors in the lysimeters also demonstrated enhanced intelligence of the SFL which yielded additional data on various soil-water parameters which included soil water content, soil electrical conductivity, temperature variability, and water potential within the lysimeters. The sensors exhibited a notable trend where the near surface sensors demonstrated higher sensitivity and responsiveness to surface environmental conditions throughout the season compared to the middle to deep-located sensors. These findings align very well with similar results reported by Baalousha et al. (2022). The electrical conductivity was found to be higher when soil moisture is high, according to Ratshiedana et al. (2023) EC becomes high when there is sufficient soil moisture to allow the movement of changes within the soil medium. EC readings can aid in salinity indication, which on our findings comparing the EC values with the South African published EC values on salinity, acidity and sodicity by Nell and Van Huyssteen (2018), no signs of salinity were found in the lysimeter EC measurements throughout the cropping season. High EC values were quickly registered by the top sensor located near the surface, similar findings have been reported by Moorhead et al. (2019). Soil moisture sensors were active throughout the cropping season measuring the amount of soil water content present at three depth levels of the lysimeter cylinder. The top sensor near the surface was the most responsive sensor detecting irrigation events immediately as irrigation starts while the middle and bottom sensors responded gradually with some delay time because of depth, crop water abstraction on the upper layer. Crop roots extract water from the soil to support their growth and metabolic processes, therefore, the near-surface roots are more likely to consume moisture, contributing to lower moisture levels in the topsoil. Contrary, at deeper soil layers, the presence of roots can be less significant, allowing more moisture to accumulate. Baalousha et al. (2022) also mentioned that bottom sensors detect water with slow response because of sub-soil compaction leading to poor soil water draining performance whereas the top sensor occupies more loose soils because of soil tillage resulting in faster water draining. Moreover, the water potential sensors at the top of the lysimeters monitored changes in the soil's water potential. Water potential reflects the soil's ability to retain or release water and is influenced by irrigation practices. The water potential sensors also showed a similar behaviour to other sensors, where the response to irrigation was quicker. It is worth noting that water potential gradient between the lysimeter soil and its surroundings determines the direction and rate of water movement, the water potential of the lysimeter soil affects the infiltration of water into the lysimeter. If the lysimeter soil has a lower water potential than the incoming irrigation water, water will move into the lysimeter through infiltration, increasing its water content and weight. Higher water potential in the soil encourages the movement of water from the soil to the atmosphere through evaporation and transpiration. This contributes to water loss from the lysimeter, reducing its water content and weight. The water potential of the lysimeter soil also influences the potential for drainage. If the lysimeter soil has a higher water potential compared to the surrounding environment, water will drain from the lysimeter, reducing its water content and weight. The water potential of the lysimeter soil determines its water holding capacity, soil with a higher water potential has a greater capacity to retain water. Therefore, soils with lower water potentials may reach field capacity more quickly and experience greater runoff or drainage, leading to changes in the water balance. Generally, these sensors have a crucial role to play, for instance, by monitoring soil water content, farmers can determine when to irrigate, how much water to apply, and avoid overwatering or under-watering. EC sensors measure the ability of the soil to conduct electrical currents, which is related

to the soil's salinity and nutrient content. High soil salinity can negatively impact crop growth and yield, as a result, through monitoring soil EC, farmers can identify areas of the field with excessive salt buildup and take corrective actions, such as adjusting irrigation practices or applying soil treatments. On the other side, temperature variability sensors monitor changes in soil temperature over time, temperature plays a critical role in various soil processes, including microbial activity, nutrient availability, and plant growth (Onwuka, 2018). Monitoring temperature variability can help farmers optimize planting and harvesting times, as well as adjusting irrigation schedules based on temperature trends, and mitigate consequences associated with extreme temperature fluctuations. Water potential sensors measure the energy required for water to move within the soil-plant system. This parameter provides insights into the availability of water to plant roots. By monitoring water potential, farmers can assess plant stress levels and water uptake efficiency which aids in optimizing irrigation schedules, ensuring that crops receive adequate water without wasting resources. The ET<sub>a</sub> values measured from the smart field weighing lysimeters were evaluated for accuracy by comparing the irrigation depth measurement from the Onset tipping bucket rain gauge with the irrigation depth measured by the smart field weighing lysimeters. A linear regression approach was applied on the measured irrigation depths from the two devices. The results demonstrated a strong positive  $r=0.84$  value indicates that there is a notable linear relationship between the two datasets. In other words, as the irrigation depths measured by one method increase or decrease, there is a corresponding increase or decrease in the measurements from the other method. This correlation coefficient value suggests a relatively robust association between the two sets of data. The  $R^2=0.7$  value provides additional information about the strength of the correlation. It represents the proportion of variance in the irrigation depths that can be explained by the rain gauge measurements. With an  $R^2$  value of 0.7, it means that 70% of the variability in the irrigation depths can be accounted for by the rain gauge measurements. The value implies that the rain gauge data has a significant influence on the irrigation measurements obtained from the smart field weighing lysimeter. Moreover, the low p-value ( $p<0.005$ ) obtained from the statistical analysis confirms the significance of the relationship between the two methods of measurement, as such the likelihood of obtaining such a strong correlation purely by chance is extremely low. Therefore, the results can be considered highly reliable and meaningful, supporting the practical application of both the rain gauge and lysimeter methods for irrigation monitoring and scheduling.

### 3.6 CONCLUSIONS

The findings from this study have confirmed that the implementation of smart field weighing lysimeters represents a highly effective tool for monitoring water usage, providing invaluable assistance in irrigation scheduling, and optimizing crop water productivity and efficiency. By offering critical insights into crop water requirements, water use efficiency, nutrient management, and soil moisture dynamics, these lysimeters play a vital role in water resource management. Throughout the course of this study, continuous and precise measurements of the water balance components have demonstrated the capabilities of smart field weighing lysimeters in improving agricultural irrigation practices, thereby contributing to the sustainable management of water resources. Moreover, the recorded data which was obtained remotely from the cloud storage system significantly reduced the need for on-site visits, which resemble the technological concept of the Internet of Things (IoT), thereby modernizing agricultural workload and operation costs. One crucial aspect to highlight in this study particularly from literature is the lack of ground actual evapotranspiration data in South Africa and the study area, necessitating further investigation into the water usage of other crop types within the Hartswater area. Smart field weighing lysimeters are becoming important tools in agricultural research and industry by providing ground-based evapotranspiration data at the field scale for validating ET models used at larger scales. They provide real-time opportunities to reduce water losses through ungoverned irrigation

plans. Their ability to create actionable strategies from the data collected has, up until now, been constrained in irrigated farming due to a lack of financial resources and expertise. To alleviate water scarcity, it is specifically advised that smart field weighing lysimeters be targeted to improve scientifically informed decision-making in agricultural water usage management. While the lysimeters employed in this study were not large, it has become evident that future research should explore the application of large lysimeters to assess the water use dynamics of the dominant pecan nut trees under irrigation in the area. This expansion into larger-scale experimentation would offer valuable insights into the irrigation needs and water requirements of major crops in the area. By using these advanced technologies, agricultural water use practices can be improved to ensure the sustainable utilization of water resources, aiding in better decision-making, water conservation, and cost reduction for farmers and the broader agricultural sector.

## CHAPTER 4: EVALUATION OF REFERENCE EVAPOTRANSPIRATION METEOROLOGICAL MODELS

### 4.1 INTRODUCTION

Water use monitoring is one of the major challenges faced globally affecting the availability, control, and distribution of natural water resources amongst various water-reliant users. The lack of monitoring techniques hinders the determination of acceptable ways to reduce the overuse and misuse of the available limited water resources. Agriculture in most countries uses more water than other industries through irrigation practices which are not guided by the actual crop water demands. Water scarcity is one of the significant challenges facing countries and communities in arid and semi-arid zones (Donnenfeld et al., 2018). South Africa is a physically water-scarce country, a condition characterized by a significant disparity between the limited availability of freshwater resources and the growing demands for water across various sectors (Otieno and Ochieng, 2007). This pressing concern has been exacerbated by an interplay of factors such as climatic variations, population growth, industrial development, and agricultural demands (Palmer et al., 2004; Pretorius, 2018). Despite the existing conditions of water scarcity, a more alarming problem is that research has projected that by the year 2025, a substantial majority of regions within South Africa will confront an even more severe and acute state of water scarcity (Otieno and Ochieng, 2007). Looking ahead to the near future, the prospects for water availability become increasingly concerning, the projected intensification of water scarcity comes with serious implications for the nation's socioeconomic, and environmental balance and the sustenance of vital hydrological ecosystems. In South Africa, crop production consumes the highest percentage of the available water resources in the country, reaching over 75%, compared to water allocation to other sectors (Pahlow et al., 2015). Efficient agricultural water management through an increment in water use efficiency and water productivity represents major solutions to avail additional water that can be allocated to increase the cultivated area or be given to other water-using sectors (Keller and Keller, 1995).

One of the most important components of the hydrological cycle is evapotranspiration (ET) which resembles a dual process of soil water and leaf-surface water loss accounting for the total water lost in a cropped environment (Zhang et al., 2023). This phenomenon can be categorized into three distinct groups: Potential evapotranspiration, Actual evapotranspiration, and Reference evapotranspiration. Potential evapotranspiration, as defined by (Irmak et al., 2003), refers to the evaporation of water from extended surfaces of a short green crop covering the ground, unable to resist water flow, and consistently supplied with water. This type of evapotranspiration is constrained and cannot surpass the evaporation from a free-water body, even under identical weather conditions. In contrast, actual evapotranspiration represents the amount of water utilized by an extensively vegetated surface with a crop in an active growth stage, featuring a canopy that covers the soil surface (Bhatt et al., 2019). Lastly, the term reference evapotranspiration was introduced to provide clarity to the potential evapotranspiration definition of a short green crop (Irmak et al., 2003).  $E_{To}$  is fundamental in the determination of crop evapotranspiration ( $E_{Tc}$ ) which represents crop water demand in agricultural environments to aid in irrigation scheduling. However, the estimation of  $E_{To}$  is a complex process influenced by various climatic factors, making it crucial to employ robust models that capture the relationships between meteorological parameters. Moreover, for regions characterized by arid environments like South Africa where water scarcity is a prevalent concern, precise  $E_{To}$  estimation becomes even more imperative.

Interest in accurate quantification of ETo has increased with increased water demands and scarcity challenges particularly in irrigated arid and semi-arid agricultural regions for crop water use modelling (Jafari et al., 2021; Koffi and Komla, 2015; Moeletsi et al., 2013; Yassen et al., 2020). The Food and Agriculture Organization of the United Nations (FAO) Penman-Monteith algorithm has frequently been proposed for estimating ETo, but its accuracy and reliability are hampered by its demand for data requirements in areas with limited data availability such as areas with limited weather stations (Moeletsi et al., 2013). The FAO developed and introduced the standard ETo model Penman-Monteith (PM) which is a combination model to solve irrigation scheduling problems worldwide (Allen, 1998). Although a standard model exists, its limitations cannot be undermined, the PM model was developed based on a reference crop fully watered and continuously growing at a constant height (Allen, 1998). The assumption of crops being under ample supply of water is not true in arid environments with limited precipitations and water resources (Hua et al., 2020). The standard ETo method was developed and validated in humid conditions with stress free crops, its transferability to dry conditions requires local calibrations (Allen, 1998; Pereira et al., 2015). As a result, different empirical micrometeorological models have been developed over the years and are commonly used for estimating ETo to solve the problems of data limitations (Vaughan and Ayars, 2009). The commonly used models are classified into four categories as: radiation models, temperature models, aerodynamic-based models, and combination models for estimating the reference ETo incorporating the relationships between meteorological variables such as solar radiation, wind speed, air temperature, and humidity (Celestin et al., 2020). These models offer the advantage of considering multiple factors that contribute to the evapotranspiration process, providing a holistic understanding of water loss from agricultural land surfaces. Their accuracy, however, remains contingent upon the calibration and validation against localized environmental conditions. The arid regions of South Africa present a unique challenge in ETo estimation due to their distinctive climatic characteristics, marked by high temperatures, limited rainfall, and substantial water deficits. Traditional ETo estimation methods, often derived from meteorological data from distant weather stations, may not accurately capture the nuances of ET dynamics in such environments. Therefore, the development and validation of locally relevant ETo estimation models are essential for effective water management strategies tailored to the region's specific needs.

Different micrometeorological models were developed because of limited availability of data in the areas where they were developed and calibrated. On evaluation of different micrometeorological models, research has demonstrated that different models are usually accurate and applicable under climate conditions at which they were developed and calibrated at (Hargreaves and Samani, 1982; Makkink, 1959). The limitations that arise on transferability of models from one region to another are based on the climatic conditions differences which vary spatially both in space and time (Myeni et al., 2021). As a result, models which are adopted and applied outside their region of origin come with high chances of yielding poor performance. With examples: compared the performance of two temperature-based models namely the Hargreaves and Samani (1985) and the Thornthwaite (1948) to estimate decadal ET in Free State South Africa, their choice was because temperature is the common available variable which is measured in most weather stations of South Africa. They found that the un-calibrated models provided very poor results underestimating ET while the calibrated Hargreaves and Samani model yielded accurate accuracy ranges compared to the calibrated Thornthwaite, the calibration here was based on the FAO's Penman-Monteith model due to lack of measuring devices of ET. A study done by Lu et al. (2018) assessed and compared six potential evapotranspiration methods categorized as Three temperature-based models namely: Thornthwaite (1948), Hamon (1961), and the Hargreaves and Samani (1985) as well as three radiation-based being: Turc (1961), Makkink (1959), and Priestley and Taylor (1972) method at a regional scale in the Southeastern United States. They found big differences amongst different methods with Turc, Priestley-Taylor and Hamon methods performing better than other models.

ETo information is crucial for determination of crop evapotranspiration (ETc) in agriculture (Irmak *et al.*, 2009; Ko and Piccinni, 2009), this information is paramount for scheduling irrigation and managing water resources (Savva and Frenken, 2002). Inaccurate ETo estimations may also result in poor modelling of crop coefficients (Kc) and ETc which would probably result in misleading model outputs affecting the entire irrigation scheduling and water management strategies (Gu *et al.*, 2021; Lea-Cox, 2012; Lian *et al.*, 2018). As a solution, internationally developed ETo models require local validation and calibration against the actual measurements under standard conditions of the environments at which they are being used at (Xing *et al.*, 2008; Kumar *et al.*, 2021). Therefore, the limitations of ground-based measured actual evapotranspiration (ETa) hinder calibrations, development, and validation of ET models in many countries, particularly developing countries (Tang *et al.*, 2012). As a result, many models are applied with no local validation or calibration because of validation data limitation (Landeras *et al.*, 2008; Moeletsi *et al.*, 2013). The biggest gap in ET models is their reliability outside areas which they originated from resulting in ET quantifications being questionable and unsuitable for use as inputs to other models. Validation of ET models in South Africa has been done using data acquired using instruments with known inaccuracies (Dzikiti *et al.*, 2014; Gokool *et al.*, 2018; Gwate *et al.*, 2018; Jovanovic *et al.*, 2015; Majozi *et al.*, 2017; Ramoelo *et al.*, 2014). South Africa is a high climate variable country with most of its regions being semi-arid, arid and small areas which are temperate and hyper-arid (Meadows and Hoffman, 2002). As a result of such conditions, accurate modelling of ETo in irrigated arid agricultural regions through validation, development and calibration of ET models is of utmost significance to enhance water resources monitoring and management. Recently, some researchers have attempted to validate and calibrate ET models based in South Africa integrating satellite and ground data (Dzikiti *et al.*, 2014; Gokool *et al.*, 2018; Gwate *et al.*, 2018; Jovanovic *et al.*, 2015; Majozi *et al.*, 2017; Ramoelo *et al.*, 2014), however; limited work on validation of micrometeorological models have been done. In the studies that have been done, the limitations were the use few models which do not correspond to the areas which they were developed from, instruments with data limitations arising from measurement errors and data gaps due to climate variability. This leaves ET reliability in South Africa being the biggest data gap in the hydrological studies due to ground-based measurement with high-accuracy instruments. A robust model for ET quantification is required to evaluate the water use efficiency. Water use monitoring by applying suitable local calibrated models is an efficient tool to assess water consumption and use efficiency in different land uses apart from agriculture.

The present study aims to bridge the existing gap by evaluating the performance of micrometeorological models in estimating reference evapotranspiration in a South African arid environment using high precision smart field weighing lysimeter. This innovative approach provides real-time and localized data on water consumption by crops, enabling the development of site-specific crop coefficients that can enhance the precision of ETo calculations. By combining the advancements in micrometeorological modelling with the insights gained from smart field weighing lysimeter technology, this research seeks to contribute to the refinement of ETo estimation techniques in arid regions. The outcomes of this study have the potential to inform more efficient irrigation practices, improve water resource management, and ultimately promote sustainable agricultural productivity in the challenging climatic conditions of South African arid environments.

## **4.2 METHODS AND MATERIALS**

### **4.2.1 Study area description.**

The study was carried out on an 18-ha experimental farm owned by the South African Barley Breeding Institute (SABBI) in Hartswater Town, an agricultural area in South Africa along the N18 road in the

Frances Baard District and the Phokwane local municipality in the Northern Cape province. The farm is located at the geographical coordinates Latitude:  $-27.72^{\circ}$  S; Longitude:  $24.74^{\circ}$  E and  $-27.72^{\circ}$  S;  $24.74^{\circ}$  E. The study area is in South Africa's largest irrigation scheme, the Vaalharts Irrigation Scheme, which was established in the early 1930s to alleviate unemployment and poverty (Ojo and Ilunga, 2018). The study area is in the country's arid region, receiving irrigation water predominantly from the Vaal River through the Bloemhof dam and via canals (Ellington *et al.*, 2004). Most farms are irrigated with pivot irrigation systems, though flood irrigation, sprinklers, drip irrigation, and other methods continue to be employed (Pretorius, 2018). Annually, between November and March, the area receives approximately 450 mm of rain on the Taung side and approximately 477 mm on the Jan Kempdorp side (Verwey and Vermeulen, 2011). Temperatures in the area have been recorded as high as  $38.8^{\circ}\text{C}$  and as low as  $-4.4^{\circ}\text{C}$  (Ratshiedana *et al.*, 2023; Verwey and Vermeulen, 2011). Le Roux *et al.* (2007) define the soils in the study area as sandy loam in texture. Salinity has been extensively researched in the area as a major issue with the area's limited groundwater usage (Verwey and Vermeulen, 2011). The area is well-known for its pecan production, but it also grows winter wheat, barley, maize, groundnuts, sorghum, cotton, lucerne, soybeans, tobacco, and other cash crops (Muller and van Niekerk, 2019). Cattle and poultry farming also exist in limited numbers (Maisela, 2007). The study area was chosen based on the availability of weather stations, a suitable arid environment with limited water, and a variety of crops to assess crop water usage.

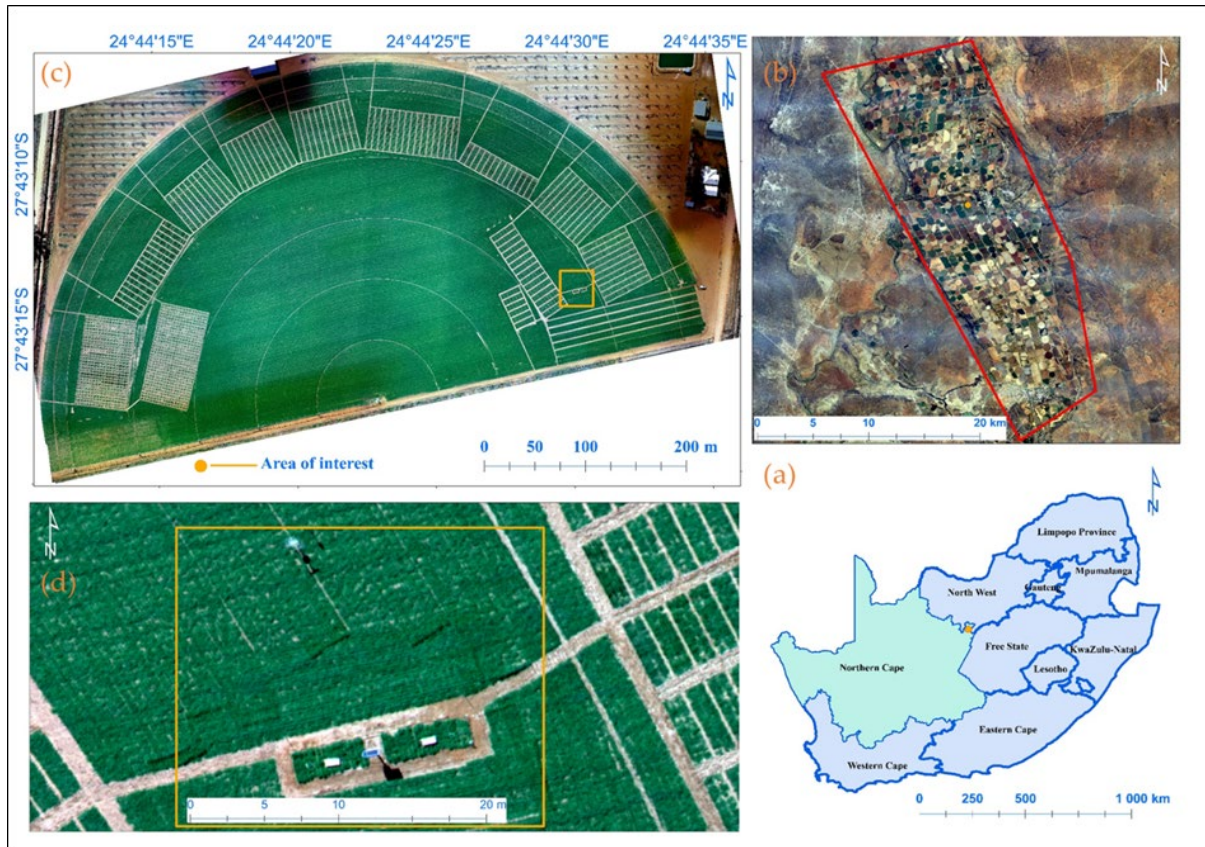
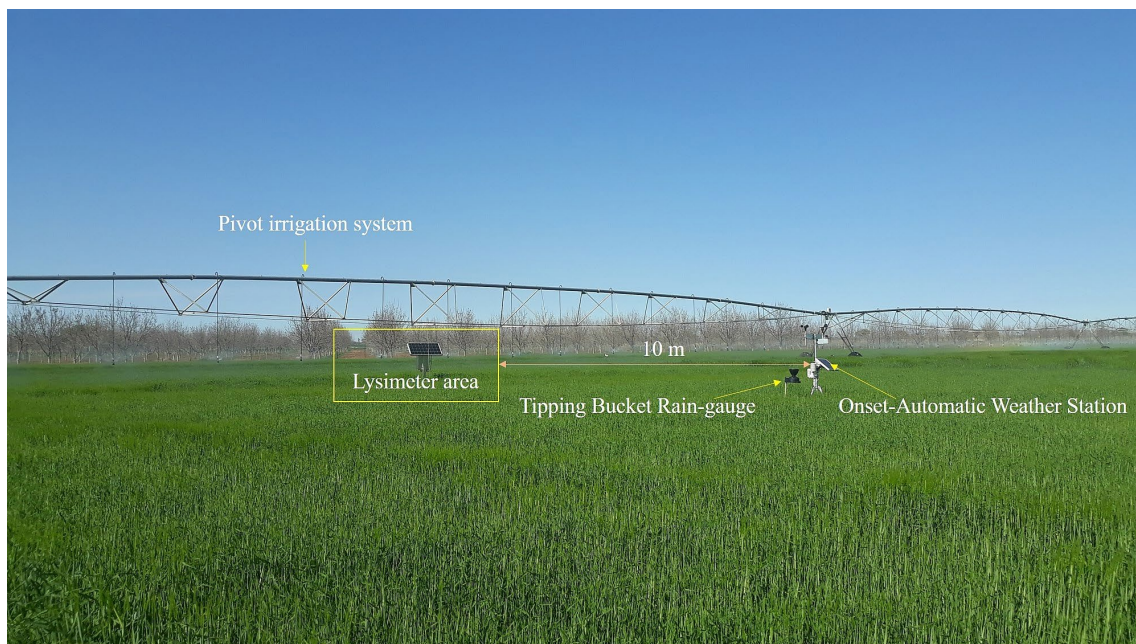


Figure 27: Locality map of the study area.

## 4.2.2 Ground-based data collection.

### 4.2.2.1 Weather data

To obtain a detailed understanding of the local climatic conditions and their impact on ET, an automatic weather station (AWS) was installed in the field. This AWS was a cutting-edge system provided by HOBOlink®, known for its precise measurements and data acquisition capabilities. The AWS was configured to record a range of climatic variables on both an hourly and daily basis. This included temperature, humidity, wind speed, solar radiation, ETo and irrigation depth (mm). The hourly and daily recording intervals were chosen to capture variations throughout the day and to assess overall daily trends in the climate. To enhance the depth of data collection and accuracy, the weather station was integrated with soil moisture and temperature sensors. These sensors were strategically placed in the soil and linked to data loggers, establishing a wireless connection with the AWS. This integration allowed for real-time monitoring of soil conditions, further aiding in the evaluation of ET by considering soil-water dynamics. Moreover, to quantify irrigation and precipitation accurately, the weather station was linked to a tipping bucket rain gauge. This facilitated precise measurements of irrigation and natural precipitation, which are important factors in understanding water availability and usage. Missing data were excluded from this study.



**Figure 28: The visual setting of an automatic weather station in relation to the weather station within the field.**

## 4.2.3 Actual Evapotranspiration Measurement

Two smart field weighing lysimeters were installed within an experimental farm to measure the water balance components important for ET quantification. The installation of smart field weighing lysimeters within an experimental farm was crucial in accurately estimating ETa by measuring the important water

balance components. This process involved carefully placing specialized lysimeter cylinders, each equipped with a weighing balance mechanism, into protective barrels occupying excavated holes in the ground. These protective barrels were sealed with impermeable rubber membranes to isolate the soil column within the lysimeters. To capture detailed data on the soil-water relationship, sensors were placed at multiple depths within each lysimeter. These sensors were designed to measure various essential parameters, including temperature, moisture content, water potential, and soil electrical conductivity. This allowed for a detailed characterization of the soil-water conditions and how they changed over time. The sensors were connected to a data logger system, which recorded data at minute intervals. This frequent data collection ensured a high-resolution dataset, providing insights into the dynamic soil-water interactions. By monitoring and analysing this data, it was possible to quantify the actual crop water usage accurately for the different seasons.

### **4.3 METHODOLOGIES**

This study has identified three types of models used for the estimation of reference evapotranspiration (ET<sub>o</sub>). The reference Evapotranspiration Calculation from Different Micrometeorological Models has been validated using relationships developed at the lysimeter level. The validated relationship between the ET<sub>o</sub> and ET<sub>a</sub> has then been used to extrapolate the measurements at the lysimeter level to larger scale.

**Table 2: Radiation based models for reference evapotranspiration estimated estimation.**

Reference Evapotranspiration Model	Equation	Input Parameters	References
ETO_P-T	$ET_0 = \frac{1}{\lambda} \left[ \alpha \frac{\Delta}{\Delta + \gamma} (R_n - G) \right]$	Elevation; Tmean; SR	(Priestley and Taylor, 1972)
ET-Makkink	$0,7 \left( \frac{Rs}{\lambda} \right) \left[ \frac{\Delta}{\Delta} + \gamma \right] - 0,12$	Elevation; Tmean; SR	(Makkink, 1959)
Turc	$0,0133 * \left( \frac{Tm}{Tm + 15} \right) * (Rs + 50) \text{ if } RH > 50\%$ $0,0133 * \left( \frac{Tm}{Tm + 15} \right) * (Rs + 50) * \left( 1 + 50 - \frac{RH}{70} \right) \text{ (if } RH < 50\%)$	Tmean; SR; RHmean	(Turc, 1961)
Irmak_Rn	$-0,611 + 0,149 * Rs + 0,079Tmean$	SR; Tmean	(Irmak et al., 2003)
Irmak_Rs	$(3,75 + 0,503u2)(es - ea)$	SR; Tmean	(Irmak et al., 2003)
Jensen-Haisen	$Rs (0.025 * T + 0.08)$	Tmean; SR	(Jensen and Haise, 1963)
Tabari 1	$-0.642 + 0.174Rs + 0.0353Tmean$	Tmean; SR	(Tabari et al., 2013)
Tabari 2	$-0.478 + 0.156Rs - 0.0112Tmax + 0.0733Tmin$	SR; Tmax; Tmin.	(Tabari et al., 2013)
Caprio	$(0,01092708 * T) + (0,0060706 * Rs)$	Tmean; SR	(Caprio, 1974)

**Table 3: Aerodynamic based models for reference evapotranspiration estimated estimation.**

Reference Evapotranspiration Model	Equation	Input Parameters	References
ET_Albrecht	$(0.1005 + 0.297 * u_2) * (e_s - e_a)$	Tmax; Tmin; THmax; MeanU2; RHmin	(Albrecht, 1950)
Trabert	$0,408 * (0,3075 * \sqrt{U_2}u) * (e_s - e_a)$	Tmax; Tmin; RHmax; MeanU2; RHmin	(Trabert, 1896)
Meyer	$(3,75 + 0,503u_2)(e_s - e_a)$	Tmax; Tmin; RHmax; MeanU2; RHmin.	(Meyer, 1926)
wmo	$(1,298 + 0,934u_2)(e_s - e_a)$	Tmax; Tmin; RHmax; MeanU2; RHmin.	(WMO, 1996)
ROhWER	$(3,3 + 0,891u_2)(e_s - e_a)$	Tmax; Tmin; RHmax; MeanU2; RHmin	(Rohwer, 1931)
Brockamp-Wenner	$(0,543u_2^{0,456})(e_s - e_a)$	Tmax; Tmin; RHmax; MeanU2; RHmin	(Brockamp and Wenner, 1963)
Penman	$0.35 * (1 + 0,24 * u_2) * (e_s - e_a)$	Tmax; Tmin; RHmax; MeanU2; RHmin	(Penman, 1948)
Mahringer	$(0,286u_2^{0,5})(e_s - e_a)$	Tmax; Tmin; RHmax; MeanU2; RHmin	(Mahringer, 1970)
Dalton	$(3,648 + 0,7223u_2)(e_s - e_a)$	Tmax; Tmin; RHmax; MeanU2; RHmin.	(Dalton, 1802).

**Table 4: Combination models for reference evapotranspiration estimated estimation.**

Reference Evapotranspiration Model	Equation	Input Parameters	References
ETO_P-M FAO-56	$ET_0 = \frac{0.408\Delta(R_a - G) + \gamma \left( \frac{900}{T + 273} \right) u_2 (e_s - e_a)}{\Delta + \gamma(1 + 0.34u_2)}$	Latitude; Tmean; Tmax; Elevation; Tmin; RHmean; RHmax; MeanU2; SR ; RHmin.	(Allen, 1998)

**Table 5: Temperature based models for reference evapotranspiration estimated estimation.**

Reference Evapotranspiration Model	Equation	Input Parameters	References
Ivanov	$0,00006 * (25 + T_{mean})^2 * (100 - RH)$	Mean Temperature; Mean Relative Humidity	(Romanenko, 1961)
Trajkovic	$\frac{[0,0023Ra(T_{mean} + 17,8)(T_{max} - T_{min})^{0,424}]}{\lambda}$	Latitude; Tmean; Tmax; Tmin	(Trajkovic, 2007)
Schendel	$16 * \left(\frac{T_{mean}}{RH}\right)$	Tmean; RH	(Schendel, 1967)
Ravazzani	$(0.817 + 0.00022 * Z)0.0023 Ra(T_{mean} + 17.8)(T - T_{min})^{0.5}$	Elevation; Tmean; Tmax; Tmin;	(Ravazzani et al., 2012)
Hamon	$k(0.1651 * 216,7)N * \left(\frac{es}{T + 272,3}\right)$	Tmean; Tmax; Sunshine Hours	(Hamon, 1961)
Papadakos	$2,5(es - ea)$	Tmax; Tmin	(Papadakis, 1965)
Droogers and Allen	$0.003 * (T_{mean} + 20)(T_{max} - T_{min})^{0,4}Ra$	Latitude; Tmean; Tmax; Tmin.	(Droogers and Allen, 2002)
Calibrated Christiansen	$0.53 * \left(\frac{Rs}{\lambda}\right)$	RS	(Abtew, 1996)
Hargreaves and Allen	$(0.0135T_{mean} + 0.2403) * \frac{Rs}{\lambda}$	Tmean; SR	(Hargreaves and Allen, 2003)
HS	$\frac{[0,0023 * Ra(T_{mean} + 17,8)(T_{max} - T_{min})^{0,5}]}{\lambda}$	Latitude; Mean Temperature; Maximum Temperature; Minimum Temperature.	(Hargreaves and Samani, 1985)

### 4.3.1 Radiation-Based Models

The radiation-based evapotranspiration methods revolve around understanding how water stored in the soil and available in plant leaves escapes into the atmosphere. This process is primarily powered by the energy from sunlight, which causes the water to evaporate. These methods carefully consider three factors which are solar radiation ( $R_s$ ), temperature ( $T$ ), and humidity ( $R_h$ ). The core idea behind these methods is that as solar radiation becomes more intense, it provides more energy that leads to increased evaporation of available water. This results in more water being lost from both the ground and plants. In these radiation-based methods, the key principle is that higher levels of solar radiation correspond to a greater potential for evapotranspiration. When temperature is incorporated into these methods, its role expands beyond just heating the air. It also warms up the surfaces of the ground and plants. Warmer surfaces prompt a higher rate of water turning into vapor and moving into the air (Caprio, 1974; Jensen and Haise, 1963). While solar radiation and temperature are critical factors, scientists have introduced an additional element into these methods which is relative humidity. Relative humidity indicates how much moisture is present in the air compared to the maximum amount it can hold at a specific temperature. This becomes particularly relevant in dry regions, where the air doesn't hold much moisture. In such cases, more water vapor can be drawn from surfaces into the air, which further increases the potential for evapotranspiration (Turc, 1961).

### 4.3.2 Temperature-Based Models

Temperature-based methods revolve around temperature as a key driving factor for evapotranspiration. These methods focus on highlighting the crucial role that temperature plays in calculating potential evapotranspiration (PET), while also acknowledging the potential effects of other factors. In these methods, the primary emphasis is placed on temperature as the main factor that determines evapotranspiration. This perspective understands that the rate at which water vapor moves from the ground into the air is mostly controlled by changes in temperature. As temperatures increase, the energy available for water molecules to change from a liquid to a vapor state also increases, leading to a greater likelihood of evapotranspiration. The radiation-based methods include another factor which is relative humidity (RH). This provides evidence that the presence of moisture in the air can significantly impact how quickly evapotranspiration occurs. These methods consider how humidity levels can either help or hinder the movement of water molecules from the ground into the air. When humidity is high, evapotranspiration might be limited since the air is already saturated with moisture. On the other hand, when humidity is low, the process of evapotranspiration can be enhanced. While temperature remains a central focus, the influence of potential radiation (PR) is also considered in these methods.

### 4.3.3 Aerodynamic-Based Models

The evapotranspiration methods based on mass transfer are designed by considering wind speed ( $u$ ), temperature, and relative humidity within a general framework. These methods share a foundational belief that the process of evapotranspiration is closely tied to how the air moves and interacts, while also factoring in the dryness of the atmosphere. This dryness is measured by the difference between the vapor pressure of the air when it's completely saturated ( $e_s$ ) and the actual vapor pressure ( $e_a$ ). In all these approaches, the effect of vapor pressure deficit is corrected by including a component related to the speed of the wind ( $u$ ). This helps account for how the air is moving. The formulas used in these methods to estimate evapotranspiration through mass transfer consider a wide range of factors and aspects. Each formula takes into consideration the complex connections between how the air moves, the temperature, and the humidity. This way, they capture the intricate processes that control ET. These unique formulas provide a detailed insight into how these different factors come together and affect how quickly evapotranspiration happens.

#### 4.3.4 Combination Models

The combination-based evapotranspiration models are structured with a broad perspective, considering various factors that influence the estimation of potential evapotranspiration. These models consider parameters like solar radiation (Rs), wind speed (u), air temperature (T), and relative humidity (RH), which together shape the evapotranspiration process. Within these methods, solar radiation plays a crucial role by providing energy to the earth's surface. The energy affects temperature changes, which in turn impact the potential for water vapor to be released into the air through evapotranspiration. The relationship between solar radiation and temperature creates a dynamic balance where higher radiation levels generally lead to increased temperatures and evapotranspiration rates. Wind speed is another significant factor in these models, influencing the speed of air movement over surfaces. Higher wind speeds facilitate the transfer of moisture from land and plants to the atmosphere, thereby increasing potential evapotranspiration rates. The interaction between wind speed and other factors enhances the accuracy of estimations. Air temperature directly affects the energy available for evaporation and transpiration. Higher temperatures accelerate the transition of water molecules from liquid to vapor state. Incorporating air temperature into the model establishes a strong connection between thermal conditions and evapotranspiration potential. Relative humidity introduces the element of moisture content in the air, which significantly impacts evapotranspiration. These methods consider how varying levels of relative humidity affect vapor pressure gradients, influencing the rate of water vapor movement from surfaces to the atmosphere. By integrating these parameters comprehensively, the combination evapotranspiration model provides a more detailed and accurate understanding of the complex processes governing potential evapotranspiration.

#### 4.3.5 Calculation of the Actual Evapotranspiration

The water balance equation is used to calculate evapotranspiration:

$$ET = P - R - \Delta S$$

ET is the water lost through evaporation (E) and plant transpiration (T) while P represents Precipitation and R denotes Rainfall while  $\Delta S$  denotes change in storage. Precipitation in this situation was taken as irrigation input, another input was water pumped back into the systems by tensiometers when the conditions were to overlap. Change in storage was measured by the water accumulation in the drainage system changes. The actual evapotranspiration from lysimeters is calculated as (Doležal et al., 2018).

$$ET_a = \frac{(LYW_n + SWW_n) - (LYW_{n+1} + SWW_{n+1})}{Lysimeter\ Area}$$

Where  $ET_a$  (mm)  $ET_a$  is the actual crop evapotranspiration,  $LYW_n$ =Lysimeter Weight at nth time,  $SWW_n$ =Drainage Weight at nth time,  $LYW_{n+1}$ =Lysimeter Weight at n+1 time,  $SWW_{n+1}$ =Drainage Weight at n+1 time.

$$Lysimeter\ Area = \pi r^2 = \pi \times (0.15)^2 = 0.0707m^2$$

When the drainage is zero, evapotranspiration can be obtained directly by multiplying the change in storage with the density of water which can be calculated as:

$$1\ kg\ of\ seepage\ water = 0.001m^3 = \frac{0.001m^3}{0.0707m^2} = 0.014\ m = 14\ mm$$

#### 4.3.6 Development of a relationship between $ET_a$ and $ET_o$

The  $ET_a$  obtained from the smart field weighing lysimeter was directly compared to the  $ET_o$  obtained from various micrometeorological models using simple linear regression model to establish a relationship for

computing ETc in areas with no lysimeters. The developed conversion equations were used for obtaining ETa in other areas within the scheme following the equation:

$$ETa = M * ET_o \pm C$$

### 4.3.7 Statistical Analysis

Descriptive statistics including mean, median, standard deviation, and range for both ETa and ETo datasets were computed. Furthermore, the correlation coefficient between ETa and each ETo estimate to assess the strength and direction of the relationship were conducted. A linear regression model to quantify the relationship between ETa and each ETo estimate was also conducted.

#### 4.3.7.1 Bias and Error Analysis

The models were evaluated for the bias and errors associated with each model by comparing model estimates with lysimeter measurements using metrics such as Mean error percentage (MAPE%), root mean square error (RMSE), explained variance (EV) and R<sup>2</sup>.

**Table 6: Statistical performance indicators used for validation of different ETo models.**

Performance evaluation measure	Denotation	Equation
Root mean square error	RMSE	$RMSE = \sqrt{\frac{\sum_{i=1}^N (y_i - y'_i)^2}{N}}$
Explained variance	EV	$EV = \frac{\sum(\hat{y}_i - \bar{Y})^2}{\sum(y_i - \bar{Y})^2}$
Mean error percentage	MAPE	$MAPE = \left(\frac{1}{n}\right) \times \sum \left( \left  \frac{(Actual - Estimated)}{Actual} \right  \right) \times 100$
Coefficient of determination	R <sup>2</sup>	$r^2 = 1 - \frac{\sum_{i=1}^N (y_i - y'_i)^2}{\sum_{i=1}^N (y_i - y''_i)^2}$

Where: N denotes the total number of data observations, y<sub>i</sub> represents the actual observed value for the i<sup>th</sup> data point, ŷ<sub>i</sub> represents the estimated value for the i<sup>th</sup> data point, Σ denotes the sum over all data points, |x| represents the absolute value of x, "Actual" being the actual value of the data point; and "Estimated" being the estimated value of the data point. Σ(ŷ<sub>i</sub> - Ȳ)<sup>2</sup> is the sum of the squared differences between the estimated values generated by the model and the mean of the dependent variable; and Σ(y<sub>i</sub> - Ȳ)<sup>2</sup> is the is the sum of the squared differences between each data point and the mean of the dependent variable. The actual values in this study are the actual measured values by the smart field weighing lysimeter while the estimated values represent the values estimated from various micrometeorological models.

#### 4.3.7.2 Model evaluation and ranking.

The assessment was conducted for the performance of each micrometeorological model based on its ability to accurately estimate ETa compared to lysimeter measurements. The models were ranked based on the statistical metrics, computational efficiency, and practical applicability.

## 4.4 RESULTS

Different ETo models were assessed to determine the performance of each model considering the indicators highlighted in table 6.

### 4.4.1 Calculated metrics at the field level during various seasons

Tables (7-22) represent the performance rankings of various micrometeorological models for estimating ETo in different crop seasons. Each table presents the performance metrics of different models categorized by their underlying principles as radiation-based, aerodynamic-based, temperature-based, and combination models. The metrics include RMSE, Bias, EV, MAPE, MAE, R, and R<sup>2</sup>. Lower values of RMSE, Bias, and MAE indicate better model performance, while higher values of EV, R, and R<sup>2</sup> indicate stronger correlations between observed and estimated ETo values.

**Table 7: Radiation-based models ranked according to metrics in the 2019 Barley Season.**

Model	RMSE	Bias	EV	MAPE	MAE	R	R <sup>2</sup>
ETOETO_P-T	2.4	2.1	58.82	29.5	2.11	0.86	0.74
ET-Makkink	3.16	2.8	69.88	38.24	2.80	0.84	0.70
Tabari 1	3.76	-1.76	0.07	38.29	2.98	0.03	0.001
Turc	4.56	4.39	75.58	66.72	4.39	0.87	0.76
Jensen-Haisen	5.06	4.28	72.566	63.19	4.28	0.85	0.73
Caprio	6.45	6.34	73.34	95.28	6.34	0.86	0.73
Tabari 2	5.06	3.97	55.19	51.41	3.97	-0.74	0.55
Irmak_Rn	5.08	-3.23	47.79	75.58	4.79	-0.69	0.48
Irmak_Rs	6.28	-4.42	39.59	95.41	6.06	-0.63	0.40

**Table 8: Aerodynamic-based models ranked according to metrics in 2019 Barley Season.**

Model	RMSE	Bias	EV	MAPE	MAE	R	R <sup>2</sup>
Penman-Monteith	2.026	-1.31	72	25.11	1.7	0.85	0.72
Meyer	2.18	1.23	46.08	30.26	1.84	0.68	0.46
WMO	2.86	-2.27	51.25	37.24	2.51	0.72	0.51
ROhWER	2.92	0.6	0.53	34.71	2.38	0.07	0.01
Dalton	3.39	0.68	2.55	38.58	2.68	-0.16	0.03
Brockamp_Wenner	5.1	1.97	1.28	62.96	4.17	-0.11	0.01
Mahringer	5.83	-5.71	75.00	86.66	5.71	0.86	0.75
Albrecht	5.89	-0.23	10.279	58.1	4.28	-0.32	0.1
Tabert	6.76	-6.52	73.571	95.15	6.52	0.86	0.74

**Table 9: Temperature based models ranked according to metrics in 2019 Barley Season.**

Model	RMSE	Bias	EV	MAPE	MAE	R	R <sup>2</sup>
Hargreaves and Allen	1.79	-0.26	57.17	20.50	1.44	0.76	0.57
HS	2.02	-1.00	47.57	19.93	1.49	0.69	0.48
Ivanov	2.23	-1.82	7.98	29.23	1.92	0.28	0.08
Hamon	2.53	-2.16	77.85	33.29	2.19	0.88	0.78
Schendel	2.62	0.79	68.33	26.94	1.94	0.83	0.68

Smart Field Lysimeter for ET-Sensing

<b>Calibrated Christiansen</b>	3.57	3.25	0.65	57.55	3.25	0.01	0.00
<b>Papadakos</b>	3.76	1.49	27.29	47.00	3.12	-0.52	0.27
<b>Trajkovic</b>	5.91	2.76	38.04	76.89	5.21	-0.62	0.38
<b>Droogers and Allen</b>	7.75	7.50	21.53	124.56	7.50	0.45	0.21
<b>Ravazzani</b>	8.33	6.38	26.74	126.30	8.05	-0.52	0.27

**Table 10: Combination model metrics in 2019 Barley Season.**

<b>Model</b>	<b>RMSE</b>	<b>Bias</b>	<b>EV</b>	<b>MAPE</b>	<b>MAE</b>	<b>R</b>	<b>R<sup>2</sup></b>
ET_PM	3.85	5.78	63.78	13.98	0.93	0.8	0.64

**Table 11: Radiation based ranked according to metrics in 2020 Maize Season.**

<b>Model</b>	<b>RMSE</b>	<b>Bias</b>	<b>EV</b>	<b>MAPE</b>	<b>MAE</b>	<b>R</b>	<b>R<sup>2</sup></b>
ETo_P_T	4.39	0.20	19.75	-0.54	39.41	0.82	0.20
ET_MK	5.76	0.32	31.56	-1.65	52.95	4.96	0.32
Turc	7.92	0.33	32.65	-4.00	76.71	7.25	0.33
Irmak_Rn	4.15	0.19	19.05	-0.37	32.70	1.94	0.19
Irmak_Rs	5.35	0.33	33.02	-1.28	46.25	4.46	0.33
Jensen_and_Haise	5.89	0.34	33.71	-1.77	60.76	-3.86	0.34
Tabari_1	5.79	0.32	31.82	-1.67	52.47	4.98	0.32
Tabari_2	5.89	0.32	32.43	-1.77	52.30	5.07	0.32
Caprio	9.91	0.34	33.06	-6.83	99.93	9.26	0.34

**Table 12: Aerodynamic based models ranked according to metrics in 2020 Maize Season.**

<b>Model</b>	<b>RMSE</b>	<b>Bias</b>	<b>EV</b>	<b>MAPE</b>	<b>MAE</b>	<b>R</b>	<b>R<sup>2</sup></b>
Meyer	3.95	1.79	19.33	35.31	3.17	0.44	0.19
Dalton	3.92	1.44	19.26	36.40	3.20	0.43	0.19
ROWER	4.02	1.62	17.74	36.40	3.25	0.42	0.18
ET_Albrecht	5.12	0.49	11.62	48.81	4.19	0.35	0.12
Brockamp Wenner	5.07	-1.14	16.03	50.97	4.11	0.39	0.16
WMO	5.90	4.86	15.09	51.20	4.94	0.39	0.15
Penman	5.81	4.87	19.83	50.36	4.94	0.45	0.20
Mahringer	9.36	8.71	14.96	93.62	8.71	0.39	0.15
Tabert	9.67	9.02	15.37	97.20	9.02	0.39	0.15

**Table 13: Temperature based models ranked according to metrics in 2020 Maize Season.**

<b>Model</b>	<b>RMSE</b>	<b>Bias</b>	<b>EV</b>	<b>MAPE</b>	<b>MAE</b>	<b>R</b>	<b>R<sup>2</sup></b>
HS	4.29	2.94	27.06	29.75	3.27	0.52	0.27
Hargreaves_and_Allen	5.72	4.72	18.63	50.55	4.87	0.43	0.19
Ivanov	4.57	-3.44	28.06	57.86	3.94	0.53	0.28
Schendel	4.64	3.42	21.72	33.99	3.64	0.47	0.22
Ravazzani	7.76	-7.10	27.03	98.39	7.10	0.52	0.27
Hamon	5.25	4.10	23.06	38.61	4.19	0.48	0.23

Model	RMSE	Bias	EV	MAPE	MAE	R	R <sup>2</sup>
Hansen	16.70	-16.31	4.05	224.07	16.31	-0.20	0.04
Calibrated_Christiansen	3.47	-0.54	31.05	33.63	2.42	0.56	0.31
Droogers_and_Allen	7.73	-7.11	27.72	99.70	7.11	0.53	0.28
Trajkovic	3.97	-1.44	34.06	40.23	2.93	0.58	0.34
Papadakis	5.99	5.08	19.73	52.26	5.12	0.45	0.20

Table 14: Combination model metrics in 2020 Maize Season.

Model	RMSE	Bias	EV	MAPE	MAE	R	R <sup>2</sup>
Penman-Monteith	2.85	3.41	44.34	60.66	1.89	0.66	0.44

Table 15: Radiation based ranked according to metrics in 2020 Barley Season.

Model	RMSE	Bias	EV	MAPE	MAE	R	R <sup>2</sup>
ETo_P_T	0.85	0.48	61.82	13.48	0.61	0.79	0.62
ET_MK	1.15	0.91	61.03	20.73	0.93	0.78	0.61
Tabari_1	0.94	0.61	20.07	15.81	0.71	0.76	0.57
Tabari_2	1.51	1.34	61.04	30.84	1.34	0.78	0.61
Turc	2.87	2.73	57.08	65.01	2.73	0.76	0.58
Irmak_Rs	6.31	-6.17	62.73	154.72	6.17	0.80	0.63
Irmak_Rn	5.85	-5.75	56.83	146.12	5.75	0.75	0.57

Table 16: Aerodynamic based models ranked according to metrics in 2020 Barley Season.

Model	RMSE	Bias	EV	MAPE	MAE	R	R <sup>2</sup>
Penman	1.31	0.73	19.63	20.84	0.93	0.31	0.20
Meyer	2.18	-1.51	19.32	49.64	1.85	0.18	0.19
Dalton	2.43	-1.71	18.77	54.67	2.03	0.13	0.19
ROWER	2.36	-1.51	17.64	52.07	1.94	0.09	0.18
Wmo	1.90	1.03	15.06	35.18	1.53	-0.04	0.15
ET_Albrecht	3.89	-1.69	12.36	73.03	2.75	-0.13	0.12
Brockamp_Wenner	4.28	-3.17	15.38	91.51	3.40	-0.03	0.16
Mahringer	3.91	3.76	14.91	90.05	3.76	-0.05	0.15
Tabert	4.12	3.98	14.62	95.64	3.98	-0.05	0.15

Table 17: Temperature based models ranked according to metrics in 2020 Barley Season.

Model	RMSE	Bias	EV	MAPE	MAE	R	R <sup>2</sup>
Ivanov	1.22	0.33	6.37	22.26	0.95	0.25	0.06
Hargreaves_and_Allen	1.23	0.19	7.57	23.22	0.99	0.28	0.08
HS	1.25	0.45	7.33	22.28	1.01	0.30	0.07
Papadakis	1.39	0.89	10.17	22.31	1.01	0.31	0.10
Hamon	1.44	1.00	9.88	23.72	1.10	0.32	0.10
Trajkovic	4.75	-4.59	43.55	116.96	4.59	0.66	0.44

Model	RMSE	Bias	EV	MAPE	MAE	R	R <sup>2</sup>
Calibrated_Christiansen	4.85	-4.74	49.43	121.56	4.74	0.70	0.49
Droogers_and_Allen	7.34	-7.17	44.02	181.02	7.17	0.66	0.44
Ravazzani	7.71	-7.52	43.12	189.73	7.52	0.66	0.43
Schendel	8.72	-7.63	19.43	50.63	7.87	0.42	0.19

Table 18: Combination model metrics in 2020 Barley Season.

Model	RMSE	Bias	EV	MAPE	MAE	R	R <sup>2</sup>
Penman-Monteith	4.09	3.90	62.73	8.90	0.70	0.79	0.63

Table 19: Radiation based models ranked according to metrics in 2021 Soybean Season.

Model	RMSE	Bias	EV	MAPE	MAE	R	R <sup>2</sup>
ET-MK	3.68	-1.55	16.02	34.82	2.47	0.40	0.16
ETo_P-T	3.74	-1.72	19.05	31.91	2.40	0.43	0.19
Tabari 1	3.70	-1.50	14.03	35.26	2.49	0.37	0.14
Irmak_Rs	3.49	-1.08	18.89	38.21	2.47	0.43	0.19
Turc	5.11	-3.78	17.97	57.37	3.78	0.42	0.18
Jensen and Haise	7.45	6.31	7.18	162.48	6.62	-0.26	0.07
Irmak_Rn	7.08	4.24	6.78	159.92	6.26	-0.26	0.07
Tabari 2	8.76	2.00	4.79	198.03	7.73	-0.21	0.05
Caprio	6.78	41.00	27.46	99.87	5.71	0.52	0.27

Table 20: Aerodynamic-based models ranked according to metrics in 2021 Soybean Season.

Model	RMSE	Bias	EV	MAPE	MAE	R	R <sup>2</sup>
Meyer	2.78	0.054	42.2	0.374	2.05	0.650	0.422
Dalton	2.77	0.216	43.4	0.383	2.08	0.659	0.434
ROWER	2.74	-0.03	44.3	0.344	1.96	0.665	0.443
ET_Albrecht	3.35	-0.29	43.3	0.378	2.29	0.658	0.433
wmo	3.86	-2.68	45.2	0.426	2.71	0.673	0.452
Brockamp-Wenner	3.54	1.28	46.0	0.467	2.53	0.678	0.460
Penman	3.69	-2.16	37.2	0.320	2.35	0.610	0.372
Tabert	6.61	-5.56	45.8	0.970	5.56	0.677	0.458

**Table 21: Temperature-based models ranked according to metrics in 2021 Soybean Season.**

Model	RMSE	Bias	EV	MAPE	MAE	R	R <sup>2</sup>
Calibrated_Christiansen	3.47	-0.54	31.05	33.63	2.42	0.557	0.31
Hargreaves_and_Allen	3.97	-1.44	33.46	40.23	2.93	0.579	0.34
HS	4.29	2.94	27.43	29.75	3.27	0.524	0.27
Schendel	4.64	3.42	22.2	34.00	3.64	0.472	0.22
Papadakis	5.99	5.08	20.2	52.26	5.12	0.449	0.20
Hamon	5.25	4.10	23.31	38.61	4.19	0.483	0.23
Ivanov	5.72	4.72	18.7	50.55	4.87	0.432	0.19
Droogers_and_Allen	7.73	-7.11	28.1	99.70	7.11	0.530	0.28
Ravazzani	7.76	-7.10	27.4	98.39	7.10	0.524	0.27

**Table 22: Combination model metrics in 2021 Soybean Season.**

Model	RMSE	Bias	EV	MAPE	MAE	R	R <sup>2</sup>
Penman-Monteith	5.78	9.22	6.41	29.91	2.23	0.004	0.06

#### 4.4.2 Overall model rankings based on compromise programming ranking.

Tables (23-25) present the overall rankings of micrometeorological models based on compromise programming (CP) ranking methodology. The rankings are segmented into three categories: radiation-based models, aerodynamic-based models, and temperature-based models.

**Table 23: Radiation based models ranking based on CP.**

Model	RMSE Rank	Bias Rank	EV Rank	MAPE Rank	MAE Rank	R Rank	R <sup>2</sup> Rank	Weighted Sum	Rank
ETo_P-T	1	1	7	1	1	5	4	3.56	1
ET-Makkink	3	3	6	2	3	4	6	3.78	2
Tabari 1	5	6	1	3	5	1	1	3.72	3
Turc	7	7	5	6	7	6	7	5.44	4
Jensen-Haisen	8	8	4	5	6	3	5	4.97	5
Caprio	9	9	3	7	8	7	5	6.11	6
Tabari 2	8	5	8	4	4	2	3	4.52	7
Irmak_Rn	6	2	9	8	2	8	8	4.88	8
Irmak_Rs	4	4	10	9	9	9	9	6.91	9

**Table 24: Aerodynamic-based models ranking based on CP.**

Model	RMS E Rank	Bias Rank	EV Rank	MAPE Rank	MAE Rank	R Rank	R <sup>2</sup> Rank	Weighted Sum	Rank
Meyer	2	3	4	2	2	2	2	2.0	1
WMO	3	2	3	3	3	3	3	15.88	2
Penman	1	4	2	1	1	1	1	17.5	3
Mahringer	7	8	1	7	7	5	5	31.38	4
ROhWER	4	6	8	4	4	6	7	31.63	5
Dalton	5	5	7	5	5	7	8	33.5	6
Albrecht	8	7	5	8	8	4	6	36.0	7
Brockamp_Wenner	6	1	6	6	6	8	9	40.5	8
Tabert	9	9	9	9	9	9	9	55.63	9

**Table 25: Temperature based models ranking based on CP.**

Model	RMSE Rank	Bias Rank	EV Rank	MAPE Rank	MAE Rank	R Rank	R <sup>2</sup> Rank	Weighted Sum	Rank
Hargreaves and Allen	1	3	1	1	1	1	1	8.25	1
Ivanov	5	4	3	4	3	3	3	24.5	2
HS	4	5	5	8	1	2	2	26.125	3
Schendel	2	2	4	5	2	4	4	26.5	4
Papadakis	3	4	6	6	3	3	3	27.5	5
Trajkovic	8	8	1	1	8	1	1	28.375	6
Droogers and Allen	10	10	4	4	10	1	1	39.125	7
Calibrated Christiansen	9	9	2	2	9	8	8	47.25	8
Ravazzani	11	11	3	3	11	1	1	40.75	9
Hamon	7	7	7	7	7	8	8	50.0	10

## 4.5 COMBINATION MODEL SELECTION ACROSS SEASONS

Penman-Monteith was ranking based on its occurrence four times to select the best model performance season. The Penman-Monteith model, employed during the 3rd season, showed the following performance metrics: RMSE of 4.09; a Bias of 3.90 EV of 62.73; MAPE of 8.90; a MAE of 0.70; an R value of 0.79, and an R<sup>2</sup> value of 0.63.

### 4.5.1 Final ranking and selection of radiation-based models across seasons.

Figure 27 illustrates the ranking of different micrometeorological models for estimating ET<sub>0</sub>. Lower rank values signify models with desirable performance, while higher ranks indicate poorer performance in ET<sub>0</sub> estimation. In essence, the figure provides a visual representation of how each model compares in terms of accuracy and reliability for estimating reference evapotranspiration.

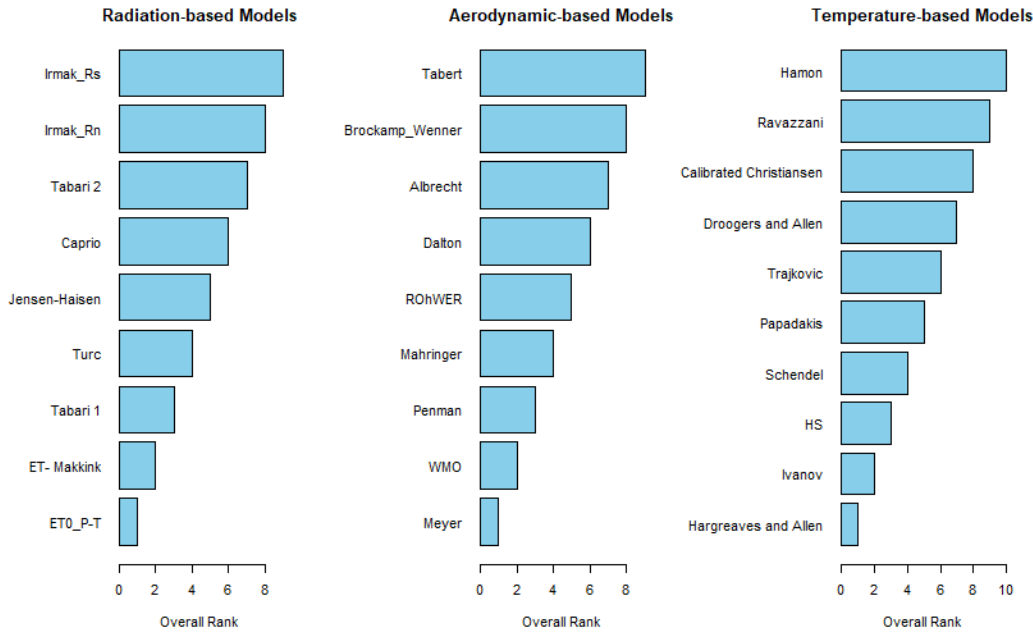


Figure 29: Model rankings throughout the seasons.

4.5.2 Final selection of the best models for estimating ET<sub>o</sub> in the arid environment.

Among all the models described on tables showing various micrometeorological models, Penman-Monteith, Hargreaves and Allen, and Makkink models have shown high significant relationship between the ET<sub>o</sub>, and ET<sub>a</sub> measured at the local level (Figure 27).

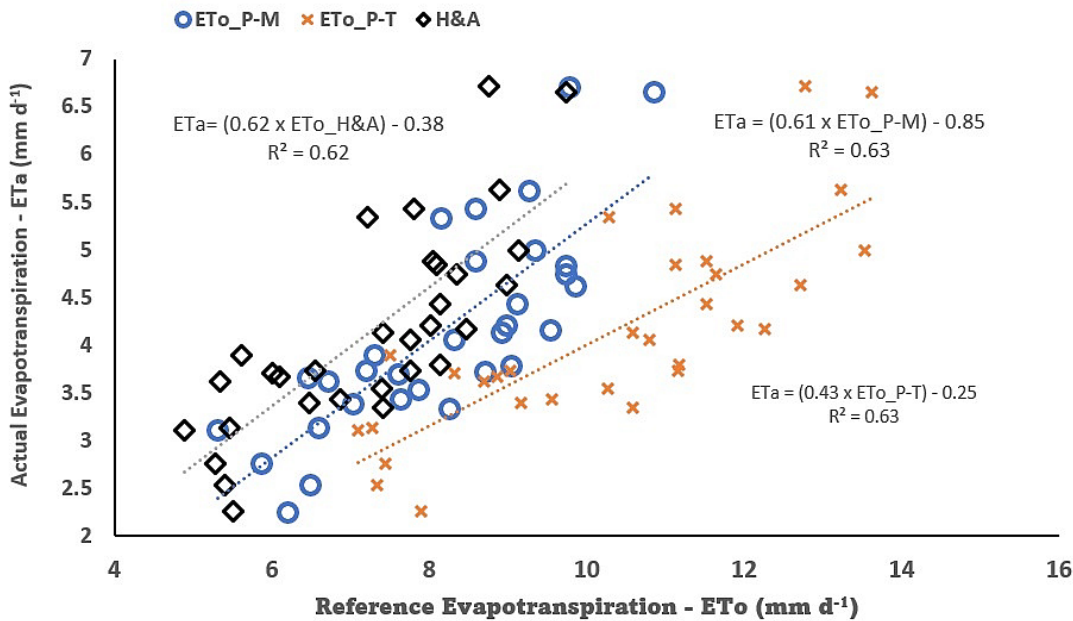


Figure 30: Selected models (Blue is the Penman-Monteith model, black is the Hargreaves and Allen model while orange is the Makkink model).

## 4.6 DISCUSSIONS

Water scarcity is a pressing global issue, compounded by the agricultural sector's excessive water usage, alongside factors like climate change and population growth. Effective management and allocation of available freshwater resources are crucial in addressing this challenge. Central to this effort is accurately determining water balance components, particularly ET, which represents a significant portion of water loss. However, precise estimation of ET throughout the season is challenging and often requires costly measuring devices. To mitigate the cost constraints associated with high-accuracy devices, this study utilized a smart field weighing lysimeter to measure  $ET_a$ , which represent  $ET_o$  multiplied by crop coefficients at different phenological stages. Correlations between  $ET_a$  and  $ET_o$  were established using lysimeter data alongside various micrometeorological models integrated with weather station observations. This correlation aimed to facilitate  $ET_a$  determination in areas lacking expensive lysimetric devices, particularly in arid environments. The study evaluated 28 micrometeorological models using data from a high-resolution smart field weighing lysimeter across four seasons, encompassing various crop types such as barley, maize, and soybean. Assessing of  $ET_o$  models come a long way from back when Makkink evaluated the Penman method using lysimeters (Makkink, 1957). Models were assessed based on statistical metrics including RMSE, MAE, Bias, R,  $R^2$ , MAPE, and EV. Categorization of models into radiation-based, aerodynamic-based, temperature-based, and combination models aimed to identify reliable options for  $ET_o$  and  $ET_a$  estimation, especially where lysimeters are impractical due to cost limitations. A compromise programming ranking methodology was employed, ranking models with superior performance. The Priestly-Taylor and Makkink models led among radiation-based models, while the Meyer and Hargreaves and Allen models excelled in aerodynamic and temperature-based categories, respectively. Subsequently, the Penman-Monteith, Priestly-Taylor, and Hargreaves and Allen models emerged as the most robust choices for  $ET_o$  and  $ET_a$  estimation in arid environments, consistently providing satisfactory results among the models evaluated across seasons. The effectiveness of the PM method across diverse climatic settings has been highlighted in studies by (Suleiman et al., 2007; Moeletsi et al., 2013). The effectiveness of Priestly-Taylor model has been found to be effective across various environments as well, such observations have been made in the study of (Muhammad et al., 2019); (Pereira, 2004) and by (Gao et al., 2020). The results of this study indicate that certain models excel in specific environmental conditions where they were developed and calibrated at with 25 models having yielded poor results. For example, the Priestly-Taylor and Makkink models demonstrate superior performance among radiation-based models, while the Meyer and Hargreaves and Allen models outperform others in aerodynamic and temperature-based categories, respectively. This result allows water managers to select the most appropriate model depending on the prevailing climatic and environmental conditions of their region. Moreover, the identification of the Penman-Monteith, Priestly-Taylor, and Hargreaves and Allen models as the most robust choices for  $ET_o$  and  $ET_a$  estimation in arid environments is particularly significant. By relying on these models, water managers can make informed decisions regarding irrigation scheduling, water allocation, and drought management in arid regions. The study emphasizes the critical role of model selection in accurately estimating  $ET_o$  and  $ET_a$ , particularly in regions where conventional measuring devices are impractical.

# CHAPTER 5: ASSESSMENT OF REMOTE SENSED EVAPOTRANSPIRATION PRODUCTS UNDER ARID ENVIRONMENT

## 5.1 INTRODUCTION

Water scarcity is a major limiting concern in providing adequate food to the world's expanding population. Agriculture, on the other hand, uses more water than other water-using industries. Quantification of crop water use at field scale is important for a better understanding of water usage, water scheduling and application rates, in the process of trying to solve water problems at a basin or larger scale field-based point equipment are usually confined to local space (Evans and Sadler, 2008). The natural environment as a system is characterized with variations in soils, water availability and climate status which requires multi-temporal information covering a large spatial extent area to understand how areas differ in water use (Kingra et al., 2016). As a result, greater emphasis is being placed on estimating crop water use or evapotranspiration (ET) at larger scales. The innovations in satellite technology have enabled the development of Global Earth Observation (GEO) ET products which permits the computation of local to regional crop water usage, soil water content status, and other important data for water resource management and planning. The lack of sufficient direct ground data measurements has always made estimating crop water use at larger scales difficult to accurately calibrate and validate (Condon et al., 2020). As a result, the gap to validate such products under different set of environments in Africa is a need. The validation and calibration of global ET products have been dominantly done in the countries located mostly on the northern hemisphere including areas in Asia, Australia, South America, and Europe (Ramoelo et al., 2014). Most products were developed in areas with conditions which fit their outputs, application of products developed using algorithms developed in different environmental setting is a problem when the models are transferred to a different environment. MOD16 ET product is generated based on the Penman-Monteith algorithm which is known to have its uncertainties in estimation of ET (Westerhoff, 2015). Apart from the algorithm itself, the misclassification of MODIS landcover add more on the errors of ET estimations (Ruhoff et al., 2012). Most evapotranspiration ground measurements are point-based and do not take spatial extent into account (Kite et al., 2001; Liou and Kar, 2014). Most ET data which is open access has been collected using flux towers located all over the world (Weerasinghe et al., 2020). There are only a few ET ground measurement stations, and only six FLUXNET stations in Africa have accessible ET data (Weerasinghe et al., 2020). Due to the limited data availability of in situ measurements, a method of evaluating ET estimations using data other than point observations are required. Rapid innovations in satellite-based ET products have yielded promising data for filling these observational gaps (Khan et al., 2018). ET cannot be directly measured from the earth's orbit, but it can be estimated using energy balance algorithms from variables that can be recognized from space. Time interpolations are also necessary because of interference from passing frequency range and cloud cover effects.

Several authors, including (Cleugh et al., 2007), used the Penman-Monteith model with data from MODIS in Australia to model and validate global ET products. (Mu et al., 2013) validated the MOD16 using the Ameriflux tower, whereas (Kim et al., 2012) validated the MOD16 ET products using the Asiaflux station. Several researchers in South Africa have attempted to validate the global ET products which includes the MOD16-ET, EUMETSAT, GLEAM, WaPOR (Jovanovic et al., 2015; Majozi et al., 2017; Ramoelo et al., 2014). The work of Jovanovic et al. (2015) on validating MOD16 using historical showed poor correlations of measured to predicted ET, they concluded that the inaccuracies might have been influenced by limited ground data used. Ramoelo et al. (2014) also undertook a study to validate MOD16 global ET product within the Savanna biome using flux tower stations located in the Kruger national park of South Africa, they found inaccuracies between the flux tower and MOD16 estimations concluding that the inaccuracies are due to scaling of flux tower ET to the size of MOD16 pixel, limitations arising from the parametrization of the MOD16 algorithm and errors in measurement of ET. (Majozi et al., 2017) also focused on validating GLEAM and the MOD16 global ET

products from two different ecosystems one in the Savanna and the other site located in the humid coastal area using flux tower in the savanna and scintillometer in the humid area, they found that no model performs well in both environments.

Mu et al. (2005) developed the MOD16 ET algorithm which later on, Mu et al. (2011) improved it. The Penman-Monteith equation serves as the foundation for MOD 16. MOD 16 has an approximate spatial resolution of 1 km<sup>2</sup> and temporal resolutions of 8-day, monthly, and annual intervals Ndara (2017). The MOD 16 ET algorithm calculates ET by combining 8-day remote sensing data (land cover, Leaf Area Index (LAI), Fraction of Photosynthetically Active Radiation, and albedo) with daily in situ data (air temperature, air pressure, humidity, and solar radiation) (Mu et al., 2011). The EUMETSAT LSA SAF ET's algorithm used to generate MET v2, DMET v2, LE, and H products uses LSA-SAF products to deliver maps over the entire MSG field of view (South America, Europe, Africa, and the Middle East) at the variable spatial resolution of Meteosat Second Generation satellites, 3.1 km at sub-satellite point. The WaPOR ET data for this work is the ET1a-WPR V2.0 products available on the WaPOR portal ("[https://wapor.apps.fao.org/home/WAPOR\\_2/1](https://wapor.apps.fao.org/home/WAPOR_2/1)," 2023). The ET1a-WaPOR is based on a modified version of the ETLook model that employs Penman-Monteith to estimate ETa adapted to remote sensing input data. The Penman-Monteith method combines the energy balance equation and the aerodynamic equation.

## 5.2 METHODOLOGY

The validation and calibration of satellite-derived evapotranspiration (ETa) using lysimeters on a pixel basis were carried out, aiming to ensure precise and dependable outcomes. This process contributed to the establishment of a robust connection between measurements taken from satellites and observations obtained on the ground. The following steps were undertaken during this process:

### 5.2.1 Lysimeter Installation and Data Collection

Two lysimeters were set up at strategic locations within the satellite pixel or grid cell. Continuous monitoring and collection of high-quality ground-based ET data were conducted using lysimeters throughout the growing season. Two smart-field weighing lysimeters (SFL-600) were installed in an 18-ha field. Each lysimeter was a stainless-steel core cylinder of 60 cm in height and 30 cm in diameter. Each lysimeter contained a core of undisturbed soil monolith with planted crops resembling field conditions. To extract the soil monolith core, three rope straps were fastened on steel hook anchors secured on the ground anchoring and supporting a jack that was placed on top of the cylinder helping push the cylinder downwards. The jack was used to push the cylinder until the soil filled the cylinders to its bottom. The lysimeter soil bottom was cut with a flat metal plate to enable an easy closure of the cylinder bottom. For each lysimeters cylinder, a gypsum-filled ceramic cap was used to close the bottom of each cylinder, assisting in regulating the boundary condition between the surrounding field and the lysimeter. To prevent leaks, a sealing rubber was placed between the cylinder and the ceramic cap contact and tensioned with a metallic strap. The weighing balance platform was fastened to the ceramic cover below using metal fasteners. Each lysimeter featured six sensors to monitor temperature, electrical conductivity, soil moisture, and water potential. The lysimeter system was put in flat station drum protective cylinder which was levelled with a spirit leveller prior its outside space in the dug hole was filled with soil to prevent movement providing a flat ground surface for the weighing balance. A complete sensor-equipped lysimeter was raised using a tripod and then gradually lowered into the supporting cylinder with the aid of a chain block. The wires connecting the Lysimeters, drainage control pipes, and tensiometer cables were attached before it reached the bottom. A tensiometer was installed adjacent to each lysimeter to ensure consistent boundary conditions both inside and outside the lysimeter. A drainage bottle with a platform for weighing the amount of water drained from the lysimeter was set in the drainage box one metre from each lysimeter. Power cables were connected from the lysimeters to the central data logger system, which was equipped with a solar panel, batteries, and a SIM-card for the logger connection to remote data storage.

### 5.2.2 Lysimeters field data measurement operation

Smart Field Weighing Lysimeters are more intelligent lysimeters compared to others. These systems are the only systems which consist of a bi-directional pump that maintains the true field conditions automatically representing the surrounding field environment within the lysimeter. Changes in storage or lysimeter weight were recorded every minute. For every 10 minutes soil moisture content in the lysimeters was measured and sent to the central lysimetric logger control system, at any case when the soil contained within the lysimeter is becoming more drier as compared to the surrounding field conditions, the water in the drainage container was automatically pumped back into the lysimeter system to maintain homogeneity between the field conditions and the lysimeter system. Contrary, when the soil contained within the lysimeter systems becomes very wet compared to the surrounding field conditions, the system pump drains the water out of the lysimeter until there is balance in moisture between the field conditions and the lysimeter system, always maintaining the actual true field conditions. Compared to other methods which have known inaccuracies, the Smart Field Weighing Lysimeters are the only devices that can measure with high accuracy the field-level actual evapotranspiration fluxes. The Smart Field Weighing Lysimeter makes use of very sensitive load cells when weighing the amount of water that comes into the system as precipitation or irrigation as well as the amount of water that leaves the lysimetric system as soil water evaporation or plant transpiration.

### 5.2.3 Lysimeter data selection and processing

Data cleaning and removal of noise that occurs from external activities such as mechanical vibrations, farm attacking animals and strong winds amongst many other factors is crucial before using data for quantification of crop evapotranspiration, data cleaning reduces false quantifications which can lead to wrongful decision making. Data recorded by both lysimeters for different seasons were inspected for anomalous values such as negative values, error readings on the weighing balance and abnormal readings causing spikes which cannot be explained. ET data focus was on rainless days with zero irrigation, zero-dew or and frost days.

The purpose of removing water input days was to allow monitoring water use after a known irrigation amount event, nevertheless; irrigation days yield negative ET due to weight differences between the less wet and irrigated soils. Cloudy days were also removed from the data set by assessing radiation fluxes acquired from the farm weather station data adjacent to the two lysimeters. Following data cleaning, the data was imported into the origin lab software and plotted against time to enable smoothing of the data for ease interpretation using average-smoothing filter at 20 minutes window to remove anomalies, manual filtering was also done for the values which could not be smoothed by the automatic filter.

Pre-processing of the lysimeter data was done to fit the hourly, daily, and monthly ETa requirements. Evapotranspiration was determined using two smart field weighing lysimeters (SFL-600) based on the weight variations of the lysimeter weighing balance when irrigation was discontinued. Evapotranspiration was computed using the lysimeters, in-situ weight readings, indicated as (LYW), and the weight of the storage vessel, designated as (SWW). The two lysimeters were connected to a data logger which was programmed to record, store and transfer measurement data from the load cells every 10 seconds. The data was downloaded from the cloud storage and saved as .csv files for analysis. For quality and maintenance purposes, monthly visits to the location where the lysimeters were installed were undertaken to assess the field conditions, vegetation planted and the drainage containers for flood checks.

The decrease in the lysimeter cylinder weight was caused by the evaporation of water from the crop and soil surfaces as well as transpiration of water through the tissues of the crop, the increase in weight was associated with irrigation, precipitation, and dew effects. The lysimeter weight changes measured in kilograms, were converted to the equivalent depth of water in millimetres, by dividing the changes in weight of the lysimeter between periods by the density of water in grams as well as the surface area of the lysimeters in square metres. The hourly ETa was calculated based on the weight changes between two consecutive hours, while daily ETa values were calculated by summing up all the daily ETa values obtained from 08:00 am and 17:00 pm on a 24-hour period in winter for barley crop and 5 am to 18:00 pm for summer crops (maize and soya

beans), the purpose of selecting data between the hours was to eliminate the diurnal fluxes caused by dew, frost and rime.

The choice was influenced by the fact that evapotranspiration occurs between sunrise and sunset when there is sufficient energy to evaporate water from surfaces, transpiration also ceases when the sunlight is reduced stopping the processes, the diurnal variations in this study were taken as dew or frost influenced. The smart field weighing lysimeters directly measures the water balance components being the amount of irrigation or incoming precipitation, frost and dew events as incoming water which causes changes in the lysimeter storage. Irrigation and precipitation were also measured directly using a Hobo-link weather station rain gauge situated 10 metres north of the two lysimeters. At every 10 minutes interval drainage was measured by the lysimeters. Adding all the measured components, the only component not measured remains the actual crop evapotranspiration.

#### 5.2.4 Calculation of actual ET at different time scales using smart field weighing lysimeters

To calculate the actual evapotranspiration fluxes, lysimetric data from smart field weighing lysimeters recorded from 2019 to the end of 2021 cropping seasons for different crops within the experimental farm were used.

$$ET_a = \frac{(LYW_n + SWW_n) - (LYW_{n+1} + SWW_{n+1})}{Lysimeter\ Area}$$

Where  $ET_a$  (mm)  $ET_a$  is the actual crop evapotranspiration,  $LYW_n$ =Lysimeter Weight at nth time,  $SWW_n$ =Drainage Weight at nth time,  $LYW_{n+1}$ =Lysimeter Weight at n+1 time,  $SWW_{n+1}$ =Drainage Weight at n+1 time.

$$Lysimeter\ Area = \pi r^2 = \pi \times (0.15)^2 = 0.0707m^2$$

When the drainage is zero, evapotranspiration can be obtained directly by multiplying the change in storage with the density of water which can be calculated as:

$$1\ kg\ of\ seepage\ water = 0.001m^3 = \frac{0.001m^3}{0.0707m^2} = 0.014\ m = 14\ mm$$

#### 5.2.5 Calculation of reference evapotranspiration at different weather stations

The FAO-56 Penman-Monteith model was used to calculate the reference evapotranspiration for all the stations within the irrigation scheme. The reference ET Penman-Monteith model calculates ET using the equation:

$$ET_0 = \frac{0.408\Delta(R_n - G) + \gamma \left( \frac{900}{T + 273} \right) u_2 (e_s - e_a)}{\Delta + \gamma(1 + 0.34u_2)}$$

Where the reference evapotranspiration is denoted by  $ET_0$  in mm/day,  $\Delta$  notation represents the slope of saturated vapour pressure against temperature curve in Kpa/°C,  $R_n$  denotes the total daily net radiation in MJm<sup>2</sup> day<sup>-1</sup>,  $G$  represents the total net soil heat flux,  $\gamma$  denotes psychrometric constant in Kpa/°C,  $T$  is the average daily temperature in °C,  $U_2$  represents the average daily wind speed in m s<sup>-1</sup>,  $e_s$  represent the average daily saturated vapour pressure in Kpa while  $e_a$  represents average daily actual vapour pressure in Kpa.

#### 5.2.6 Relationship between $ET_a$ and $ET_0$

The relationship between  $ET_a$  and  $ET_0$  was developed with the aim of extrapolating  $ET_a$  from a field scale to the scheme scale through empirical equation.

### 5.2.6.1 Satellite Data Acquisition

Satellite-derived ET<sub>a</sub> data for the corresponding pixel or grid cell were retrieved through google earth engine (GEE) for different ET products. A time series was retrieved for every weather station point containing ET values for comparison and evaluation purposes. The MODIS-16, WaPOR and NOAH products were retrieved for this purpose. Attention was given to ensuring that the temporal resolution of the satellite data matched the intervals of ground-based observations.

**Table 26: Global ET products data acquisition.**

Product	Spatial resolution	Temporal resolution	Source
MOD16 global ET product	500 m <sup>2</sup>	8-Day	<a href="https://modis.gsfc.nasa.gov/data/dataproduct/mod16.php">https://modis.gsfc.nasa.gov/data/dataproduct/mod16.php</a>
NOAH product	1 km <sup>2</sup>	Daily	<a href="https://ntrs.nasa.gov">https://ntrs.nasa.gov</a>
FAO- WAPOR	250 m <sup>2</sup>	Decadal	<a href="https://wapor.apps.fao.org/catalog/WaPOR_2/1/L1_AE_TIA">https://wapor.apps.fao.org/catalog/WaPOR_2/1/L1_AE_TIA</a>

### 5.2.6.2 Spatial and Temporal Synchronization

Measures were taken to ensure proper alignment between the locations of the weather stations and the ET products pixels within the Vaalharts irrigation scheme. Additionally, adjustments were made to synchronize the temporal resolution of each ET products with the weather station measurements depending on the temporal resolution of ET satellite products.

### 5.2.6.3 Quality Control and Preprocessing

Both weather station estimates, and satellite ET products data underwent rigorous quality control procedures which included filtering and avoiding days with cloud cover to identify and eliminate any outlying values.

### 5.2.6.4 Comparison and Analysis

Direct comparison was conducted between satellite-derived ET products pixel values and weather station-based ET estimates for each corresponding station location and timeframe. Statistical metrics, such as correlation coefficients, coefficient of determination, bias, root mean square error, mean absolute error and mean absolute percentage error, were employed including assessing the significance between observations to quantify the level of agreement.

### 5.2.6.5 Validation approach

In this study two approaches have been adopted. First, a direct comparison between the ET<sub>a</sub> from the remote sensed products and ET<sub>a</sub> measurements from lysimeters. The second method is to use lysimeter data to correct and validate meteorological measurements and use the meteorological relationship for the validation. The acquired ET<sub>a</sub>-WaPOR was exposed to a thorough analysis with the in-situ ET<sub>a</sub> data obtained from the smart field weighing lysimeters over ten days, aligning with the temporal resolution of the WaPOR system product. For this adjustment, the ET<sub>a</sub>-WaPOR values corresponding to Level-1 (250 m) were utilized, given that this level provided coverage over the region of South Africa. The extraction of pixel values took place in the vicinity of the lysimeter area, a location chosen based on the basis that the pixel accurately represents the measurement footprint of the smart field weighing lysimeter area. Following data processing, statistical analysis was performed, and classical statistics parameters were used as the basis for validity checks. The process was done for all ET products retrieved including the NOAH and the MOD16 ET products.

### 5.3 RESULTS

Remote sensing is a valuable tool for monitoring and studying various environmental parameters, including water resources in arid areas. Satellite remote sensing can provide a wide-scale view of water resources in arid areas, allowing for the identification and monitoring of key features of the hydrological cycle. Additionally, it can fill the gap of data scarcity in arid areas. This validation process is crucial for ensuring the accuracy and reliability of satellite-based evapotranspiration data in arid regions and data-scarce regions, as it allows for better-informed decision-making and resource management. Satellite remote sensing products have global coverage advantages (Figure 29) on one hand and the issue of resolution on the other hand (Table 26). Daily evapotranspiration can be retrieved using coarse satellite data with high temporal resolution such as MODIS and NOAA. However, the main limitation of such high temporal resolution products is the cloud cover on most of the areas. Most of the ET products are using temporal composite such as 8-days in MODIS and 10-days as found in WaPOR products. The 10-days ET product time series during the study period is shown on figure 30.

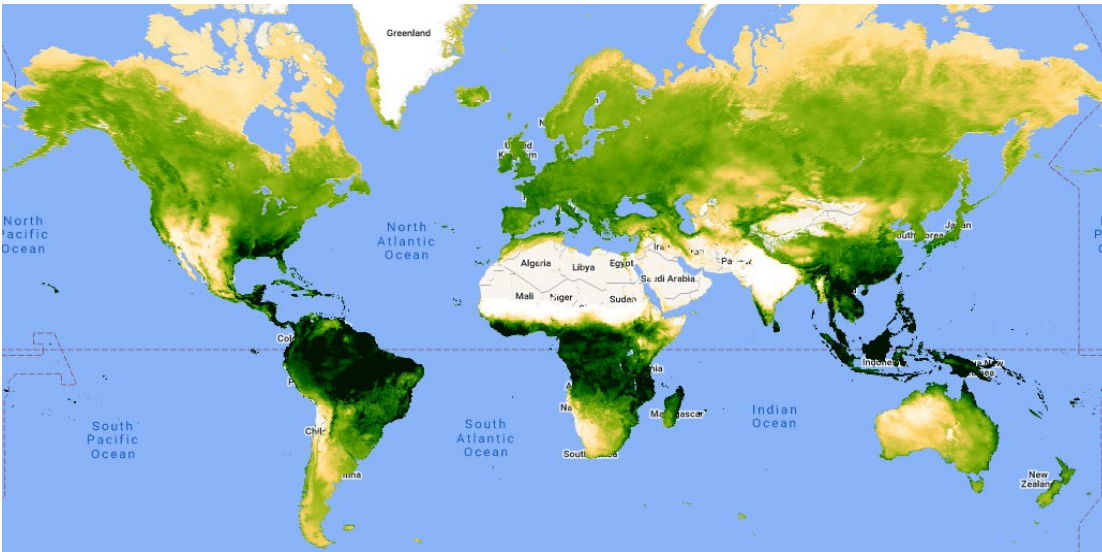


**Figure 31: Satellite-based evapotranspiration coverage using MODIS data.**

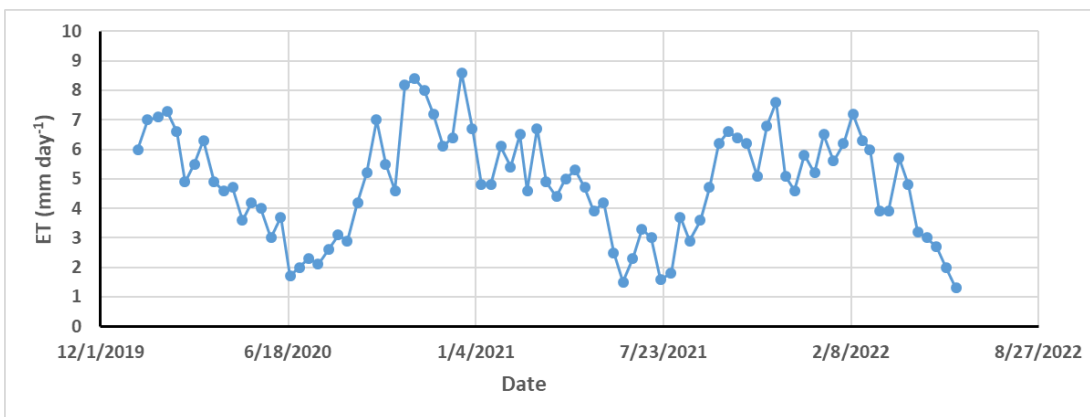


**Figure 32: 10-Days WaPOR-FAO evapotranspiration products extracted at the lysimeter site in the period between September 2019 and August 2022.**

The relationship between  $E_{To}$  and  $E_{Ta}$  using WaPOR products follow the same trend that has been found between the  $E_{To}$  and  $E_{Ta}$  from the lysimeter data (Figure 33).

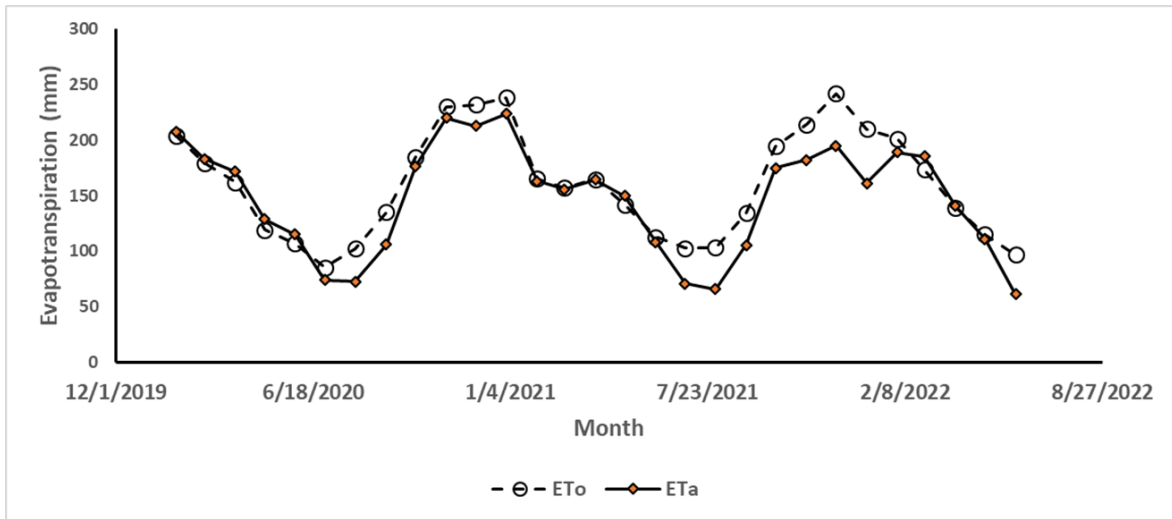


Figure 33: Relationship between ETo and ETa using WaPOR products.

The MODIS ETa data has been extracted using Google Earth Engine (GEE) platform (Figure 34). The GEE can allow us to extract data from different sites and different periods without the need to download the actual products.

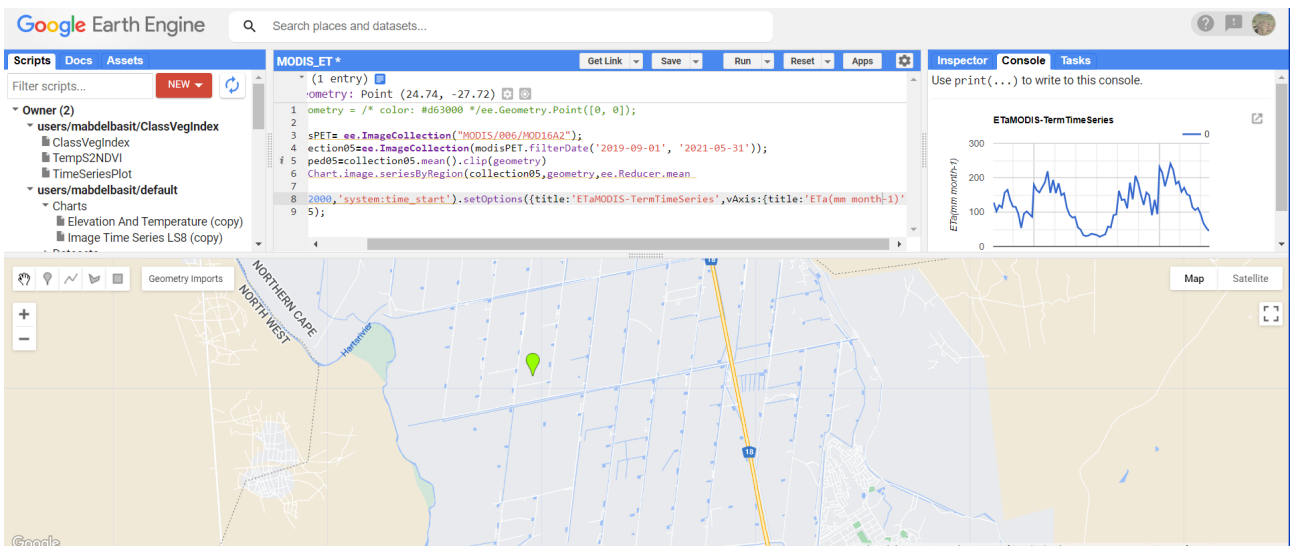
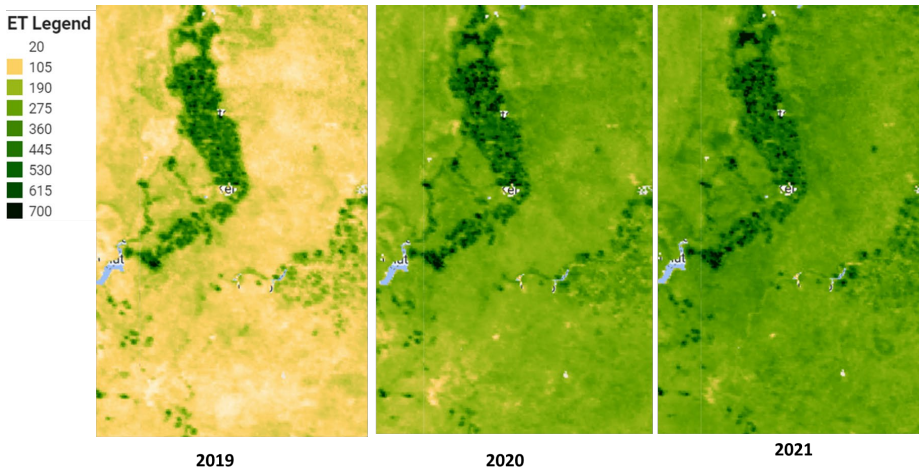


Figure 34: Extraction of MODIS ETa products using Google Earth Engine.

The MOD16 ETa data can also be processed on an 8-day, monthly and annual ETa can be calculated make it an easy tool for water balance assessment (Figure 35).



**Figure 35: Annual evapotranspiration data for Vaalharts irrigation scheme using MODIS ETa product.**

There is general trend between the ET products, however, there was high discrepancies on the magnitude of the ETa (Figure 36). This issue has specifically indicated the problem of resolution and data extraction. The lysimeter data cannot be directly extrapolated to the large scale without using proxy data that can help in regionalisation the accurate lysimeter data. The meteorological ET function was developed at the lysimeter scale and has been used to validate the satellite data.

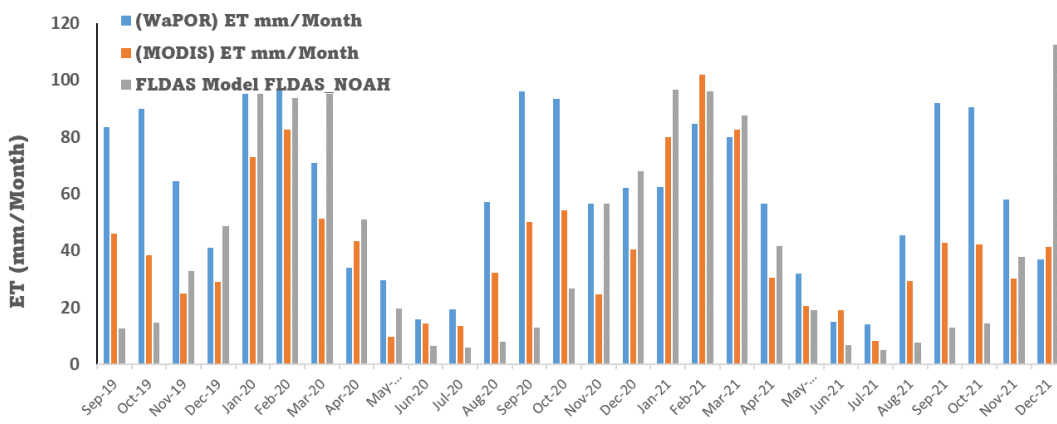


**Figure 36: Different evapotranspiration products used in this study.**

Three ET<sub>o</sub> functions with different data requirements have been used to develop the relationship between ET<sub>o</sub> and ET<sub>a</sub> using the lysimeter data (Figure 37).

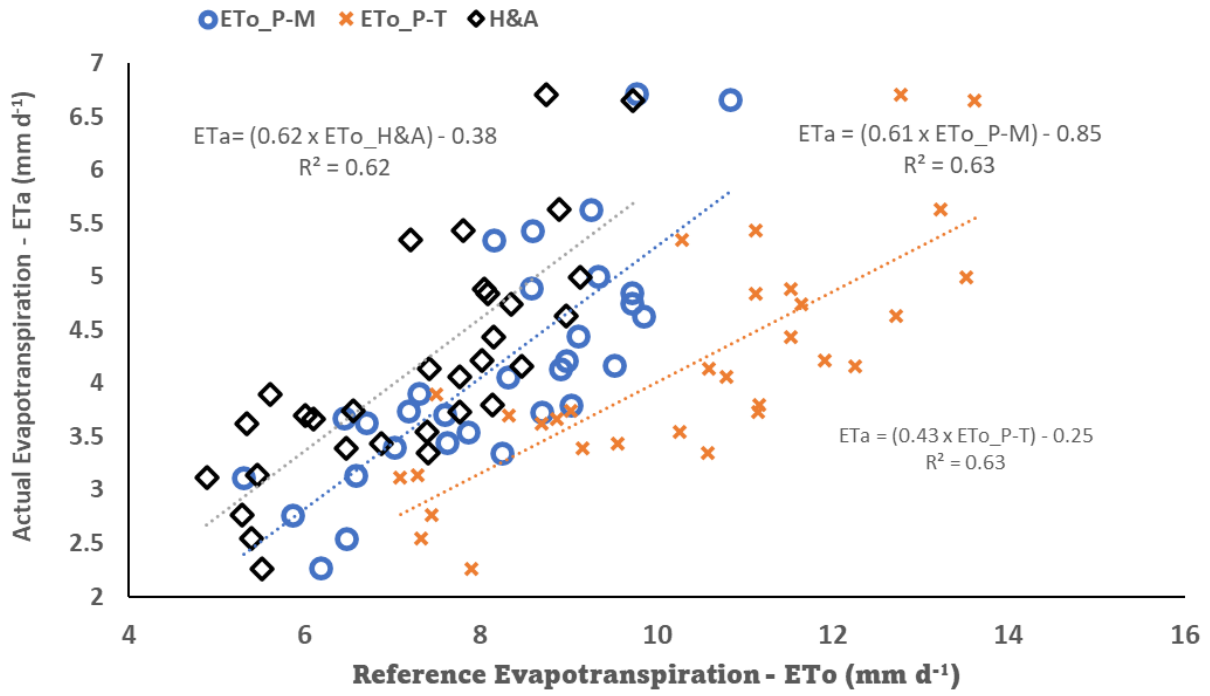


Figure 37: Relationship between ETo and ETa using meteorological functions and lysimeter data logger

**Table 27: Validation of NOAH pixels with ground data across four seasons**

Station	Season	N	R <sup>2</sup>	R	RMSE (mm/8d)	MAE (mm/8d)	Bias (mm/8d)	MAPE %	P-value
Ganspan	2019 Barley	91	0.41	-0.64	0.459	0.361	1.549506e-15	18.9122	6.938445e-12
	2020 Maize	183	0,41	-0.64	1.164008	1.082683	1.082683	119.4102	6.938445e-12
	2020 Barley	122	0,41	-0.64	0.79	0.72	-0.2113236	36.23468	6.938445e-12
	2021 Soybean	182	0.0117	-0.108	0.2314703	0.1611061	9.214021e-17	21.30587	0.1447246
Tadcaster	2019 Barley	91	0.4905758	-0.7004	0.4283556	0.3387537	-2.718845e-18	17.93062	1.09872e-14
	2020 Maize	183	0.04	0.20	0.31	0.14	2.039683	41.82	0.46144
	2020 Barley	121	0.43	-0.65	2.28	0.521	2.44	54.24	0.461
	2021 Soybean	181	0.003	-45	0.79	0.72	-0.2113236	36.23468	6.938445e-12
SABBI	2019 Barley	91	0.39	-0.63	0.54	0.38	-4.098515e-15	6.056501e-16	0.45201
	2020 Maize	183	0.0003	3.19	0.43	0.14	-3.08415e-15	6.056501e-16	0.43001
	2020 Barley	11	0.48	0.69	2.79	2.30	-9.689219e-16	28.03	0.0181
	2021 Soybean	16	0.005	1.164008	1.082683	1.082683	119.4102	6.938445e-12	1.164008
Jan Kempdorp	2019 Barley	4.6992	3.84	9.690008e-16	79.40	0.771	5.328203e-16	31.14	0.219
	2020 Maize	6.03	5.46192	3.941292e-15	42.44	0.022	-5.051515e-15	35.43	0.461
	2020 Barley	4.24	3.55	-4.737891e-16	37.17	0.61657	-5.181011e-16	13.70741	0.00140963
	Soybean 2021	6.19	5.09	1.665335e-15	40.92	0.0670	-7.648203e-16	40.3413	2.671839e-07

**Table 28: Validation of WaPOR pixels with ground data across four seasons**

Station	Season	N	R <sup>2</sup>	R	RMSE (mm/8d)	MAE (mm/8d)	Bias (mm/8d)	MAPE %	P-value
Ganspan	2019 Barley	10	0,54	0,74	0,75	0,67	-4,21915E-16	21,02	0.015
	2020 Maize	17	0,39	0,63	1,04	0,90	4.702631e-16	24,56	0.0072
	2020 Barley	12	0,58	0,76	0,68	0,51	-1.849355e-17	17,81	0,0030
	2021 Soybean	18	0.48	0.69	0.802	0.63	-5.181011e-16	13.711	0.00140963
Tadcaster	2019 Barley	27	0.66	0,81	1,26	1,02	-7.648203e-16	40.34	2.671839e-07
	2020 Maize	18	0,29	0,54	1,84	1,57	1.851275e-16	66.45	0.021
	2020 Barley	12	0,46	0,68	1,30	1,05	3.700834e-16	28.93	0.01524
	2021 Soybean	18	0,63	0,79	0,97	0,78	-1.356578e-16	24.27	8.724665e-05
SABBI	2019 Barley	9	0,55	0,74	0,73	0,67	2.072428e-15	11.29	0.0223
	2020 Maize	18	0.56	0.75	0.911	0.77	-5.18119136521913e-16	19.97	0.00032
	2020 Barley	12	0.54	0.732	1.0063	0.74	-1.14721238874312e-15	14.48	0.00673
	2021 Soybean	18	0.55	0.742	0.842	0.67	-1.24588984480281e-15	14.60	0.00041
Jan Kempdorp	2019 Barley	9	0.71	0.841	0.2468	-1.35696936904665e-16	0.2006	14.65	0.0044
	2020 Maize	18	0.34	0.586	1.03423	0.87215	3.70917609898096e-17	31.21	0.0104
	2020 Barley	12	0.01	0.109	0,55	0,50	-2.313145e-16	36.71	0.7340176

Smart Field Lysimeter for ET-Sensing

	2021 Soybean	18	0,61	0.78	0.72	0,54	1.776357e-15	16.98	0.000138
--	--------------	----	------	------	------	------	--------------	-------	----------

**Table 29: Validation of MOD16 pixels with ground data across four seasons**

Station	Season	N	R <sup>2</sup>	R	RMSE (mm/8d)	MAE (mm/8d)	Bias (mm/8d)	MAPE %	P-value
Ganspan	2019 Barley	11	0.49	0.70	2.746898	2.29067	4.198701e-15	28.53456%	0.02
	2020 Maize	16	0.02	0.16	5.90	4.93	-1.110223e-16	52.46	0.56
	2020 Barley	15	0.09	0.30	2.40	1.81	-7.106006e-16	37.37	0.28
	2021 Soybean	22	0.02	0.14	4.48	3.87	-3.471931e-15	38.11	0.52
Tadcaster	2019 Barley	11	0.48	0.69	2.79	2.30	-9.689219e-16	28.03	0.02
	2020 Maize	16	0.005	0.07	5.96	5.03	-4.440892e-16	53.03	0.79
	2020 Barley	15	0.11	0.34	2.65	2.32	5.328203e-16	31.14	0.22
	2021 Soybean	16	0.04	0.20	5.51	4.66	-5.051515e-15	35.43	0.46
SABBI	2019 Barley	11	0.23	0.48	4.14	3.388	-4.845398e-16	56.76	0.13
	2020 Maize	23	0.16	0.41	7.41	6.32	-1.389966e-15	81.50	0.06
	2020 Barley	15	0.30	0.55	3.58	2.79	0,1	28.65	0.03
	2021 Soybean	22	0.46	0.68	5.45	4.26	6.056501e-16	37.81	0.00047
Jan Kempdorp	2019 Barley	11	0.01	0.10	4.70	3.84	9.690008e-16	79.40	0.77
	2020 Maize	16	0.31	0.56	6.03	5.46192	3.941292e-15	42.44	0.02
	2020 Barley	15	0.01	0.14	4.24	3.55	-4.737891e-16	37.17	0.62
	2021 Soybean	16	0.22	0.47	6.19	5.09	1.665335e-15	40.92	0.07

5.3.1 Evaluation of NOAH ET product against in situ ET data across various stations

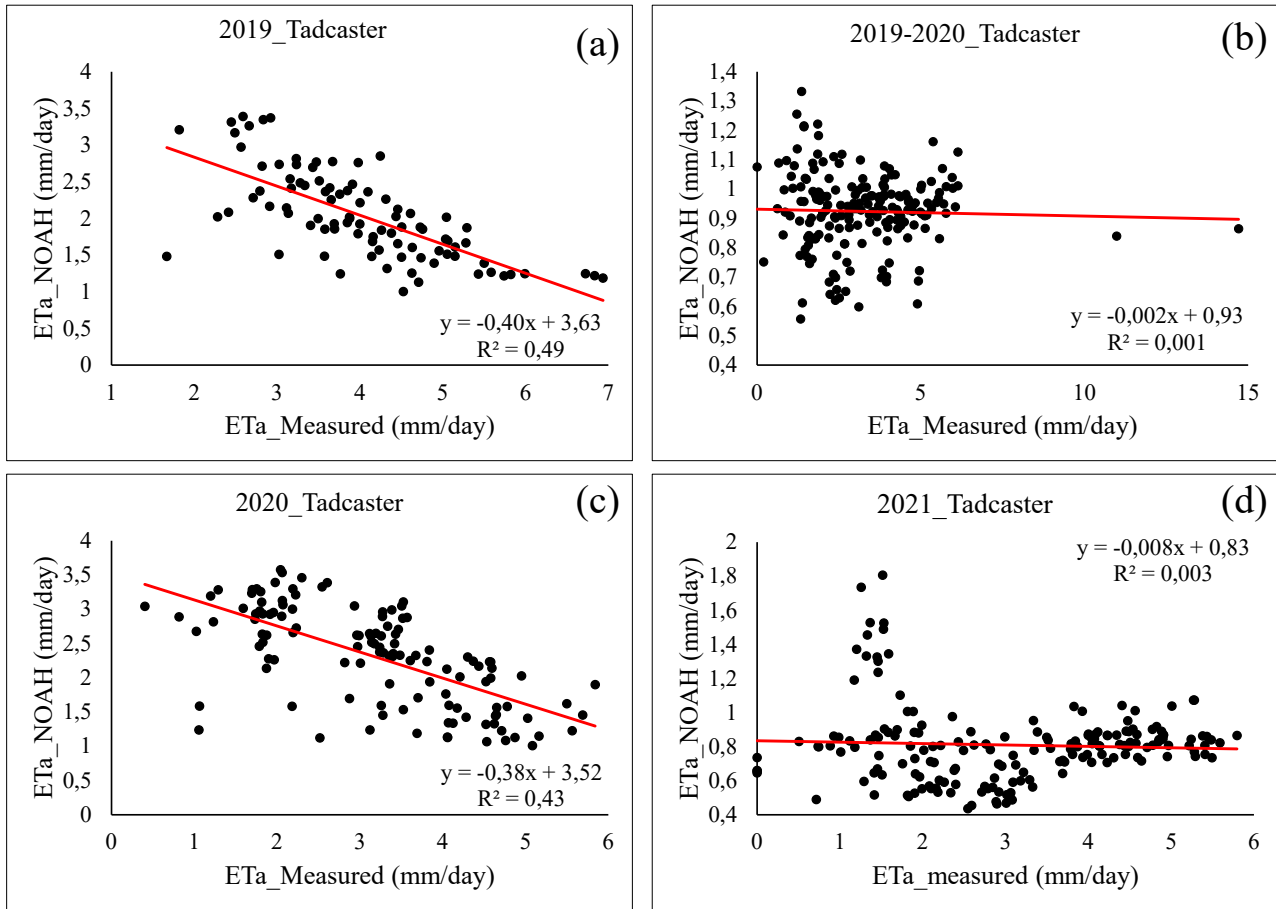


Figure 38: NOAH ET evaluation at Tadcaster station for all seasons

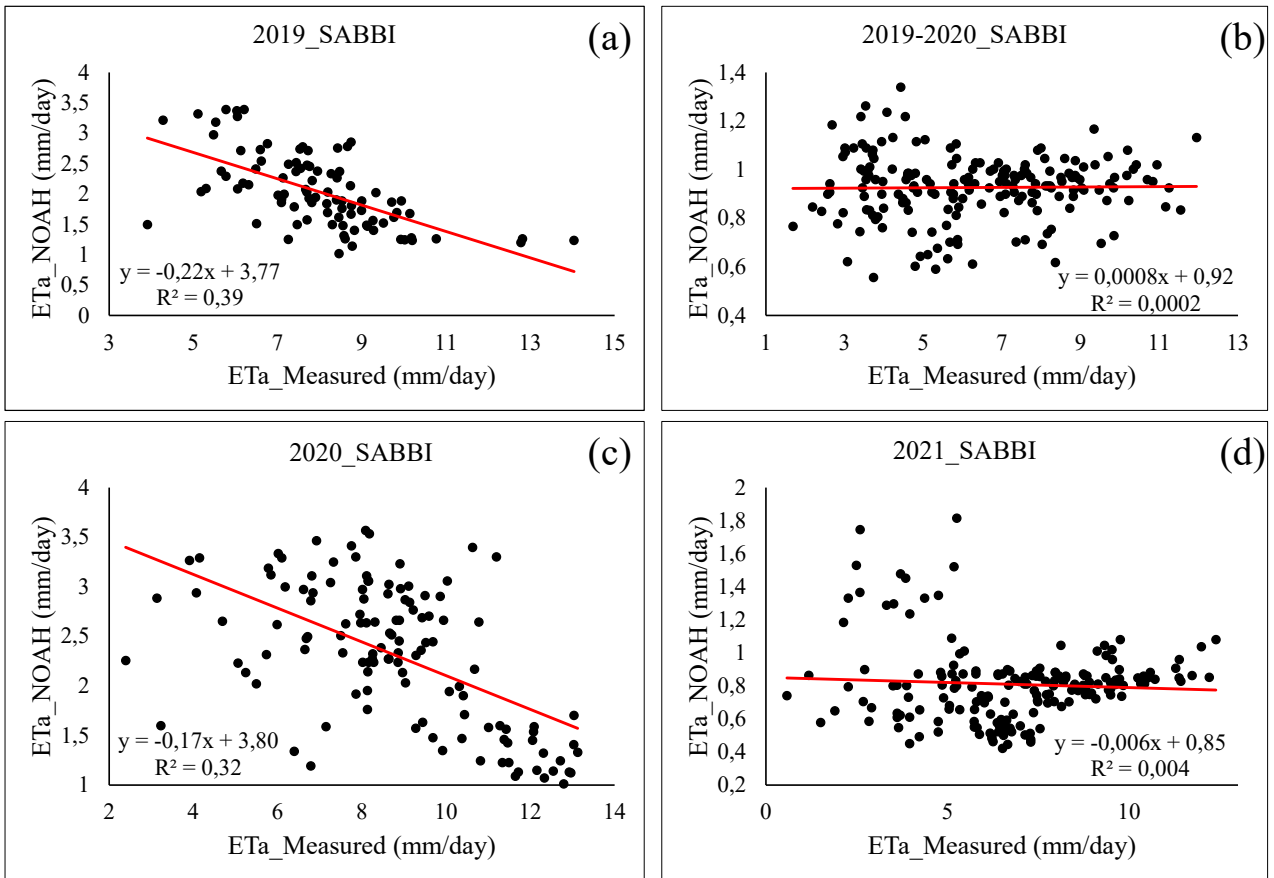


Figure 39: NOAH ET evaluation at SABBI station.

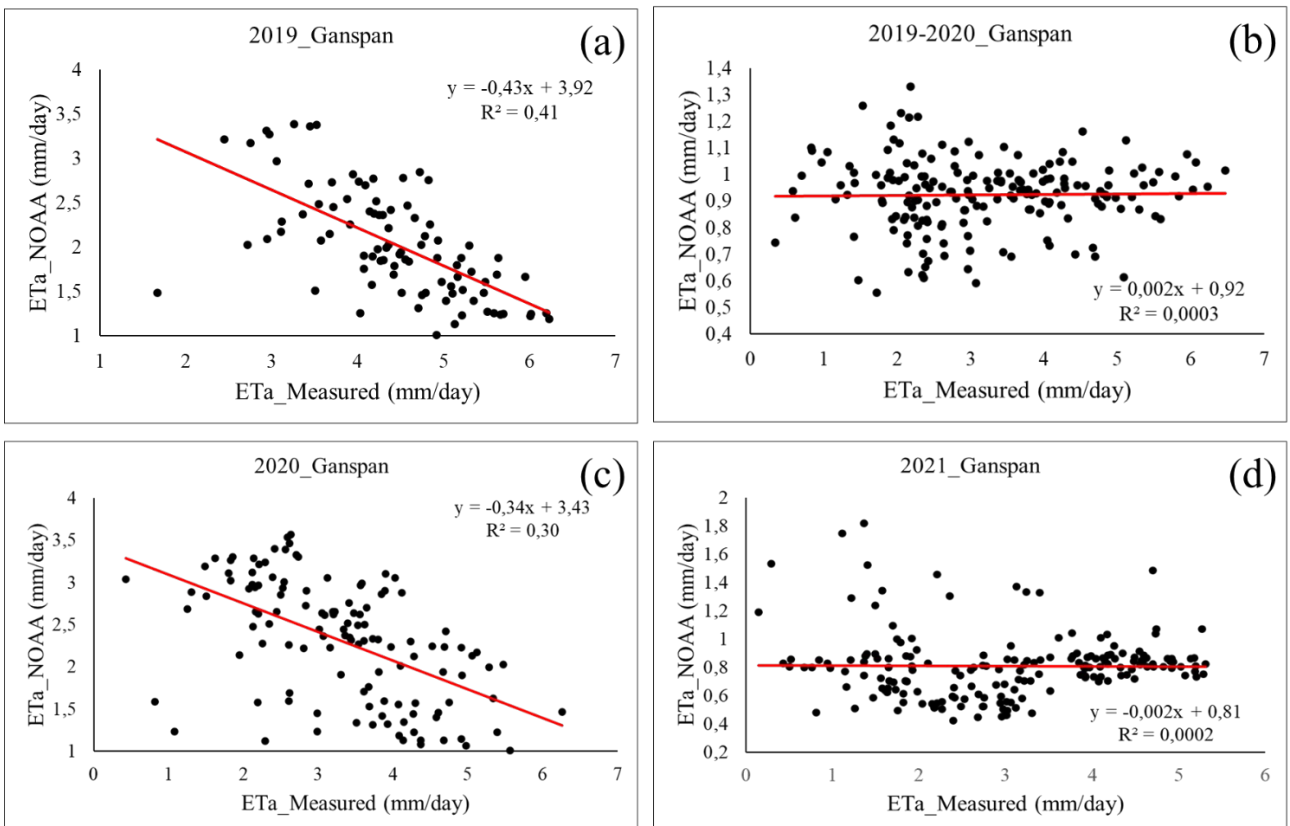


Figure 40: NOAH evaluation at Ganspan station.

5.3.2 WaPOR evaluation across different stations and seasons

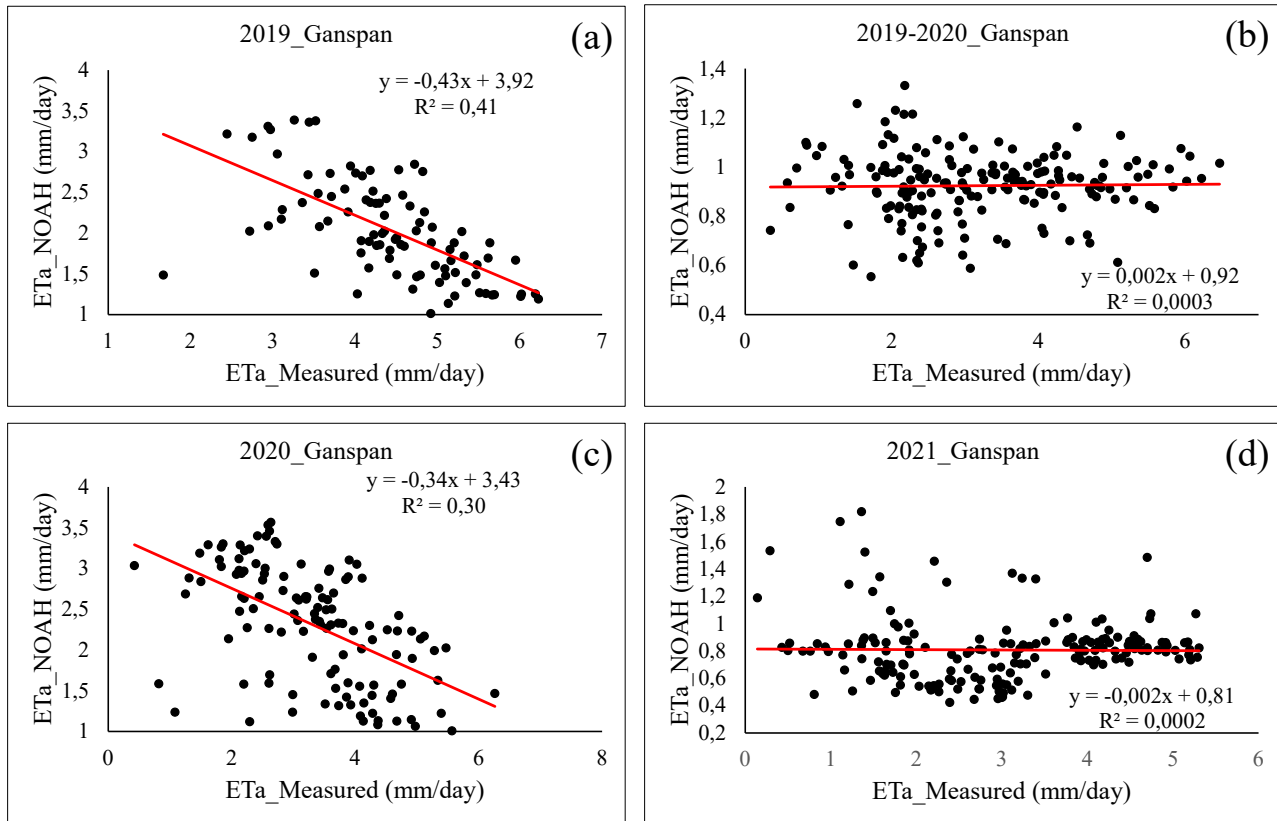


Figure 41: WaPOR evaluation at Ganspan station

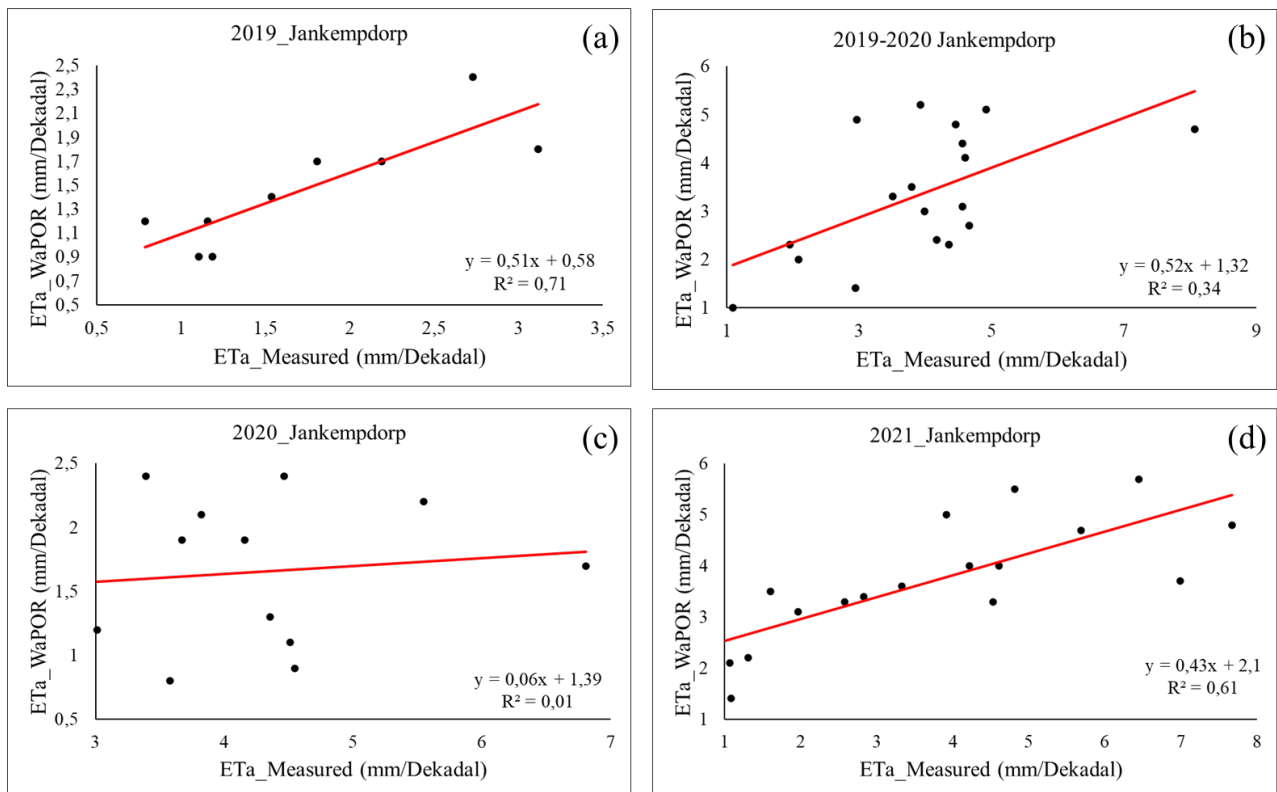


Figure 42: WaPOR evaluation at Jan Kempdorp station

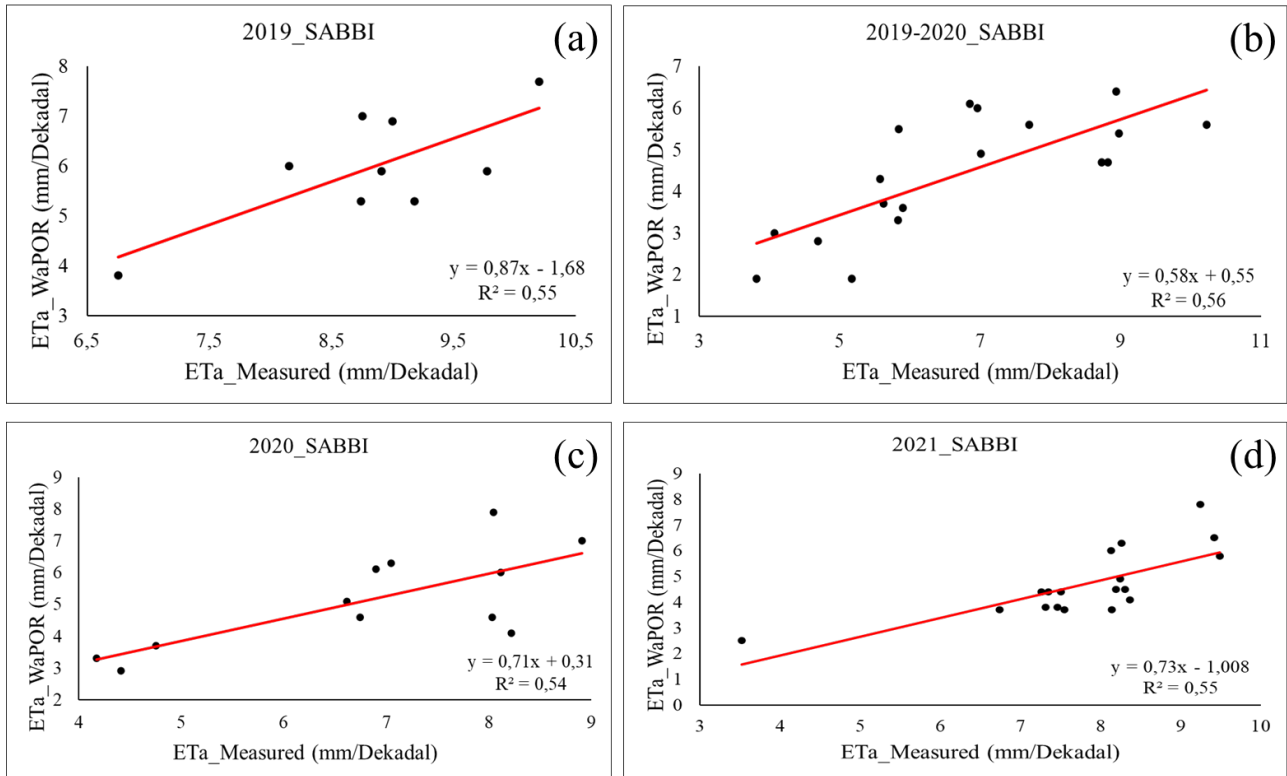


Figure 43: WaPOR evaluation at SABBI station.

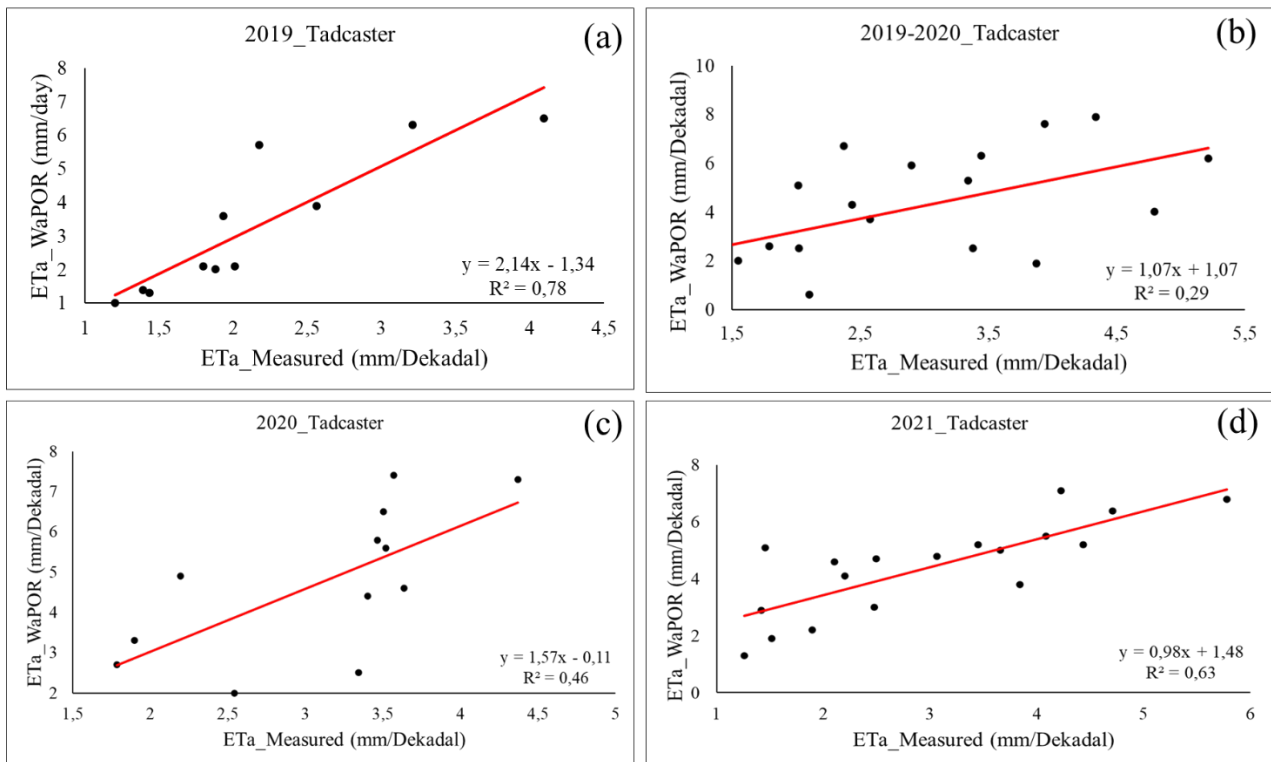


Figure 44: WaPOR evaluation at Tadcaster station.

5.3.3 Evaluation of MOD16 across various stations and seasons

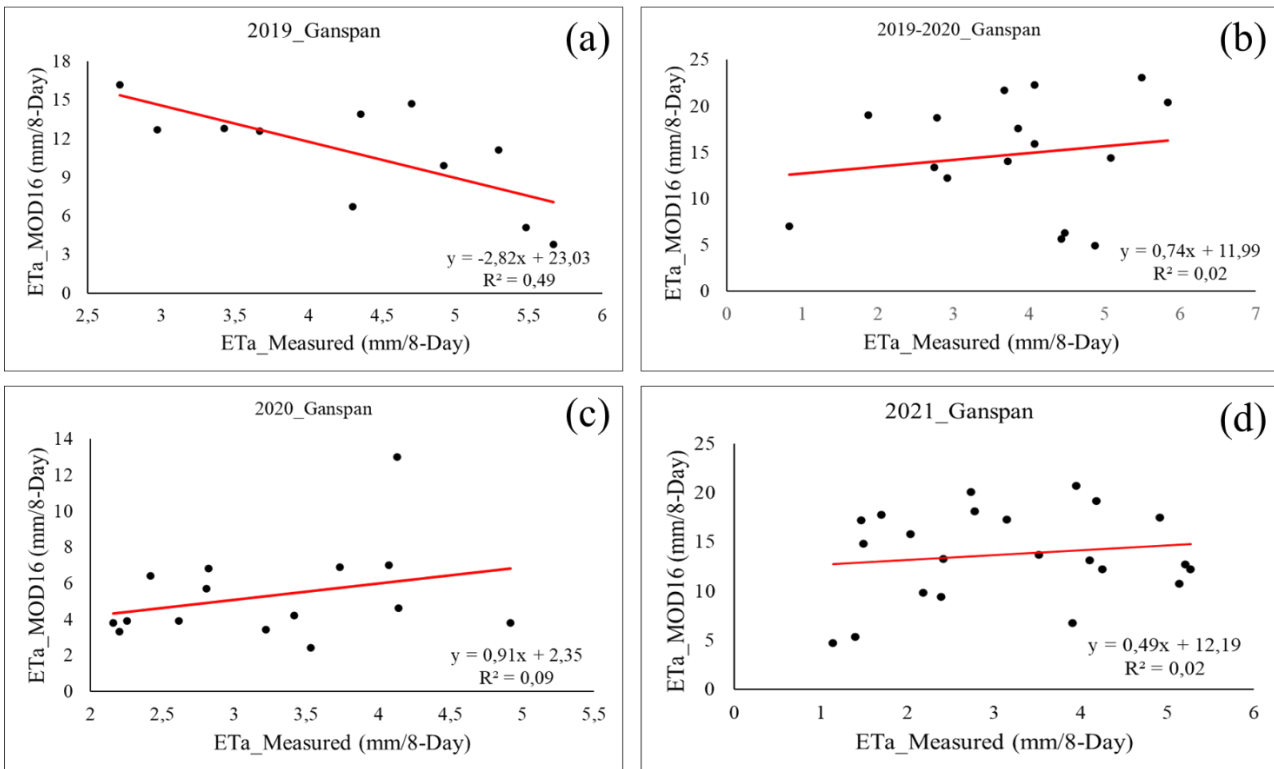


Figure 45: Evaluation of MOD16 at Ganspan station

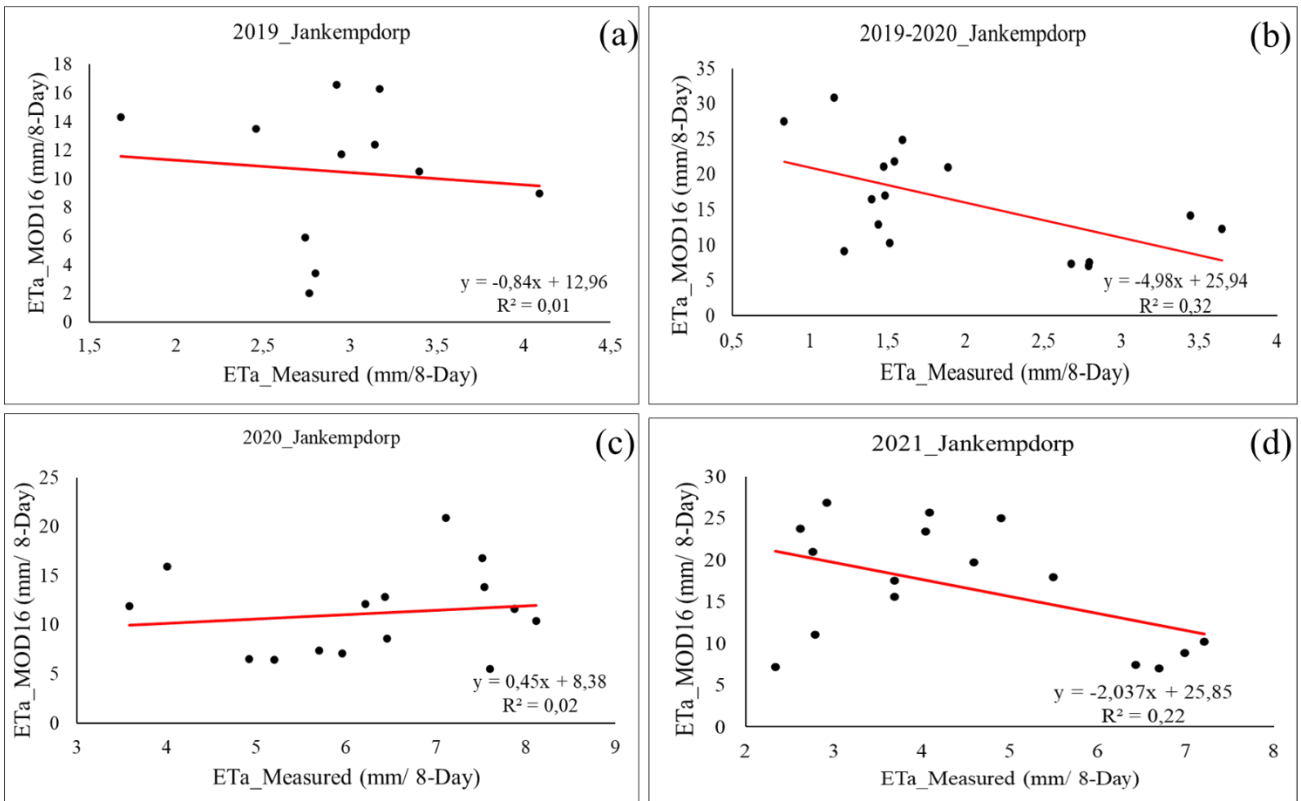


Figure 46: Scatter plot of MOD16 vs in situ data at Jan Kempdorp

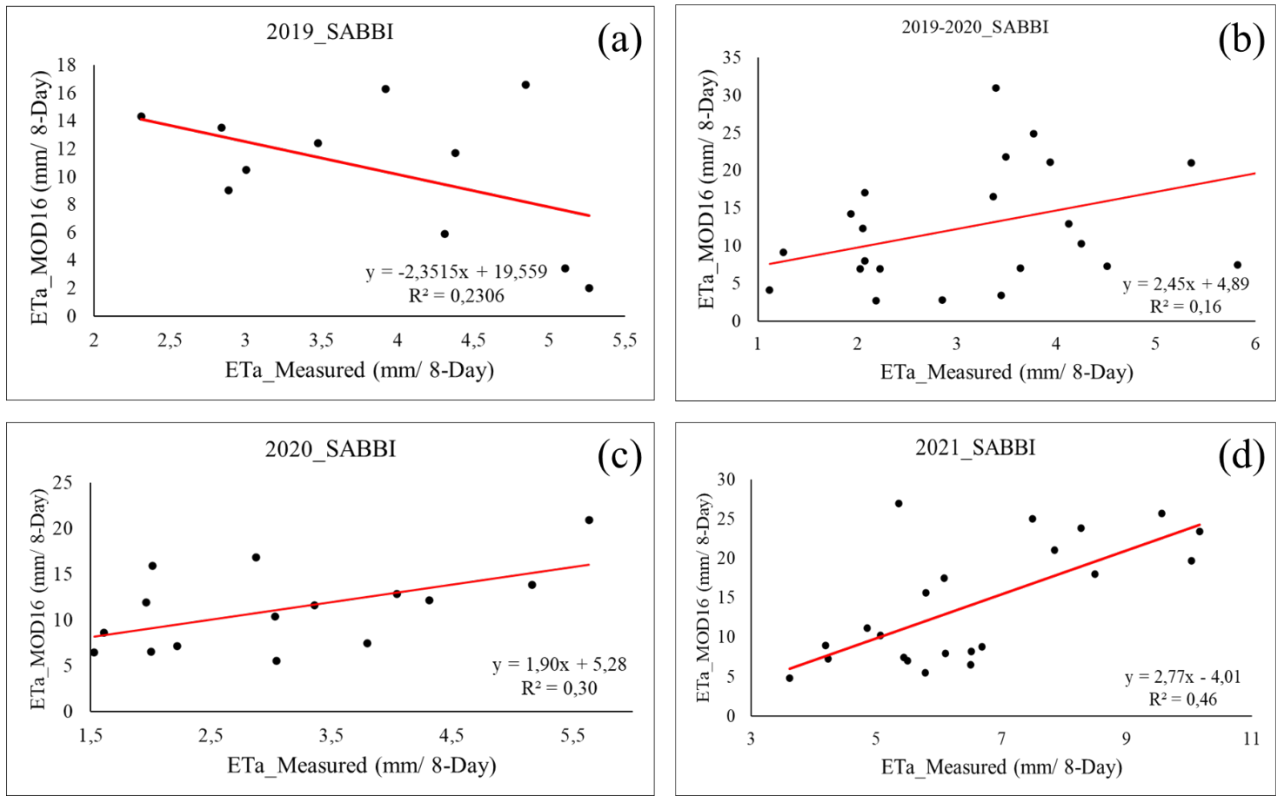


Figure 47: Scatter plot of MOD16 vs measured ETa at SABBI

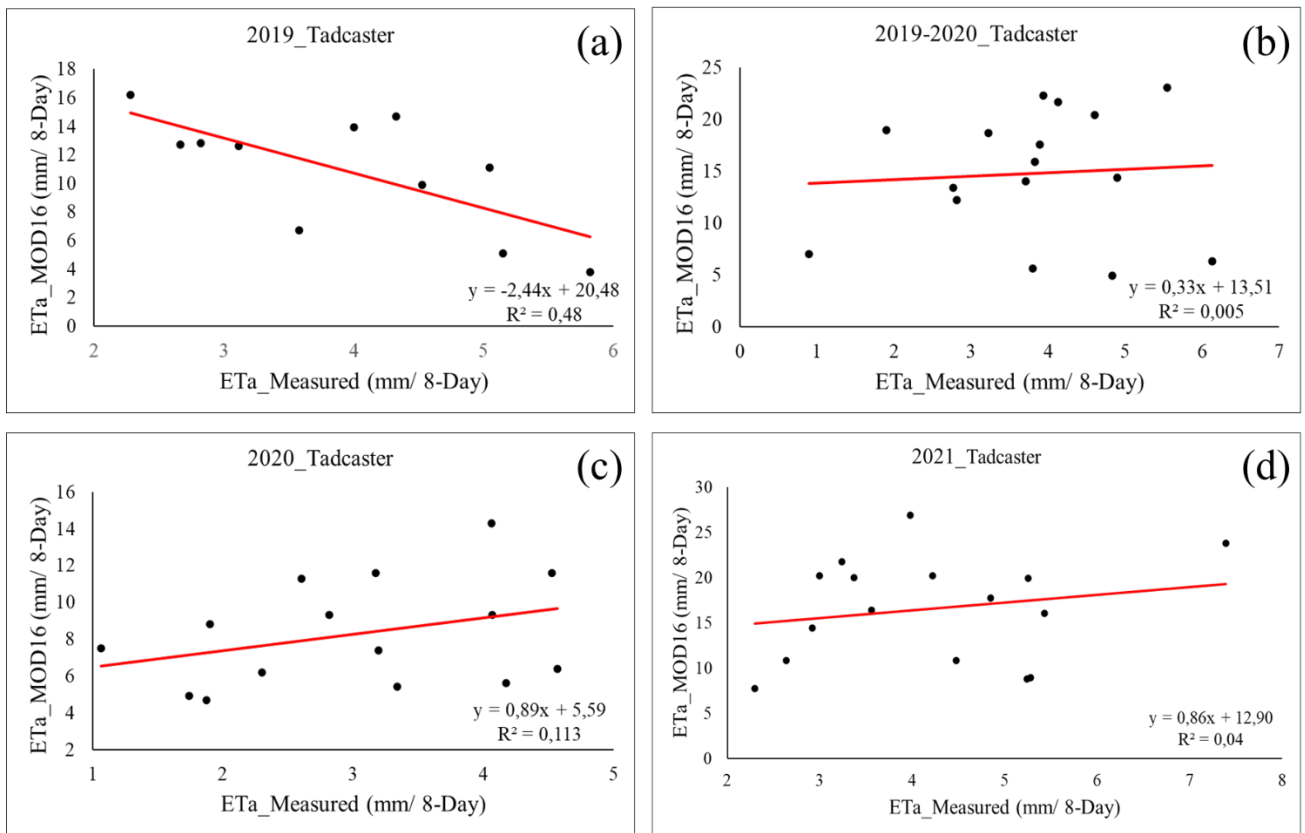


Figure 48: Scatter plot of MOD16 vs measured ETa data at Tadcaster station.

## 5.4 DISCUSSIONS

This study aimed to evaluate the accuracy of three global Evapotranspiration (ET) products across different spatial resolutions: the NOAA Land Data Assimilation System (LDAS) at 1 km<sup>2</sup>, MOD16 ET at 500 m<sup>2</sup>, and WaPOR at 250 m<sup>2</sup>. Evaluation involved comparing ET outputs from these products with in-situ data. The assessment was conducted in two stages.

Firstly, at the field scale, ET<sub>a</sub> from smart field weighing lysimeters was compared with ET<sub>o</sub> determined using the Penman-Monteith model. This comparison helped develop a mathematical approach to extrapolate ET<sub>a</sub> in areas with weather stations but no lysimeters. Secondly, this relationship was used to convert ET<sub>o</sub> at four weather stations into ET<sub>a</sub>. The converted station ET<sub>a</sub> was then directly compared to ET<sub>a</sub> outputs from the global products at various time stamps. Evaluation metrics included R<sup>2</sup>, R, RMSE, MAE, Bias, and MAPE, and significance tests were conducted using P-values.

Findings revealed that ET<sub>a</sub>\_WaPOR showed better performance compared to in situ data, while ET<sub>a</sub>\_NOAH and MOD16 exhibited poor correlations. The discrepancies between MOD16 and NOAA products and in situ data could be attributed to their coarse resolutions, algorithm parametrization, and errors in land use classification. Furthermore, inconsistencies between products and in situ data may arise due to pixel information mixing, where different land cover types coexist within one pixel. Among the evaluated products, WaPOR showed promise for hydrological studies and irrigation scheduling. However, its 10-day outputs may not provide sufficient temporal resolution for immediate decision-making. Recommendations include improving WaPOR's spatial resolutions for better quantification, particularly in regions like South Africa.

Inaccuracies between the MOD16 pixels and in situ data were observed in this study. The disparities between the MOD16 pixels and the ground data can be attributed to several factors such as (i) the spatial and temporal resolution differences, the MOD16 ET product has a coarser spatial resolution (1 km pixel) compared to a point-based weather station or lysimeter, which can lead to differences in the representation of land cover types and surface heterogeneity. An observation in the study area was that within 1 km<sup>2</sup> pixel more than one plots exists with different land cover types apart from agriculture, water dams in each plot exists, trees and different crops also exist. The MOD16 estimates land parameters as an amalgam of activities occurring within one pixel, that means that ET is based on different activities occurring within the MODIS pixel which has the potential to yield inaccurate estimates which result in contradictory results (Aguilar et al., 2018). Moreover, the MOD16 product is available at a specific temporal interval of 8-day composites, while weather station and lysimeter data may make measurements at higher temporal resolutions (minutes, hourly and daily), because of the differences in spatial and temporal resolution discrepancies between the two datasets, the uncertainties might arise (Ndara, 2017). Furthermore, vegetation cover dynamics could also be seen as another factor influencing disparities. The MOD 16 ET estimates are based on remote sensing data which may not fully capture the complex dynamics of vegetation, such as changes in leaf area index, crop phenology, and crop growth stages. Variations in vegetation characteristics between MODIS pixels and the actual field conditions can lead to non-correlation between MODIS and in situ measurements (Ramoelo et al., 2014).

Calibration and validation of the ET product is another factor that could be the reason of disparities between estimated and in situ data. The accuracy of MODIS ET estimates depends on the calibration and validation of the algorithm using ground-based measurements, such as lysimetric data. However, the calibration and validation datasets may not fully represent the range of environmental conditions and land cover types present in the study area, leading to discrepancies between MODIS and weather station-based ET estimates. Another important factor not to overlook is measurement errors, both MODIS and ground data can be subjected to measurement errors, the errors include errors in satellite retrievals, sensor calibration, and data processing. Consequently, such errors can propagate through the ET estimation process and contribute to non-correlation between the two datasets. The differences in estimation methods can also add to inaccuracies between two datasets. MODIS ET estimates are based on remote sensing data and empirical algorithms, while weather

station ET estimates may be derived from empirical models or physical-based approaches. Variations in the underlying estimation methods can lead to discrepancies between MODIS and ground-based ET estimates.

The land surface heterogeneity is another factor that contributes to inaccuracies. The study area exhibited heterogeneous land surface characteristics, such as variations in soil properties, land cover types, and irrigation practices. The MODIS pixels may represent an average value for these heterogeneous surfaces, leading to discrepancies between MODIS and weather station ET estimates at smaller spatial scales. The variations within a single pixel have been described by Mu et al. (2011) who mentioned that the MODIS land cover has some inaccuracies which contributes to inaccuracies of ET. Fang et al. (2013) demonstrated the impact of land cover misclassification on leaf area index (LAI) which is one variable used as an input in the MOD16's Penman-Monteith algorithm.

The NOAH ET products demonstrated poor results when compared to in-situ measurements. The disparity between the NOAH and ground-based ET can be attributed to the coarse resolution of NOAH pixel while it can also be attributed to the errors on ground measurements. According to Moorhead et al. (2015), the data that is used in development of the NOAH's daily ETo layers are generated from measurements over land cover surfaces that are different from short or tall reference crops, in non-agricultural environments, which provides an unknown difference between estimated values and actual conditions. However, Moorhead et al. (2015) observed good correlations between ground measurements and NOAH pixels in a non-agricultural setting. The disparities in the current study can be attributed to the land cover which is an agricultural setting with mixed vegetation parcels occurring in one pixel.

The WaPOR ET product runs on the ETLOOK algorithm developed by Bastiaanssen et al. (2012) with a land cover classification layer of 100 m resolution. Product covering South Africa covers a spatial extent of 250 m<sup>2</sup>. This resolution provides a better understanding of land cover variability compared to MOD16 and the NOAH product. This product offered a better agreement with the measured in-situ data because of less lumping of land cover types in one pixel except for fields which share boundaries within the same pixel while their management and irrigation practices are different. Similar observations were made by Geshnigani et al. (2018). The disparities between WaPOR and measured ETa can also be related to the parametrization of the ETlook algorithm that depends on the Penman-Monteith model which is known to have inaccuracies in land cover.

# CHAPTER 6: ASSESSMENT OF SATELLITE-BASED EVAPOTRANSPIRATION ALGORITHMS UNDER AGRICULTURAL ARID ENVIRONMENT

## 6.1 INTRODUCTION

The increasing challenges surrounding water utilization, particularly within irrigated agricultural regions, are rooted in the limitations of accurate monitoring technologies to guide the existing managing water consumption strategies (Evans and Sadler, 2008; Schultz and De Wrachien, 2002). This issue is significantly exacerbated within arid environments, where limited precipitation inputs and high evaporation rates create an uncertain balance between water demands and supply (Lu et al., 2018). Consequently, enhancing the productivity of arable land and optimizing the utilization of available water resources poses an intense challenge within the context of the water scarcity era (Mancosu et al., 2015). In such circumstances, the need for water often far exceed the available resources (Jalali, 2007). To cope with these challenges, areas faced with aridity often resort to water transfers from areas with ample water sources, such as dams and rivers (Oweis and Hachum, 2003). However, their reliance on external water sources does not only impact production within these zones; it also triggers negative consequences for the very water sources from which they draw their sustenance water. This, in turn, disrupts the equilibrium of freshwater ecosystems, which serve as vital habitats for aquatic life forms including the riparian vegetation especially in rivers (Malmqvist and Rundle, 2002).

Agriculture in South Africa contributes about 70% in fresh water consumption in competition with other water dependent sectors (Musvoto et al., 2015). The key contributor to water losses in agricultural settings is the process of evapotranspiration (ET), which manifests as both evaporation from soil surfaces and transpiration from crop canopies, it is typically difficult to separate the two occurrences as they occur simultaneously (Allen, 1998). ET is a vital component of the water balance resembling water output in a given system, as a result ET component plays an essential role in quantification of the exact amount of water lost post irrigation or precipitation event (Minhas et al., 2020). Therefore, acquiring accurate spatiotemporal trends of ETa within irrigated arid regions becomes crucial, the data serves as a base for various critical aspects of agricultural water and soil management. One of the primary implications of accurate ETa is its role in guiding agricultural irrigation practices, with accurate knowledge of how ETa fluctuates across different crop stages and seasons, farmers and irrigation technicians can make informed decisions about when to irrigate. This does not only conserve water resources by avoiding unnecessary irrigation but also helps prevent over-irrigation that can lead to soil salinity and waterlogging issues. However, quantifying ET is not a simple task to do, this rests on the fact that water balance components requires expensive and sophisticated devices to accurately measure such as using the weighing lysimeters which provides direct quantification of ETa fluxes (Kool et al., 2014; Moorhead et al., 2019).

The increasing global scarcity and demand for water highlights the critical necessity for its efficient utilization, particularly within the agricultural sector, which stands out as the single largest consumer of this indispensable resource. Beyond the widening gap between crop demand and water supply, the situation is exacerbated by the gross mismanagement of water resources and a pervasive neglect of the environmental impact on water sources. Crop evapotranspiration serves as an important indicator of crop water demand, influenced by dynamic factors such as weather conditions and crop health. Presently, most water demand models lack spatial considerations, relying instead on point data derived from reference evapotranspiration and crop coefficient values found in the existing literature particularly those published by FAO. The crop coefficient ( $K_c$ ) emerges as a crucial parameter in irrigation scheduling and water allocation. While crop coefficient values obtained from literature may offer practical guidance for scheduling irrigation, the inherent empirical nature of these values introduces some margin of error in estimating crop water requirements. Consequently, there arises an imperative need to rectify and adjust crop coefficient values in accordance with local conditions. This

recognition initiates a departure from a one-size-fits-all approach, emphasizing the importance of accounting for regional disparities and environmental variables that significantly impact the accurate determination of crop water needs. Implementing these localized corrections in crop coefficient values becomes essential for refining the precision of irrigation scheduling and, in turn, optimizing water allocation practices within the agricultural domain.

While methods like the Bowen ratio, Eddy Covariance systems, lysimeters, Scintillometers, and Surface renewal systems provide direct means of measuring crop evapotranspiration (ET<sub>c</sub>), they are limited in their scope (Ramjeawon, 2016; Savage, 2010). These techniques capture data from specific localized areas, failing to account for spatial variability. Given the impracticality of deploying expensive devices like lysimeters and eddy covariance systems extensively, the adoption of the standard reference evapotranspiration (ET<sub>o</sub>) equation, like the Penman-Monteith (PM) equation, has become conventional (Zhang et al., 2023). This equation integrates data from meteorological stations and crop coefficients provided by the Food and Agriculture Organization (FAO-56) guidelines of the United Nations covering most crops which are common globally (Allen, 1998). However, this approach also has its own challenges which include; meteorological station scarcity, especially in developing nations with limited technologies, and the unavailability of certain parameters necessary for the equation's completion compromise its accuracy (Hashmi and Garcia, 1998). For example, areas with high humidity always lack radiation component while arid regions always lack the humidity component to feed into the equation compromising the accuracy of ET<sub>o</sub> quantification.

In response to these complexities, various reference evapotranspiration models have been developed and used in different environmental settings categorized into radiation, aerodynamic, temperature, and combination models (Gossard, 1998). These models aim to bridge data gaps and provide accurate estimations of ET<sub>o</sub>. Despite the existence of these models and their years of utilization, weather stations, confined to specific points, lack the spatial distribution needed for comprehensive large-scale ET<sub>o</sub> investigations highlight the need for site-specific models to ensure accurate ET<sub>o</sub> determination. Furthermore, data gaps arising from weather station maintenance and vandalism further constrain efforts to precisely quantify evapotranspiration patterns (Louw et al., 1998). With challenges associated with ground-based point measurement devices, remote sensing ET products were developed from satellite-based data.

Remote sensing products were developed to solve the issue of spatial limitations with the idea of capturing the variabilities at global scales. Most global ET products were developed to run following the standard PM algorithm combining datasets from different sensors. Such products include the existence of the Water Productivity (WAPoR) ET product with the spatial resolution ranging from 30 m to 250 m with South Africa covered on the 250 m spatial resolution per pixel, the Moderate Resolution Imaging Spectroradiometer (MODIS) Evapotranspiration product (MOD-16) at 1 km and the Land Surface Analysis Satellite Application Facility (LSA SAF) Evapotranspiration product at 3 km spatial resolution. The challenges associated with these products remains their coarse resolutions which were considered ideally to capture the fluxes at global scales such that they become less effective zooming into an individual farm scale, there are no pixels defining variabilities in ET.

Studies on the use of global ET products have been undertaken by several researchers in South Africa (Majozi et al., 2017; Ramoelo et al., 2014) For example, the MOD-16 product in South Africa lacks validity as it has demonstrated underestimations of ET in some environments while it has not been evaluated in most environments including agricultural environments (Gibson et al., 2011; Ndara, 2017). Another study in South Africa with efforts by (Ramoelo et al., 2014) also highlighted the inconsistency of MOD-16 accuracy due to limited data for validation available in the country as well as measurement errors produced by the Eddy Covariance systems and also raising concerns that the inaccuracies in their site of experiments might be related to the parametrization of the Penman-Monteith algorithm that runs the MOD-16 product. (Majozi et al., 2017) also evaluated the GLEAM product using Scintillometer and Eddy covariance data in two ecosystems in South Africa achieving very low correlations and coefficients of determinations. The lack of inconsistencies

reported in South African studies necessitates the development and improvement of satellite-based ET products (Gibson et al., 2011).

As a result, models incorporating better resolution satellite products such as incorporating Landsat data and Sentinel data were developed. These models include the Surface Energy Balance Algorithm for Land (SEBAL), Mapping Evapotranspiration at High Resolution with Internalized Calibration (METRIC), Atmosphere-Land Exchange Inverse (ET-ALEXI), Surface Energy Balance (SEBS) and the Three-Temperature Model (3T Model). The advancement of models like SEBAL developed by (Bastiaanssen et al., 1999) has enabled the estimation of evapotranspiration (ET) with varying accuracies in diverse environments. Studies in different regions have demonstrated the applicability and potential enhancements of these models. In Iran, (Rahimzadegan and Janani, 2019) evaluated SEBAL's effectiveness in estimating pistachio crop evapotranspiration using Landsat 8 images, highlighting SEBAL's potential for precise ET mapping. (Silva et al., 2018) employed SEBAL in Brazil, producing compatible ET estimates with literature values, demonstrating its utility in various landscapes. In Turkey, (Shamloo et al., 2021) validated SEBAL's estimations for corn against multiple methods, showcasing its robustness. However, studies involving the utilization of remote sensing data for assessing water use in South Africa have been conducted employing the SEBAL model alongside data from Landsat at field scales (Klaasse et al., 2008; Klaasse and Jarmain, 2011; Singels et al., 2018). Additionally, (Ndou et al., 2018) applied SEBAL to model groundwater levels in South Africa, revealing significant correlations between potential evapotranspiration and groundwater depth. These advantages of these field-scale investigations was the potential for on-site validation (Gibson et al., 2013). The SEBAL validation approach has been successfully employed in several of the previously researched studies with the use of water balance, eddy covariance and Scintillometer with no lysimeter validation related work that has been published. These studies collectively highlight the SEBAL's versatile applicability and offer insights into refining its models for improved accuracy in different environments.

The Surface Energy Balance System (SEBS) was developed in 2002 by (Su, 2002), to estimate evapotranspiration through satellite imagery. The model's adeptness in estimating evapotranspiration and energy flux has been substantiated by (Jia et al., 2003) and (McCabe and Wood, 2006). While generally reliable, instances of excessive latent heat flux overestimation have been reported (McCabe and Wood, 2006), particularly in forested areas (Badola, 2009), and overestimations of daily ET at grassland sites (Rwasoka et al., 2011). Given the model's original focus on agricultural environments, it is reasonable that certain parameterizations might not be fully optimal for non-agricultural land types (Gibson et al., 2013). In the South African context, Gibson *et al.* (2011) introduced the SEBS model, alongside MODIS satellite data, validated with eddy covariance data from a substantial apple orchard in the Western Cape. This validation process revealed an underestimation of sensible heat flux due to constraints imposed by wet conditions. On the same study, daily ET from the eddy covariance system ranged from 55 to 96% of SEBS estimates, signifying an overestimation. (Gokool et al., 2018) conducted a study to validate satellite-derived ET against data obtained from a surface renewal system and eddy covariance in a sugarcane farm in Mpumalanga province, South Africa. They also aimed to assess the feasibility of two infilling techniques to create a daily satellite-derived ET time series. They used MODIS imagery with SEBS for ET modelling and their results indicated that SEBS ET estimates were about 47% higher, yielding  $R^2$  and RMSE values of 0.33 and 2.19  $\text{mm}\cdot\text{d}^{-1}$ , respectively, compared to in-situ ET values. Inaccuracies were attributed to errors in ET measurements. In another study, (Govender, 2022) employed the SEBS model to evaluate the impact of land use changes and climate variability on ET fluxes using Landsat 8 data. Validation was conducted against Penman-Monteith derived ET values, demonstrating significant relationships. However, this study did not provide more information into water balance components due to a lack of validation devices on the study site. Given that SEBS was primarily designed for agricultural contexts, the absence of validation devices in South Africa underscores the need for accurate measurement tools for assessing water balance components.

(Madugundu et al., 2017) utilized the METRIC algorithm on Landsat-8 images from June to October 2013 to map evapotranspiration (ET) for a 50-hectare irrigated alfalfa field in Saudi Arabia. They validated METRIC's accuracy against data from an eddy covariance (EC) flux tower and found it provided accurate ET estimations

with RMSE values of 0.13 and 4.15 mm/d. The algorithm performed better in full canopy conditions. Although hourly ET was slightly overestimated by 6.6%, daily ET was underestimated by 4.2%. (Lian and Huang, 2015) estimated ET fluctuations across diverse land cover types in an oasis using 14 Landsat-8 images. They employed the METRIC model, applying an innovative approach by selecting hot extreme pixels separately for desert and oasis areas. Their findings revealed significant temporal-spatial ET variations, with highest values over water bodies, arable land, low-lying terrain, and forests. METRIC, when using appropriate extreme pixel selection, displayed reasonable accuracy for heterogeneous land use, achieving  $R^2=0.9$  and an RMSE of 1.1 mm respectively. Although such findings are evident in other countries, limited studies utilizing the METRIC model in South Africa in literature were noted.

Given the challenges posed by conventional methods for estimating and measuring ET in capturing the spatial variations of ET, satellite-based ET estimation emerges as the only viable approach for quantifying water loss in agricultural environments. However, widely available global ET products, due to their coarse spatial resolutions and algorithm parameterization issues, are inadequate for precise field-level ET estimations. While some countries have achieved satisfactory results using remotely sensed models that integrate higher-resolution satellite imagery, the challenge in South Africa lies in obtaining accurate measured data to effectively assess the applicability of models for generating field-scale ET products.

To overcome these limitations and enhance the understanding of spatial variability in evapotranspiration, this study aims to integrate high-temporal-resolution smart field weighing lysimeters which will play a crucial role in determining and refining  $ET_a$  values using Landsat 8 data and established remote sensing models, with a focus on SEBAL, SEBS,  $ET_a_{VI}$ , and  $ET_a_{CWSI}$  ET approaches. Landsat 8 data offers finer spatial resolution, which is particularly beneficial when investigating field-scale dynamics of crop water usage in agricultural landscapes. By integrating Landsat 8 data with  $ET_o$  values obtained from weather stations and  $ET_a$  measurements derived from lysimeters, a more comprehensive understanding of  $ET_a$  distribution can be achieved.

## 6.2 METHODOLOGY

### 6.2.1 Study area.

The Vaalharts Irrigation Scheme is a large-scale irrigation project located in the Northern Cape province of South Africa. It is one of the country's most significant and extensive irrigation systems. The scheme was established in the 1930s and has since played a crucial role in agricultural development within the arid region. The Vaalharts Scheme primarily utilizes water from the Vaal River, sourced from the Vaal Dam. This water is channelled through an intricate network of canals and pipelines to supply water to around 35,000 hectares of land, making it one of the largest irrigation projects in South Africa (Barnard, 2013). Pivot irrigation dominates the area (Ratshiedana et al., 2023) whereas other irrigation systems such as drip irrigation, flood irrigation and sprinklers amongst others exist (Figure 28). The use of groundwater in this area is not suitable due to high salinity levels (Pretorius, 2018). The main goal of the scheme is to enable the cultivation of various crops, including fruits, vegetables, and field crops, in an area that would otherwise be too arid for sustained agricultural activity (Pretorius, 2018). To ensure efficient water distribution, the scheme employs advanced water management practices, such as controlled canal systems and modern irrigation technologies. Farmers within the scheme receive allocated water quotas based on the size of their land holdings and the types of crops they cultivate. The success of the Vaalharts Irrigation Scheme has had a positive impact on the local economy by creating jobs, generating agricultural products, and contributing to food security. It has also paved the way for agricultural diversification and economic growth within the region. However, challenges related to water scarcity, maintenance, and equitable water distribution have also been part of the scheme's history.

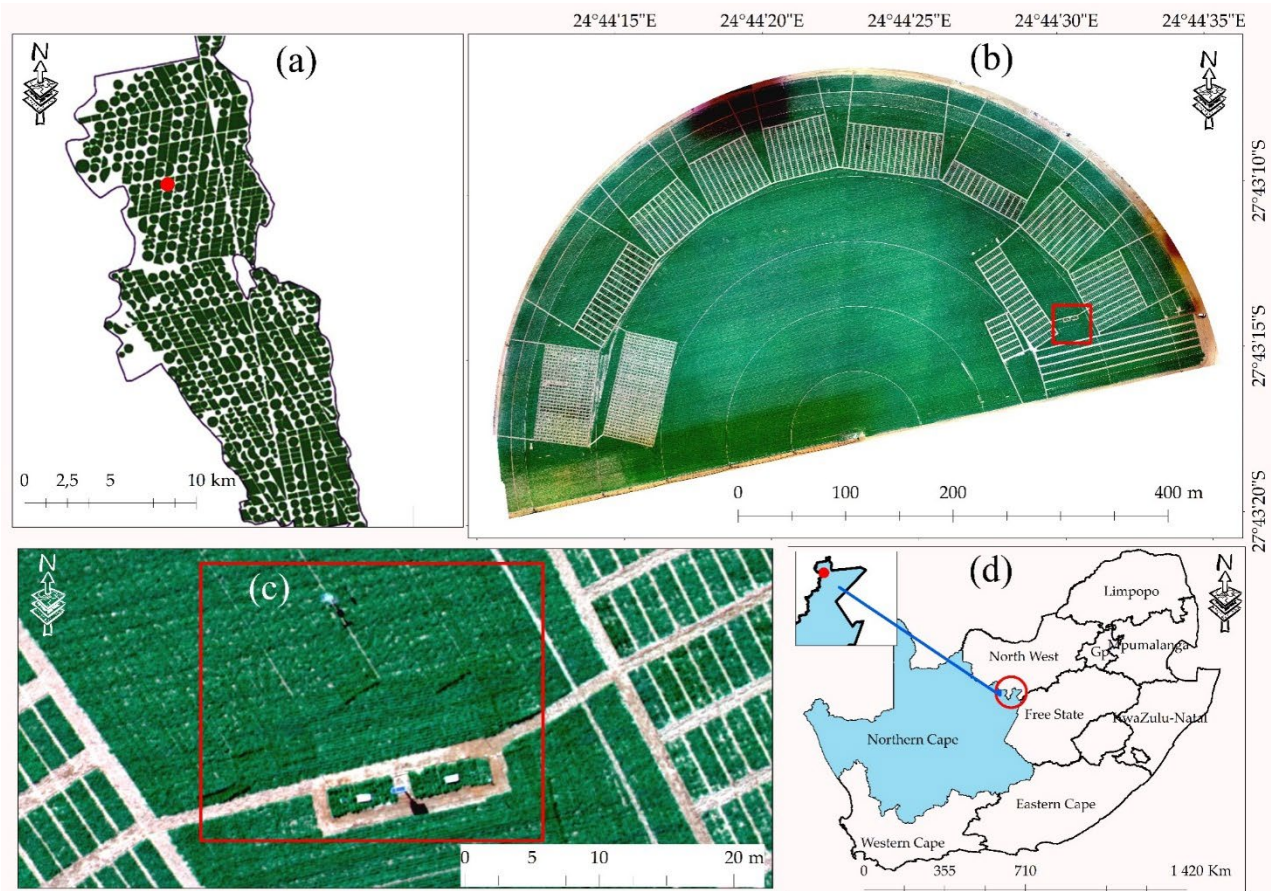


**Figure 49: The map depicting the study area distinct regions, (a) delineates the Vaalharts Irrigation Scheme, (b) identifies the experimental farm, and (c) indicates the study area's position in relation to various South African provinces.**

### 6.2.2 Data Acquisition

Landsat 8 images were obtained from the United States Geological Survey (USGS) Earth Explorer portal (<https://earthexplorer.usgs.gov/>, 2022). A total of 24 cloud free days were obtained matching the days with zero irrigation and precipitation in the experimental farm to align with the direct  $ET_a$  measurements. To acquire the images a selection criterion of zero % clouds and Level-1 Terrain Corrected (L1T) was inputted into the Earth Explorer interface, the system retrieved and displayed the available Landsat 8 images which matched the search parameters. The L1T products were downloaded being radiometrically calibrated and georeferenced to the study area. The L1T products included 11 bands which are given in table 1. However, the selection of days with zero cloud limited the number of images available for the study. For a detailed comparison with lysimeter  $ET_a$  at the pixel scale, images that matched lysimeter data on days with zero irrigation and the satellite pass were directly assessed. On days when this matching was not possible, an imperial approach was employed, considering a broader perspective for evaluation using a relationship between crop evapotranspiration based on various weather stations within the study area. This approach aimed to align the satellite-derived  $ET_a$  with ground-based measurements.

**Table 30: Landsat 8 Satellite Data from Operational Land Imager (OLI) and Thermal Infrared Sensor (TIRS)**

Band Name	Wavelength	Significance in Mapping Scenarios
Band 1 – coastal aerosol	0.43-0.45 nm	Useful for studying coastal regions and aerosols.
Band 2 – blue	0.45-0.51 nm	Applied in bathymetric mapping, soil-vegetation differentiation, and distinguishing between deciduous and coniferous vegetation.
Band 3 – green	0.53-0.59 nm	Highlights peak vegetation, aiding in plant vigor assessment.
Band 4 – red	0.64-0.67 nm	Detects variations in vegetation slopes.
Band 5 – Near Infrared (NIR)	0.85-0.88 nm	Emphasizes biomass content and shoreline features.
Band 6 – Short-wave Infrared (SWIR) 1	1.57-1.65 nm	Discriminates soil and vegetation moisture content and can penetrate thin clouds.
Band 7 – Short-wave Infrared (SWIR) 2	2.11-2.29 nm	Enhanced detection of soil and vegetation moisture, and penetration of thin clouds.
Band 8 – Panchromatic	0.50-0.68 nm	Offers 15-meter resolution for sharper image definition.
Band 9 – Cirrus	1.36-1.38 nm	Improved identification of cirrus cloud interference.
Band 10 – TIRS 1	10.60-11.19 $\mu\text{m}$	Provides 100-meter resolution for thermal mapping and estimated soil moisture assessment.
Band 11 – TIRS 2	11.50-12.51 $\mu\text{m}$	Enhanced 100-meter resolution for thermal mapping and estimated soil moisture assessment.

### 6.2.3 Data Pre-processing

The pre-processing of Level-1 Terrain Corrected (L1TP) data was executed utilizing the Semi-Automatic Classification Plugin in QGIS. The obtained L1TP Landsat 8 images were directly imported into QGIS without any sub-setting. By performing radiometric calibration, the data was transformed from digital numbers (DN) to top-of-atmosphere (TOA) reflectance values. This conversion was achieved by utilizing the metadata linked to each image file. Since the L1TP data had already been georeferenced, geometric correction was unnecessary. Atmospheric correction was applied to mitigate the impact of atmospheric scattering and absorption. For the thermal bands, processing was carried out to derive temperature values in degrees Celsius ( $^{\circ}\text{C}$ ). Additionally, each image underwent pan sharpening to enhance the spatial resolution of the multispectral bands.

### 6.2.4 Actual Evapotranspiration Based on Reference Evapotranspiration and vegetation index.

The reference evapotranspiration in this study was calculated using the Penman-Monteith evapotranspiration model. Actual crop evapotranspiration was directly measured using a smart field weighing lysimeter at a field scale. Extending the ETa data to locations without lysimeters at weather stations involved the development of an empirical relationship between reference evapotranspiration and actual evapotranspiration. This developed relationship was then applied to the reference evapotranspiration values to estimate the actual crop

evapotranspiration in areas without lysimeters, enabling a broader understanding of water consumption patterns across different locations.

The general equation for actual crop evapotranspiration is given by the equation:

$$ET_a = ET_o * K_c$$

The reference evapotranspiration ( $ET_o$ ) was acquired from meteorological stations, and the crop coefficient ( $K_c$ ) was employed.  $ET_o$  was determined for various stations within the study region using the conventional Penman-Monteith equation for computing reference evapotranspiration, as introduced by Allen (1998) as:

$$ET_o = \frac{0.408\Delta(R_n - G) + \gamma \left( \frac{C_n}{T + 273} \right) U_2 (e_s - e_a)}{(\Delta + \gamma(1 + C_d U_2))}$$

Where  $ET_o$  denotes the standardized reference evapotranspiration in millimetres per day (mm/d) or millimetres per hour (mm/h). The symbol  $\Delta$  represents the slope of saturation vapour pressure against air temperature in kilopascals per degree Celsius ( $kPa/^\circ C$ ).  $R_n$  corresponds to the total or net radiation on the studied crop surface, measured in mega joules per square metre per day ( $MJ/m^2/d$ ) over a 24-hour period, while  $G$  signifies the heat flux density at the soil surface during the same 24-hour interval.  $T$  stands for the average daily air temperature per hour in degrees Celsius ( $^\circ C$ ), and  $U_2$  represents the mean hourly wind speed measured at a height of 2 metres in metres per second (m/s). The variable  $e_s$  denotes the saturation vapour pressure in kilopascals (kPa),  $e_a$  signifies the actual vapour pressure in kilopascals (kPa), and the difference  $e_s - e_a$  indicates the saturation vapour pressure deficit, also measured in kilopascals (kPa). Additionally,  $\gamma$  represents the psychrometric constant in kilopascals per degree Celsius ( $kPa/^\circ C$ ), whereas  $C_n$  and  $C_d$  are constants that vary based on the reference surface being employed (Allen, 1998).

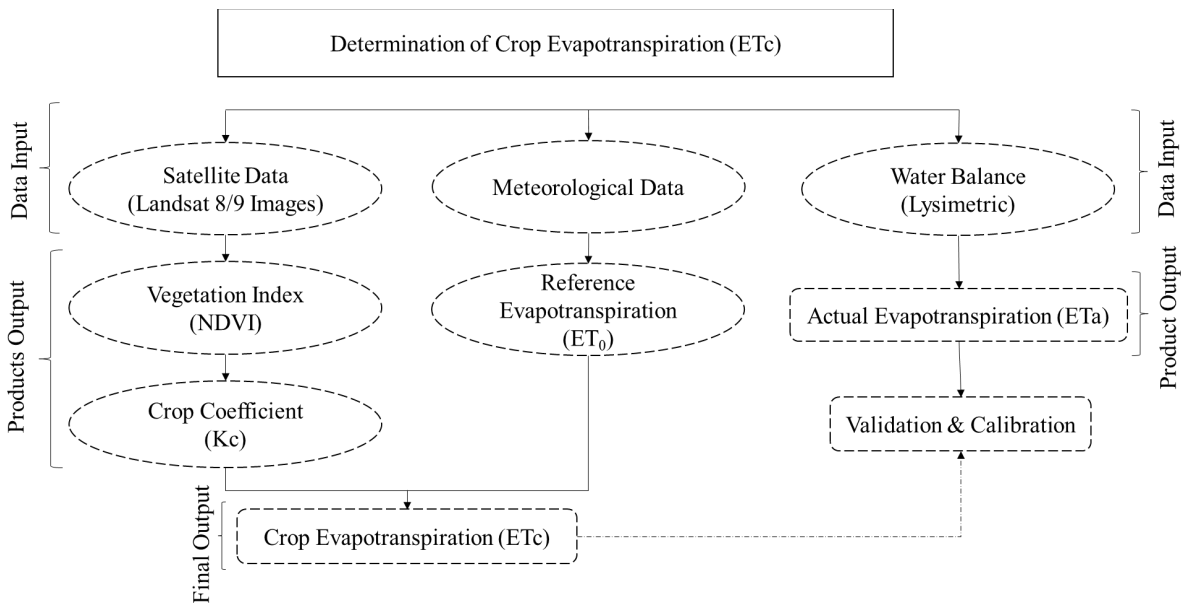


**Figure 50: Conceptual framework for the determination of crop evapotranspiration based on vegetation index.**

To determine the  $K_c$  values, NDVI and fractional vegetation cover were used applying the following equations:

$$K_c = K_{cb} + K_e$$

$K_{cb}$  denotes the fundamental crop coefficient, while  $K_e$  stands for the soil evaporation coefficient.

$$K_{cb} = 1.07 \times \left[ 1 - \left( \frac{NDVI_v - NDVI_s}{NDVI_v - NDVI_s} \right)^{0.84} \right]^{0.54}$$

NDVI<sub>v</sub> and NDVI<sub>l</sub> represent the highest and lowest daily NDVI values, respectively.

$$K_e = \beta \times (1 - fV_c)$$

Where  $\beta$  is a constant and  $fV_c$  is the fractional vegetation cover representing the ratio of vegetation to bare soils. The value of  $\beta$  was assumed to be 0.25 as adopted from the studies that were undertaken by (Abid et al., 2018) and (Ren et al., 2023) which both adopted a  $\beta$  value of 0.25, drawn from the report of (Allen, 1998) based on irrigation supply which was approximately within 10 days.

#### 6.2.4.1 The SEBAL Model

The retrieval of ET based on the SEBAL model was based on the energy balance given by the expression:

$$ET = R_n - G - H$$

Where  $R_n$  is the net radiation,  $G$  is the soil heat flux and  $H$  is the sensible heat flux, ET is the evapotranspiration component equivalent to the latent heat flux (LE).

The net radiation ( $R_n$ ) was computed using the energy balance equation, considering albedo, incoming solar radiation, and outgoing thermal radiation. The net radiation was calculated based on the equation:

$$R_n = (1 - \alpha)RS \downarrow + \varepsilon \times RL \downarrow - (1 - \varepsilon)RL \uparrow$$

Where  $RS \downarrow$  represents the total solar radiation that reaches the earth's surface from the sun. The parameter  $\alpha$  represents the earth surface's albedo, which is the percentage of incoming solar radiation that is reflected into space. The outgoing longwave radiation emitted by the Earth's surface is denoted by  $RL \downarrow$ . While  $\varepsilon$  denotes the emissivity which describes how efficiently a surface emits thermal radiation, it is a dimensionless value between 0 and 1, with 0 being a perfect reflector and 1 representing a perfect emitter. The term  $\varepsilon \times RL \downarrow$  accounts for the emitted longwave radiation because of the temperature of the earth's surface, whereas  $RL \uparrow$  denotes the longwave radiation emitted by the atmosphere and directed towards the earth's surface and it is caused by the greenhouse effect, as well as the fact that the atmosphere emits radiation back to the surface.

Surface albedo was calculated for both types of land surfaces using the reflectance values from the visible and near-infrared bands of the Landsat 8 imagery. Albedo represents the proportion of incoming solar radiation that's reflected by the land surface. The albedo was calculated based on the equation:

$$\alpha = \left( \frac{(0.356 \times \text{Blue Band}) + (0.130 \times \text{Red Band}) + (0.373 \times \text{NIR Band}) + (0.085 \times \text{SWIR}) + (0.072 \times \text{SWIR}) - 0.018}{1.016} \right)$$

The longwave radiation was calculated based on the equation:

$$RL \uparrow = \varepsilon \times \sigma \times T_s^4$$

Where  $\sigma$  is the Stefan-Boltzmann constant which is a fundamental physical constant that relates the temperature of an object to the amount of thermal radiation it emits. It has a value of approximately  $5.67 \times 10^{-8}$   $5.67 \times 10^{-8}$  W/ (m<sup>2</sup>·K<sup>4</sup>). The constant  $\sigma$  converts the temperature of the surface to the amount of emitted radiation.

The outgoing longwave radiation was calculated based on the equation:

$$RL \downarrow = \sigma \times \varepsilon_a \times T_a^4$$

Where  $\varepsilon_a$  is the emissivity of the material and it is a dimensionless value between 0 and 1 that describes how efficiently an object emits thermal radiation compared to a perfect blackbody radiator and can be calculated using the equation:

$$\varepsilon_a = 9.2 \times 10^{-6} \times (T_a + 273)^2$$

Where  $T_a$  is the ambient temperature in degrees Celsius. The value 273 was added to  $T_a$  to convert the temperature from degrees Celsius to Kelvin, as the Kelvin scale starts from absolute zero which is equal to  $-273.15^\circ\text{C}$ . The value  $9.2 \times 10^{-6}$  is a constant coefficient that determines the relationship between the temperature and emissivity.

$$\varepsilon = \varepsilon_s \times (1 - Pv) + \varepsilon_v + Pv$$

Where ( $\varepsilon_s$ ) represent a non-vegetated surface and ( $\varepsilon_v$ ) represent a vegetated surface while the  $Pv$  represents the fraction of the surface covered by vegetation. The constants  $E_s=B10=0.971$   $B11=0.977$   $E_v$   $b10=987$   $b11=989$  were used for Landsat 8 data.

The fractional vegetation cover was calculated based on the equation:

$$Pv = \left( \frac{NDVI - NDVI_{min}}{NDVI_{max} - NDVI_{min}} \right)^{0.5}$$

Where NDVI is the Normalized Difference Vegetation Index calculated based on the near infrared band and the red band. NDVI\_min is the minimum NDVI value which was observed in the study area which corresponds to areas with minimal or no vegetation, while NDVI\_max represent the maximum NDVI value which was observed in the study area representing the highest NDVI value that corresponds to areas with dense and healthy vegetation. Where  $NDVI_{max} = 0.5$  and  $NDVI_{min} = 0.15$  according to Schulze, 1997 b

The soil heat flux ( $G$ ) was calculated based on the equation:

$$G = \left( \frac{T_s - 273.16}{\alpha} \right) \times (0.0038\alpha + 0.0074\alpha^2)(1 - 0.98(NDVI^4))R_n$$

Where  $T_s$  is the surface temperature in degrees Celsius.

$$LST = \left( \frac{LST_{10} - LST_{11}}{2} \right)$$

To calculate the sensible heat flux, the following equation was used:

$$H = \frac{p \times c_p \times dT}{rah}$$

Where  $p$  is the air density, which signifies the mass of air per unit volume.  $C_p$  is the specific heat capacity of air, indicating the amount of heat energy required to raise the temperature of a unit mass of air by one degree Celsius.  $T$  represent the temperature difference between the earth's surface and the overlying air. The  $rah$ -term is the aerodynamic resistance to heat transfer, which accounts for the resistance offered by the atmosphere to the exchange of heat between the surface and the air.

The change in temperature was calculated based on the equation:

$$dT = aT_s + b$$

Where  $a$  is the coefficient that quantifies the relationship between the change in temperature and the surface temperature while  $b$  is the Constant term representing an additional temperature change that is not directly proportional to the surface temperature.

The aerodynamic resistance to heat transfer ( $rah$ ) parameter quantifies how much the atmosphere resists the exchange of heat between the earth's surface and the air which was calculated using the equation:

$$rah = \ln \ln \frac{Z_2 - Z_1}{U_*} k$$

Where  $Z_2-Z_1$  is the difference in measurement heights being the vertical distance between two points in the atmosphere where temperature measurements were taken.  $U^*$  being the friction velocity that characterizes the turbulence and momentum exchange near the earth's surface and the parameter  $k$  is the Von Kármán constant.  $U^*$  is calculated using the equation:

$$U^* = \frac{Kux}{\ln} \left( \frac{Zx}{Zom} \right)$$

Where  $(Ku)$  is the friction velocity scale factor the wind speed at height  $x$  ( $Ux$ ), and the natural logarithm of the ratio of the measurement height  $Zx$  to the roughness length for momentum ( $Zom$ ).

While net radiation flux ( $Rn$ ), sensible heat flux ( $H$ ), and Earth's temperature flux ( $G$ ) are instantaneous measurements during the satellite's passage, the latent heat flux values are instantaneous as well. The instantaneous evapotranspiration rate now of satellite pass was calculated using the (Frahmand et al., 2020) formula:

$$ET_{inst} = 3600 \times \frac{\lambda ET}{\lambda}$$

Where  $\lambda ET$  is the heat of vaporization, which is the amount of heat required to convert a unit mass of liquid into vapour at a constant temperature. While  $\lambda$  is the latent heat flux, which is the rate of heat transfer associated with the phase change which in this case refers to the transition of water from liquid to vapour.

The value of  $\lambda$  was computed using the formula presented in the work by (Ndou et al., 2018) given as:

$$\lambda = [2.501 - 0.00236(TS - 273)] \times 10^6$$

The daily ET values were determined through the utilization of the reference evapotranspiration fraction ( $ETrF$ ) and reference plant evapotranspiration ( $ETr$ ) where  $ETrF$  signifies the proportion of calculated  $ET_{inst}$  for each pixel in relation to the reference ET derived from meteorological data, as outlined in the research efforts by (Allen et al., 2011).

$$ETrF = \frac{ET_{inst}}{ETr}$$

The calculation for daily evapotranspiration values was performed as follows:

$$ET_{24} = ETrF \times (ETr_{-24}).$$

## 6.2.4.2 Crop water stress-based ETa.

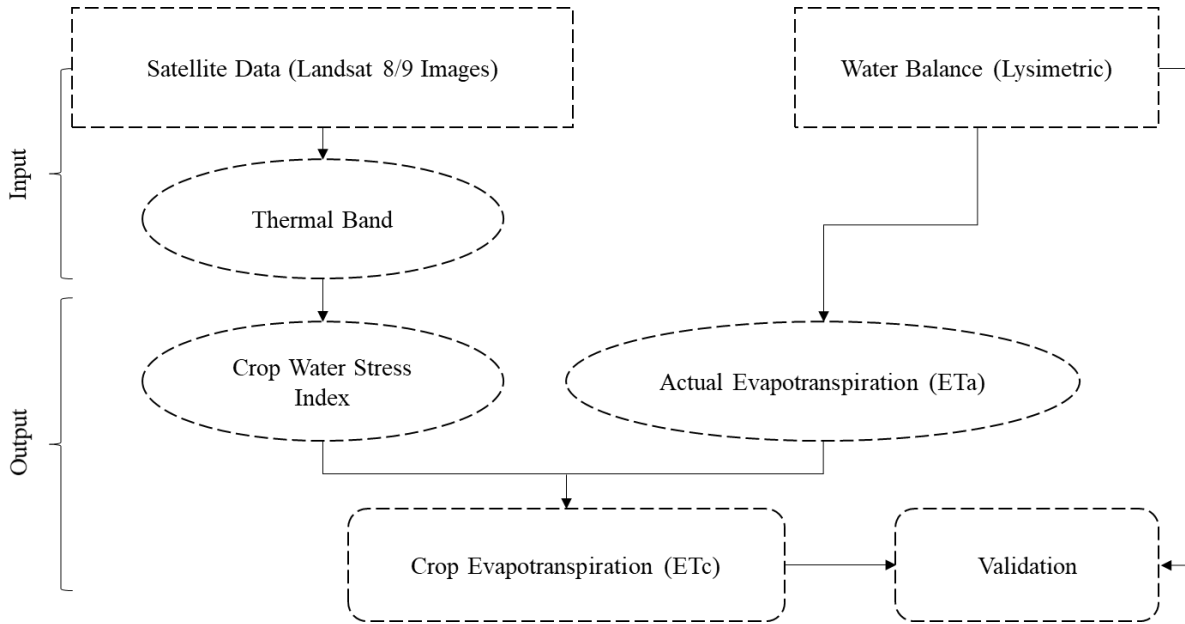


**Figure 51: Conceptual framework for the determination of crop evapotranspiration based on CWSI.**

(Jackson et al., 1981) established a mathematical relationship between the crop water stress index (CWSI) and the water consumption of plants. Their findings indicated that when CWSI equalled one, no water was being used, and if CWSI reached zero, ETa matched ETc, signifying an absence of water shortage. This highlighted the utility of both CWSI and ETc as effective tools for quantifying agricultural water consumption. To compute ETa, they devised the equation:

$$ETa = ET0 * (1 - CWSI)$$

In this study, Landsat 8 thermal data was employed to formulate the crop water stress index, utilizing the equation developed by (Jackson et al., 1981):

$$CWSI = \frac{\Delta T - \Delta Tm}{\Delta Tx - \Delta Tm}$$

Where  $\Delta T$  represents the difference in air temperature as determined by LST,  $\Delta Tm$  indicates the least change in LST<sub>air</sub>, and  $\Delta Tx$  denotes the greatest divergence between LST and air temperature.

## 6.2.4.3 SEBS model approach

(Su, 2002) introduced the Surface Energy Balance System (SEBS) as a methodology for estimating heat flow fluxes and evaporative fractions. This model shares similarities with the SEBAL model, with a distinction being the incorporation of soil heat flux in the SEBS model. The inclusion of soil heat flux in SEBS enhances its capability to provide a more comprehensive assessment of the surface energy balance. The soil heat flux was calculated as:

$$G_0 = R_n [T_c + (1 - F_{vc})(T_s - T_c)]$$

Where,  $G_0$  is the soil heat flux,  $R_n$  represents the net radiation,  $T_c$  stands for the psychrometric constant for the canopy air layer,  $T_s$  represents the psychrometric constant for the soil and  $F_{vc}$  is the fractional vegetation cover.

## 6.3 RESULTS

Landsat 8 images between 2019 and 2021 study experimental period are detailed in table 2 below. The criterion for image selection was based on cloud free scenes, however on 16<sup>th</sup> February 2020, an image with 4.23% was selected because it was cloud free within the area of interest which is the irrigation scheme. Details of the crop within the experimental farm are also given in the last column of the table.

**Table 31: Details on satellite images used in this study.**

Path/Row	Date Acquired	Satellite pass time	Cloud cover	Crop type
172/79	2019/09/09	08:15:19	0.01	Winter Barley
172/79	2020/01/15	08:15:15	0.22	Maize
172/79	2020/01/31	08:15:10	0.00	Maize
172/79	2020/02/16	08:15:06	4.23	Winter Barley
172/79	2020/08/10	08:15:03	0.01	Winter Barley
172/79	2020/09/11	08:15:18	0.00	Winter Barley
172/79	2020/09/27	08:15:23	0.00	Winter Barley
172/79	2020/10/13	08:15:25	0.05	Winter Barley
172/79	2021/01/17	08:15:14	0.00	Soybean
172/79	2021/02/18	08:15:08	0.01	Soybean
172/79	2021/03/22	08:14:53	0.15	Soybean

**Table 32: Showing the daily ETa (mm) from the lysimeter and estimated from four remote sensing models.**

Date	ETa_Lysimeter	ETa_SEBAL	ETa_SEBS	ETa_VI	ETa_CWSI
09-Sep-19	6,27	7	7,16	4,86	6,99
15-Jan-20	5,23	7,44	11,94	10,03	9,66
31-Jan-20	1,29	3,83	3,65	10,78	5,83
16-Feb-20	8,18	10,45	12,2	10,38	9,04
10-Aug-20	5,74	7,15	12,8	4,12	4,22
11-Sep-20	3,35	4,15	11,07	7,7	2,49
27-Sep-20	4,17	4,88	9,4	6,84	6,4
13-Oct-20	5,19	8,05	9,83	6,44	1,92
17-Jan-21	5,38	5,81	6,71	8,22	6,91
18-Feb-21	2,32	4,77	6,74	12,55	4,46
22-Mar-21	2,87	5,76	4,5	10,06	6,58

### 6.3.1 Statistical analysis between ETa from lysimeter and the estimated ETa from four models

Table 4 below shows the statistical metrics between the lysimeter and ETa remote sensing models. On assessing the RMSE, SEBAL achieves the lowest RMSE (1.97), indicating the smallest average magnitude of error between predicted and observed values. This suggests that SEBAL is the most accurate model in terms of precision. The ETa\_CWSI also performs well with a reasonably low RMSE (2.71), displaying its effectiveness in estimating ETa. However, the SEBS model falls in the middle range, having a moderate RMSE (4.77). Findings portray that it is less precise than SEBAL and ETa\_CWSI but outperforms ETa\_VI based on that the ETa\_VI shows the highest RMSE (5.35), suggesting a larger average discrepancy between predicted and observed values.

Assessing the Mean Absolute Error (MAE), the SEBAL model excels with the lowest MAE (1.75), indicating accurate predictions and minimal bias. While ETa\_CWSI also performs well with a relatively low MAE (2.35), demonstrating its competence in providing accurate ETa estimates. The SEBS model again on MAE falls in the middle range with a moderate MAE (4.18), suggesting slightly less accuracy compared to SEBAL and ETa\_CWSI. The ETa\_VI Exhibits the highest MAE (4.37), indicating a larger average absolute error in predictions. When using the Percentage Bias, the SEBAL Shows a negative PBIAS (-38.61), suggesting an underestimation of lysimeter values on average. Despite this bias, the model still demonstrates good precision. The ETa\_CWSI also exhibits a negative PBIAS (-29.03), indicating a slight underestimation. However, it is less biased than SEBAL. The SEBS model shows a significantly negative PBIAS (-92.04), indicating a considerable underestimation of lysimeter values. This suggests a systematic bias in SEBS predictions. The ETa\_VI presents a negative PBIAS (-83.99), indicating a substantial underestimation similar to SEBS. On assessing the Coefficient of Determination (R), the SEBAL achieves the highest R value (0.88), indicating a strong positive linear relationship between predicted and observed values. This suggests SEBAL's effectiveness in capturing the variability in lysimeter values. The ETa\_CWSI also demonstrates a relatively high R value (0.38), indicating a positive but weaker linear relationship compared to SEBAL. The SEBS model exhibits a moderate R value (0.65), suggesting a reasonable but not as strong correlation as SEBAL. The ETa\_VI presents a negative R value (-0.43), indicating a poor fit and an inverse relationship with lysimeter values.

Lastly, on assessing the Mean Absolute Percentage Error (MAPE), the SEBAL Shows the lowest MAPE (55.77%), indicating a lower percentage error on average. This further emphasizes SEBAL's accuracy. The ETa\_CWSI presents a moderate MAPE (79.75%), indicating a higher percentage error compared to SEBAL but still within an acceptable range. The SEBS model exhibits a higher MAPE (110.44%), indicating a larger average percentage error. The ETa\_VI demonstrates the highest MAPE (169.75%), indicating a higher relative error compared to other models.

**Table 33: Comparison of estimated and lysimeter ET values using statistical indicators.**

Method	SEBAL	SEBS	ETa_VI	ETa_CWSI
RMSE	1.97	4.77	5.347736	2.711841
MAE	1.75	4.18	4.368182	2.346364
PBIAS	-38.61	-92.04	-83.9968	-29.02581
R <sup>2</sup>	0,78	0,43	0,19	0,14
MAPE	55.77	110.44	169.7515	79.74747
R	0.88	0.65	-0.4335184	0.3804239

Figures (31 and 32) displays the spatial distribution of Evapotranspiration (ETa), which has been derived using the SEBAL model. This model stands out as the most robust among the various models evaluated, with the assessment conducted against the ground-truth lysimeter ETa data.

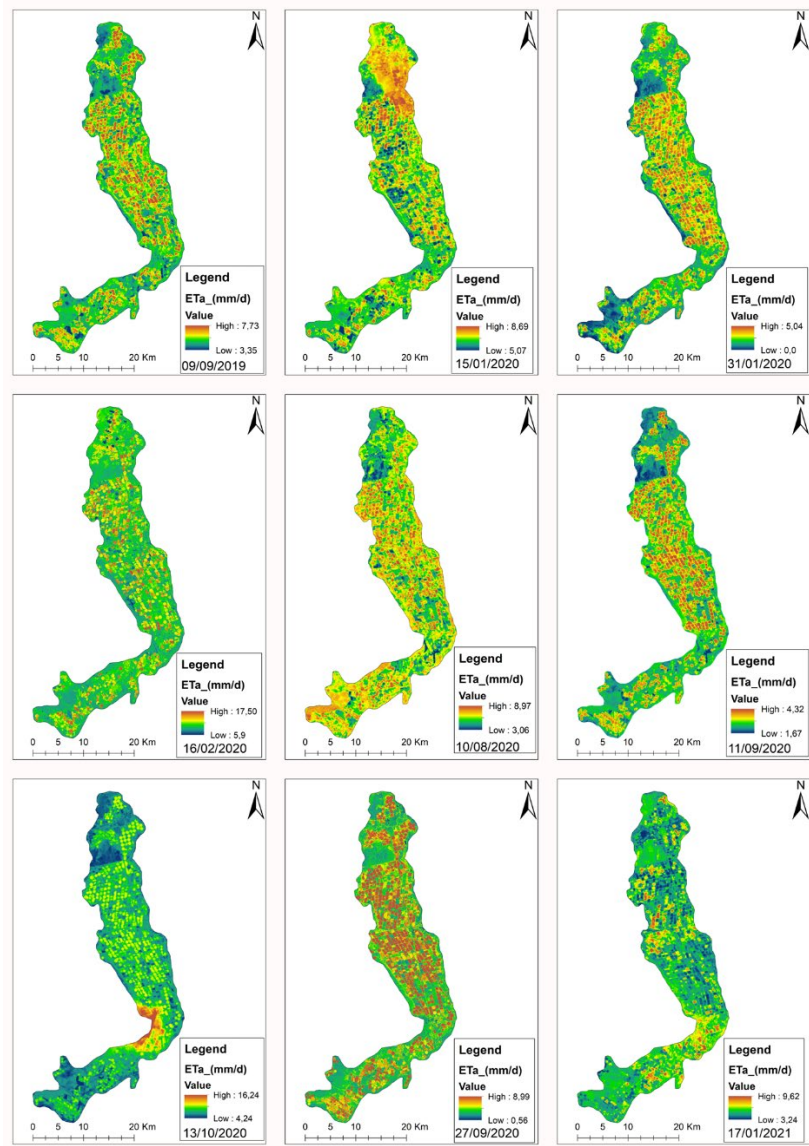
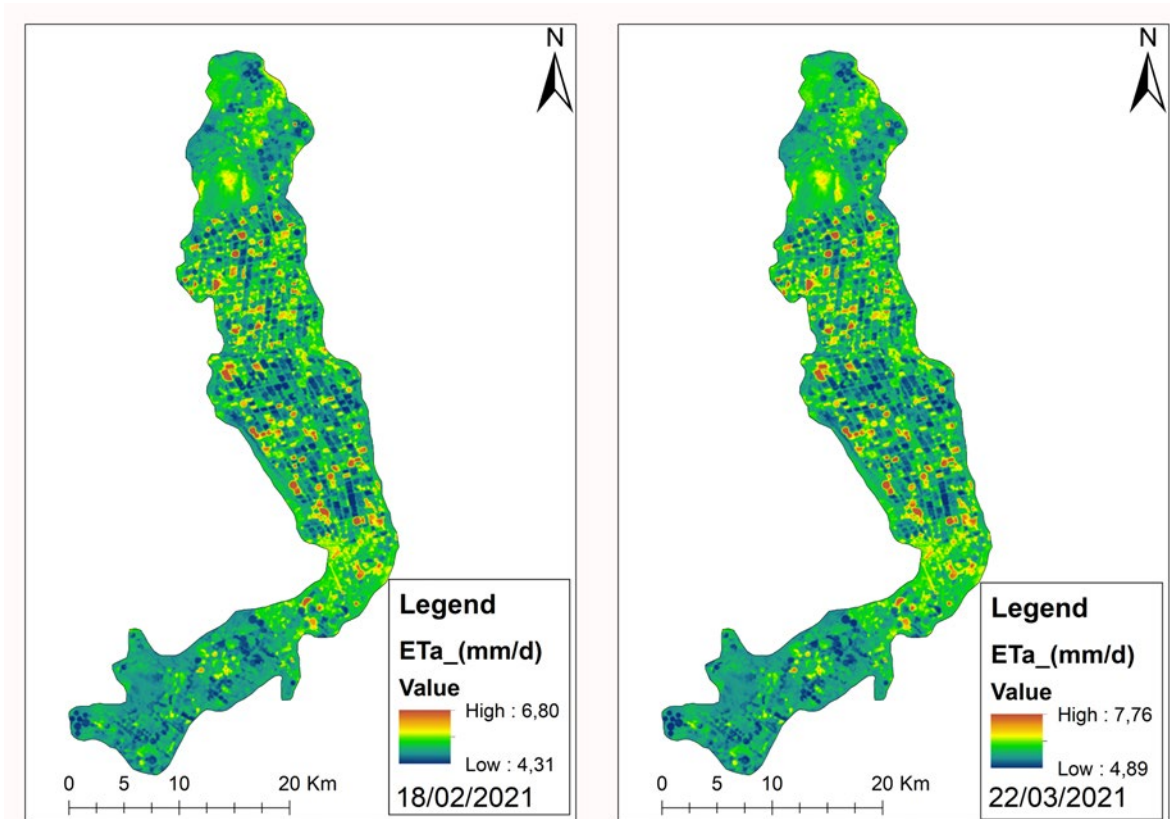


Figure 52: Shows the spatial distribution of ETa values estimated by SEBAL algorithm compared to the lysimeter method.



**Figure 53: Shows the spatial distribution of ETa values estimated by SEBAL algorithm compared to the lysimeter method.**

## 6.4 DISCUSSIONS

This study was undertaken over the course of four successive cropping seasons with a comprehensive evaluation of the capacity of satellite-derived ET using SEBAL, SEBS, vegetation index (VI) and crop water stress index (CWSI) based models and lysimetric approach in monitoring evapotranspiration (ET) across barley, maize, and soybean fields from 2019 to 2021. The primary objective of this study was to bridge the existing research gap concerning the accurate estimation of crop coefficient ( $K_c$ ) and crop evapotranspiration ( $ET_c$ ) at a farm-scale utilizing remotely sensed data. To achieve this, the study employed Landsat 8 satellite sensors to generate detailed time-series maps of ET based on SEBAL, SEBS, VI and CWSI throughout the entirety of the cropping seasons. The choice of Landsat 8, with its advanced capabilities, allowed for a more nuanced understanding of the spatial and temporal dynamics of vegetation and water stress in the selected crops. The basal crop coefficient ( $K_{cb}$ ) was meticulously modelled by analysing the NDVI time-series data. Concurrently, the daily FAO56 reference evapotranspiration ( $ET_o$ ) was derived from a nearby weather station, serving as a crucial benchmark for assessing the accuracy of the remotely sensed data. To validate and augment the study's findings, a smart field weighing lysimeter was installed to directly measure crop evapotranspiration during corresponding seasonal periods. These lysimeter provided ground-truth data, contributing to the reliability and robustness of the study's conclusions.

The SEBAL Model demonstrated to be the most effective model in estimating  $ET_a$ . Similar findings have been reported by (Zoratipour et al., 2023) when comparing SEBAL, SEBS and lysimeter values. However, the SEBAL's superior performance can be attributed to its comprehensive physical basis, higher spatial and temporal resolution and a balanced incorporation of various factors influencing energy balance. While  $ET_{a\_CWSI}$  may provide a reasonable alternative, especially in cases where SEBAL is not practical, SEBS and  $ET_{a\_VI}$  exhibit limitations that affect their accuracy and correlation with lysimeter values.

Achieving the objectives of this study encountered limitations, particularly in terms of aligning image availability with the days of zero-irrigation when lysimeter ETa was calculated. This constraint resulted in a reduced number of available images throughout the study period.

The statistical metrics portrayed the performance metrics of four methods for estimating ETa. The SEBAL model exhibited the lowest errors with a RMSE of 1.97 and MAE of 1.75, along with a strong positive correlation ( $R = 0.88$ ) and a relatively good fit ( $R^2 = 0.78$ ). SEBS demonstrated higher errors compared to SEBAL, with a RMSE of 4.77 and a larger MAE of 4.18, indicating substantial underestimation (PBIAS = -92.04) and a moderate positive correlation ( $R = 0.65$ ). ETa\_VI exhibited the highest errors among all methods with a RMSE of 5.35 and a high MAPE of 169.75, indicating significant underestimation (PBIAS = -83.9968) and a weak negative correlation ( $R = -0.433$ ). ETa\_CWSI falls in between, with moderate errors and correlations. Overall, SEBAL appears to be the most suitable method for estimating ETa in the given context, showing the lowest errors and the strongest correlation with observed values, while ETa\_VI exhibits the poorest performance.

Some inconsistencies were observed across the evaluated ET algorithms although the same images were used. One of the primary challenges with CWSI-based ET compared to lysimeter measurements is the indirect nature of CWSI. While CWSI provides valuable information about crop water stress levels, it relies on assumptions and models to estimate actual ET rates based on canopy temperature differences. These estimates may not always perfectly align with the actual water use measured by lysimeters. CWSI measurements may not capture the spatial and temporal variability of water stress within a field accurately. Variations in crop type, soil properties, irrigation practices, and microclimatic conditions can all influence the effectiveness of CWSI for estimating ET. Factors such as cloud cover, humidity, wind speed, and sensor viewing angle can introduce noise and errors into CWSI measurements, making it challenging to isolate the effects of water stress accurately.

## CHAPTER 7: CONCLUSIONS & RECOMMENDATIONS

### 7.1 CONCLUSIONS

Limited and scarcity of water resources in South Africa is the main challenge for applying improving policies and strategies in the agricultural sector. The eradication efforts by the government of the extreme poverty, improvement of livelihood and environmental sustainability cannot be achieved without a robust plan for available natural resources management and, specifically, the water resources. Therefore, horizontal, and vertical expansion policies in food production were considered major tasks to achieve the millennium strategic goals. The recent drought spells in the Western Cape areas and other parts of South Africa have increased public awareness of the water shortage and suggest severe water cuts in agricultural sectors. Developing new water-saving strategies and tools for estimating water use efficiency (WUE) at different scales and environments can improve farmers, abilities to adapt to the increasing water shortage and climate change. At the same time, increasing WUE has undoubtedly positive effects on the sustainable use of water resources in agriculture. South Africa is a semi-arid country with various characteristics that make water availability quite variable in time and space. As water scarcity represents a major limitation for food production and rangeland productivity, developing technologies that can categorise resource use efficiency is highly recommended. The field smart lysimeter combined with the satellite measurements, can provide essential information about the plant water use and water productivity at the field level. The utilisation of satellite-based technology can provide and efficient tools to help farmer to monitor their crop water use at the farm level. This study was aimed to apply smart field lysimeters to generate accurate evapotranspiration data that can be used to calibrate and validate evapotranspiration measurement derived from the remote sensing data. The study has involved three levels, namely: 1. Application of the smart weighing lysimeter to measure the water use of winter and summer crops under arid conditions, 2. To validate some of the widely used evapotranspiration products derived from remotely sensed data, and 3. To assess different algorithm used to estimate the evapotranspiration from Landsat satellite imagery.

The findings from this study have confirmed that the implementation of smart field weighing lysimeters represents a highly effective tool for monitoring water usage, providing invaluable assistance in irrigation scheduling, and optimizing crop water productivity and efficiency. By offering critical insights into crop water requirements, water use efficiency, nutrient management, and soil moisture dynamics, these lysimeters play a vital role in water resource management. Throughout the course of this study, continuous and precise measurements of the water balance components have demonstrated the capabilities of smart field weighing lysimeters in improving agricultural irrigation practices, thereby contributing to the sustainable management of water resources. Moreover, the recorded data which was obtained remotely from the cloud storage system significantly reduced the need for on-site visits, which resemble the technological concept of the Internet of Things (IoT), thereby modernizing agricultural workload and operation costs. One crucial aspect to highlight in this study particularly from literature is the lack of ground actual evapotranspiration data in South Africa and the study area, necessitating further investigation into the water usage of other crop types within the Hartswater area. Smart field weighing lysimeters are becoming important tools in agricultural research and industry by providing ground-based evapotranspiration data at the field scale for validating ET models used at larger scales. They provide real-time opportunities to reduce water losses through ungoverned irrigation plans. Their ability to create actionable strategies from the data collected has, up until now, been constrained in irrigated farming due to a lack of financial resources and expertise. To alleviate water scarcity, it is specifically advised that smart field weighing lysimeters be targeted to improve scientifically informed decision-making in agricultural water usage management. While the lysimeters employed in this study were not large, it has become evident that future research should explore the application of large lysimeters to assess the water use dynamics of the dominant pecan nut trees under irrigation in the area. This expansion into larger-scale experimentation would offer valuable insights into the irrigation needs and water requirements of major crops in the area. By using these advanced technologies, agricultural water use practices can be improved to ensure

the sustainable utilization of water resources, aiding in better decision-making, water conservation, and cost reduction for farmers and the broader agricultural sector.

The study has proved that the direct comparison of the ET<sub>a</sub> from the lysimeter and the satellite and the remote sensing products will be unrealistic due to the differences in the spatial measurement domains. In order to extrapolate the lysimeter local measurements to the field and catchment scale, there was a need to develop and upscaling method. The method has been suggested in this study is to use various meteorological models to develop a relationship between the ET<sub>a</sub> and ET<sub>o</sub> at different sites. The study has evaluated a total of 28 ET<sub>o</sub> micrometeorological models' performance using a smart field weighing lysimeter. All models were evaluated using statistical metrics which demonstrated how good or bad each model is when compared to lysimeter ET data. The idea behind these processes was to find a more appropriate model that can be used in arid environments of South Africa which match the exact characteristics of the study area. The Penman-Monteith, Priestly-Taylor, and the Hargreaves and Allen models were identified as the robust models suitable for estimating ET in arid environments. These findings are important for water managers in irrigation scheduling, water allocation, and drought management, emphasizing the significance of model selection in accurately estimating ET, especially where conventional measuring devices are impractical or not economically feasible.

The conclusions drawn from the performance metrics of various methods for estimating ET<sub>a</sub> highlights the critical role of accurate estimation techniques as demonstrated by the SEBAL method, in guiding efficient water management, irrigation practices, and enhancing water use efficiency in agriculture. By prioritizing the selection of reliable methods like SEBAL, water managers can optimize irrigation scheduling, minimize water wastage, and improve crop water use efficiency contributing to water conservation efforts and sustainable agricultural development. These findings show the importance of informed decision-making in water management, emphasizing the need for precise ET<sub>a</sub> estimation to address global water scarcity challenges and promote resource-efficient agricultural practices through accurate remote sensing models.

## 7.2 RECOMMENDATIONS

Accurate measurements of ET<sub>a</sub> remain the biggest data gap in the South African water management practices. This is due to the limitations associated with lack of ground-based measuring devices. In the entire Africa only six Fluxnet stations exist with only one located in South Africa (<https://fluxnet.org/sites/site-summary/>). Majority of these stations are in Europe and United Kingdom countries where most validations and calibrations of ET models and products have been done. This limitation in South Africa makes it difficult to carry out the validation of models and products that were developed to provide global solutions before adopting them into the water management practices. Based on the above-mentioned challenges and findings of this project, we recommend to the WRC that:

- Based on the limitations in ET measuring stations, there is a need to focus on development of ET monitoring network systems across the country with data that is available to the public while the data has potential to help in the validation and calibration of indirect ET models.
- Lysimeters are not cheap, but their accuracy in determining the water balance components make them top priority tools that can be used for crop water use in large commercial farms to aid in irrigation scheduling. As such future research should focus on the development of lysimeters for use at various scales for the purpose of evaluating and calibrating ET models, this can either be from greenhouses or farm scales.
- To our knowledge the smart field weighing lysimeter used in this study is the first in Africa, however the lysimeter of its kind provides more information on the soil-plant-water conditions. More devices of this nature are recommended for future research purposes including those that can be used for horticultural purposes.

- The study was done at a field scale within the Vaalharts irrigation scheme, as such findings obtained here might not actually apply to the entire country, as such evaluation of ET based on the results of this study may not always produce accurate results if used in a different area with different climatic, topographic and soil conditions. We recommend that future research should focus on implementing projects of this nature to solve the issue of environmental variabilities for accurate outputs.
- The current study focused on three crops which were barley, maize, and soybean, we recommend the determination of ETa for many other crops which can help in the development of local crop coefficients that can be used for irrigation scheduling.
- During the project, we observed the limitations in the use of SFL-600 lysimeter for maize ETa determination where we could only determine ETa for early to development stages of the crop with errors being observed on the weighing balance measurement due to long maize roots reaching the lysimeter bottom. We recommend that, future research should focus on the use of larger lysimeters when dealing with crops that have long roots.
- The study made use of micrometeorological models to aid in extrapolating ETa from a point level into the larger extent of the irrigation scheme using four weather stations. We recommend the continuous installation of meteorological stations in the study area to capture more variabilities in ET which can be used to develop more robust ET models that could aid in improving the water management practices in the scheme.
- The study made use of ET products at varying scales, the coarse resolutions such as NOAH and MODIS products demonstrated poor results when compared with ETa from ground measurements. While on the other side, WaPOR product showed some promising results at 250 m<sup>2</sup> resolution. The WaPOR product in some countries contains a 100 m<sup>2</sup> and 30 m<sup>2</sup> resolution ET products. We recommend the FAO to improve the resolution of WaPOR also covering South Africa and more African countries.
- The project made use of Landsat 8 data for estimation of ET using SEBAL, SEBS, CWSI and vegetation index-based algorithms obtaining varying observations when compared to ground measurements. We recommend the integration of better resolution images such as sentinel datasets and the use of Unmanned aerial vehicles (UAV) for ET estimation. The use of UAV will add more value to solve the issues of spatial and temporal resolutions and weather challenges such as clouds which are common when using satellite images.
- Future research should apply irrigation scheduling based on ETa observations and assess crop yields thereafter.

## REFERENCES

- Abid, N., Bargaoui, Z., Mannaerts, C.M., 2018. Remote-sensing estimation of the water stress coefficient and comparison with drought evidence. *International journal of remote sensing* 39, 4616-4639.
- Abtew, W., 1996. Evapotranspiration measurements and modeling for three wetland systems in South Florida 1. *JAWRA Journal of the American Water Resources Association* 32, 465-473.
- Abutaleb, K., Ngie, A., Darwish, A., Ahmed, M., Arafat, S., Ahmed, F., 2015. Assessment of urban heat island using remotely sensed imagery over Greater Cairo, Egypt. *Advances in Remote Sensing* 4, 35.
- Albrecht, 1950. The methods for determining the evaporation of the natural earth's surface. 2, 1-38.
- Allen, L.H., Pan, D., Boote, K.J., Pickering, N.B., Jones, J.W., 2003. Carbon dioxide and temperature effects on evapotranspiration and water use efficiency of soybean. *Agronomy Journal* 95, 1071-1081.
- Allen, R.G. (Ed.), 1998. Crop evapotranspiration: guidelines for computing crop water requirements, FAO irrigation and drainage paper. Food and Agriculture Organization of the United Nations, Rome.
- Allen, R.G., Pereira, L.S., Howell, T.A., Jensen, M.E., 2011. Evapotranspiration information reporting: I. Factors governing measurement accuracy. *Agricultural Water Management* 98, 899-920.
- Allen, R.G., Pereira, L.S., Raes, D., Smith, M., 1998. FAO Irrigation and Drainage Paper No. 56, Crop Evapotranspiration, guidelines for computing crop water requirements, Food and Agriculture Organization of the United Nations.
- Anapalli, S.S., Fisher, D.K., Reddy, K.N., Rajan, N., Pinnamaneni, S.R., 2019. Modeling evapotranspiration for irrigation water management in a humid climate. *Agricultural Water Management* 225, 105731.
- Anderson, M., Gao, F., Knipper, K., Hain, C., Dulaney, W., Baldocchi, D., Eichelmann, E., Hemes, K., Yang, Y., Medellín-Azuara, J., 2018. Field-scale assessment of land and water use change over the California Delta using remote sensing. *Remote Sensing* 10, 889.
- Annandale, J., Stirezaker, R., Singels, A., Van Der Laan, M., Laker, M., 2011. Irrigation scheduling research: South African experiences and future prospects. *WSA* 37, 751-764. <https://doi.org/10.4314/wsa.v37i5.12>
- ARC, 2023. Climate Monitoring Services [WWW Document]. URL <https://www.arc.agric.za/arc-iscw/Pages/Climate-Monitoring-Services.aspx> (accessed 4.4.23).
- Ávila-Dávila, L., Soler-Méndez, M., Bautista-Capetillo, C.F., González-Trinidad, J., Júnez-Ferreira, H.E., Robles Rovelo, C.O., Molina-Martínez, J.M., 2021. A compact weighing lysimeter to estimate the water infiltration rate in agricultural soils. *Agronomy* 11, 180.
- Baalousha, H.M., Ramasomanana, F., Fahs, M., Seers, T.D., 2022. Measuring and Validating the Actual Evaporation and Soil Moisture Dynamic in Arid Regions under Unirrigated Land Using Smart Field Lysimeters and Numerical Modeling. *Water* 14, 2787. <https://doi.org/10.3390/w14182787>
- Badola, A., 2009. Validation of Surface Energy Balance System (SEBS) over forest land cover and sensitivity analysis of the model [WWW Document]. URL <http://essay.utwente.nl/92700/> (accessed 8.25.23).
- Bakhshoodeh, R., Ocampo, C., Oldham, C., 2022. Exploring the evapotranspirative cooling effect of a green façade. *Sustainable Cities and Society* 81, 103822. <https://doi.org/10.1016/j.scs.2022.103822>
- Bardsley, W.E., Campbell, D.I., 2000. Natural Geological Weighing Lysimeters: Calibration Tools for Satellite and Ground Surface Gravity Monitoring of Subsurface Water-Mass Change. *Natural Resources Research* 9, 147-156. <https://doi.org/10.1023/A:1010147527484>
- Barnard, J.H., 2013. On-farm management of salinity associated with irrigation for the Orange-Riet and Vaalharts schemes (Thesis). University of the Free State.
- Bastiaanssen, W.G.M., 2000. SEBAL-based sensible and latent heat fluxes in the irrigated Gediz Basin, Turkey. *Journal of hydrology* 229, 87-100.
- Bastiaanssen, W.G.M., Thiruvengadachari, S., Sakthivadivel, R., Molden, D.J., 1999. Satellite Remote Sensing for Estimating Productivities of Land and Water. *International Journal of Water Resources Development* 15, 181-194. <https://doi.org/10.1080/07900629949005>
- Becker, F., Li, Z.-L., 1990. Temperature-independent spectral indices in thermal infrared bands. *Remote sensing of environment* 32, 17-33.
- Berliner, P.R., Oosterhuis, D.M., 1987. Effect of root and water distribution in lysimeters and in the field on the onset of crop water stress. *Irrig Sci* 8. <https://doi.org/10.1007/BF00257509>
- Bhatt, R., Hossain, A., Singh, P., 2019. Scientific interventions to improve land and water productivity for climate-smart agriculture in South Asia. *Agronomic Crops: Volume 2: Management Practices* 499-558.

- Brockamp, B., Wenner, H., 1963. Verdunstungsmessungen auf den Steiner see bei münster. Dt Gewässerkundl Mitt 7, 149-154.
- Buttar, N.A., Yongguang, H., Shabbir, A., Lakhari, I.A., Ullah, I., Ali, A., Aleem, M., Yasin, M.A., 2018. Estimation of evapotranspiration using Bowen ratio method. IFAC-PapersOnLine 51, 807-810. <https://doi.org/10.1016/j.ifacol.2018.08.096>
- Caprio, J.M., 1974. The solar thermal unit concept in problems related to plant development and potential evapotranspiration. Phenology and seasonality modeling 353-364.
- Carlson, T., 2007. An Overview of the "Triangle Method" for Estimating Surface Evapotranspiration and Soil Moisture from Satellite Imagery. Sensors 7, 1612-1629. <https://doi.org/10.3390/s7081612>
- Celestin, S., Qi, F., Li, R., Yu, T., Cheng, W., 2020. Evaluation of 32 simple equations against the Penman-Monteith method to estimate the reference evapotranspiration in the Hexi Corridor, Northwest China. Water 12, 2772.
- Chen, J.M., Liu, J., 2020. Evolution of evapotranspiration models using thermal and shortwave remote sensing data. Remote Sensing of Environment 237, 111594.
- Chen, S., McColl, K.A., Berg, A., Huang, Y., 2021. Surface flux equilibrium estimates of evapotranspiration at large spatial scales. Journal of Hydrometeorology 22, 765-779.
- Cheng, M., Jiao, X., Liu, Y., Shao, M., Yu, X., Bai, Y., Wang, Z., Wang, S., Tuohuti, N., Liu, S., Shi, L., Yin, D., Huang, X., Nie, C., Jin, X., 2022. Estimation of soil moisture content under high maize canopy coverage from UAV multimodal data and machine learning. Agricultural Water Management 264, 107530. <https://doi.org/10.1016/j.agwat.2022.107530>
- Chiwetalu, U.J., Egwuagu, O., Okechukwu, M.E., Nebechukwu, A.C., 2022. Determination of Crop Evapotranspiration (ETc) and Crop Coefficient (Kc) for Maize Using Drainage Lysimeter in Dry Season Period in Enugu State, Nigeria.
- Cleugh, H.A., Leuning, R., Mu, Q., Running, S.W., 2007. Regional evaporation estimates from flux tower and MODIS satellite data. Remote Sensing of Environment 106, 285-304.
- Condon, L.E., Atchley, A.L., Maxwell, R.M., 2020. Evapotranspiration depletes groundwater under warming over the contiguous United States. Nature communications 11, 873.
- Corbari, C., Skokovic Jovanovic, D., Nardella, L., Sobrino, J., Mancini, M., 2020. Evapotranspiration estimates at high spatial and temporal resolutions from an energy-water balance model and satellite data in the capitanata irrigation consortium. Remote Sensing 12, 4083.
- Costa, L.D., Gianquinto, G., 2002. Water stress and watertable depth influence yield, water use efficiency, and nitrogen recovery in bell pepper: lysimeter studies. Aust. J. Agric. Res. 53, 201. <https://doi.org/10.1071/AR00133>
- Cuxart, J., Boone, A.A., 2020. Evapotranspiration over land from a boundary-layer meteorology perspective. Boundary-Layer Meteorology 177, 427-459.
- Dalton, J., 1802. Experimental essays, on the constitution of mixed gases; on the force of steam or vapour from water and other liquids in different temperatures, both in a Torricellian vacuum and in air; on evaporation; and on the expansion of elastic fluids by heat. (No Title).
- Dash, P., Göttsche, F.-M., Olesen, F.-S., Fischer, H., 2002. Land surface temperature and emissivity estimation from passive sensor data: Theory and practice-current trends. International Journal of remote sensing 23, 2563-2594.
- Denager, T., Looms, M.C., Sonnenborg, T.O., Jensen, K.H., 2020. Comparison of evapotranspiration estimates using the water balance and the eddy covariance methods. Vadose zone j. 19. <https://doi.org/10.1002/vzj2.20032>
- Ding, R., Kang, S., Li, F., Zhang, Y., Tong, L., Sun, Q., 2010. Evaluating eddy covariance method by large-scale weighing lysimeter in a maize field of northwest China. Agricultural Water Management 98, 87-95.
- Djaman, K., Irmak, S., Futakuchi, K., 2017. Daily reference evapotranspiration estimation under limited data in Eastern Africa. Journal of Irrigation and Drainage Engineering 143, 06016015.
- Doležal, F., Hernandez-Gomis, R., Matula, S., Gulamov, M., Miháliková, M., Khodjaev, S., 2018. Actual Evapotranspiration of Unirrigated Grass in a Smart Field Lysimeter. Vadose Zone Journal 17, 1-13. <https://doi.org/10.2136/vzj2017.09.0173>
- Donnenfeld, Z., Hedden, S., Crookes, C., 2018. A delicate balance: Water scarcity in South Africa.
- Doorenbos, J., Pruitt, W.O., 1981. Guidelines for predicting crop water requirements.
- Droogers, P., Allen, R.G., 2002. Estimating reference evapotranspiration under inaccurate data conditions. Irrigation and drainage systems 16, 33-45.

- Dzikiti, S., Jovanovic, N.Z., Bugan, R., Israel, S., Maitre, D.L., 2014. Measurement and modelling of evapotranspiration in three fynbos vegetation types. *Water SA* 40, 189-198. <https://doi.org/10.4314/wsa.v40i2.1>
- Ellington, R.G., Usher, B.H., van Tonder, G.J., 2004. Quantification of the impact of irrigation on the aquifer under the Vaalharts Irrigation Scheme, in: *Water Resources of Arid Areas: Proceedings of the International Conference on Water Resources of Arid and Semi-Arid Regions of Africa*, Gaborone, Botswana, 3-6 August 2004. Taylor & Francis, p. 60.
- Elnmer, A., Khadr, M., Kanae, S., Tawfik, A., 2019. Mapping daily and seasonally evapotranspiration using remote sensing techniques over the Nile delta. *Agricultural Water Management* 213, 682-692.
- Evans, R.G., Sadler, E.J., 2008. Methods and technologies to improve efficiency of water use: INCREASING WATER USE EFFICIENCIES. *Water Resour. Res.* 44. <https://doi.org/10.1029/2007WR006200>
- Fernández, M.D., Bonachela, S., Orgaz, F., Thompson, R., López, J.C., Granados, M.R., Gallardo, M., Fereres, E., 2010. Measurement and estimation of plastic greenhouse reference evapotranspiration in a Mediterranean climate. *Irrigation science* 28, 497-509.
- Frahmand, A., Akyuz, D., Sanli, F., Bektaş Balçık, F., 2020. CAN REMOTE SENSING AND SEBAL FILL THE GAP ON EVAPOTRANSPIRATION? A CASE STUDY: KUNDUZ CATCHMENT, AFGHANISTAN. *Journal of Environmental Protection and Ecology* 21, 423-432.
- Franc, G.B., Cracknell, A.P., 1994. Retrieval of land and sea surface temperature using NOAA-11 AVHRR-data in north-eastern Brazil. *International Journal of Remote Sensing* 15, 1695-1712.
- Francois, C., Otlé, C., 1996. Atmospheric corrections in the thermal infrared: global and water vapor dependent split-window algorithms-applications to ATSR and AVHRR data. *IEEE transactions on geoscience and remote sensing* 34, 457-470.
- Friedl, M.A., 2002. Forward and inverse modeling of land surface energy balance using surface temperature measurements. *Remote sensing of environment* 79, 344-354.
- Fuzzo, D.F. da S.S., Rocha, J.V., 2018. Simplify the triangle method for estimating evapotranspiration and its use in agrometeorological modeling. *Applied Research & Agrotechnology* 11, 07-15.
- Gao, Z., Shi, W., Wang, X., Wang, Y., 2020. Non-rainfall water contributions to dryland jujube plantation evapotranspiration in the Hilly Loess Region of China. *Journal of Hydrology* 583, 124604.
- Gebler, S., Hendricks Franssen, H.-J., Pütz, T., Post, H., Schmidt, M., Vereecken, H., 2015. Actual evapotranspiration and precipitation measured by lysimeters: a comparison with eddy covariance and tipping bucket. *Hydrol. Earth Syst. Sci.* 19, 2145-2161. <https://doi.org/10.5194/hess-19-2145-2015>
- Ghaderi, A., Dasineh, M., Shokri, M., Abraham, J., 2020. Estimation of actual evapotranspiration using the remote sensing method and SEBAL algorithm: a case study in Ein Khosh Plain, Iran. *Hydrology* 7, 36.
- Gibson, L., Jarmain, C., Su, Z., Eckardt, F., 2013. Review: Estimating evapotranspiration using remote sensing and the Surface Energy Balance System – A South African perspective. *WSA* 39, 477-484. <https://doi.org/10.4314/wsa.v39i4.5>
- Gibson, L.A., Münch, Z., Engelbrecht, J., 2011. Particular uncertainties encountered in using a pre-packaged SEBS model to derive evapotranspiration in a heterogeneous study area in South Africa. *Hydrol. Earth Syst. Sci.* 15, 295-310. <https://doi.org/10.5194/hess-15-295-2011>
- Gillespie, A., Rokugawa, S., Matsunaga, T., Cothorn, J.S., Hook, S., Kahle, A.B., 1998. A temperature and emissivity separation algorithm for Advanced Spaceborne Thermal Emission and Reflection Radiometer (ASTER) images. *IEEE transactions on geoscience and remote sensing* 36, 1113-1126.
- Gokool, S., Riddell, E.S., Swemmer, A., Nippert, J.B., Raubenheimer, R., Chetty, K.T., 2018. Estimating groundwater contribution to transpiration using satellite-derived evapotranspiration estimates coupled with stable isotope analysis. *Journal of Arid Environments* 152, 45-54.
- Gossard, C., 1998. *Evapotranspiration Estimates for the Closed Norman, Oklahoma Landfill*.
- Govender, T., 2022. Remote sensing and multispectral imaging of hydrological responses to land use/land cover and climate variability in contrasting agro-ecological systems in Mountainous catchment, Western Cape.
- Gowda, P.H., Chávez, J.L., Howell, T.A., Marek, T.H., New, L.L., 2008. Surface energy balance based evapotranspiration mapping in the Texas high plains. *Sensors* 8, 5186-5201.
- Green, G.C., 1974. Lysimetric determination of citrus tree evapotranspiration. *Agrochimophysics* 6, 35-41.
- Groh, J., Pütz, T., Gerke, H.H., Vanderborght, J., Vereecken, H., 2019. Quantification and prediction of nighttime evapotranspiration for two distinct grassland ecosystems. *Water Resources Research* 55, 2961-2975.

- Gu, Z., Zhu, T., Jiao, X., Xu, J., Qi, Z., 2021. Neural network soil moisture model for irrigation scheduling. *Computers and Electronics in Agriculture* 180, 105801. <https://doi.org/10.1016/j.compag.2020.105801>
- Gwate, O., Mantel, S.K., Palmer, A.R., Gibson, L.A., Munch, Z., 2018. Measuring and modelling evapotranspiration in a South African grassland: Comparison of two improved Penman-Monteith formulations. *Water SA* 44, 482-494.
- Häfner, M., 1994. Pesticides in soil: A German approach of predicting their movement into ground and surface water, in: *Pesticides in Ground and Surface Water*. Springer, pp. 247-288.
- Hamon, W.R., 1961. Estimating potential evapotranspiration. *Journal of the Hydraulics Division* 87, 107-120.
- Hargreaves, G.H., Allen, R.G., 2003. History and evaluation of Hargreaves evapotranspiration equation. *Journal of irrigation and drainage engineering* 129, 53-63.
- Hargreaves, G.H., Samani, Z.A., 1985. Reference crop evapotranspiration from temperature. *Applied engineering in agriculture* 1, 96-99.
- Hargreaves, G.H., Samani, Z.A., 1982. Estimating potential evapotranspiration. *Journal of the Irrigation and Drainage Division* 108, 225-230.
- Hashem, A.A., Engel, B.A., Bralts, V.F., Marek, G.W., Moorhead, J.E., Radwan, S.A., Gowda, P.H., 2020. Assessment of Landsat-Based Evapotranspiration Using Weighing Lysimeters in the Texas High Plains. *Agronomy* 10, 1688. <https://doi.org/10.3390/agronomy10111688>
- Hashmi, M.A., Garcia, L.A., 1998. Spatial and Temporal Errors in Estimating Regional Evapotranspiration. *J. Irrig. Drain Eng.* 124, 108-114. [https://doi.org/10.1061/\(ASCE\)0733-9437\(1998\)124:2\(108\)](https://doi.org/10.1061/(ASCE)0733-9437(1998)124:2(108))
- Hoffman, M.T., 2014. Changing Patterns of Rural Land Use and Land Cover in South Africa and their Implications for Land Reform. *Journal of Southern African Studies* 40, 707-725. <https://doi.org/10.1080/03057070.2014.943525>
- Hook, S.J., Gabell, A.R., Green, A.A., Kealy, P.S., 1992. A comparison of techniques for extracting emissivity information from thermal infrared data for geologic studies. *Remote Sensing of Environment* 42, 123-135.
- Hough, J.J.H., Rudolph, D.C., 2003. Vaalharts Groundwater Protocol for on-site sanitation. Report fr VKE Engineers, by GHT. GHT Consulting Report No. RVN 331, 482. <https://earthexplorer.usgs.gov/>, 2022. [https://wapor.apps.fao.org/home/WAPOR 2/1](https://wapor.apps.fao.org/home/WAPOR%202/1), 2023.
- Hua, D., Hao, X., Zhang, Y., Qin, J., 2020. Uncertainty assessment of potential evapotranspiration in arid areas, as estimated by the Penman-Monteith method. *Journal of Arid Land* 12, 166-180.
- Hutson, J.L., 1980. A weighing lysimeter facility at Roodeplaat for crop evapotranspiration studies. *Water SA* 6, 41-48.
- Irmak, S., Allen, R.G., Whitty, E.B., 2003. Daily grass and alfalfa-reference-Evapotranspiration calculations as part of the ASCE standardization effort. *Journal of Irrigation and Drainage Engineering-ASCE* 129, 360-370.
- Irmak, S., Istanbuluoglu, E., Irmak, A., 2008. An evaluation of evapotranspiration model complexity against performance in comparison with Bowen ratio energy balance measurements. *Transactions of the ASABE* 51, 1295-1310.
- Jackson, R.D., Idso, S.B., Reginato, R.J., Pinter, P.J., 1981. Canopy temperature as a crop water stress indicator. *Water Resources Research* 17, 1133-1138. <https://doi.org/10.1029/WR017i004p01133>
- Jafari, M., Kamali, H., Keshavarz, A., Momeni, A., 2021. Estimation of evapotranspiration and crop coefficient of drip-irrigated orange trees under a semi-arid climate. *Agricultural Water Management* 248, 106769.
- Jalali, M., 2007. Salinization of groundwater in arid and semi-arid zones: an example from Tajarak, western Iran. *Environ Geol* 52, 1133-1149. <https://doi.org/10.1007/s00254-006-0551-3>
- Jarchow, C.J., Waugh, W.J., Nagler, P.L., 2022. Calibration of an evapotranspiration algorithm in a semiarid sagebrush steppe using a 3-ha lysimeter and Landsat normalized difference vegetation index data. *Ecohydrology* 15. <https://doi.org/10.1002/eco.2413>
- Jensen, M.E., Haise, H.R., 1963. Estimating evapotranspiration from solar radiation. *Journal of the Irrigation and Drainage Division* 89, 15-41.
- Jia, L., Su, Z., Van Den Hurk, B., Menenti, M., Moene, A., De Bruin, H.A.R., Yrisarry, J.J.B., Ibanez, M., Cuesta, A., 2003. Estimation of sensible heat flux using the Surface Energy Balance System (SEBS) and ATSR measurements. *Physics and Chemistry of the Earth, Parts A/B/C* 28, 75-88. [https://doi.org/10.1016/S1474-7065\(03\)00009-3](https://doi.org/10.1016/S1474-7065(03)00009-3)

- Jiang, L., Wu, H., Tao, J., Kimball, J.S., Alfieri, L., Chen, X., 2020. Satellite-Based Evapotranspiration in Hydrological Model Calibration. *Remote Sensing* 12, 428. <https://doi.org/10.3390/rs12030428>
- Johnson, R.S., Williams, L.E., Ayars, J.E., Trout, T.J., 2005. Weighing lysimeters aid study of water relations in tree and vine crops. *California Agriculture* 59.
- Jovanovic, N., Mu, Q., Bugan, R.D., Zhao, M., 2015. Dynamics of MODIS evapotranspiration in South Africa. *Water SA* 41, 79-90.
- Kahle, A.B., Madura, D.P., Soha, J.M., 1980. Middle infrared multispectral aircraft scanner data: Analysis for geological applications. *Applied Optics* 19, 2279-2290.
- Kealy, P.S., 1990. Estimation of emissivity and temperature using alpha coefficients, in: *Proceedings of the Second Thermal Infrared Multispectral Scanner (TIMS) Workshop*. pp. 11-16.
- Kealy, P.S., Hook, S.J., 1993. Separating temperature and emissivity in thermal infrared multispectral scanner data: Implications for recovering land surface temperatures. *IEEE Transactions on Geoscience and Remote Sensing* 31, 1155-1164.
- Keller, A.A., Keller, J., 1995. Effective efficiency: A water use efficiency concept for allocating freshwater resources. Center for Economic Policy Studies, Winrock International Arlington, VA, USA.
- Khan, M.S., Liaqat, U.W., Baik, J., Choi, M., 2018. Stand-alone uncertainty characterization of GLEAM, GLDAS and MOD16 evapotranspiration products using an extended triple collocation approach. *Agricultural and Forest Meteorology* 252, 256-268.
- Kim, H.W., Hwang, K., Mu, Q., Lee, S.O., Choi, M., 2012. Validation of MODIS 16 global terrestrial evapotranspiration products in various climates and land cover types in Asia. *KSCE Journal of Civil Engineering* 16, 229-238.
- Kim, Y., Jabro, J.D., Evans, R.G., 2011. Wireless lysimeters for real-time online soil water monitoring. *Irrigation Science* 29, 423-430.
- Kingra, P.K., Majumder, D., Singh, S.P., 2016. Application of remote sensing and GIS in agriculture and natural resource management under changing climatic conditions. *Agricultural Research Journal* 53.
- Kite, G., Granger, R., Jayasinghe, G., 2001. Evapotranspiration at the basin scale estimated from satellite data and by a hydrological model., in: *Remote Sensing and Hydrology 2000. Selected Papers from a Conference Held at Santa Fe, New Mexico, USA, 2-7 April 2000*. IAHS Press, pp. 265-270.
- Klaasse, A., Bastiaanssen, W., Jarmain, C., Roux, A., 2008. Water use efficiency of table and wine grapes in Western Cape, South Africa. *WaterWatch report*, Wageningen, The Netherlands.
- Klaasse, A., Jarmain, C., 2011. GrapeLook: Improving Agricultural Water Management using Satellite Earth Observation. *Agriculture, Articles, Earth Observation, Water Availability*.
- Ko, J., Piccinni, G., 2009. Corn yield responses under crop evapotranspiration-based irrigation management. *Agricultural water management* 96, 799-808.
- Koffi, D., Komla, G., 2015. Trend analysis in reference evapotranspiration and aridity index in the context of climate change in Togo. *Journal of Water and Climate Change* 6, 848-864.
- Kool, D., Agam, N., Lazarovitch, N., Heitman, J.L., Sauer, T.J., Ben-Gal, A., 2014. A review of approaches for evapotranspiration partitioning. *Agricultural and Forest Meteorology* 184, 56-70. <https://doi.org/10.1016/j.agrformet.2013.09.003>
- Kovacs, G., 1976. THE USE OF LYSIMETERS IN THE HYDROLOGICAL INVESTIGATION OF THE UNSATURATED ZONE / Utilisation des lysimètres pour l'examen hydrologique de la zone non saturée. *Hydrological Sciences Bulletin* 21, 499-516. <https://doi.org/10.1080/02626667609491670>
- Kumar, H., Srivastava, P., Ortiz, B.V., Morata, G., Takhellambam, B.S., Lamba, J., Bondesan, L., 2021. Field-Scale Spatial and Temporal Soil Water Variability in Irrigated Croplands. *Transactions of the ASABE* 64, 1277-1294. <https://doi.org/10.13031/trans.14335>
- Kumar, U., Srivastava, A., Kumari, N., Sahoo, B., Chatterjee, C., Raghuwanshi, N.S., 2021. Evaluation of Spatio-Temporal Evapotranspiration Using Satellite-Based Approach and Lysimeter in the Agriculture Dominated Catchment. *J Indian Soc Remote Sens* 49, 1939-1950. <https://doi.org/10.1007/s12524-021-01367-w>
- Labbé, S., Lebourgeois, V., Jolivot, A., Marti, R., 2012. Thermal infra-red remote sensing for water stress estimation in agriculture. *Options Méditerranéennes Série B. Etudes et Recherches* 67, 175-184.
- Landeras, G., Ortiz-Barredo, A., López, J.J., 2008. Comparison of artificial neural network models and empirical and semi-empirical equations for daily reference evapotranspiration estimation in the Basque Country (Northern Spain). *Agricultural water management* 95, 553-565.
- Le Roux, P.A.L., du Preez, C., Strydom, M., van Rensburg, L., Bennie, A., 2007. Effect of irrigation on soil salinity profiles along the Lower Vaal River, South Africa. *Water Sa* 33.

- Lea-Cox, J.D., 2012. Using wireless sensor networks for precision irrigation scheduling. Problems, perspectives and challenges of agricultural water management. InTech Press, Rijeka, Croatia 233-258.
- Li, Z.-L., Becker, F., Stoll, M.P., Wan, Z., 1999. Evaluation of six methods for extracting relative emissivity spectra from thermal infrared images. *Remote sensing of Environment* 69, 197-214.
- Lian, J., Huang, M., 2015. Evapotranspiration Estimation for an Oasis Area in the Heihe River Basin Using Landsat-8 Images and the METRIC Model. *Water Resour Manage* 29, 5157-5170. <https://doi.org/10.1007/s11269-015-1110-z>
- Lian, X., Piao, S., Huntingford, C., Li, Y., Zeng, Z., Wang, X., Ciais, P., McVicar, T.R., Peng, S., Ottlé, C., 2018. Partitioning global land evapotranspiration using CMIP5 models constrained by observations. *Nature Climate Change* 8, 640-646.
- Liang, S., Fang, H., Chen, M., Shuey, C.J., Walthall, C., Daughtry, C., Morissette, J., Schaaf, C., Strahler, A., 2002. Validating MODIS land surface reflectance and albedo products: Methods and preliminary results. *Remote sensing of environment* 83, 149-162.
- Liou, Y.-A., Kar, S.K., 2014. Evapotranspiration estimation with remote sensing and various surface energy balance algorithms—A review. *Energies* 7, 2821-2849.
- Lohman, H.A.C., Trimmer, J.T., Katende, D., Mubasira, M., Nagirinya, M., Nsereko, F., Banadda, N., Cusick, R.D., Guest, J.S., 2020. Advancing Sustainable Sanitation and Agriculture through Investments in Human-Derived Nutrient Systems. *Environ. Sci. Technol.* 54, 9217-9227. <https://doi.org/10.1021/acs.est.0c03764>
- Louw, C., Van Heerden, J., Olivier, J., 1998. The South African fog-water collection experiment: Meteorological features associated with water collection along the eastern escarpment of South Africa. *WATER SA-PRETORIA* – 24, 269-280.
- Lu, Y., Ma, D., Chen, X., Zhang, J., 2018. A Simple Method for Estimating Field Crop Evapotranspiration from Pot Experiments. *Water* 10, 1823. <https://doi.org/10.3390/w10121823>
- Lyon, C.K., Garrett, V.H., Black, D.R., Applewhite, T.H., Goldblatt, L.A., 1965. Thermal Conductivity of Castor Oil-Based Rigid Urethane Foams. *Industrial & Engineering Chemistry Product Research and Development* 4, 189-191.
- Ma, H.-I., Hwang, W.-J., Chen-Sea, M.-J., 2005. Reliability and validity testing of a Chinese-translated version of the 39-item Parkinson's Disease Questionnaire (PDQ-39). *Qual Life Res* 14, 565-569. <https://doi.org/10.1007/s11136-004-0687-0>
- Madugundu, R., Al-Gaadi, K.A., Tola, E., Hassaballa, A.A., Patil, V.C., 2017. Performance of the METRIC model in estimating evapotranspiration fluxes over an irrigated field in Saudi Arabia using Landsat-8 images. *Hydrol. Earth Syst. Sci.* 21, 6135-6151. <https://doi.org/10.5194/hess-21-6135-2017>
- Mahringer, W., 1970. Verdunstungsstudien am neusiedler See. *Archives for Meteorology Geophysics and Bioclimatology Series B Theoretical and Applied Climatology* 18, 1-20.
- Maisela, R.J., 2007. Realizing agricultural potential in land reform: The case of Vaalharts irrigation scheme in the Northern Cape Province (Thesis). University of the Western Cape.
- Majozi, N., Mannaerts, C., Ramoelo, A., Mathieu, R., Mudau, A., Verhoef, W., 2017. An Intercomparison of Satellite-Based Daily Evapotranspiration Estimates under Different Eco-Climatic Regions in South Africa. *Remote Sensing* 9, 307. <https://doi.org/10.3390/rs9040307>
- Makkink, G.F., 1959. Limitations and perspectives of lysimeter research, in: Colloque de Hannoversch-Muenden 8-14 September 1959= Symposium of Hannoversch-Muenden 8-14 September 1959. AIHS, pp. 13-25.
- Malmqvist, B., Rundle, S., 2002. Threats to the running water ecosystems of the world. *Envir. Conserv.* 29, 134-153. <https://doi.org/10.1017/S0376892902000097>
- Mancosu, N., Snyder, R., Kyriakakis, G., Spano, D., 2015. Water Scarcity and Future Challenges for Food Production. *Water* 7, 975-992. <https://doi.org/10.3390/w7030975>
- McCabe, M.F., Wood, E.F., 2006. Scale influences on the remote estimation of evapotranspiration using multiple satellite sensors. *Remote Sensing of Environment* 105, 271-285. <https://doi.org/10.1016/j.rse.2006.07.006>
- McNally, A., 2016. FLDAS Noah Land Surface Model L4 monthly 0.1 x 0.1 degree for Eastern Africa (GDAS and RFE2) V001. Goddard Earth Sciences Data and Information Services Center (GES DISC). Accessed: June 18, 2017.
- Meadows, M.E., Hoffman, M.T., 2002. The nature, extent and causes of land degradation in South Africa: legacy of the past, lessons for the future? *Area* 34, 428-437.

- Meissner, R., Rupp, H., Seeger, J., Ollesch, G., Gee, G.W., 2010. A comparison of water flux measurements: passive wick-samplers versus drainage lysimeters. *European Journal of Soil Science* 61, 609-621. <https://doi.org/10.1111/j.1365-2389.2010.01255.x>
- Meyer, A., 1926. Concerning several relationships between climate and soil in Europe. *Chemie der Erde* 2, 209-347.
- Minacapilli, M., Cammalleri, C., Ciraolo, G., Rallo, G., Provenzano, G., 2016. Using scintillometry to assess reference evapotranspiration methods and their impact on the water balance of olive groves. *Agricultural Water Management* 170, 49-60.
- Minhas, P.S., Ramos, T.B., Ben-Gal, A., Pereira, L.S., 2020. Coping with salinity in irrigated agriculture: Crop evapotranspiration and water management issues. *Agricultural Water Management* 227, 105832. <https://doi.org/10.1016/j.agwat.2019.105832>
- Moeletsi, M.E., Walker, S., Hamandawana, H., 2013. Comparison of the Hargreaves and Samani equation and the Thornthwaite equation for estimating dekadal evapotranspiration in the Free State Province, South Africa. *Physics and Chemistry of the Earth, Parts A/B/C* 66, 4-15.
- Moorhead, J.E., Marek, G.W., Gowda, P.H., Lin, X., Colaizzi, P.D., Evett, S.R., Kutikoff, S., 2019. Evaluation of evapotranspiration from eddy covariance using large weighing lysimeters. *Agronomy* 9, 99.
- Morse, A., Kramber, W.J., Allen, R.G., Tasumi, M., 2004. Use of the METRIC evapotranspiration model to compute water use by irrigated agriculture in Idaho, in: *IGARSS 2004. 2004 IEEE International Geoscience and Remote Sensing Symposium*. IEEE, pp. 2134-2137.
- Mpelasoka., B., M., B., S., G., 2001. Water use, yield and fruit quality of lysimeter-grown apple trees: responses to deficit irrigation and to crop load. *Irrigation Science* 20, 107-113. <https://doi.org/10.1007/s002710100041>
- Mu, Q., Zhao, M., Running, S.W., 2013. MODIS global terrestrial evapotranspiration (ET) product (NASA MOD16A2/A3). Algorithm Theoretical Basis Document, Collection 5, 600.
- Mu, Q., Zhao, M., Running, S.W., 2011. Improvements to a MODIS global terrestrial evapotranspiration algorithm. *Remote sensing of environment* 115, 1781-1800.
- Mu, Q., Zhao, M., Running, S.W., 2005. Brief introduction to MODIS evapotranspiration data set (MOD16). *Water Resour. Res* 45, 1-4.
- Muhammad, M.K.I., Nashwan, M.S., Shahid, S., Ismail, T. bin, Song, Y.H., Chung, E.-S., 2019. Evaluation of empirical reference evapotranspiration models using compromise programming: A case study of Peninsular Malaysia. *Sustainability* 11, 4267.
- Mukammal, E.I., McKay, G.A., Turner, V.R., 1971. Mechanical balance-electrical readout weighing lysimeter. *Boundary-Layer Meteorol* 2, 207-217. <https://doi.org/10.1007/BF00192130>
- Muller, S., van Niekerk, A., 2019. Within-Field Monitoring of Secondary Salinity in Irrigated Areas of South Africa, in: *Soil Degradation and Restoration in Africa*. CRC Press, pp. 88-110.
- Musvoto, C., Nortje, K., Wet, B. de, Mahumani, B.K., Nahman, A., 2015. Imperatives for an agricultural green economy in South Africa. *South African Journal of Science* 111, 1-8. <https://doi.org/10.17159/sajs.2015/20140026>
- Myeni, L., Moeletsi, M.E., Clulow, A.D., 2021. Field calibration of DFM capacitance probes for continuous soil moisture monitoring. *Water SA* 47, 88-96.
- Ndara, N., 2017. Analysis of monthly MOD16 evapotranspiration rates at sites with different climatic characteristics; Heuningnes and Letaba catchments in South Africa.
- Ndou, N.N., Palamuleni, L.G., Ramoelo, A., 2018. Modelling depth to groundwater level using SEBAL-based dry season potential evapotranspiration in the upper Molopo River Catchment, South Africa. *The Egyptian Journal of Remote Sensing and Space Science* 21, 237-248. <https://doi.org/10.1016/j.ejrs.2017.08.003>
- Nell, J.P., Van Huyssteen, C.W., 2018. Prediction of primary salinity, sodicity and alkalinity in South African soils. *South African Journal of Plant and Soil* 35, 173-178. <https://doi.org/10.1080/02571862.2017.1345015>
- Ngie, A., Abutaleb, K., Ahmed, F., Darwish, A., Ahmed, M., 2014. Assessment of urban heat island using satellite remotely sensed imagery: a review. *South African Geographical Journal= Suid-Afrikaanse Geografiese Tydskrif* 96, 198-214.
- Niu, H., Hollenbeck, D., Zhao, T., Wang, D., Chen, Y., 2020. Evapotranspiration Estimation with Small UAVs in Precision Agriculture. *Sensors* 20, 6427. <https://doi.org/10.3390/s20226427>

- Ojo, O.I., Ilunga, F., 2018. Geospatial Analysis for Irrigated Land Assessment, Modeling and Mapping, in: Rustamov, R.B., Hasanova, S., Zeynalova, M.H. (Eds.), Multi-Purposeful Application of Geospatial Data. InTech. <https://doi.org/10.5772/intechopen.73314>
- Onwuka, B., 2018. Effects of Soil Temperature on Some Soil Properties and Plant Growth. APAR 8. <https://doi.org/10.15406/apar.2018.08.00288>
- Otieno, F., Ochieng, G., 2007. Water management tools as a means of averting a possible water scarcity in South Africa by the year 2025. WSA 30, 120-124. <https://doi.org/10.4314/wsa.v30i5.5181>
- Oweis, T.Y., Hachum, A.Y., 2003. Improving water productivity in the dry areas of West Asia and North Africa., in: Kijne, J.W., Barker, R., Molden, D. (Eds.), Water Productivity in Agriculture: Limits and Opportunities for Improvement. CABI Publishing, UK, pp. 179-198. <https://doi.org/10.1079/9780851996691.0179>
- Pahlow, M., Snowball, J., Fraser, G., 2015. Water footprint assessment to inform water management and policy making in South Africa. Water Sa 41, 300-313.
- Palmer, M., Bernhardt, E., Chornesky, E., Collins, S., Dobson, A., Duke, C., Gold, B., Jacobson, R., Kingsland, S., Kranz, R., Mappin, M., Martinez, M.L., Micheli, F., Morse, J., Pace, M., Pascual, M., Palumbi, S., Reichman, O.J., Simons, A., Townsend, A., Turner, M., 2004. Ecology for a Crowded Planet. Science 304, 1251-1252. <https://doi.org/10.1126/science.1095780>
- Papadakis, J., 1965. Crop ecologic survey in relation to agricultural development of Western Pakistan. Draft report.
- Payero, J.O., Irmak, S., 2008. Construction, installation, and performance of two repacked weighing lysimeters. Irrig Sci 26, 191-202. <https://doi.org/10.1007/s00271-007-0085-9>
- Penman, H.L., 1948. Natural evaporation from open water, bare soil and grass. Proceedings of the Royal Society of London. Series A. Mathematical and Physical Sciences 193, 120-145.
- Pereira, A.R., 2004. The Priestley-Taylor parameter and the decoupling factor for estimating reference evapotranspiration. Agricultural and Forest Meteorology 125, 305-313.
- Pereira, L.S., Allen, R.G., Smith, M., Raes, D., 2015. Crop evapotranspiration estimation with FAO56: Past and future. Agricultural Water Management 147, 4-20.
- Pereira, L.S., Paredes, P., Melton, F., Johnson, L., Wang, T., López-Urrea, R., Cancela, J.J., Allen, R.G., 2020. Prediction of crop coefficients from fraction of ground cover and height. Background and validation using ground and remote sensing data. Agricultural Water Management 241, 106197. <https://doi.org/10.1016/j.agwat.2020.106197>
- Pereira, L.S., Perrier, A., Allen, R.G., Alves, I., 1999. Evapotranspiration: concepts and future trends. Journal of irrigation and drainage engineering 125, 45-51.
- Peters, A., Nehls, T., Schonsky, H., Wessolek, G., 2014. Separating precipitation and evapotranspiration from noise – a new filter routine for high-resolution lysimeter data. Hydrol. Earth Syst. Sci. 18, 1189-1198. <https://doi.org/10.5194/hess-18-1189-2014>
- Prata, A.J., Caselles, V., Coll, C., Sobrino, J.A., Ottele, C., 1995. Thermal remote sensing of land surface temperature from satellites: Current status and future prospects. Remote sensing reviews 12, 175-224.
- Pretorius, W.M., 2018. Vaalharts : environmental aspects of agricultural land and water use practices (Thesis). North-West University.
- Price, J.C., 1984. Land surface temperature measurements from the split window channels of the NOAA 7 Advanced Very High Resolution Radiometer. Journal of Geophysical Research: Atmospheres 89, 7231-7237.
- Priestley, C.H.B., Taylor, R.J., 1972. On the assessment of surface heat flux and evaporation using large-scale parameters. Monthly weather review 100, 81-92.
- Qin, Z., Karnieli, A., Berliner, P., 2001. A mono-window algorithm for retrieving land surface temperature from Landsat TM data and its application to the Israel-Egypt border region. International journal of remote sensing 22, 3719-3746.
- Rahimzadegan, M., Janani, A., 2019. Estimating evapotranspiration of pistachio crop based on SEBAL algorithm using Landsat 8 satellite imagery. Agricultural Water Management 217, 383-390. <https://doi.org/10.1016/j.agwat.2019.03.018>
- Ramjeawon, M.R., 2016. Developing a method to estimate the water use of South African natural vegetation using remote sensing. (Thesis).

- Ramoelo, A., Majozi, N., Mathieu, R., Jovanovic, N., Nickless, A., Dziki, S., 2014. Validation of Global Evapotranspiration Product (MOD16) using Flux Tower Data in the African Savanna, South Africa. *Remote Sensing* 6, 7406-7423. <https://doi.org/10.3390/rs6087406>
- Ratshiedana, P.E., 2022. Monitoring crop water use using unmanned aerial vehicle (UAV) and surface energy balance algorithms: a case study of Vaalharts Irrigation Scheme, Northern Cape Province, South Africa.
- Ratshiedana, P.E., Abd Elbasit, M.A.M., Adam, E., Chirima, J.G., Liu, G., Economon, E.B., 2023. Determination of Soil Electrical Conductivity and Moisture on Different Soil Layers Using Electromagnetic Techniques in Irrigated Arid Environments in South Africa. *Water* 15, 1911. <https://doi.org/10.3390/w15101911>
- Ravazzani, G., Corbari, C., Morella, S., Gianoli, P., Mancini, M., 2012. Modified Hargreaves-Samani equation for the assessment of reference evapotranspiration in Alpine river basins. *Journal of irrigation and drainage engineering* 138, 592-599.
- Raziei, T., Bordi, I., Pereira, L.S., 2011. An Application of GPCC and NCEP/NCAR Datasets for Drought Variability Analysis in Iran. *Water Resour Manage* 25, 1075-1086. <https://doi.org/10.1007/s11269-010-9657-1>
- Realmuto, V.J., 1990. Separating the effects of temperature and emissivity: Emissivity spectrum normalization, in: In Proc. of the Second Thermal Infrared Multispectral Scanner (TIMS) Workshop. JPL Publication 90-55, pp. 31-35.
- Ren, H., Chen, C., Li, Y., Zhu, W., Zhang, L., Wang, L., Zhu, L., 2023. Response of Vegetation Coverage to Climate Changes in the Qinling-Daba Mountains of China. *Forests* 14, 425.
- Rodell, M., Famiglietti, J.S., Chen, J., Seneviratne, S.I., Viterbo, P., Holl, S., Wilson, C.R., 2004. Basin scale estimates of evapotranspiration using GRACE and other observations. *Geophysical Research Letters* 31, 2004GL020873. <https://doi.org/10.1029/2004GL020873>
- Rohwer, C., 1931. Evaporation from free water surfaces. US Department of Agriculture.
- Romanenko, V.A., 1961. Computation of the autumn soil moisture using a universal relationship for a large area. *Proc. of Ukrainian Hydrometeorological Research Institute* 3, 12-25.
- Roundy, R.W., 1985. Clean water provision in rural areas of less developed countries. *Social Science & Medicine* 20, 293-300. [https://doi.org/10.1016/0277-9536\(85\)90244-8](https://doi.org/10.1016/0277-9536(85)90244-8)
- Ruhoff, A.L., Paz, A.R., Collischonn, W., Aragao, L.E., Rocha, H.R., Malhi, Y.S., 2012. A MODIS-based energy balance to estimate evapotranspiration for clear-sky days in Brazilian tropical savannas. *Remote Sensing* 4, 703-725.
- Rwasoka, D.T., Gumindoga, W., Gwenzi, J., 2011. Estimation of actual evapotranspiration using the Surface Energy Balance System (SEBS) algorithm in the Upper Manyame catchment in Zimbabwe. *Physics and Chemistry of the Earth, Parts A/B/C* 36, 736-746. <https://doi.org/10.1016/j.pce.2011.07.035>
- Sagar, A., Hasan, M., Singh, D.K., Al-Ansari, N., Chakraborty, D., Singh, M.C., Iqbal, M.A., Kumar, A., Malkani, P., Vishwakarma, D.K., Elbeltagi, A., 2022. Development of Smart Weighing Lysimeter for Measuring Evapotranspiration and Developing Crop Coefficient for Greenhouse Chrysanthemum. *Sensors* 22, 6239. <https://doi.org/10.3390/s22166239>
- Salman, A.K., Durner, W., Naseri, M., Joshi, D.C., 2023. The Influence of the Osmotic Potential on Evapotranspiration. *Water* 15, 2031. <https://doi.org/10.3390/w15112031>
- Santamouris, M., Papanikolaou, N., Livada, I., Koronakis, I., Georgakis, C., Argiriou, A., Assimakopoulos, D.N., 2001. On the impact of urban climate on the energy consumption of buildings. *Solar energy* 70, 201-216.
- Santos, C.A.C. dos, Bezerra, B.G., Silva, B.B. da, Rao, T.V.R., 2010. Assessment of daily actual evapotranspiration with SEBAL and S-SEBI algorithms in cotton crop. *Revista Brasileira de Meteorologia* 25, 383-392.
- Savage, M.J., 2010. Sensible heat flux for estimating evaporation.
- Savva, A.P., Frenken, K., 2002. Crop water requirements and irrigation scheduling. FAO Sub-Regional Office for East and Southern Africa Harare.
- Schendel, 1967. Vegetation water consumption and water requirements. 1-11.
- Schmugge, T., Hook, S.J., Coll, C., 1998. Recovering surface temperature and emissivity from thermal infrared multispectral data. *Remote Sensing of Environment* 65, 121-131.
- Schultz, B., De Wrachien, D., 2002. Irrigation and drainage systems research and development in the 21st century. *Irrig. and Drain.* 51, 311-327. <https://doi.org/10.1002/ird.67>

- Seshoka, J., De Lange, W., Faysse, N., 2004. The transformation of irrigation boards into water user associations in South Africa: case studies of the Lower Olifants, Great Letaba and Vaalharts Water User Associations. International Water Management Institute, Colombo, Sri Lanka.
- Shahrajabian, M., Soleymani, A., 2017. A Lysimeter Study, a Unique Tool for Botanists, Agronomists and Other Plant Scientists. ARJA 4, 1-9. <https://doi.org/10.9734/ARJA/2017/32492>
- Shamloo, N., Taghi Sattari, M., Apaydin, H., Valizadeh Kamran, K., Prasad, R., 2021. Evapotranspiration estimation using SEBAL algorithm integrated with remote sensing and experimental methods. International Journal of Digital Earth 14, 1638-1658. <https://doi.org/10.1080/17538947.2021.1962996>
- Shekhar, S., Mailapalli, D.R., Raghuvanshi, N.S., 2022. Effect of Alternate Wetting and Drying Irrigation Practice on Rice Crop Growth and Yield: A Lysimeter Study. ACS Agric. Sci. Technol. 2, 919-931. <https://doi.org/10.1021/acsagscitech.1c00239>
- Silva, B.B.D., Mercante, E., Boas, M.A.V., Wrublack, S.C., Oldoni, L.V., 2018. Satellite-based ET estimation using Landsat 8 images and SEBAL model. REVISTA CIÊNCIA AGRONÔMICA 49. <https://doi.org/10.5935/1806-6690.20180025>
- Singels, A., Jarman, C., Bastidas-Obando, E., Olivier, F., Paraskevopoulos, A., 2018. Monitoring water use efficiency of irrigated sugarcane production in Mpumalanga, South Africa, using SEBAL. WSA 44. <https://doi.org/10.4314/wsa.v44i4.12>
- Singh, R., Senay, G., Velpuri, N., Bohms, S., Scott, R., Verdin, J., 2013. Actual Evapotranspiration (Water Use) Assessment of the Colorado River Basin at the Landsat Resolution Using the Operational Simplified Surface Energy Balance Model. Remote Sensing 6, 233-256. <https://doi.org/10.3390/rs6010233>
- Sobrino, J.A., Jiménez-Muñoz, J.C., Paolini, L., 2004. Land surface temperature retrieval from LANDSAT TM 5. Remote Sensing of environment 90, 434-440.
- Sobrino, J.A., Li, Z.-L., Stoll, M.P., Becker, F., 1994. Improvements in the split-window technique for land surface temperature determination. IEEE Transactions on Geoscience and Remote Sensing 32, 243-253.
- Sobrino, J.A., Souza Da Rocha, N., Skoković, D., Suélen Käfer, P., López-Urrea, R., Jiménez-Muñoz, J.C., Alves Rolim, S.B., 2021. Evapotranspiration Estimation with the S-SEBI Method from Landsat 8 Data against Lysimeter Measurements at the Barrax Site, Spain. Remote Sensing 13, 3686. <https://doi.org/10.3390/rs13183686>
- Stoll, M., Baecke, S., Kenning, P., 2008. What they see is what they get? An fMRI-study on neural correlates of attractive packaging. J of Consumer Behaviour 7, 342-359. <https://doi.org/10.1002/cb.256>
- Streutker, A., 1977. The dependence of permatent crop production on efficient irrigation and drainage at the Vaalharts Government Water scheme. Water SA 3, 90-102.
- Su, Z., 2002. The Surface Energy Balance System (SEBS) for estimation of turbulent heat fluxes. Hydrol. Earth Syst. Sci. 6, 85-100. <https://doi.org/10.5194/hess-6-85-2002>
- Suleiman, A.A., Tojo Soler, C.M., Hoogenboom, G., 2007. Evaluation of FAO-56 crop coefficient procedures for deficit irrigation management of cotton in a humid climate. Agricultural Water Management 91, 33-42. <https://doi.org/10.1016/j.agwat.2007.03.006>
- Sun, J., Wang, G., Sun, X., Lin, S., Hu, Z., Huang, K., 2020. Elevation-dependent changes in reference evapotranspiration due to climate change. Hydrological Processes 34, 5580-5594.
- Tabari, H., Grismer, M.E., Trajkovic, S., 2013. Comparative analysis of 31 reference evapotranspiration methods under humid conditions. Irrigation Science 31, 107-117.
- Tang, R., Li, Z.-L., Chen, K.-S., Zhu, Y., Liu, W., 2012. Verification of land surface evapotranspiration estimation from remote sensing spatial contextual information. Hydrological Processes 26, 2283-2293.
- Tanner, C.B., 1967. Measurement of evapotranspiration. Irrigation of agricultural lands 11, 534-574.
- Thomas, A., 2000. Spatial and temporal characteristics of potential evapotranspiration trends over China. Int. J. Climatol. 20, 381-396. [https://doi.org/10.1002/\(SICI\)1097-0088\(20000330\)20:4<381::AID-JOC477>3.0.CO;2-K](https://doi.org/10.1002/(SICI)1097-0088(20000330)20:4<381::AID-JOC477>3.0.CO;2-K)
- Thornthwaite, C.W., 1948. An approach toward a rational classification of climate. Geographical review 38, 55-94.
- Tolk, J.A., Evett, S.R., 2009. Lysimetry versus Neutron Moisture Meter for Evapotranspiration Determination in Four Soils. Soil Science Soc of Amer J 73, 1693-1698. <https://doi.org/10.2136/sssaj2009.0037>
- Trabert, 1896. New observations on evaporation rates. 13, 261-263.
- Trajkovic, S., 2007. Hargreaves versus Penman-Monteith under humid conditions. Journal of Irrigation and Drainage Engineering 133, 38-42.

- Turc, L., 1961. Water requirements assessment of irrigation, potential evapotranspiration: simplified and updated climatic formula, in: *Annales Agronomiques*. L'Institut National de la Recherche Agronomique (INRA) Paris, France, pp. 13-49.
- Van Halsema, G.E., Vincent, L., 2012. Efficiency and productivity terms for water management: A matter of contextual relativism versus general absolutism. *Agricultural Water Management* 108, 9-15. <https://doi.org/10.1016/j.agwat.2011.05.016>
- Van Vliet, M.T.H., Jones, E.R., Flörke, M., Franssen, W.H.P., Hanasaki, N., Wada, Y., Yearsley, J.R., 2021. Global water scarcity including surface water quality and expansions of clean water technologies. *Environ. Res. Lett.* 16, 024020. <https://doi.org/10.1088/1748-9326/abbfc3>
- Vaughan, P.J., Ayars, J.E., 2009. Noise reduction methods for weighing lysimeters. *Journal of irrigation and drainage engineering* 135, 235-240.
- Verwey, P., Vermeulen, P., 2011. Influence of irrigation on the level, salinity and flow of groundwater at Vaalharts Irrigation Scheme. *WSA* 37. <https://doi.org/10.4314/wsa.v37i2.65861>
- Walker, E., García, G.A., Venturini, V., Carrasco, A., 2019. Regional evapotranspiration estimates using the relative soil moisture ratio derived from SMAP products. *Agricultural Water Management* 216, 254-263.
- Wan, Z., Zhang, Y., Zhang, Q., Li, Z., 2002. Validation of the land-surface temperature products retrieved from Terra Moderate Resolution Imaging Spectroradiometer data. *Remote sensing of Environment* 83, 163-180.
- Wang, L., D'Odorico, P., Evans, J.P., Eldridge, D.J., McCabe, M.F., Caylor, K.K., King, E.G., 2012. Dryland ecohydrology and climate change: critical issues and technical advances. *Hydrol. Earth Syst. Sci.* 16, 2585-2603. <https://doi.org/10.5194/hess-16-2585-2012>
- Wang, T., Melton, F.S., Pôças, I., Johnson, L.F., Thao, T., Post, K., Cassel-Sharma, F., 2021. Evaluation of crop coefficient and evapotranspiration data for sugar beets from landsat surface reflectances using micrometeorological measurements and weighing lysimetry. *Agricultural Water Management* 244, 106533. <https://doi.org/10.1016/j.agwat.2020.106533>
- Watson, K., 1992. Spectral ratio method for measuring emissivity. *Remote sensing of Environment* 42, 113-116.
- Weerasinghe, I., Bastiaanssen, W., Mul, M., Jia, L., Van Griensven, A., 2020. Can we trust remote sensing evapotranspiration products over Africa? *Hydrology and Earth System Sciences* 24, 1565-1586.
- Westerhoff, R.S., 2015. Using uncertainty of Penman and Penman-Monteith methods in combined satellite and ground-based evapotranspiration estimates. *Remote Sensing of Environment* 169, 102-112.
- WMO, 1996. *Measurement and Estimation of Evaporation and Evapotranspiration*.
- Xing, Z., Chow, L., Meng, F.-R., Rees, H.W., Stevens, L., Monteith, J., 2008. Validating evapotranspiration equations using bowen ratio in New Brunswick, Maritime, Canada. *Sensors* 8, 412-428.
- Yang, J., Li, B., Shiping, L., 2000. A large weighing lysimeter for evapotranspiration and soil-water-groundwater exchange studies. *Hydrol. Process.* 14, 1887-1897. [https://doi.org/10.1002/1099-1085\(200007\)14:10<1887::AID-HYP69>3.0.CO;2-B](https://doi.org/10.1002/1099-1085(200007)14:10<1887::AID-HYP69>3.0.CO;2-B)
- Yang, X., Wu, J.J., Shi, P.J., Yan, F., 2008. Modified triangle method to estimate soil moisture status with MODerate resolution Imaging Spectroradiometer (MODIS) products. *Proc. Int. Arch. Photogramm. Remote Sens. Spat. Inf. Sci* 37, 555-560.
- Yassen, A.N., Nam, W.-H., Hong, E.-M., 2020. Impact of climate change on reference evapotranspiration in Egypt. *Catena* 194, 104711.
- Zhang, J., Wang, Y., Li, Y., 2006. A C++ program for retrieving land surface temperature from the data of Landsat TM/ETM+ band6. *Computers & geosciences* 32, 1796-1805.
- Zhang, X., Duan, J., Cherubini, F., Ma, Z., 2023. A global daily evapotranspiration deficit index dataset for quantifying drought severity from 1979 to 2022. *Scientific Data* 10, 824.
- Zhao, L., Xia, J., Xu, C., Wang, Z., Sobkowiak, L., Long, C., 2013. Evapotranspiration estimation methods in hydrological models. *J. Geogr. Sci.* 23, 359-369. <https://doi.org/10.1007/s11442-013-1015-9>
- Zhao, S., Yang, Y., Zhang, F., Sui, X., Yao, Y., Zhao, N., Zhao, Q., Li, C., 2015. Rapid evaluation of reference evapotranspiration in Northern China. *Arab J Geosci* 8, 647-657. <https://doi.org/10.1007/s12517-013-1263-0>
- Zoratipour, E., Mohammadi, A.S., Zoratipour, A., 2023. Evaluation of SEBS and SEBAL algorithms for estimating wheat evapotranspiration (case study: central areas of Khuzestan province). *Applied Water Science* 13, 137.

Zsembeli, J., Czeller, K., Sinka, L., Kovács, G., Tuba, G., 2019. Application of lysimeters in agricultural water management. Creating a platform to address the techniques used in creation and protection of environment and in economic management of water in the soil 5-21.